



TEZ ŞABLONU ONAY FORMU
THESIS TEMPLATE CONFIRMATION FORM.

1. Şablonda verilen yerleşim ve boşluklar değiştirilmemelidir.
2. **Jüri tarihi** Başlık Sayfası, İmza Sayfası, Abstract ve Öz'de ilgili yerlere yazılmalıdır.
3. İmza sayfasında jüri üyelerinin unvanları doğru olarak yazılmalıdır. Tüm imzalar **mavi pilot kalemle** atılmalıdır.
4. **Disiplinlerarası** programlarda görevlendirilen öğretim üyeleri için jüri üyeleri kısmında tam zamanlı olarak çalıştıkları anabilim dalı başkanlığının ismi yazılmalıdır. Örneğin: bir öğretim üyesi Biyoteknoloji programında görev yapıyor ve biyoloji bölümünde tam zamanlı çalışıyorsa, İmza sayfasına biyoloji bölümü yazılmalıdır. İstisnai olarak, disiplinler arası program başkanı ve tez danışmanı için disiplinlerarası program adı yazılmalıdır.
5. Tezin **son sayfasının sayfa** numarası Abstract ve Öz'de ilgili yerlere yazılmalıdır.
6. Bütün chapterlar, referanslar, ekler ve CV sağ sayfada başlamalıdır. Bunun için **kesmeler** kullanılmıştır. **Kesmelerin kayması** fazladan boş sayfaların oluşmasına sebep olabilir. Bu gibi durumlarda paragraf (¶) işaretine tıklayarak kesmeleri görünür hale getirin ve yerlerini **kontrol edin**.
7. Figürler ve tablolar kenar boşluklarına taşmamalıdır.
8. Şablonda yorum olarak eklenen uyarılar dikkatle okunmalı ve uygulanmalıdır.
9. Tez yazdırılmadan önce PDF olarak kaydedilmelidir. Şablonda yorum olarak eklenen uyarılar PDF dokümanında yer almamalıdır.
10. Tez taslaklarının kontrol işlemleri tamamlandığında, bu durum öğrencilere METU uzantılı öğrenci e-posta adresleri aracılığıyla duyurulacaktır.
11. Tez yazım süreci ile ilgili herhangi bir sıkıntı yaşarsanız, **Sıkça Sorulan Sorular (SSS)** sayfamızı ziyaret ederek yaşadığınız sıkıntıyla ilgili bir çözüm bulabilirsiniz.

1. Do not change the spacing and placement in the template.
2. Write **defense date** to the related places given on Title page, Approval page, Abstract and Öz.
3. Write the titles of the examining committee members correctly on Approval Page. **Blue ink** must be used for all signatures.
4. For faculty members working in **interdisciplinary programs**, the name of the department that they work full-time should be written on the Approval page. For example, if a faculty member staffs in the biotechnology program and works full-time in the biology department, the department of biology should be written on the approval page. Exceptionally, for the interdisciplinary program chair and your thesis supervisor, the interdisciplinary program name should be written.
5. Write **the page number of the last page** in the related places given on Abstract and Öz pages.
6. All chapters, references, appendices and CV must be started on the right page. **Section Breaks** were used for this. **Change in the placement** of section breaks can result in extra blank pages. In such cases, make the section breaks visible by clicking paragraph (¶) mark and **check their position**.
7. All figures and tables must be given inside the page. Nothing must appear in the margins.
8. All the warnings given on the comments section through the thesis template must be read and applied.
9. Save your thesis as pdf and Disable all the comments before taking the printout.
10. This will be announced to the students via their METU students e-mail addresses when the control of the thesis drafts has been completed.
11. If you have any problems with the thesis writing process, you may visit our **Frequently Asked Questions (FAQ)** page and find a solution to your problem.

Yukarıda bulunan tüm maddeleri okudum, anladım ve kabul ediyorum. / I have read, understand and accept all of the items above.

Name : _____
Surname : _____
E-Mail : _____
Date : _____
Signature : _____

RECYCLING OF POLYMER WASTE USING DIFFERENT TECHNIQUES

A THESIS SUBMITTED TO
THE GRADUATE SCHOOL OF NATURAL AND APPLIED SCIENCES
OF
MIDDLE EAST TECHNICAL UNIVERSITY

BY
SEDA SIVRI

IN PARTIAL FULFILLMENT OF THE REQUIREMENTS
FOR
THE DEGREE OF DOCTOR OF PHILOSOPHY
IN
CHEMICAL ENGINEERING

JANUARY 2023

Approval of the thesis:

RECYCLING OF POLYMER WASTE USING DIFFERENT TECHNIQUES

submitted by **SEDA SİVRİ** in partial fulfillment of the requirements for the degree of **Doctor of Philosophy in Chemical Engineering, Middle East Technical University** by,

Prof. Dr. Halil Kalıpçılar
Dean, Graduate School of **Natural and Applied Sciences**

Prof. Dr. Pınar Çalık
Head of the Department, **Chemical Engineering**

Prof. Dr. Naime Aslı Sezgi
Supervisor, **Chemical Engineering, METU**

Assoc. Prof. Dr. Çerağ Dilek Hacıhabiboğlu
Co-Supervisor, **Chemical Engineering, METU**

Examining Committee Members:

Prof. Dr. Gürkan Karakaş
Chemical Engineering, METU

Prof. Dr. Naime Aslı Sezgi
Chemical Engineering, METU

Prof. Dr. Göknur Bayram
Chemical Engineering, METU

Prof. Dr. Nuray Oktar
Chemical Engineering, Gazi University

Assist. Prof. Dr. Zeynep Obalı
Material Science and Nanotechnology Engineering, TOBB

Date: 26.01.2023

I hereby declare that all information in this document has been obtained and presented in accordance with academic rules and ethical conduct. I also declare that, as required by these rules and conduct, I have fully cited and referenced all material and results that are not original to this work.

Name Last name : SEDA SİVRİ

Signature :

ABSTRACT

RECYCLING OF POLYMER WASTE USING DIFFERENT TECHNIQUES

Sivri, Seda
Doctor of Philosophy, Chemical Engineering
Supervisor: Prof. Dr. Naime Aslı Sezgi
Co-Supervisor: Assoc. Prof. Dr. Çerağ Dilek Hacıhabiboğlu

January 2023, 289 pages

Poly(lactic acid) (PLA) is the most widely known renewable biodegradable polymer due to its mass production, good processability, optical, mechanical, thermal, and barrier properties. Hence, the production rate of PLA increased gradually during the last decade. However, PLA is known to have slow degradation rate in soil and marine environments, leading to significant waste accumulation with widespread usage of the polymer. Thus, recycling of PLA waste will become a significant environmental concern in near future unless the effective techniques emerge.

Focusing on this problem, the degradation of PLA was performed with and without metal loaded silica aerogel catalysts using custom-designed pyrolysis system and high-pressure reaction system under different reaction parameters. The production of lactide isomers, lactic acid, propionic acid, acetaldehyde, carbon monoxide, carbon dioxide and hydrogen were achieved. The maximum lactide isomer yield was determined to be 49 wt.% at 225 °C, 480 min, 70 rpm under 50 ml/min argon flow in pyrolysis system, while 89 wt.% lactide isomer yield was achieved at 200 °C, 120 min, 70 rpm and 206 bar in high-pressure system. In addition, Al, Fe, and Mg loaded catalysts were found to be effective in the degradation of PLA. The highest lactide

isomer yield was found to be 58 wt.% with SAUFe15 catalyst at 225 °C, 60 min, 70 rpm under 50 ml/min argon flow.

These outputs show that supercritical carbon dioxide medium, mesoporous catalysts and pyrolysis technique are promising for the recycling of PLA with the aim of closed loop production of PLA.

Keywords: Polylactic Acid, Degradation, Pyrolysis, Supercritical Carbon Dioxide, Mesoporous Catalysts

ÖZ

ÇEŞİTLİ TEKNİKLER KULLANILARAK POLİMER ATIKLARIN GERİ DÖNÜŞÜMÜ

Sivri, Seda
Doktora, Kimya Mühendisliği
Tez Yöneticisi: Prof. Dr. Naime Aslı Sezgi
Ortak Tez Yöneticisi: Doç. Dr. Çerağ Dilek Hacıhabiboğlu

Ocak 2023, 289 sayfa

Polilaktik asit (PLA), seri üretimi, iyi işlenebilirliği, optik, mekanik, termal ve bariyer özelliklerinden dolayı en yaygın olarak bilinen yenilenebilir, biyolojik olarak parçalanabilen polimerdir. Bu nedenle, PLA üretim hızı son on yılda önemli ölçüde arttı. Bununla birlikte, PLA'nın toprakta ve deniz ortamlarında yavaş bozunma hızına sahip olduğu ve polimerin yaygın kullanımı ile önemli atık birikimine yol açtığı bilinmektedir. Bu nedenle, PLA atıklarının geri dönüşümü, yeni teknikler ortaya çıkmadıkça yakın gelecekte önemli bir çevresel sorun haline gelecektir.

Bu probleme odaklanılarak, PLA'nın bozunması farklı reaksiyon parametreleri altında özel olarak tasarlanmış piroliz sistemi ve yüksek basınçlı reaksiyon sistemi kullanılarak metal yüklü silika aerogel katalizörleriyle ve bunlar olmaksızın gerçekleştirilmiştir. Laktit izomerleri, laktik asit, propiyonik asit, asetaldehit, karbon monoksit, karbon dioksit ve hidrojenin üretimi sağlanmıştır. Piroliz sisteminde 50 ml/dk argon akışı altında 225 °C, 480 dk, 70 rpm'de maksimum laktit izomer verimi ağırlıkça %49 olarak belirlenirken, yüksek basınç sisteminde 200 °C, 120 dk, 70 rpm ve 206 bar'da ağırlıkça %89 laktit izomer verimi elde edildi. Ayrıca Al, Fe ve Mg

yüklü katalizörlerin PLA'nın parçalanmasında etkili olduğu görülmüştür. En yüksek laktit izomer verimi SAUFe15 katalizörü ile 225 °C, 60 dk, 70 rpm'de, 50 ml/dk argon akışında ağırlıkça %58 olarak bulunmuştur.

Bu çıktılar, süperkritik karbondioksit ortamı, mezogözenekli katalizörler ve piroliz tekniğinin, PLA'nın kapalı döngü üretimi amacıyla PLA'nın geri dönüşümü için umut verici olduğunu göstermektedir.

Anahtar Kelimeler: Polilaktik Asit, Bozunma, Piroliz, Süperkritik Karbondioksit, Mezogözenekli Katalizörler

To my beloved parents and Alp

&

To the memory of my grandmother and Chen

ACKNOWLEDGMENTS

I turned a new leaf when I started working in this field, which gave me the opportunity to expand my wings, and now I feel immense pleasure to come to an end in this chapter. As a beginning, I would like to express my sincere appreciation for the ongoing global efforts to address plastic pollution and the promotion of recycling technologies and green chemistry. The use of bioplastics as a sustainable alternative to traditional plastics is a crucial step towards mitigating the negative impacts of plastic waste on the environment. It is my hope that this research will contribute to efforts to promote sustainability and protect our planet for future generations. Throughout my thesis studies, I was surrounded by many people. I could not complete this work without their assistance and hard labor.

First and foremost, I would like to express my sincere gratitude to my supervisors, Prof. Dr. Naime Aslı Sezgi and Assoc. Prof. Dr. Çerağ Dilek Hacıhabioğlu for their invaluable guidance, support, and encouragement throughout this journey. Their expertise and insight have been instrumental in shaping the direction and quality of my research. Your willingness to listen, and to challenge me to think critically and deeply has helped me become a more confident and capable researcher.

I would also like to extend my appreciation to the members of my committee, Prof. Dr. Gürkan Karakaş and Prof. Dr. Nuray Oktar for their valuable feedback and constructive criticism, which have greatly improved the overall quality of my work. I am also grateful to Dr. Gökhan Çelik and Arzum Ceren Aydoğdu for their assistance with MS analyses.

I am grateful to the Chemical Engineering Department for providing me with the necessary resources and facilities to conduct my research. I would also like to acknowledge the support of TEZ-D-304-2020-10182, GAP-304-2020-10143, and TUBİTAK-122M088 projects for financially supporting this thesis. I would like to

extend my sincere thanks to the ODTU Technology Transfer Office for their support of patent registration processes.

I am deeply grateful to my dear friends Ezgi Yavuzyılmaz, Merve Sarıyer, Merve Özkutlu, and Fatma Şahin. They have stood by me not only during the happy times but also during the challenging moments, offering their unwavering support and encouragement. Their presence in my life has been invaluable, and I cherish the bond that we share. I cannot thank them enough for being there for me whenever I needed them and for making my life better in so many ways.

My friends, lab-mates and colleagues Çağla Bozcuoğlu, Soner Yaşar, Aslı Karausta, Nisa Erişen, Taner Astarlıoğlu, Betül Teke, Oğuzhan Sarıyer, Arzu Arslan Bozdağ, İlker Şener, Zeynep Karakaş, Veysi Halvacı, Selin Karahan, Asena Kızıl, Azad Yılmaz, Almira Çaldıkhoğlu, Candan Karaevvaz, Alican Ertaş, Salih Ermiş, Sevil Göktürk and Abdul Rehman Rajabalı Habib have been a tremendous source of support throughout my journey, and I would like to express my gratitude towards them. Their unwavering encouragement and assistance have kept me going, and I couldn't have made it this far without their help.

Finally, I want to express my gratitude to the most significant people for me who are in my family. Presence of each one gives me happiness, strength and peace. I want to acknowledge many thanks to my bighearted aunt Serpil İnan who has provided a great influence on my personality. I also thank to my uncles and to their lovely wives Naci-Serap Sivri, Hüseyin-Buket Sivri, Fatoş-Selim Sivri and Hasan-Hatice Yön. I am also thankful to Korkut İnan for her distinctive humour which had never failed to cheer me up when I needed. I am also grateful to my cousins, Serra İnan, Berra İnan, Yasin Sivri, Yasemin Sivri, Atilla Sivri, Handan Uğurlu, Ela Sivri, Duru Sivri, who fill my life with endless joy.

I am most thankful for my parents and my brother Alp. My dear mom, I cannot express my gratitude enough for you, for being the most positive person I have ever known, for being so caring all the time and for showing me unconditional love which

lets me make my own mistakes and learn from them. My lovely father, thank you for always staying besides me and giving me confidence to stand on my own feet. My beloved brother Alp for helping me not only in this thesis but also all the stages of my life. Thanks to you I smile more, I love more and I challenge myself more. I am so grateful to have you

TABLE OF CONTENTS

ABSTRACT.....	v
ÖZ	vii
ACKNOWLEDGMENTS	x
TABLE OF CONTENTS.....	xiii
LIST OF TABLES	xix
LIST OF FIGURES	xxi
LIST OF ABBREVIATIONS	xxx
LIST OF SYMBOLS	xxxi
CHAPTERS	
1 INTRODUCTION	1
2 BACKGROUND INFORMATION AND LITERATURE SURVEY	7
2.1 The core material in the evolution of an age.....	7
2.2 Plastics: The other side of the medallion	12
2.3 Plastic Waste: Current state, strategies, and solutions.....	15
2.4 Recycling of the Current Plastic Waste as a Major Solution to Plastic Crisis	207
2.5 Recycling Methods of Plastic Waste	20
2.6 Advanced techniques and approaches on the Plastic Waste	22
2.6.1 Mesoporous Catalysts in the Degradation of Plastics.....	22
2.6.2 Supercritical Fluids in the Degradation of Plastics.....	25
2.7 Bioplastics as an alternative to common plastics.....	30
2.8 A Promising Biodegradable Plastic: Polylactic Acid	35
2.9 Recycling of Polylactic Acid	42

2.9.1	Biological Recycling of Polylactic Acid	43
2.9.2	Mechanical Recycling of PLA	46
2.9.3	Chemical Recycling of PLA.....	47
2.9.3.1	Hydrolysis and Solvolysis of PLA.....	48
2.10	Thermal Degradation of PLA.....	55
2.10.1	Thermal Degradation of PLA using Thermogravimetric Technique	55
2.10.2	Determination of the Kinetic Parameters of Degradation Reaction of PLA	56
2.10.3	The Influence of Agents on the Thermal Behaviour of PLA	57
2.10.4	Thermal Degradation of PLA Composites and Blends	57
2.10.5	The Influence of Biomass on the Thermal Behaviour of PLA.....	58
2.10.6	Molecular Simulations on the Degradation of PLA	58
2.10.7	Reaction Mechanism and Products in the Degradation of PLA Composites and Blends	60
2.10.8	Pyrolysis System	60
2.11	Chemical Recycling of Plastics with Supercritical Carbon Dioxide.....	63
2.12	Aim of the Study	65
3	EXPERIMENTAL	69
3.1	Synthesis and Characterization of Silica Aerogel Based Catalysts.....	69
3.1.1	Synthesis of Silica Aerogel Support.....	69
3.1.2	Impregnation of Metal into Silica Aerogel Support	70
3.1.3	Characterization of Silica Aerogel Based Catalysts	71
3.2	Thermal Degradation of PLA using Thermogravimetric Method.....	72
3.3	PLA Degradation Experiments.....	73

3.3.1	PLA Pyrolysis System	73
3.3.1.1	Experimental Procedure for the Non-catalytic Degradation of PLA in Pyrolysis System	74
3.3.1.2	Experimental Procedure for Degradation of PLA with Metal Loaded Silica Aerogel Catalysts:	75
3.3.2	Supercritical PLA Degradation System	76
3.3.2.1	The Experimental Procedure for the Degradation Reaction of PLA in the Supercritical CO ₂ Environment	77
3.4	Analyses of the Products	78
3.4.1	GC Analyses of the Condensable, Gas and Solid Products	78
3.4.2	Analyses of the Solid in the Pyrolysis Reactor	79
4	RESULTS AND DISCUSSION	81
4.1	Degradation of PLA with Different Techniques	82
4.1.1	Thermal Degradation of PLA using Thermogravimetric Method	82
4.1.2	Degradation of PLA by Pyrolysis	83
4.1.2.1	Design and Operation of the Pyrolysis System for the Degradation Reaction of PLA	83
4.1.2.2	The Effect of the Mixing Rate on the Product Type and Distribution	84
4.1.2.3	The Effect of the Reaction Temperature on the Product Type and Distribution	90
4.1.2.4	The Effect of the Reaction Time on the Product Type and Distribution	104
4.1.2.5	The Effect of the Flow Rate on the Product Type and Distribution	114
4.1.3	Degradation of PLA in Supercritical Carbon Dioxide	118

4.1.3.1	The Effect of Mixing Rate on the Product Type and Distribution.....	119
4.1.3.2	The Effect of Reaction Time on the Product Type and Distribution.....	122
4.1.3.3	The Effect of Reaction Temperature on the Product Type and Distribution.....	126
4.1.3.4	The Effect of Reaction Pressure on the Product Type and Distribution.....	128
4.1.4	Comparison of PLA Degradation Techniques	132
4.2	Catalytic Degradation of PLA	138
4.2.1	Degradation of PLA with Aluminum Loaded Catalyst.....	139
4.2.1.1	Characterization of Aluminum Loaded Catalyst.....	139
4.2.1.1.1	Characterization of Silica Aerogel Material	139
4.2.1.1.2	Characterization of Aluminum Loaded Silica Aerogel Catalyst	147
4.2.1.2	Determination of Activation Energy of PLA Degradation Reaction in the Presence of Aluminum Loaded Silica Aerogel Catalyst..	157
4.2.1.3	Degradation of PLA in the presence of Aluminum Loaded Silica Aerogel Catalyst	159
4.2.1.4	Characterization of the Used Catalysts	171
4.2.2	Degradation of PLA with Iron Loaded Catalyst.....	173
4.2.2.1	Characterization of Iron Loaded Silica Aerogel Catalyst	173
4.2.2.2	Determination of Activation Energy of PLA Degradation Reaction in the Presence of Iron Loaded Silica Aerogel Catalyst.....	177
4.2.2.3	Degradation of PLA in the presence of Iron Loaded Silica Aerogel Catalyst	179

4.2.2.4	Characterization of the Used Iron Loaded Silica Aerogel Catalysts.....	189
4.2.3	Degradation of PLA with Magnesium Loaded Catalyst.....	192
4.2.3.1	Characterization of Magnesium Loaded Catalyst.....	193
4.2.3.2	Determination of Activation Energy of PLA Degradation Reaction in the Presence of Magnesium Loaded Silica Aerogel Catalyst	195
4.2.3.3	Degradation of PLA in the presence of Magnesium Loaded Silica Aerogel Catalyst	197
4.2.3.4	Characterization of the Used Magnesium Loaded Silica Aerogel Catalysts.....	207
4.2.4	Comparison of Activities of Different Metal Loaded Catalysts in PLA Degradation.....	209
5	CONCLUSIONS.....	217
6	RECOMMENDATIONS	221
7	REFERENCES	223
A.	Determination of Activation Energy for Thermal Degradation Reaction of PLA.....	267
B.	Calculation of Solid, Condensable and Non-condensable Product Yields and Weight Fraction of Compounds in Condensable Product for the Pyrolysis System.....	270
C.	Calculations of Relative Response Factor and Number of Moles of the Components in the Condensable and Solid Products	271
D.	Calculation of Mole Fraction of Components in Non-condensable Product	274
E.	DSC Analysis of PLA-2003D.....	276

F.	Determination of the Viscosity Average Molecular Weight of the Solid in the Reactor	277
G.	Calculation of the Solid and Gas Yields in Supercritical Reaction System	282
H.	XRD Data	283
	CURRICULUM VITAE	287

LIST OF TABLES

TABLES

Table 2.1. Recycling rates of plastic bottles sourced in the United States in 2020.	20
Table 2.2. The studies on recycling of polymers in the presence of supercritical medium.	28
Table 2.3. The studies on recycling of polymers in the presence of supercritical medium-cont'd.	29
Table 2.4. The studies on recycling of polymers in the presence of supercritical medium-cont'd.	30
Table 3.1. Metal loaded silica aerogel-based catalysts.	71
Table 3.2. The components of the pyrolysis system.	73
Table 3.3. Reaction parameters of the non-catalytic degradation of PLA.	75
Table 3.4. The components of the supercritical reaction system.	76
Table 3.5. Reaction Parameters of Thermal Degradation of PLA in Supercritical CO ₂	78
Table 4.1. Degradation temperatures of solid products at 5% and 60% weight losses.	97
Table 4.2. Degradation temperatures of solid products at 5% and 60% weight losses.	107
Table 4.3. The physical properties of uncalcined and calcined silica aerogels. ...	144
Table 4.4. The physical properties of aluminum loaded silica aerogel catalysts..	149
Table 4.5. Total acidic capacities of aluminum loaded silica aerogel catalysts....	152
Table 4.6. The physical properties of 15 (wt.%) aluminum loaded silica aerogel catalysts.	155
Table 4.7. Activation energies of PLA degradation reaction in the presence of Al loaded silica aerogels.	159
Table 4.8. The physical properties of used aluminum loaded silica aerogel catalysts.	173

Table 4.9. Degradation temperature values at 5%, 30%, and 60% weight losses with the SAUFe15 catalyst.	179
Table 4.10. The physical properties of the used iron loaded silica aerogel catalysts.	191
Table 4.11. Degradation temperature values at 5%, 30%, and 60% weight losses with the SAUMg15 catalyst.	197
Table 4.12. The physical properties of used aluminum loaded silica aerogel catalysts.	208

LIST OF FIGURES

FIGURES

Figure 2.1. The distribution of the commodity plastics worldwide in 2018 (Statista, 2021).	9
Figure 2.2. The distribution of global plastic material production in 2019 by region.	10
Figure 2.3. The distribution of global plastic material production in 2019	11
Figure 2.4. Huge plastic masses created by human beings	12
Figure 2.5. Plastic waste generation by industrial sector	13
Figure 2.6. The estimated degradation time of commercial materials in marine environment	14
Figure 2.7. The current global plastic use and waste with global plastic use and waste projections scenarios by 2060	16
Figure 2.8. The recycling rate of the plastic waste and packaging plastic waste on European countries in 2018.	19
Figure 2.9. Global bioplastic production capacity.	31
Figure 2.10. The market value of bioplastics	32
Figure 2.11. The distribution of biodegradable plastics by production capacity in 2019	33
Figure 2.12. The global production capacity of bioplastics by usage areas.	34
Figure 2.13. Production routes of PLA	36
Figure 2.14. Market value forecast of polylactic acid in the United States from 2019 to 2025 by application (in million U.S. dollars)	41
Figure 2.15. Production and recycling methods of PLA	43
Figure 2.16. Hydrolysis of PLA in artificial seawater (SW) and water (FW) at 25 °C	46
Figure 2.17. The degradation of PLA with different techniques.	67
Figure 3.1. Installed pyrolysis system	73
Figure 3.2. Supercritical reaction system	76

Figure 4.1. Thermal degradation of PLA by thermogravimetric method.....	82
Figure 4.2. The effect of mixing rate on the yield of the products (225 °C, 60 min, 70 rpm, 50 ml/min).....	85
Figure 4.3. The effect of mixing rate on the condensable product distribution (225 °C, 60 min, 50 ml/min).	86
Figure 4.4. The isomers of lactide	87
Figure 4.5. The effect of mixing rate on the non-condensable product distribution at the 15 th min. (225 °C, 60 min, 50 ml/min).	88
Figure 4.6. The effect of mixing rate on the non-condensable product distribution at the 50 th min. (225 °C, 60 min, 50 ml/min).	89
Figure 4.7. The yields of products obtained from three runs at different times (275 °C, 60 min, 70 rpm, 50 ml/min).....	91
Figure 4.8. Product distribution of the condensable product obtained from three runs at different times (275 °C, 60 min, 70 rpm, 50 ml/min).....	92
Figure 4.9. The gas composition obtained from three runs at the 15 th min (275 °C, 60 min, 70 rpm, 50 ml/min).....	93
Figure 4.10. The gas composition obtained from three runs at the 50 th min (275 °C, 60 min, 70 rpm, 50 ml/min).....	93
Figure 4.11. The effect of reaction temperature on the yield of products (60 min, 70 rpm, 50 ml/min).....	94
Figure 4.12. Degradation profiles of the solid products obtained at reaction temperature range of 200 °C and 250 °C.	96
Figure 4.13. The viscosity average molecular weight of the solid product with respect to reaction temperature (60 min, 70 rpm, 50 ml/min).....	98
Figure 4.14. The effect of reaction temperature on condensable product distribution (60 min, 70 rpm, 50 ml/min).	99
Figure 4.15. The effect of reaction temperature on the area of unidentified product.	101
Figure 4.16. The effect of reaction temperature on non-condensable product distribution at the 15 th min. (60 min, 70 rpm, 50 ml/min).....	102

Figure 4.17 The effect of reaction temperature on non-condensable product distribution at the 50 th min. (60 min, 70 rpm, 50 ml/min).	104
Figure 4.18. The effect of reaction time on the yield of product (225 °C, 70 rpm, 50 ml/min).....	105
Figure 4.19. Degradation profile of the solid reaction products obtained at different reaction times.	106
Figure 4.20 The viscosity average molecular weight of the solid products with respect to reaction time (225 °C, 70 rpm, 50 ml/min).....	108
Figure 4.21. The effect of reaction time on condensable product distribution (225 °C, 70 rpm, 50 ml/min).	109
Figure 4.22. The effect of reaction time on non-condensable product distribution (225 °C, 70 rpm, 50 ml/min).	110
Figure 4.23. The effect of reaction time on the yield of products (300 °C, 70 rpm, 50 ml/min).....	111
Figure 4.24. The effect of reaction time on condensable product distribution (300 °C, 70 rpm, 50 ml/min).	112
Figure 4.25. The effect of reaction time on the area of unidentified product (U1).	113
Figure 4.26. The effect of reaction time on non-condensable product distribution (300 °C, 70 rpm, 50 ml/min).	114
Figure 4.27. The effect of flow rate on the yield of products (225 °C, 70 rpm, 60 min).	115
Figure 4.28. The effect of flow rate on condensable product distribution (225 °C, 70 rpm, 60 min).....	116
Figure 4.29. The effect of flow rate on non-condensable product distribution at the 15 th minute (225 °C, 70 rpm, 60 min).	117
Figure 4.30. The effect of flow rate on non-condensable products distribution at the 50 th minute (225 °C, 70 rpm, 60 min).	118
Figure 4.31. The effect of the mixing rate on the yield of the products (200 °C, 103 bar, 120 min).	120

Figure 4.32. The effect of the mixing rate on the solid product distribution (200 °C, 103 bar, 120 min).	121
Figure 4.33. The effect of reaction time on the yield of products (200 °C, 103 bar, 70 rpm).	123
Figure 4.34. The effect of reaction time on the solid product distribution (200 °C, 103 bar, 70 rpm).	124
Figure 4.35. The effect of reaction time on the yield of products (220 °C, 103 bar, 70 rpm).	125
Figure 4.36. The effect of reaction time on the solid product distribution (220 °C, 103 bar, 70 rpm).	126
Figure 4.37. The effect of reaction temperature on the yield of products (103 bar, 120 min., 70 rpm).	127
Figure 4.38. The effect of reaction temperature on the solid product distribution (103 bar, 120 min, 70 rpm).	128
Figure 4.39. The effect of reaction pressure on the yield of products (200 °C, 120 min, 70 rpm).	129
Figure 4.40. The effect of reaction pressure on the solid product distribution (200 °C, 120 min, 70 rpm).	130
Figure 4.41. The effect of reaction pressure on the yield of products (220 °C, 30 min, 70 rpm).	131
Figure 4.42. The effect of reaction pressure on the solid product distribution (220 °C, 30 min, 70 rpm).	132
Figure 4.43. The effect of reaction temperature on the yield of compounds in condensable products (60 min, 70 rpm, 50 ml/min).	133
Figure 4.44. The effect of reaction time on the yield of compounds in condensable products (225 °C, 70 rpm, 50 ml/min).	134
Figure 4.45. The effect of reaction temperature on the yield of compounds in solid products (120 min, 103 bar, 70 rpm).	135
Figure 4.46. The effect of reaction time on the yield of compounds in solid products (200 °C, 103 bar, 70 rpm).	136

Figure 4.47. The produced silica aerogel material.....	140
Figure 4.48. Nitrogen adsorption/desorption isotherms of different uncalcined (SAU) silica aerogel material batches.....	141
Figure 4.49. Nitrogen adsorption/desorption isotherms of uncalcined (SAU) and calcined (SA) silica aerogel materials.....	142
Figure 4.50. Comparison of the pore size distributions of uncalcined (SAU) and calcined (SA) silica aerogels.....	143
Figure 4.51. SEM images of the uncalcined silica aerogel (SAU) with 100kX magnification.	145
Figure 4.52. FTIR spectra of uncalcined (SAU) and calcined (SA) silica aerogels.	146
Figure 4.53. Nitrogen adsorption/desorption isotherms of aluminum loaded silica aerogel catalysts with different weight ratios	147
Figure 4.54. The pore size distributions of aluminum loaded silica aerogel materials.	148
Figure 4.55. SEM images of the aluminum loaded silica aerogel catalysts: a. SAA110, b. SAA115 with 100kX magnification.	149
Figure 4.56. EDX analysis of the SAA115 catalyst.....	151
Figure 4.57. NH ₃ -TPD curves of aluminum loaded silica aerogel catalysts.	152
Figure 4.58. Nitrogen adsorption/desorption isotherms of 15 wt.% aluminum loaded silica aerogel catalysts (filled and empty symbols represent adsorption and desorption branches, respectively).....	153
Figure 4.59. The pore size distribution of 15% aluminum loaded silica aerogel materials.	154
Figure 4.60. SEM images of 15 wt.% aluminum loaded uncalcined silica aerogel catalyst: a. 25kX magnification b. 50 kX magnification.	155
Figure 4.61. DRIFTS spectra of the pyridine adsorbed 15 wt.% aluminum loaded into uncalcined & calcined silica aerogels.	156
Figure 4.62. Degradation profile of PLA in the presence of the aluminum loaded catalyst.	158

Figure 4.63. The effect of reaction temperature on the yield of products (SAUA115, 60 min, 70 rpm, 50 ml/min).....	160
Figure 4.64. Comparison of the catalytic degradation of PLA with the the non-catalytic degradation of PLA in terms of reaction temperature and product yield (60 min, 70 rpm, 50 ml/min).....	162
Figure 4.65. The effect of reaction temperature on condensable product distribution (SAUA115, 200-275 °C, 60 min, 70 rpm, 50 ml/min).....	164
Figure 4.66. Comparison of the catalytic degradation of PLA with the the non-catalytic degradation of PLA in terms of reaction temperature and product distribution in condensable product (60 min, 70 rpm, 50 ml/min).....	165
Figure 4.67. The effect of reaction temperature on non-condensable product distribution at the 15 th minute (SAUA115, 60 min, 70 rpm, 50 ml/min).....	166
Figure 4.68. The effect of reaction temperature on non-condensable product distribution at the 50 th minute (SAUA115, 60 min, 70 rpm, 50 ml/min).....	168
Figure 4.69. Comparison of the catalytic degradation of PLA with the the non-catalytic degradation of PLA in terms of reaction temperature and product distribution in non-condensable product at the 15 th min (60 min, 70 rpm, 50 ml/min).	169
Figure 4.70. Comparison of the catalytic degradation of PLA with the the non-catalytic degradation of PLA in terms of reaction temperature and product distribution in non-condensable product at the 50 th min (60 min, 70 rpm, 50 ml/min).	170
Figure 4.71. Nitrogen adsorption/desorption isotherms of used aluminum loaded silica aerogel catalysts	171
Figure 4.72. Comparison of the pore size distributions of used aluminum loaded silica aerogel catalysts.	172
Figure 4.73. Nitrogen adsorption/desorption isotherms of 15 wt.% iron loaded silica aerogel catalyst.....	174
Figure 4.74. The pore size distribution of 15% iron loaded silica aerogel material.	175

Figure 4.75. SEM image of 15 wt.% iron loaded silica aerogel catalyst with 50kX magnification.	176
Figure 4.76. DRIFTS spectrum of the pyridine adsorbed 15 wt.% iron loaded silica aerogel catalyst.....	177
Figure 4.77. Degradation profile of PLA in the presence of the iron loaded catalyst.	178
Figure 4.78. The effect of reaction temperature on the yield of products (SAUFe15, 60 min, 70 rpm, 50 ml/min.)	180
Figure 4.79. Comparison of the catalytic degradation of PLA with the the non-catalytic degradation of PLA in terms of reaction temperature and product yield (60 min, 70 rpm, 50 ml/min).	181
Figure 4.80. The effect of SAUFe15 on condensable product distribution (200-275 °C, 60 min, 70 rpm, 50 ml/min).	183
Figure 4.81. Comparison of the PLA degradation of PLA in the presence of SAUFe15 with the non-catalytic degradation of PLA in terms of reaction temperature and product distribution in condensable product (60 min, 70 rpm, 50 ml/min).....	184
Figure 4.82. The effect of reaction temperature on non-condensable product distribution at the 15 th min (SAUFe15, 60 min, 70 rpm, 50 ml/min).....	185
Figure 4.83. The effect of reaction temperature on non-condensable product distribution at the 50 th min (SAUFe15, 60 min, 70 rpm, 50 ml/min).	186
Figure 4.84. Comparison of the catalytic degradation of PLA with the the non-catalytic degradation of PLA in terms of reaction temperature and product distribution in non-condensable product at the 15 th min (60 min, 70 rpm, 50 ml/min).....	187
Figure 4.85. Comparison of the degradation of PLA in the presence of SAUFe15 with the the non-catalytic degradation of PLA in terms of reaction temperature and product distribution in non-condensable product at the 50 th min (60 min, 70 rpm, 50 ml/min).....	188

Figure 4.86. Nitrogen adsorption/desorption isotherms of the used iron loaded silica aerogel catalysts (filled and empty symbols represent adsorption and desorption branches, respectively).	189
Figure 4.87. Comparison of the pore size distributions of the used iron loaded silica aerogel catalysts.....	190
Figure 4.88. XRD patterns of fresh and used SAUFe15 catalysts.	192
Figure 4.89. Nitrogen adsorption/desorption isotherms of magnesium loaded silica aerogel catalyst	193
Figure 4.90. The pore size distribution of magnesium loaded silica aerogel catalyst.	194
Figure 4.91. DRIFTS spectrum of the pyridine adsorbed 15 wt.% magnesium loaded silica aerogel catalyst.	195
Figure 4.92. Degradation profile of PLA in the presence of the magnesium loaded catalyst.	196
Figure 4.93. The effect of reaction temperature on the yield of products (SAUMg15, 60 min, 70 rpm, 50 ml/min).....	198
Figure 4.94. Comparison of the degradation of PLA in the presence of SAUMg15 with the the non-catalytic degradation of PLA in terms of reaction temperature and product yield (60 min, 70 rpm, 50 ml/min).	199
Figure 4.95. The effect of SAUMg15 on condensable product distribution (60 min, 70 rpm, 50 ml/min).....	201
Figure 4.96. Comparison of the degradation of PLA in the presence of SAUMg15 with the the non-catalytic degradation of PLA in terms of reaction temperature and product distribution in condensable product (60 min, 70 rpm, 50 ml/min).	202
Figure 4.97. The effect of reaction temperature on non-condensable product distribution at 15 minute (SAUMg15, 60 min, 70 rpm, 50 ml/min).	203
Figure 4.98. The effect of reaction temperature on non-condensable product distribution at 50 minute (SAUMg15, 60 min, 70 rpm, 50 ml/min).	204
Figure 4.99. Comparison of the degradation of PLA in the presence of SAUMg15 with the non-catalytic degradation of PLA in terms of reaction temperature and	

product distribution in non-condensable product at the 15 th minute (60 min, 70 rpm, 50 ml/min).....	205
Figure 4.100. Comparison of the degradation of PLA in the presence of SAUMg15 with the the non-catalytic degradation of PLA in terms of reaction temperature and product distribution in non-condensable product at the 50 th minute (60 min, 70 rpm, 50 ml/min).....	206
Figure 4.101. Nitrogen adsorption/desorption isotherms of the used magnesium loaded silica aerogel catalysts	207
Figure 4.102. The pore size distributions of the used magnesium loaded silica aerogel catalysts.	208
Figure 4.103. The effect of the type of metal in the catalyst on the yield of products (200-275 °C, 60 min, 70 rpm, 50 ml/min).	210
Figure 4.104. The effect of type of metal in the catalyst on condensable product distribution (200-275 °C, 60 min, 70 rpm, 50 ml/min).....	212
Figure 4.105. The effect of the type of the metal in the catalyst on non-condensable product distribution at the 15 th minute of the reaction (60 min, 70 rpm, 50 ml/min).	214
Figure 4.106. The effect of the type of metal in the catalyst on non-condensable product distribution at the 50 th minute of the reaction (60 min, 70 rpm, 50 ml/min).	215

LIST OF ABBREVIATIONS

D,L,L	The mixture of D Lactide and L Lactide
DRIFTS	Diffuse Reflectance Infrared Fourier Transform Spectroscopy
DSC	Differential Scanning Calorimetry
FTIR	Fourier Transform Infrared Spectroscopy
GC	Gas Chromatography
GC-MS	Gas Chromatography-Mass Spectroscopy
LA	Lactic Acid
Meso L	Meso Lactide
MS	Mass Spectroscopy
NC	Non-Catalytic
PA	Propionic Acid
PLA	Polylactic Acid
Py-GC/MS	Pyrolysis-Gas Chromatography-Mass Spectroscopy
SA	Calcined Silica Aerogel
SAA12.5	2.5 wt.% aluminum loaded calcined silica aerogel catalyst
SAA10	10 wt.% aluminum loaded calcined silica aerogel catalyst
SAA15	15 wt.% aluminum loaded calcined silica aerogel catalyst
SAU	Uncalcined Silica Aerogel
SAUA15	15 wt.% aluminum loaded uncalcined silica aerogel catalyst
SAUFe15	15 wt.% iron loaded uncalcined silica aerogel catalyst
SAUMg15	15 wt.% magnesium loaded uncalcined silica aerogel catalyst
TGA	Thermal Gravimetric Analyzer
TPD	Temperature Programmed Desorption
U	Unidentified Product

LIST OF SYMBOLS

A:	Pre-exponential factor, 1/s
A_i	GC area of the compound i, $mV^2 \cdot sec$
c	Concentration of polymeric solution, g/dL
E_a	Activation energy of the reaction, kJ/mol
$m_{condensable}$	Weight of the condensable product, mg
m_i	Weight of the product i, mg
M_i	Molecular weight of compound i, g/mol
$m_{initial\ PLA}$	Initial weight of the PLA polymer, mg
$m_{non-condensable}$	Weight of the non-condensable product, mg
m_{solid}	Weight of the solid product, mg
M_v	Viscosity average molecular weight, g/mol
n	Overall reaction order
n_i	Moles of compound i, mol
R	Gas constant, 8.314 J/K.mol
RF_i	Response factor of compound i
RRF_i	Relative response factor of compound i
t	Time, min
T	Temperature, °C
V_i	Volume of compound i, ml
w_i	Weight fraction of compound i
W_o	Initial weight of sample, mg
W_t	Weight of sample at time t, mg
W_α	Weight of sample at infinite time, mg
y_i	Mole fraction of component i
ΔP	The hydrostatic pressure head generated, Pa

Greek Letters

η	Viscosity of the solvent, Pa.s
η_{inh}	Inherent viscosity, dL/g
η_o	Viscosity of the solution, Pa.s
η_{red}	Reduced viscosity, dL/g
η_{sp}	Specific viscosity
ρ_i	Density of compound i, g/cm ³
β_i	Beta factor of compound i
α	Fraction of PLA decomposed at time t
$[\eta]$	Intrinsic viscosity, dL/g

CHAPTER 1

INTRODUCTION

A special group of polymers known as plastics has played a dominant role in constituting modern life today. Plastics are outstanding products due to their availability and versatility; however, above all, they are virtually irreplaceable in terms of great performance at low cost (Nicholson et al., 2022). Nowadays, the impact of plastics on industry, economy, and society is far more ascendant than any other type of material. Thus, the production and use of plastic products are still on the rise with advanced production techniques and expanding usage areas. Global plastic production reached roughly 367 million metric tons in 2020 (Plastics Europe, 2022). The plastics industry is anticipated to expand in the upcoming years and surpass 810 billion U.S. dollars by the year 2030. (Grand View Research, 2021). Yet, the striking consequences of plastic pollution generated by profit-oriented production, the take-make-dispose model, continue to be revealed concretely today.

As a consequence of the linear economy approach, there is now a massive amount of plastic waste on the planet. It is apparent that many commodity plastics remain intact on the earth and in the oceans for generations after their life span has expired. Great Pacific Garbage Patch, 1.6 million km² of 79,000 tonnes of enormous floating plastic waste, is now known as the 7th continent (Toussaint et al., 2019). The accumulation of plastics in landfills and natural environments contributes to the major environmental problems such as global warming, microplastic accumulation, and the contamination of natural water resources, which pose a significant threat to living life and the ecosystem (Sohn et al., 2020; Carney Almroth & Eggert et al., 2019; Chae et al., 2018). It is projected that by 2050, the amount of plastic waste in

the seas will be higher than that of fishes (European Parliament, 2021). The evidence of microplastics have found in the human placenta in the latest research (Ragusa, 2021). These facts and projections show that the plastic crisis continues to grow.

Within this scope, it becomes a necessity to adopt new environmentally conscious approaches in the production, consumption, and utilization of plastic wastes to serve the zero-waste principle which is on the agenda in the world and our country recently. Biodegradable polymers have come to the fore in redesigning plastic materials in accordance with sustainable principles (European Commission, 2022; Brockhaus et al., 2016). Biodegradable polymers can be decomposed by biological agents only in suitable environmental conditions (pH, temperature, humidity, etc.) (Emadian et al., 2016). This biodegradability feature contributes to the prevention of the environmental problems caused by commercial plastics that remain imperishable (Brockhaus et al., 2016; Alvarez-Chavez et al., 2012; Papong et al., 2014). Biodegradable polymers that can be produced through synthetic and renewable resources provide high performance in many applications, while also overcoming the problems such as energy efficiency, high carbon footprint, fossil resource utilization, microplastic deposition and global warming caused by petroleum-based commercial polymers (Nanda et al., 2022; Samir et al., 2022).

Polylactic acid, commonly known as PLA, is currently one of the most popular biodegradable plastics produced industrially and used in daily life instead of fossil-based plastics (Sin et.al, 2012; Auras, 2004; Castro-Aguirre et al., 2016; Rezvani Ghomie et al., 2021). PLA is employed in many medical applications due to its biodegradability and biocompatibility properties (Basu et al., 2016; Masutani and Kimura, 2014). Besides, due to its easy processing and thermal, barrier and mechanical properties, it is also used in non-medical oriented applications such as packaging material, the resin in 3D printers, fast-moving consumer goods (cups, sachets and bottles, etc.), as well as in automotive and electronic industry (Castro-Aguirre et al., 2016; Hanon et al., 2021; Bouzouita, 2016). Recently, instead of conventional fossil-based plastics, PLA is rapidly being utilized in packaging

materials which have short lifespans. Packaging materials are the product group that has the biggest share in plastic production and the amount of plastic waste generated. In 2019, 353 million tons of plastic waste were produced globally, with 141 million tons of this waste classified as packaging material (OECD, 2022). According to the 2015 data, the production number of plastics in the packaging group is 146 million tons annually, while the amount of waste generated is 141 million annually (Geyer et al., 2017). Single-use plastics lead to a decrease in resource efficiency and an increase in plastic waste. PLA, when preferred in such product groups, offers safe usage and more option for recycling. In addition to packaging, with a 33% of market share, the polymer has been widely used as a resin in 3D printing (3D Hubs, 2018).

There has been a great effort on reducing the production costs and improving the performance of PLA materials (Masutani and Kimura, 2014; Drumright et al., 2000), which promote a gradual increase in the scope of application of the biodegradable polymer. This has also led to a significant increase in the production rate of PLA in recent years (Grandview Research, 2019). PLA is now regarded one of the most common commercial bioplastics in the world, with 0.2 million tons produced in 2015 and 0.3 million tons in 2019 (Rezvani Ghomi et al., 2021). While the increasing demand for the polymer leads to an increase in its production capacity and a corresponding decrease in its cost value, the amount of waste generated by widespread use of the polymer is expected to reach a striking value soon. However, recycling of PLA waste has not yet reached a technologically advanced stage.

Although PLA was introduced to the market as a solution to the accumulation of plastic waste, in a short period, a waste problem resulting from PLA will be arisen due to market misconceptions about the biodegradability of the polymer. This waste problem will be caused by the fact that PLA is not completely biodegradable under a wide range of environmental conditions, including landfills, seas and oceans (Emadian et al., 2017). Biodegradation only occurs at appropriate pH, temperature, nutrient and water concentration (Folino et al., 2020; Kale et al., 2007; Sangwan and Wu, 2008) that will render the biological degradation of PLA wastes insufficient and

lead to the continuity of waste. Also, since the hydrolysis process requires higher temperatures, hydrolysis of waste PLA in the sea and oceans is not possible due to water temperatures (Bagheri et al., 2017). There have been studies on mechanical and thermal-mechanical recycling of PLA (Badia et al., 2012; Brüster et al., 2016; Åkesson et al., 2016; Hopmann et al., 2015; Mclauchlin and Ghita, 2016; Badia and Ribes-Greus, 2016); however, in these studies, polymer can be processed up to a level and the contribution of mechanical recycling to the sustainability of the process can be considered as relatively low. Thus, since it is possible to obtain valuable chemicals and energy from waste, the chemical recycling of PLA is advantageous over these techniques. However, the chemical recycling technology of PLA has not matured yet. Within this scope, the development of recycling and recovery technologies of PLA-based materials is important in terms of preventing the waste accumulation and supporting the production and use of the polymer.

This work focuses on the recycling technologies of PLA which will gain a more special meaning in the coming years in accordance with the sustainability principle. This recycling technology serves to the protection of existing water resources, elimination of the negative effects of plastic wastes on the environment and the development of sustainable plastic technologies based on the circular economy. The aim is to provide a comprehensive evaluation of different techniques for the degradation of PLA to reduce waste accumulation and convert the waste into value-added chemicals.

In this regard, the degradation of PLA was performed using thermal gravimetric analyzer (TGA), pyrolysis system and supercritical reaction system. The reactions were carried out with and without mesoporous catalysts designed specifically for the PLA degradation. The synthesis of metal containing mesoporous catalysts were carried out and their physical and chemical properties obtained by various characterization techniques. The activities of the catalysts were determined using TGA for further system studies.

Novel approaches are offered in this work using metal containing mesoporous catalysts that are tailor-made for the process, and supercritical carbon dioxide, a green solvent, rather than the use of organic solvents that have negative consequences for human health and the environment. Furthermore, the degradation of PLA was studied in an installed pyrolysis system in a more realistic manner rather than fast pyrolysis systems. The aforementioned techniques can be applied to prevent PLA waste from creating a negative impact on the natural life cycle and transform them into valuable materials to ensure economic efficiency. These studies will contribute to the industrial and research-oriented studies related to the recycling of the polymer and offer new recycling routes.

CHAPTER 2

BACKGROUND INFORMATION AND LITERATURE SURVEY

2.1 The core material in the evolution of an age

Baekeland, Staudinger, Goodyear, and other prominent researchers' vision has revealed a special group of polymers called as "plastics" that ushered a new perspective to an age. It is clear that this material has played a dominant role in constituting modern life in the 20th century. Nowadays, the impact of plastics on industry, economy, and society is far more ascendant than other types of material.

Since roughly 1600 BC, when ancient Mesoamericans first molded natural rubber into balls, figurines, and bands, humans have benefited from the usage of polymers (Andrady et al., 2009; Hosler et al., 1999). Although the invention of synthetic polymers had been initiated in the beginning of the 1900s, the massive production of plastics was clearly triggered by World War II (The Brooklyn Rail, 2005; Geyer et al., 2017). A systematic technological innovation and development program was built on the industrial infrastructure for the plastic sector in the USA with the contribution of the government investment and the Society for Plastic Industries (SPI) (The Brooklyn Rail, 2005). During this period, the research and development of the plastics were carried out in the cutting-edge laboratories of the leading chemical companies.

In the post war era, plastic was rapidly spread in the consumer markets (WWF, 2022). The industry had the capability of the mass production of plastics towards to military equipment; however, this production capability did not prove for the other consumer goods yet. During this period, new markets and applications were explored

for the usage of this material globally. Since then, the production and use of plastic-based materials have shown an uncontrolled growth profile worldwide supported by various incentives from the mid-20th century to the present day due to the concept of the linear economy (take-make-dispose).

Plastics are outstanding products due to availability and versatility; however, above all, they are virtually irreplaceable in terms of great performance at low cost (Nicholson et al., 2022). Plastics have a number of distinctive features, including the ability to be employed at a broad range of temperatures, its chemical resistance, strength, and robustness; yet it can be easily processed as a hot melt (Andrady et al., 2009). Additionally, plastics' success as a material has been tremendous; they have shown to be adaptable for usage in a variety of sorts and forms, including natural polymers, customized natural polymers, thermosets, thermoplastics, and more lately, biodegradable plastics (Andrady et al., 2009).

There are numerous plastic materials available today that serve a variety of purposes. The most commonly used plastics are polypropylene (PP), polyethylene (PE, LLDPE, LDPE, HDPE etc.), polyvinylchloride (PVC), polyethylene terephthalate (PET), polyurethane (PUR), polystyrene (PS, EPS), acrylonitrile butadiene styrene (ABS), acrylonitrile styrene acrylate (ASA), styrene-acrylonitrile (SAN) and so on. The distribution of the plastic products is presented in Figure 2.1.

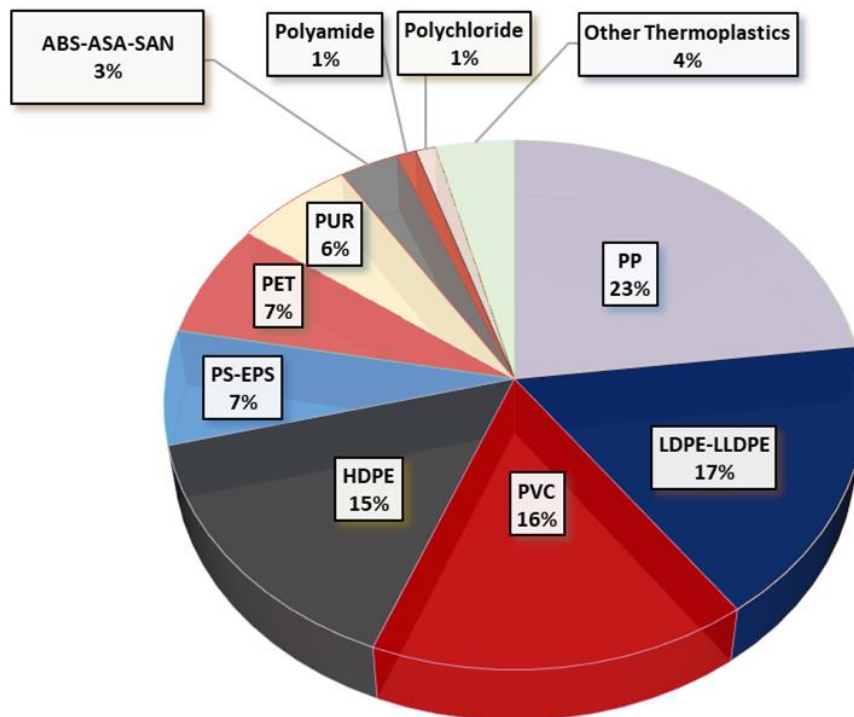


Figure 2.1. The distribution of the commodity plastics worldwide in 2018 (Statista, 2021).

In 2020, the global production of plastics reached approximately 367 million metric tons (Plastics Europe, 2022). In addition, the worldwide plastics industry was valued at 593 billion U.S. dollars in 2021. The plastics industry is expected to grow in the upcoming years and exceed over 810 billion U.S. dollars by 2030, with a compound annual growth rate (CAGR) of 3.7% from 2022 to 2030 (Plastics Europe, 2022).

Due to the mature production and processing methods of commercial plastics, the common plastics have been produced in all continents. The vast majority of these plastics have been produced in China according to the latest data (Plastics Europe; 2022). The distribution of global plastic materials production is presented in 2019 by region in Figure 2.2.

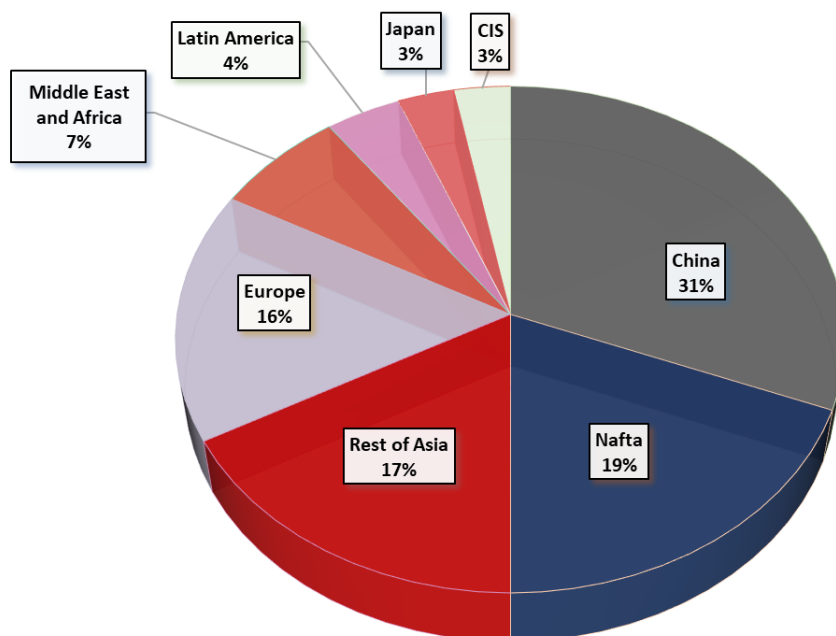


Figure 2.2. The distribution of global plastic material production in 2019 by region (Plastics Europe, 2022).

The production and use of plastic products have still on the rise with advanced production techniques and expanding usage areas. The demand for the plastic resins was established as 49.1 million tons in the European Union (Plastics Europe, 2021). The distribution of global plastic materials production in 2019 by region is given in Figure 2.3. By far the most important end-use markets are packaging and building and construction. The automotive industry is the third largest end-use market.

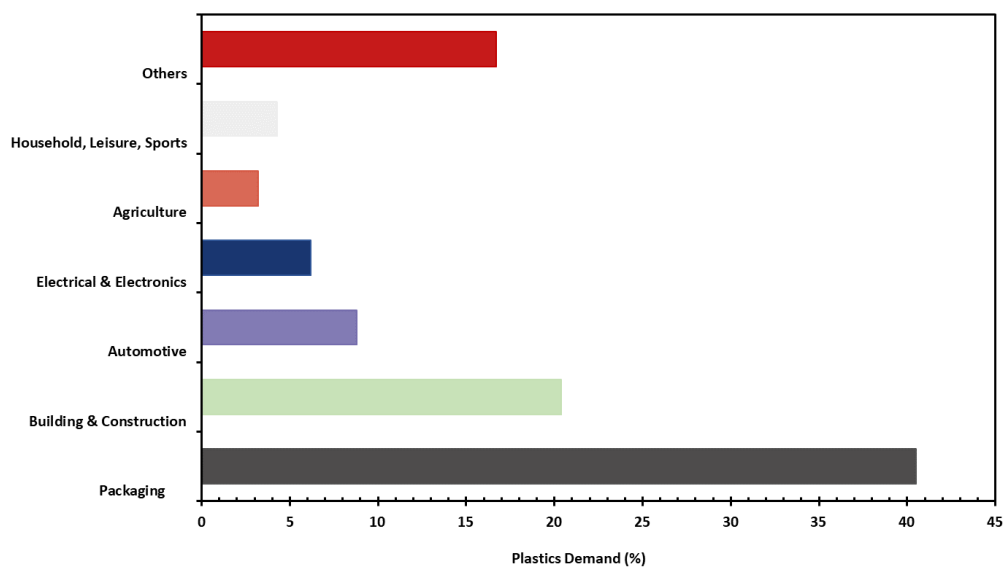


Figure 2.3. The distribution of global plastic material production in 2019 (Statista, 2021).

In European Union 28 Member States, over 1.5 million people work directly in the plastic industry, and there are more than 55.000 companies (Plastics Europe, 2020). Although the plastics contribute to economic and social benefits, it is apparent that the main incentive on plastic usage is the economic feasibility. The roots of the profitability of the plastics have arisen due to the single objective plastic model that only includes up to the production stage of the material. However, the striking consequences of plastic pollution generated by profit-oriented production continue to be revealed concretely today.

When the service life of conventional plastics is over, they remain intact on earth and in the oceans for centuries. Due to that fact, major environmental problems such as climate change, microplastic accumulation, and the pollution of natural water resources have arisen, which pose a significant threat to living life and the ecosystem (Nanda et al., 2022).

2.2 Plastics: The other side of the medallion

The traditional economy on plastics is based on the understanding of “take, make and dispose”. As the output of linear economy approach, there has been a great deal amount of plastic waste on the earth. Even, some organizations and authorities insist that plastic wastes should be accepted as the 7th natural resource after water, air, oil, natural gas, coal, and minerals (Bureau of International Recycling, 2019). Nowadays, the consequences of plastic waste have risen to the surface. Great pacific garbage patch, has a size greater than three times of the area of Spain, is now known as the 7th continent (Toussaint et al., 2019).



Figure 2.4. Huge plastic masses created by human beings (More than Green, 2021).

In 2018, 343 million tons of plastic waste were produced globally, with 158 million tons of this waste classified as packaging material. In addition, it is estimated that

each EU citizen produced 174.1 kg of packaging waste in 2018, with plastic-based products accounting for 19% of this waste (Eurostat, 2022). Particularly, the COVID-19 epidemic has contributed to an increase in the use and disposal of single-use plastics (European Environmental Agency, 2021). During the COVID-19 outbreak, approximately 8.4 million metric tons of mishandled plastic garbage were produced worldwide (The Guardian, 2021).

There still has been a steady increase in accumulation of plastic waste nowadays. Cheap, fast produced and disposed packaging materials have the majority in plastic waste generation by industrial sector (Geyer, 2017). The distribution of the plastic waste generation by industrial sector is given in Figure 2.5. The plastics utilized in textile was in the second place for the plastic waste distribution.

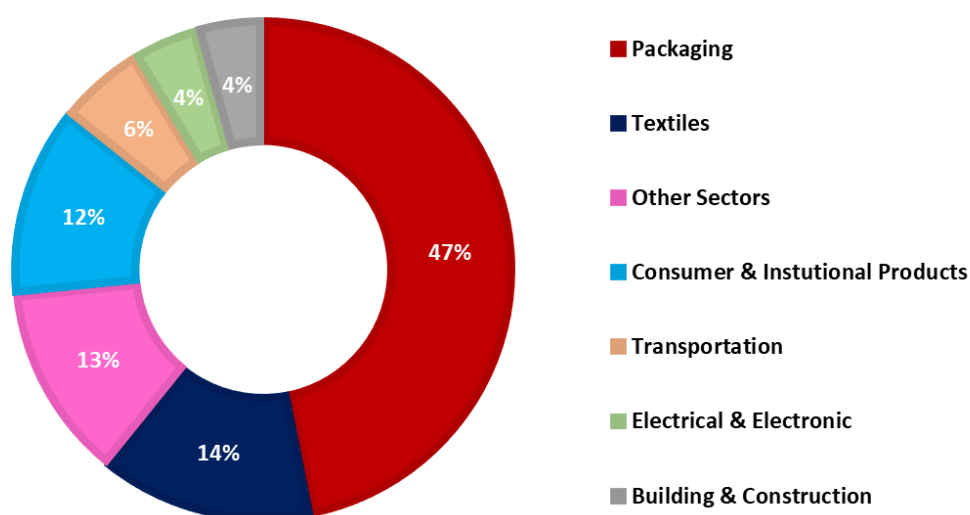


Figure 2.5. Plastic waste generation by industrial sector (Geyer, 2017).

The estimated number of years for these plastics to biodegrade in a marine environment differs from 50 years to 600 years for styrofoam cups, respectively (McCarthy, 2018). The estimated degradation time of commercial goods in marine environment is presented in Figure 2.6.

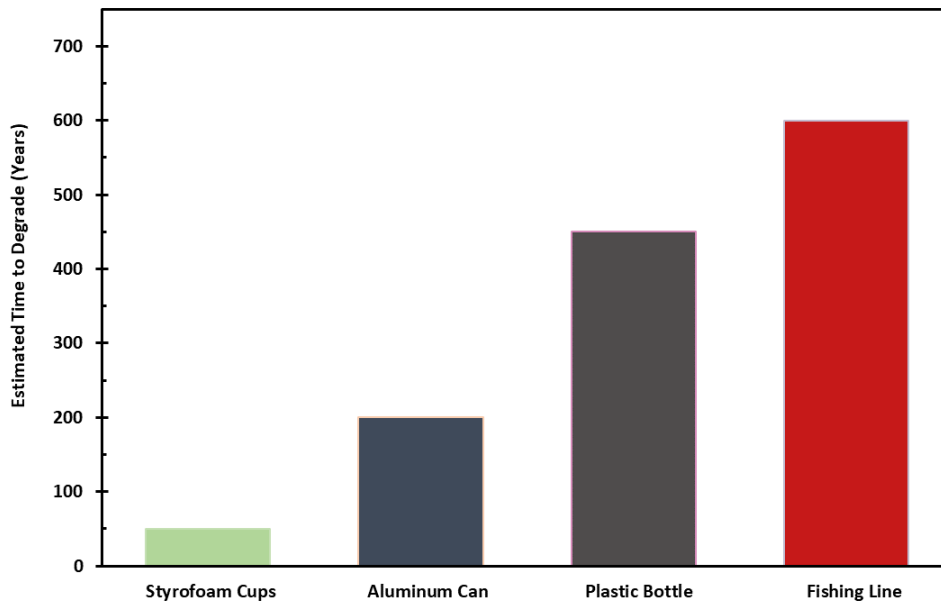


Figure 2.6. The estimated degradation time of commercial materials in marine environment (McCarty, 2018).

It is foreseen that many living species on earth will die in a short period due to plastic waste that can be broken down in nature over the years and many living spaces will become uninhabitable. Annually, around 8 million tons of plastic wastes enter the oceans, and it is anticipated that the cumulative volume of plastic wastes in the oceans is between 100 and 200 million tons, causing massive harm and the mortality of marine animals (Jem et al., 2020). 1.1 million marine organisms die annually due to plastic wastes in the macro and micro dimensions in the seas and oceans (Global Citizen, 2020). It is projected that by 2050, the amount of plastic waste in the seas will be higher than that of marine organisms (BBC, 2016).

The recent research demonstrates conclusively that microplastics can absorb toxins and metals in the environment, which are in the food chain, endangering not just marine life but also human health (Jem et al., 2020). The evidence of microplastics have found in the human placenta in the latest research (Ragusa, 2021). Studies

showed that bottle-fed infants consume millions of microplastics in a day (Li et al., 2020). Furthermore, the extensive plastic usage in agriculture has been considered as a significant source of microplastics in soil (Heidbreger et al., 2019; Liu et al., 2014; Steinmetz et al., 2016).

The production and accumulation of plastic waste induce climate change due to increased carbon emissions. Plastic production is one of the manufacturing industries with the highest greenhouse gas emissions (City to Sea, 2022). In 2019, the plastics sector has contributed more than 850 million metric tonnes of greenhouse emissions to the environment. This quantity corresponds to the output of 189 coal-fired power plants. Plastic's greenhouse gas emissions are accelerating climate breakdown and endangering our potential to maintain a sustainable planet.

These facts and projections show that the plastic crisis continues to grow. The plastic waste issue has only occurred in the past century. Yet, it will be effective on upcoming centuries unless new solutions are addressed to this problem emerge. Within this scope, it becomes a necessity to adopt new environmental-conscious approaches in the production, consumption and utilization of plastic wastes to serve the zero-waste principle, which is on the agenda in the world and our country recently.

2.3 Plastic Waste: Current state, strategies, and solutions

Since plastic materials induce an evolution in this era, the 20th century is known as “plastic age” (Thompson et al., 2019). Both industry and society are reshaped with these polymers, and they are highly dependent on plastic materials now. Between 1950 and 2017, 9200 million metric tonnes of plastic were manufactured, with 5000 million tonnes of waste had estimated (Statista, 2019). In 2019, plastic waste production was predicted to reach 353 million metric tons globally. By 2060, this amount is predicted to almost triple under present policy (OECD, 2021). The global plastic use and waste projections scenarios for 2060 is given in Figure 2.7.

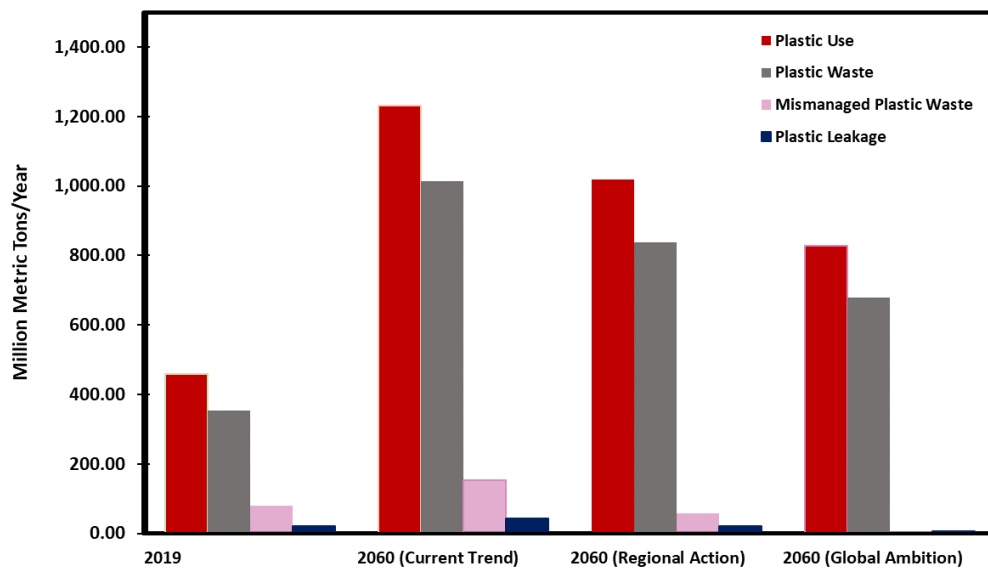


Figure 2.7. The current global plastic use and waste with global plastic use and waste projections scenarios by 2060 (OECD, 2021).

Since plastics have a short shelf life, there is a direct correlation between plastic use and plastic waste as seen in Figure 2.7. When the distribution of plastic waste was investigated, it was found that 46% of this waste consisted of packaging (Statista, 2021). China and the United States were reported to be the leading generators of single-use plastic waste in 2019 (Statista, 2021). The quantity of single-use plastic waste in China was estimated to be 25.4 million metric tons, whereas the quantity in the United States was predicted to be 17.2 million metric tons.

Thus, the production, consumption, and recycling habits on plastic materials must be reorganized based on the sustainability principle with system wide accountability. While global awareness of the hazards of plastic waste to the environment and human health is growing quickly, a number of international initiatives have been launched to find solutions to the plastic waste problem. The main principles of these initiatives are the sustainable management of plastic wastes, waste prevention and resource efficiency and recycling, raising awareness about plastic waste issue and

focusing on education and research activities. In this direction, policies are implemented by taking socioeconomic benefits into account. The European Union (EU) Commission issued and launched the European Green Deal in 2019 in order to promote the growth of a sustainable and competitive economy and the fair improvement of the social welfare level (European Commission, 2021). In the Circular Economy Action Plan, one of the pillars of this strategy, plastics-related actions are emphasized to promote a more sustainable use of plastics (European Commission, 2020). In this regard, the EU commission has released the European Strategy for Plastics in the Circular Economy (European Commission, 2021). The primary objective of this policy is to minimize the 25 million tons of plastic waste produced annually in Europe (European Commission, 2018). The four major objectives of this approach are about generating cost-effective and efficient plastic recycling, controlling plastic waste, promoting investment and innovation to build circular solutions, and initiating global action across borders to address plastic waste.

To provide sustainability and prevent plastic waste accumulation, the production and consumption must be in accordance with circular economy. The traditional approach, linear economy serves capitalism by providing maximum profit in manufacturing. However, as the consequences of rapidly growing population, increasing environmental issues and restricted natural and power sources limit the feasibility of single-use production and consumption approach. Therefore, new perspectives and approaches are offered to resolve the problems caused by traditional plastics.

2.4 Recycling of the Current Plastic Waste as a Major Solution to Plastic Crisis

There are generally two main strategies in order to reduce the negative impacts of plastic wastes on the environment. The first strategy is on the recycling of formed and existing plastic wastes on the earth. 6.3 billion tonnes of plastic waste was

produced since 1950 (Geyer et al., 2017). Only 9% of these wastes was recycled, 12% was burned, and the remaining 79% was left to landfills or natural environment. In 2015, about 20% of plastic wastes were recycled, while 25% was burned and the remaining 55% was left to landfills or natural environment. According to the projected estimates, the recycling and incineration rate is expected to reach 44% and 50% in 2050, respectively, and the rate of untreated wastes is expected to be 6% (Geyer et al., 2017).

The concerns on the plastic issue have been more pronounced in the European countries and some of the Far East countries such as South Korea and Japan. The recycling of the current waste has gained importance due to efficient management of environment and natural resources in these countries.

In 2018, 29.1 million metric tons of plastic waste were collected for the treatment in European Union Countries (Plastics Europe, 2020). 42.6% of this waste was utilized for energy recovery. 32.5% was treated by recycling, whereas the remaining portion of this waste (24.9%) was sent to landfill. Between the years of 2006 and 2018, the amount of plastic waste received for recycling has doubled. Energy recovery from plastic waste has grown by 77%, whereas plastics sent to landfill have decreased by 44%.

Packaging waste comprises a greater portion of the plastic waste; approximately 17.8 million tonnes of plastic packaging waste have been collected (Plastics Europe, 2020)

42% of this waste was sent to recycling, 39.5% has been treated for energy recovery (Plastics Europe, 2020). Between 26% and 52% of the plastic packaging waste is recycled in Europe. The average recycling rate of plastic packaging is 42%. The recycling rates for the European countries in 2018 are given Figure 2.8. The current Packaging and Packaging Waste Directive (EU) 2019/852 establishes higher recycling targets as 50% for plastic packaging by 2025 and 55% by 2030.

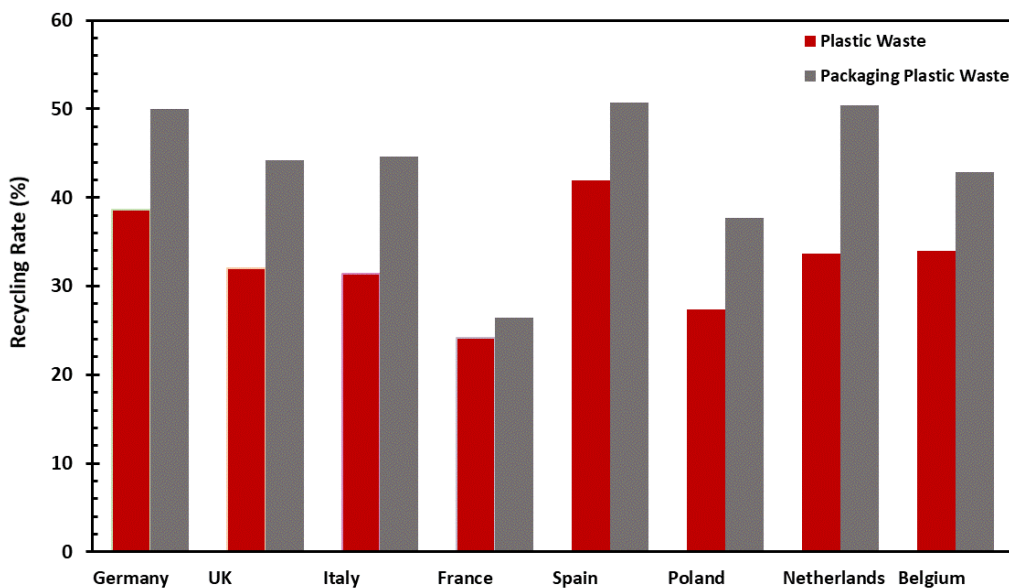


Figure 2.8. The recycling rate of the plastic waste and packaging plastic waste on European countries in 2018 (Plastics Europe, 2020).

China, the major producer of plastic materials, has 22.2% plastic recycling rate in 2019, this rate was decreased to 17.6% in 2020 due to COVID-19 pandemic (Chyxx, 2021). The recycling rate of plastic waste in South Korea was established as 56.7% in 2018 (ME (South Korea), 2022).

The recycling rates of the plastics vary greatly by depending on the polymer's popularity and the state of available recycling infrastructure. Table 2.1 shows the recycling rates of commodity plastics manufactured into bottles. Amongst the recycling rates of U.S. sourced plastic bottles, colored HDPE had the highest recycling rate in 2020 (Association of Plastic Recyclers, 2022).

Table 2.1. Recycling rates of plastic bottles sourced in the United States in 2020.

Polymer Type	Recycling Rate (%)
HDPE-Coloured	30.8
HDPE-Natural	26.4
HDPE-Total	28.8
PET	27.1
PP	15.4

The recycling industry has a significant potential due to the contribution of recycled materials to the economy. The market value of the plastic recycling was found as 34 billion U.S. dollars in 2019 (Transparency Market Research, 2021) and 48 billion U.S. dollars in 2020 (IDTechEx, 2020), while it is expected to rise to 60 billion U.S. dollars in 2027 (Transparency Market Research, 2021). In 2030, it is anticipated that polymer recycling will generate a global income of 162 billion U.S. dollars. On the other hand, global market value for recycled plastic and waste-to-oil was determined as 542.8 million U.S. dollars in 2014 and it was expected to rise 1971.4 million U.S. dollars in 2024 (PR Newswire, 2016). Based on the understanding of the circular economy, 4 million tonnes of plastic recyclates have entered the European economy (Plastics Europe, 2020). A greater part of the recyclates was used in building and construction (46%), and packaging (24%).

With the usage of recycled polymers instead of virgin materials, a substantial monetary savings can be attained related to the reduction in energy consumption (Rahimi and Garcia, 2017). This reduction can vary between 40% to 90%.

2.5 Recycling Methods of Plastic Waste

In general, recycling technologies are divided into three main groups, which are physical, chemical and biological methods. Another classification can be explained

in recycling methods as primary, secondary, tertiary and quaternary (Rahimi and Garcia, 2017; Grigore, 2017). Primary recycling involves reusing products in their original form (Grigore, 2017). Existence of a limit on the number of cycles for each component is the drawback of this procedure.

Mechanical recycling is mainly used for the secondary usage of polymeric materials. Among all recycling methods, mechanical recycling is known as the most common method. Only thermoplastics can be utilized in this method due to their thermal processing ability. The material is melted and reprocessed into final products. The mechanical recycling provides a physical transformation of the polymer; however, with limitations due to the decreased performance of the converted material. The drawbacks of this process include the heterogeneity of the plastic waste and the decline of the product's qualities in each cycle as a result of the lower molecular weight (Grigore, 2017). Chain scission reactions triggered by the presence of water and residues of acidic impurities tends to a decline in the molecular weight of the polymer. Thus, several techniques are offered to alleviate this problem such as rigorous drying, chain extender compounds, or reprocessing with vacuum degassing.

Chemical recycling is the transformation of polymers into value-added products such as monomers, oligomers, or other chemicals. The monomers obtained from chemical recycling directly contributes to circular economy. Chemical reactions take place to decompose polymers into monomers or value-added products. Hydrogenation, glycolysis, gasification, hydrolysis, methanolysis, pyrolysis, thermal cracking, catalytic cracking, reforming, photodegradation and ultrasound degradation are the processes used to degrade polymers (Grigore, 2017). There have been extensive efforts on the development of pyrolysis technologies. Pyrolysis can be described as thermal cracking of polymers in inert atmospheres to recycle or recover polymeric materials into valuable materials or energy. The technique is used in many applications to treat polymer wastes or hydrocarbons. However, there have been obstacles related to secondary pollution and the efficiency of the process. Thus, catalytic pyrolysis cracking is another option for recycling. Catalytic pyrolysis is a

promising way to obtain the products by minimizing the energy requirement and with higher selectivity. The pyrolysis process conducted in the presence of the catalyst is more advantageous compared to the non-catalytic thermal decomposition technique because it takes place at lower temperatures and with higher degradation rate.

Quaternary recycling method provides the energy recovery. This process involves the recovery of the plastics in terms of energy content. Incineration is the most common technique for the energy recovery from waste. Although the technique presents energy recovery, it does not offer an ecological recycling due to the release of toxic substances such as dioxins, heavy metals, chlorine containing substances, toxic carbon, and oxygen-based free radicals (Grigore, 2017).

Chemical recycling is the only appropriate recycling process according to the principles of sustainable development due to the production of monomers (Grigore, 2017). In Japan, approximately 270 thousand metric tons of plastic waste were recycled using the chemical recycling method in 2020 (Statista, 2022) whereas thermal recycling was applied to 5090 thousand metric tons of plastic waste (Statista, 2022). 1730 thousand metric tons of plastic waste was recycled by means of mechanical recycling. In 2022, the estimated cost of chemical recycling of plastic packaging was 49.24 Japanese Yen per kg in Japan (JCPRA, 2022). On the other hand, the average cost of mechanical recycling was higher than the cost of chemical recycling. It was calculated as 60.33 Japanese Yen per kg (Statista, 2022).

2.6 Advanced techniques and approaches on the Plastic Waste

2.6.1 Mesoporous Catalysts in the Degradation of Plastics

In chemical industries, roughly 90% of the processes are utilized with catalysts (Schlexer, 2017). Catalysts are effective on the rate of a chemical reaction by altering the activation energy required for the reaction to initiate or proceed and the speed of

the reactions by a factor of millions or even more (Cooper et al., 2000). Catalysts are commonly used to achieve lower reaction temperatures and improved selectivity in recycling processes (Molnar, 2011). Since polymers with complex structure and high molecular weight are more resistant to degrade, textural forms and structural properties of the catalysts are highly important to attain an enhanced degradation profile of such polymers. Large molecules have restricted access to active regions in the catalyst (Chaianansutcharit et al., 2007, Garforth et al., 1997, Chou et al., 2006). Mesoporous catalysts present better reaction kinetics in the degradation of commodity plastics due to their pore characteristics (Habib, 2019). Thus, some of the catalytic materials are designed to incorporate mesopores in their structures in order to improve the diffusion of larger molecules such as biopolymers (Ennaert et al., 2016). Mesoporous silica structures such as MCM-41 and FSM-16, which have similar characteristics to zeolites but larger pore sizes, are preferred for plastic degradation reactions (Chaianansutcharit et al., 2007). Due to their hexagonal pore shape, mesoporous structures with no acidic characteristics were found to be effective on the degradation of polypropylene (Uddin et al., 1998; Gaca et al., 2007). Yet, degradation reactions of linear polymers such as polyethylene and polypropylene and cracking reactions of fossil fuels and biomass are mainly dependent on the breakage of the C-C bond and extremely acidic catalysts were typically used to promote this bond breaking (Ennaert et al., 2016; Almeida et al., 2016; Gornall, 2011; Mark et al., 2020). In this regard, amorphous aluminosilicates, zeolites, and other mesoporous structures are found to be effective in the degradation of commodity plastics (Aydemir et al., 2013, 2016; Obalı et al., 2009, 2011, 2012).

Silica aerogels are unique engineering materials with remarkable features such as high surface area between 500 and 1200 m²/g, high porosity in the range of 80-99.8%, and low density around 0.003 g/cm³ (Dorcheh et al., 2008). The production of silica aerogel can be done via using silica precursors such as methyltrimethoxysilane (MTMS), tetraethoxysilane (TEOS), tetramethoxysilane (TMOS), water-glass, rice husk ash, or certain co-precursors in a two-step sol-gel

technique by following a supercritical drying, freeze drying, or ambient pressure drying (Duan et al., 2016; Huang et al., 2017; Li et al., 2012). The silicon precursors include four equal hydrolyzable alkoxy groups such as ethoxy and methoxy, whereas one of the alkoxy groups in the co-precursors is replaced by a non-hydrolyzable alkyl group (methyl, ethyl, n-propyl, iso-butyl, n-octyl, vinyl or phenyl) (Al Oweini et al., 2009). Recent research on ambient pressure drying has contributed to the commercialization and industrialization of the applications of silica aerogel materials (Dorcheh et al., 2008; Schwertfeger et al., 1998; Lee et al., 2002; Rao et al., 2005).

Silica aerogels are superior over conventional catalysts in the degradation process of polymeric wastes due to their high pore diameter and surface area with inherent thermal stability. Silica aerogels are low density mesoporous structures (Kuznetsova and Eremenko, 2014; Schmidt and Schwertfeger, 1998). Due to their physical properties, silica aerogels are used as a support material for the catalytic material (Dunn et al., 2005). While the pore diameter of the material varies between 2-50 nm, the pores are three dimensional depending on each other (Anderson et al., 2002). Silica aerogel supported catalysts are often used in gas phase reactions, Fischer-Tropsch synthesis, oxidation reactions (Amonette and Matyáš, 2017). A reaction-specific catalyst must be created for chemical recycling processes to be successful in the presence of a catalyst. In terms of reaction efficiency, the catalyst material to be used must have a high surface area, mesoporosity, high thermal resistance. In this way, the product distribution can be adjusted to the desired range and selectivity, and energy savings can be achieved as the reaction takes place at a lower temperature.

The use of silica aerogel catalysts improves reaction kinetics by reducing mass transfer limitations (Anderson et al., 2002; Leventis et al., 1999; Dunn et al., 2005). Three dimensional network of silica aerogel provides that the rapid diffusion of reaction products similar to that in the gas phase. Consequently, the silica network structure does not hinder the movement of atoms and molecules in the gas phase within the pore (Anderson et al., 2002; Leventis et al., 1999; Dunn et al., 2005). In the thermal breakdown of polymers, it is preferable to use silica aerogel-based

catalysts with large pore diameter and volume. Fischer-Tropsch synthesis occurs at a temperature comparable to the decomposition reactions, which is typically around 265 °C (Xu et al., 2003; Dunn et al., 2005). Considerable amounts of hydrocarbons in the C₉-C₁₅ range were produced using cobalt-loaded silica aerogel catalysts for Fischer-Tropsch synthesis. Due to the rapid desorption of the produced olefins, a high level of efficiency was achieved. In contrast to SBA-15, these substances were not trapped within the pores (Dunn et al., 2005). Therefore, it is advantageous to use silica aerogel based catalysts having large pore diameter and volume in thermal decomposition of polymers. Silica aerogel supported catalysts were found to be effective on the degradation of polyethylene and polypropylene (Habib, 2019). The catalyst demonstrated high thermal stability and low coke formation.

2.6.2 Supercritical Fluids in the Degradation of Plastics

In most of the chemical reactions, organic solvents are typically used in higher concentrations than reagents. Furthermore, a substantial amount of solvent is required for extraction, purification, separation and cleaning of the product in the reaction mixture.

The annual production of organic solvents widely used in the industry on a large scale is determined to be 20 million tons and many of these solutions pose a significant threat to the environment (Clark et al., 2015). The solvents used in the processes constitute a large portion of the organic pollution and a significant amount of energy is consumed during the purification of the products obtained from the solvent.

The Montreal Protocol (1987) on the development and adoption of sustainable processes and technologies involving the use of “green” solvents in industry has been the driving force (limiting and gradually eliminating the production and use of ozone-depleting chlorofluorocarbons) (Clarke et al., 2018; Velders et al., 2007). Recently, in 2015, the United Nations (UN) put the sustainability development plan

called “Transforming Our World: The 2030 Agenda for Sustainable Development” on the agenda (UN, 2015). With this important project, the importance and necessity of green and sustainable research for the future is emphasized once again.

Supercritical fluids are green solvents with temperature and pressure values above the critical temperature (T_c) and critical pressure (P_c) (Savage et al., 1995). Supercritical fluids are used in many applications as solvent instead of conventional solvents due to their adjustable properties. Supercritical fluids are solvents that resemble liquids in terms of density and gases in terms of diffusion and viscosity and possess solvation power and transport qualities by adjusting the temperature and pressure (Knez et al., 2014).

Significant changes in physicochemical properties of the material provides while preserving the chemical structure of the substance. The physicochemical properties of supercritical fluid such as density, diffusivity, dielectric constant values vary between those of gas and liquid (Wei et al., 2020; Moltalban et al., 2022). By changing the pressure and temperature values of the supercritical fluid, the physicochemical properties can be adjusted as desired (Tutuk et al., 2021). In this way, a single solvent can be used in a variety of applications (reaction, separation, etc.) with the desired solvent properties (Knez et al., 2014). The use of supercritical fluids reduces the separation requirements and enables the development of sustainable alternative industrial processes. Supercritical fluids are used in industry in extraction, purification, and reaction processes (Knez et al., 2014).

Supercritical fluids have a great influence on the rate constant due to solvent effect, which has a strong dependence on pressure (Johnston et al., 1987, Savage et al., 1995). In addition, due to a more efficient mass transfer of the reactants, reactions conducted in a supercritical fluid medium proceed at a faster rate than those utilizing organic solvents (Fan et al., 1999; Ramsey et al., 2009; York et al., 2004).

The decision of supercritical fluid to be utilized in a reaction is crucial. When selecting the supercritical fluid to be used in the reaction, the solubility of the reactant

in the supercritical fluid, the chemical stability of the reactant, and the compatibility of the reactant with the supercritical fluid must be considered. In addition, supercritical fluids that are inexpensive, readily accessible, non-toxic, non-explosive, and non-combustible are desirable for the applications.

In chemical recycling processes of polymers, supercritical fluids are performed as green solvents (Goto et al., 2009, 2016; Colnik et al., 2022). Tables 2.2, 2.3 and 2.4 provides a summary of studies on the recycling of commercial polymers, carbon fibre reinforced plastics (CFRP), printed circuit boards (PCBs) and fiber reinforced plastics (FRP) in the presence of a supercritical media. The majority of the research presented focuses on commercial polymers that are widely employed. The most widely used supercritical fluids are water, methanol, and ethanol. Due to the high critical temperature and pressure of water and alcohols, degradation processes in a supercritical water and alcohol medium must be conducted at elevated reaction temperatures and pressures.

Table 2.2. The studies on recycling of polymers in the presence of supercritical medium.

Plastic	Supercritical Fluid	Catalyst or Agent	Rxn Temperature (°C)	Rxn Pressure (MPa)	Rxn Time (min)	Reference
PE	Water	-	450-480	min. 25	1--30	Su et al., 2004
PE	Water	-	350-400	40	1	Watanabe et al., 2003
PE	Water	-	563	12.9	ND	Bozorgmehr et al., 2014
	Ethanol		564	11.3		
	Methanol		697	27		
PE, PP, PS	Water	RuO ₂ /Al ₂ O ₃ NiO/Al ₂ O ₃	450	10--38	60	Onwudili et al., 2016
PP	Water	-	380-400	26	30 70 120	Lei et al., 2007
PE, PET	Ethanol	-	225	11.65	30 60 120	Favaro et al., 2013
PET	Carbon Dioxide	H ₂ O SO ₄ /TiO ₂	100–160	8–15	180–720	Li et al., 2015
PET	Methanol	-	300-350	20	2 - 120	Goto et al., 2002

Table 2.3. The studies on recycling of polymers in the presence of supercritical medium-cont'd.

Plastic	Supercritical Fluid	Catalyst or Agent	Rxn Temperature (°C)	Rxn Pressure (MPa)	Rxn Time (min)	Reference
PBT	Methanol Ethanol Propanol	-	210-270	ND	5--90	Yang et al., 2010
PET	Ethylene Glycol	-	450	15.3	25-45	Imran et al., 2010
PS	Toluene	-	310–370	ND	0-40	Huang et al., 2006
PS	Water	N ₂ or Air	380	25.5		Dubois et al., 1996
SBR	Water	H ₂ O oxidizing agent	300-450	>40	20-60	Park et al., 2001
Epoxy	Water	O ₂ /Ar oxidizing agent	410	24	0, 60	Fromonteil et al., 2000
Nylon	Carbon Dioxide	NO ₂ oxidizing agent	140	10	60	Yanagihara et al., 2013
CFRP	Methanol 1-propanol 2-propanol 1-butanol 2-butanol tert-butanol Acetone methyl-ethyl ketone	-	320	6-12.2	6-120	Okajima et al., 2017

Table 2.4. The studies on recycling of polymers in the presence of supercritical medium-cont'd.

Plastic	Supercritical Fluid	Catalyst or Agent	Rxn Temperature (°C)	Rxn Pressure (MPa)	Rxn Time (min)	Reference
CFRP	Water	NaOH, KOH	400-420	20-25	0	Onwudili et al., 2013
FRP	Methanol Ethanol	(CH ₃) ₂ NC ₅ H ₄ N	275	9.7-12.6 7.2-8.9	90-540	Kamimura et al., 2008
PCB	Methanol	-	300-420	9--21	30-120	Xiu et al., 2010
FRP	Diethylene glycol Mono methylethter Benzyl alcohol	K ₃ PO ₄	190-350	>4.57	60-480	Iwaya et al., 2008

2.7 Bioplastics as an alternative to common plastics

Biodegradable polymers have come to the fore in redesigning the plastic materials in accordance with sustainability principles. Only under certain environmental conditions such as pH, temperature and humidity, biodegradable polymers can be decomposed by biological agents (Emadian et al., 2016). This characteristic of biodegradability serves to the prevention of environmental issues caused by commercial plastics that stay durable for decades (Brockhaus et al., 2016; Alvarez-Chavez et al., 2012; Papong et al., 2014). Biodegradable polymers that can be produced through synthetic and renewable resources provide high performance in many applications, while overcoming the problems such as global warming, high carbon and water footprint, fossil resource utilization and microplastic deposition

caused by petroleum based commercial polymers (Nanda et al., 2022; Samir et al., 2022).

Despite the fact that bioplastics have been accessible for more than a century, the mass production of bioplastics is still immature (Lettner et al., 2017). Bioplastic represents a new line and approach in terms of the raw material for the mass polymer production in the late 90s. The utilization of biopolymers is recognized as a major aspect of sustainable product development (Lettner et al., 2017). The bioplastics can be either bio-based (non-degradable) or biodegradable (Figure 2.9). The global production capacity of bioplastics was 2.4 million tons in 2021 (European Bioplastics, 2021). It is expected that this value will reach approximately to 7.6 million tons in 2026.

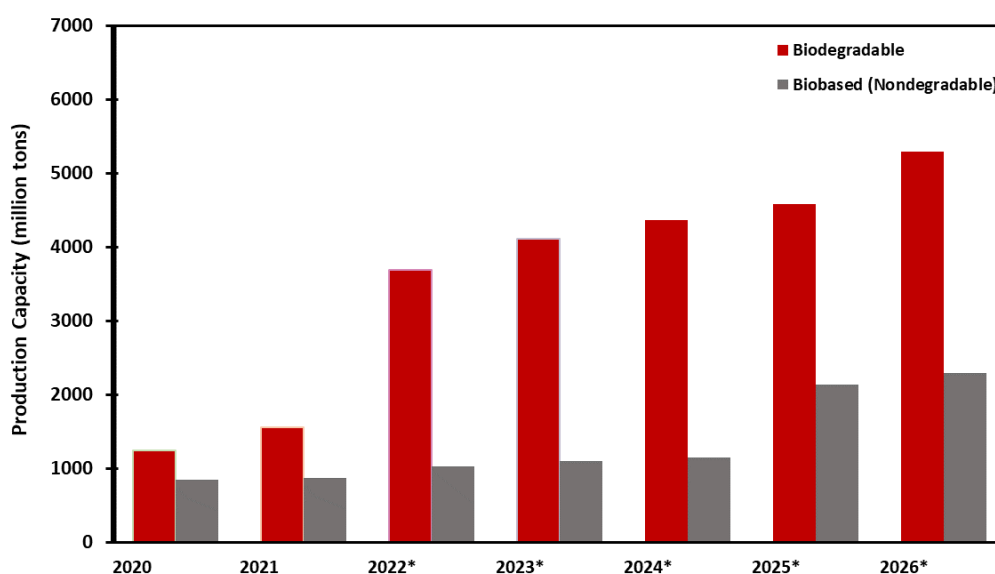


Figure 2.9. Global bioplastic production capacity (European Bioplastics, 2021).

**The projected global bioplastic production capacity in the years between 2022 and 2026.*

The market value of bioplastics was also evaluated. As of 2021, the global market for bioplastics was worth roughly 7.6 billion dollars (Fortune Business, 2021). The

global market value of bioplastics is anticipated to reach \$15.55 billion U.S. dollars by 2028. The COVID-19 pandemic had a negative effect on the bioplastics industry, with a fall of 5.02 percent in 2020 versus the average annual increase of bioplastics from 2017 to 2019. The numbers are presented in Figure 2.10.

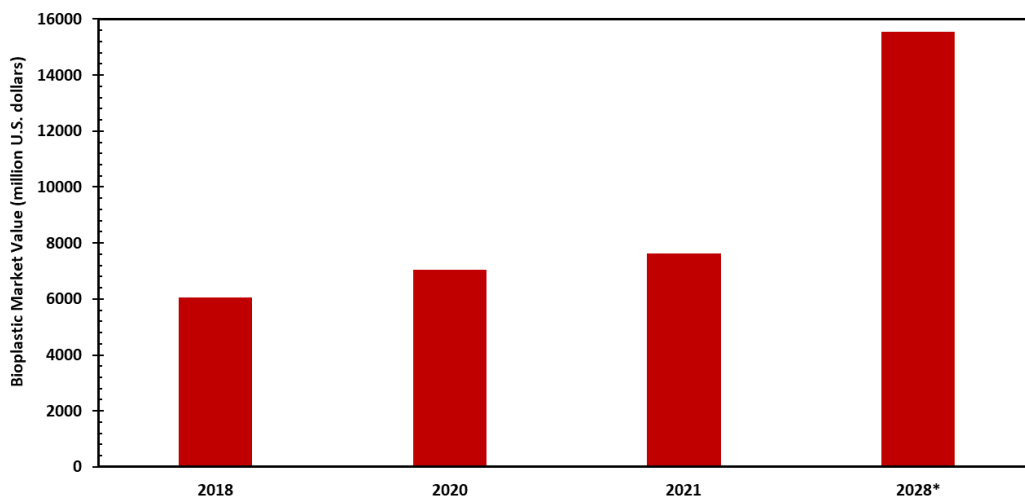


Figure 2.10. The market value of bioplastics (Fortune Business, 2021).

**The projected market value of bioplastics in 2026.*

As of the year 2020, the market value of bioplastics in Europe was estimated as \$3.5 billion (Fortune Business, 2021). This accounted for roughly half of the global market value for bioplastics in 2021. On the other hand, the global biodegradable plastics capacity was obtained as 1.1 million tons in 2019 (MRFR, 2021). The distribution of the production capacity of biodegradable plastics worldwide in 2019 is given in Figure 2.11. Starch blends, polylactic acid and polybutyrate adipate terephthalate are among the most common biodegradable plastics.

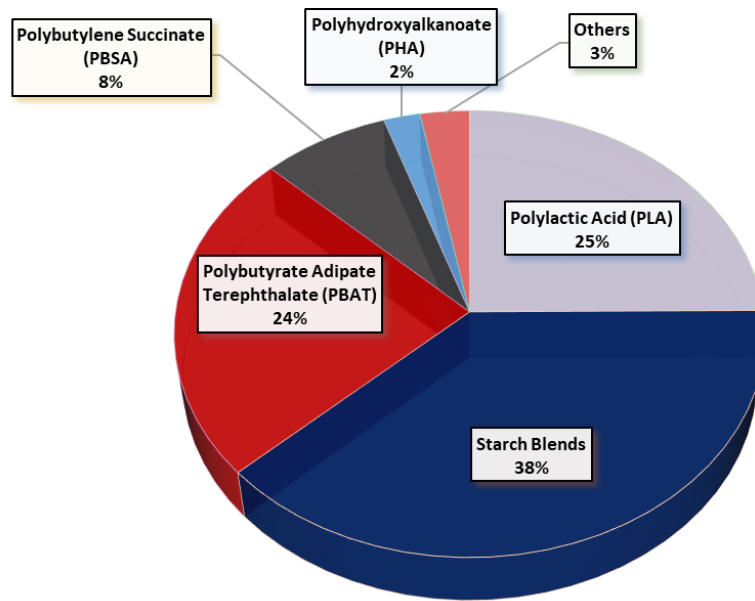


Figure 2.11. The distribution of biodegradable plastics by production capacity in 2019 (MRFR, 2021).

The usage areas of biodegradable plastics are given in Figure 2.12 with the data obtained in the year of 2021 and the projections for 2026 (European Bioplastics, 2021).

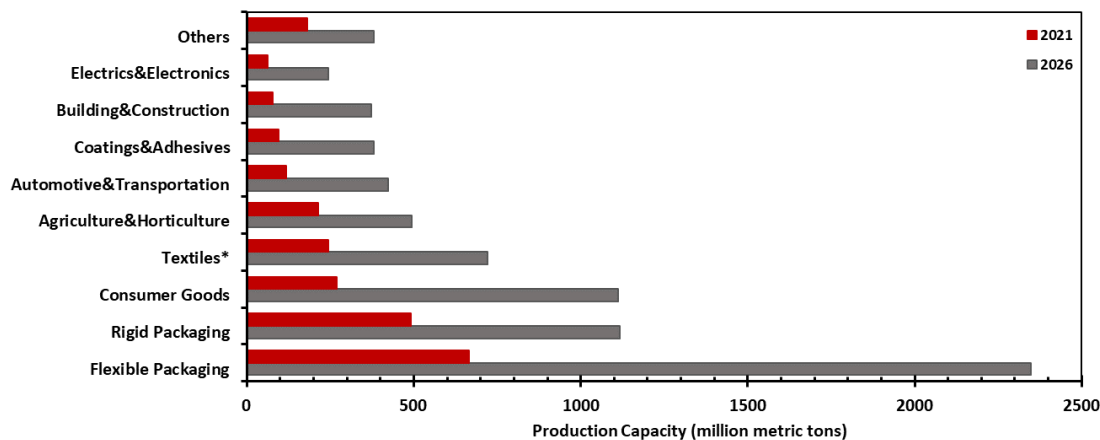


Figure 2.12. The global production capacity of bioplastics by usage areas (European Bioplastics, 2021).

In 2021, the global bioplastic manufacturing capacity for flexible and packaging was found to be 1157 thousand metric tons (European Bioplastics, 2021). It is anticipated that this number will reach to a value of 3465 thousand metric tons (European Bioplastics, 2021). Despite the popularity of the bioplastics, currently, only a few classes of biopolymers are considered competitive, mostly due to their high prices (Lettner et al., 2017; Vroman et al., 2009). Within this scope, polyhydroxyalkanoates (PHA) and polylactic acid are two of the most promising biopolymers at present (Chanprateep, 2010).

Another view on the usage of the bioplastics involves the decrease of the agricultural lands. In 2021, the total area of agricultural land used for the manufacture of bioplastics was roughly 0.7 million hectares (European Bioplastics, 2021). By 2026, this region is expected to expand to about three million hectares. This would represent around 0.058 percent of the world's agricultural land. A systematic harvesting and utilization of renewable sources and biological wastes into bioplastics present to a more sustainable approach than fossil based plastic processes (Rosenboom et al., 2022).

2.8 A Promising Biodegradable Plastic: Polylactic Acid

Polylactic acid is an industrially produced biodegradable polymer widely used in the market (Sin, 2012; Auras, 2004; Castro-Aguirre et al., 2016). PLA is mostly used in many medical applications due to its biodegradability and biocompatibility properties. Besides, due to its easy processing and thermal, barrier and mechanical properties, it is also used in non-medical oriented applications such as packaging material, the resin in 3D printers, fast-moving consumer goods (cups, sachets, and bottles, etc.), as well as in automotive and electronic industry. PLA, which is used in place of the conventional polymers, performs high performance. Although the polymer is commonly used and popular today, the discovery of the polymer was back in the 19th century. In 1845, chemist Théophile-Jules Pelouze synthesized PLA for the first time. Wallace Hume Carothers et al. established a technique for polymerizing lactide into PLA in 1932. Later, in 1954, Du Pont patented this method (Masutani and Kimura, 2014). In the late 1970s, PLA based materials were started to be used in biomedical applications and tissue engineering such as drug delivery, protein encapsulation and delivery, microspheres, hydrogels, scaffold materials, sutures and prostheses (Masutani and Kimura, 2014). In the early 1990s, a significant advancement was achieved in the manufacture of PLA. In the mid-1990s, Natureworks excelled in industrially polymerizing high molecular weight polylactic acid using ring-opening polymerization (ROP) of l-lactide and commercialized the polylactic acid (Masutani and Kimura, 2014). The technique provides low cost continuous process for manufacturing (Drumright et al., 2000). The adoption of PLA as a cost effective alternative to petrochemical-based commodity plastics would raise demand for agricultural resources such as maize and sugar beets and reduce plastics' dependence on petroleum (Drumright et al., 2000). There have been three major techniques to synthesize PLA (Stefaniak and Mazek, 2021). These techniques are condensation of lactic acid, azeotropic dehydrative condensation of lactic acid and ring opening polymerization. The production routes are given in Figure 2.13.

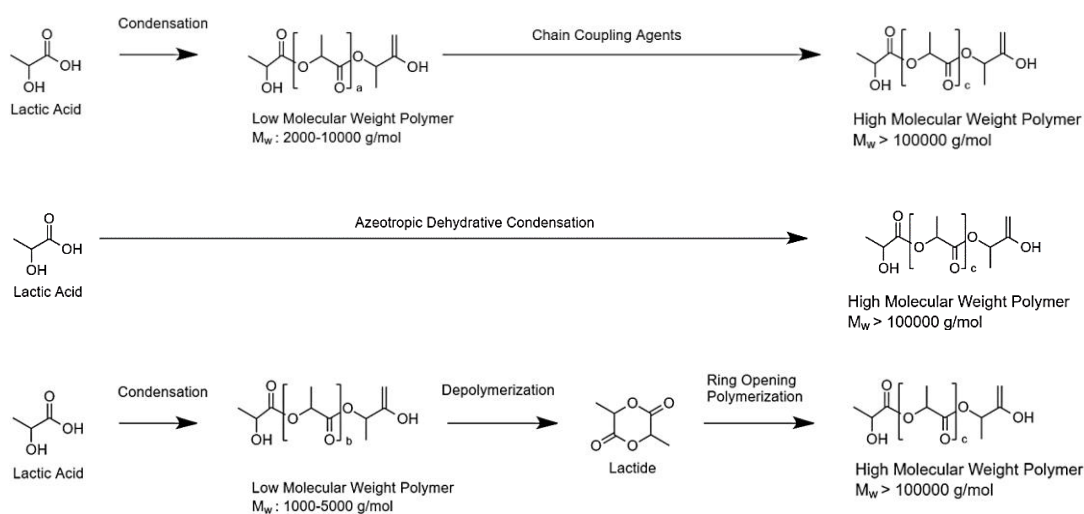


Figure 2.13. Production routes of PLA(Stefaniak and Mazek, 2021).

In direct polycondensation process, lactic acid is converted to low molecular PLA by condensation, then PLA further polymerize to increase molecular weight of the polymer (Stefaniak and Mazek, 2021). Yet, the water trapped in the polymer prevents to reach desired molecular weight. Additionally, there is a need for the use of chain coupling agents. The process requires higher temperature in the range of 180 and 200 °C with low pressure just as 1 mm Hg for extended reaction times up to 30 hours (Moon et al., 2000, Masanobu et al., 1995, Maharana et al., 2009). Thus, this process hardly takes place in industry (Stefaniak and Mazek, 2021; Masanobu et. al, 1995).

An alternative method proposed by the Mitsui Chemicals Company in Tokyo, Japan (Stefaniak and Mazek, 2021). With the azeotropic dehydrative condensation, the negative effect of by-product water on the process is minimized. The method offers high molecular weight PLA. Although chain extenders are not utilized, there is a need for the usage of high boiling point organic solvents. Hence, the technique is not considered as green and sustainable.

Lastly, ring opening polymerization process allows the production of high molecular PLA with organometal catalysts (Stefaniak and Mazek, 2021). The method consists of several steps: condensation of lactic acid, production of lactide that is a cyclic dimer of lactic acid, and ring opening polymerization. To eliminate moisture, the first step involves dehydration and polycondensation of lactic acid at high temperatures under vacuum. After that, low molecular weight PLA is depolymerized catalytically under reduced pressure. Then, the lactide is purified with crystallization or distillation by removing lactic acid and meso lactide in the mixture. The purified lactide is polymerized to obtain high molecular weight PLA by ring opening polymerization. The reaction temperature is set between melting point of lactide and the degradation temperature of PLA.

The ring opening polymerization method offers high molecular weight PLA with narrow molecular weight distribution at relatively mild conditions. Common polymerization reaction parameters are 180-210 °C, 100-1000 ppm tin octoate concentration, and 2-5 hours to achieve 95% conversion of lactide to PLA and first-order polymerization is observed (Drumright et al., 2000). The reaction is also carried out at both low reaction temperature around 130 °C and shorter reaction times (Kowalski et al., 2000, Hyon et al., 1997). Common conditions include the use of Lewis acid catalysts at temperatures between 130 and 180 °C without using a solvent (Basu et al., 2016).

The mechanism of ring opening polymerization can be cationic, anionic, and coordinative (Stefaniak and Mazek, 2021). In cationic ring opening polymerization, the potential of racemization arises due to the replacement of a monomer at a chiral center at each stage of polymer chain growth. This technique produces a polymer with a low molecular weight. Therefore, it is not used industrially (Zenkiewicz et al., 2009; Stefaniak and Mazek, 2021). In the anionic ring opening polymerization mechanism of PLA, higher reaction rate and efficiency are attained with less side reactions. When 99.9% pure L-lactide was used, racemization was less than 5% (Jedliriski et al., 1991; Kurcok et al., 1995; Stefaniak and Mazek, 2021). Stannous

octoate ($\text{Sn}(\text{Oct})_2$) is the common catalyst used in the manufacture of high molecular weight polylactic acid (Stefaniak and Mazek, 2021). The catalysts provides low degree of racemization even at higher reaction temperatures and forming atactic PLA chains (Cameron and Shaver, 2011; Stefaniak and Mazek, 2021). Lastly, the usage of the catalysts is FDA approved for the biomedical applications (Karidi et al., 2013; Stefaniak and Mazek, 2021). Apart from stannous octoate, metal complexes comprising Al, Mg, Zn, Ca, Sn, Fe, Y, Sm, Lu, Ti, and Zr have been utilized extensively as catalysts in the ROP of different lactone monomers including lactides (Masutani and Kimura, 2014).

The price of PLA is affordable and comparable with common plant-based and fossil-based plastics based on the maturity of the production (Shogren et al., 2019). The price of PLA was found to be 1 \$/lb while the price of commodity plastics (PE, PP, PET, PS and PVC) is in the range of 0.65-1.2\$/lb.

In comparison to widely used commodity plastics such as polypropylene, poly(ethylene terephthalate), and polystyrene, PLA has also comparable optical, mechanical, thermal, and barrier characteristics by broadening its commercial range of uses (Castro-Aguirre et al., 2016; Schwark, 2009). Further, good properties such as strength, hardness, stiffness, and elasticity, as well as good processability for injection moulding, extrusion equipment, and film-blowing, expand the possible applications of PLA-based materials as well (Schwark, 2009). Injection molding, sheet and film extrusion, blow molding, foaming, fiber spinning, and thermoforming commonly used to process high molecular weight PLA (Castro-Aguirre et al., 2016). The high transparency, the strong odor and taste barrier, the high moisture barrier, and the high resistance to grease and oil provides PLA taking place in many packing applications (Schwark, 2009). Yet, the material's brittleness and poor plastic elongation are its greatest drawbacks (Schwark, 2009). Packaging materials are the product group that has the biggest share in plastic production and the amount of plastic waste generated. According to the 2015 data, the production amount of plastics in the packaging group is 146 million tons annually, while the amount of

waste generated is 141 million annually (Geyer et al., 2017). Single-use plastics lead to a decrease in resource efficiency and an increase in plastic waste. It was demonstrated that PLA bottles are more environmentally friendly than PET bottles due to their lower consumption of fossil fuels and reduced toxicity to humans (Papong et al., 2014). Furthermore, PLA can be utilized in replacement of PS and PET for the applications requiring high stiffness and minimal elongation (RC Bopp, 2012). PLA, when preferred in such product groups, offers safe usage and more option for recycling.

As another scope, PLA still presents a promising platform for biomedical innovation and basic understanding of how synthetic polymers may coexist safely with biological systems (Silva et al., 2018). In the vast amount of research and hundreds of clinical reports covering the usage of PLA devices since the 1980s, only a minor number of papers indicate the harmful effects of PLA on patients (Silva et al., 2018). PLA and its glycolic acid copolymers were authorized for absorbable sutures by the US Food and Drug Administration (FDA) in the 1970s. Ever since, PLA-based polymers have been employed in a variety of biomedical and tissue engineering applications, including as drug delivery, absorbable implantable devices and coatings, scaffolds, absorbable sutures, stents, adhesion prevention films and orthopaedic plates and screws (Basu et al., 2016).

PLA-based medical devices have recently gained popularity due to its suitability as a material for technological innovations such as 3D printing. PLA is one of the most frequently utilized biodegradable polymers for 3D printing scaffolds (Silva et al., 2018). Its properties and low glass transition temperature (55–65 °C) allow it to be deformed at a temperature range of 190–220 °C, making it one of the most often utilized filaments in this technology. It is currently feasible to employ 3D printing in the biomedical industry, where it has been widely adopted (Perez Davila et al., 2021). Three-dimensional polymeric scaffolds have become an integral aspect of tissue engineering (Rezwan et al., 2006). The biodegradability of PLA makes it a highly desirable material for in vivo implantation (Silva et al., 2018). Recently, various

combinations of PLA with other components like as glass particles and PEG have been employed to properly regulate the physical and mechanical properties of scaffolds and to enhance the printing process (Serra et al., 2013, 2014; Stoppato et al., 2013; Silva et al., 2018).

Apart from biomedical applications, the polymer is safely removed from the body by the enzymes present in the human body in the event of possible contact with the human being, thereby preventing possible microplastic accumulation in vivo. PLA can enzymatically breakdown into lactic acid (Silva et al., 2018). Lactic acid (LA) is a naturally occurring molecule that serves as the precursor to the pyruvate metabolic product (Silva et al., 2018). The cells, that include neutrophils, macrophages, and fibroblasts, release a variety of enzymes, including proteinase K, pronase, acid phosphatase and lactate dehydrogenase, that promote PLA breakdown (Silva et al., 2018). Due to ester bonds in the structure of the polymer, PLA is hydrolytically cleavable and excreted from the body by decomposing into metabolizable parts (Basu et al., 2016). In vivo studies showed that the polymer has an average half-life of 30 weeks; however, this might be prolonged or decreased based on therapeutic needs (Silva et al., 2018). Hence, the polymer supports safe usage. Furthermore, the negative impacts of PLA waste on the environment are less than those of petrochemical-based plastics. Therefore, there has been a great effort on reducing the production costs and improving the performance of PLA materials. For these reasons, the scope of application of the biodegradable polymer is increasing day by day.

Among bioplastics, PLA has the highest production capacity (20.7 %) according to the latest market data in 2022 (European Bioplastics, Nova Institute, 2022). Recently, PLA is rapidly being utilized in packaging materials, have a short lifespan compared to conventional fossil-based plastics. In addition to packaging, with a 33% of market share, the polymer has been widely used as a resin in 3D printing (3D Hubs, 2018). The global market for PLA, which is used in 3D printing, is expected to grow by about six times in the next 10 years. In 2028, the market is expected to

be worth 504.7 million US dollars. In 2025, the compound annual growth rate (CAGR) of PLA is anticipated to expand to 23%, reaching \$5.4 billion (Lucintel, 2022). The market forecast of PLA by products is given in Figure 2.14.

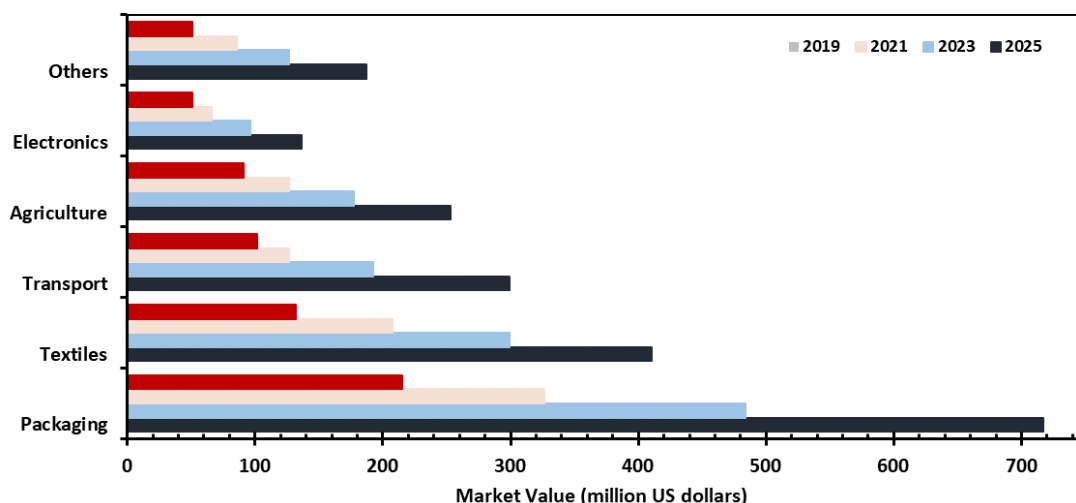


Figure 2.14. Market value forecast of polylactic acid in the United States from 2019 to 2025 by application (in million U.S. dollars) (Statista, 2019).

In parallel with the market research conducted in the world, it has been determined that there has been a significant increase in the use of PLA polymer in our country in recent years. According to the foreign trade statistics, there has been a 25-fold increase in the importation of PLA from 2015 to 2019. In 2019, approximately two hundred and seventy-three thousand kilogram of PLA polymers has been imported into our country (Turkish Statistical Institute (TurkStat), 2015, 2019). Between 2015 and 2020, the import value of PLA in Turkey's international trade increased steadily. According to the Turkish Statistical Institute (Turkstat), the value of international trade imports in 2015 was around 39,000 dollars (Turkstat, 2015), while the value of foreign trade imports in 2020 is projected to be approximately 4,600,000 dollars (Turkstat, 2020).

2.9 Recycling of Polylactic Acid

While the increasing demand for the polymer leads to an increase in production capacity and a decrease in cost value, the amount of waste generated as a result of widespread use of the polymer will reach a striking value soon. In spite of the fact that PLA was introduced to the market as a solution to the accumulation of plastic waste, in a short period, a waste problem resulting from PLA will be arisen due to market misconceptions about the biodegradability of the polymer. This waste problem will be caused by the fact that PLA is not completely biodegradable under a wide range of environmental conditions, including landfills and oceans. Since PLA only degrades at certain conditions, the polymer can be defined as “Conditionally Ecocyclable” (Brandon et al., 2019). However, the limited number of microorganisms that cause degradation of the polymer, the absence of these microorganisms in soil and the fact that degradation only occurs at appropriate pH, temperature, nutrient and water concentration will render the biological degradation of PLA wastes insufficient and lead to the continuity of waste. Also, since the hydrolysis process requires higher temperatures, hydrolysis of waste PLA in the sea and oceans is not possible due to water temperature. Therefore, the development of recycling and recovery technologies of PLA-based materials is important in terms of preventing the waste accumulation of the polymer and supporting the production and use of the polymer; however, there is limited work in the literature compared to the commodity plastics and the recycling technology of PLA has not matured yet. The current production and recycling methods of PLA is given in Figure 2.15.

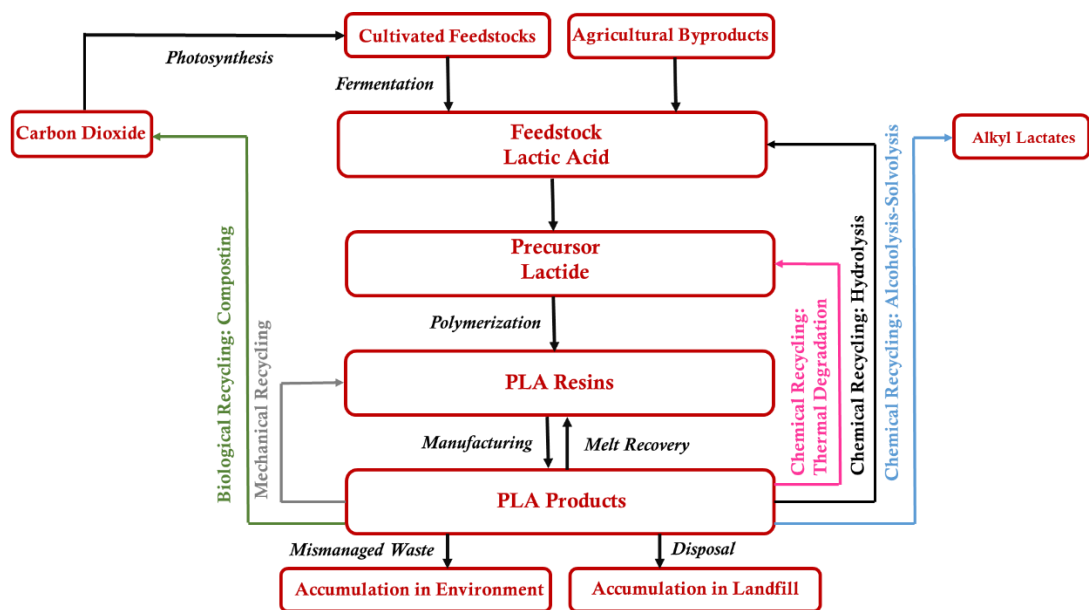


Figure 2.15. Production and recycling methods of PLA.

Different reaction products are obtained based on the recycling method. Biological recycling provides the degradation of PLA into carbon dioxide. PLA transforms into its resin by mechanical recycling. Lastly, value added chemicals and feedstocks can be obtained by chemical recycling techniques such as hydrolysis, alcoholysis, and thermal degradation.

2.9.1 Biological Recycling of Polylactic Acid

The biodegradability property of PLA is advantageous in biomedical applications. PLA, which is used in biomedical applications, is decomposed by the enzymes found in the human body and discharged from the body safely and does not constitute a hazard to human health. Due to its biodegradability, PLA polymer is frequently used in controlled release drug systems, tissue repair applications and orthopedic implants. Owing to the formulations and technologies that have been developed, the rate of polymer breakdown in the body may be adjusted according to its application

in humans. At the end of the application period, the polymer is entirely eliminated from the body and no additional surgical treatment is required. The biodegradability feature of PLA also prevents PLA-induced microplastic accumulation in the human body.

However, biodegradation of PLA polymer in solid waste landfill site is not possible under all circumstances. Although the polymer is biodegradable, it requires to achieve ideal conditions such as temperature, nutrient and water concentration and a long time for the biological degradation process to occur (Kale et al., 2007; Sangwan and Wu, 2008; Plichta et al., 2014).

The biodegradation process essentially consists of two stages. In the first step, the PLA polymer is subjected to hydrolysis or oxidative reaction to break down the polymer chain into smaller segments or oligomers and form lactic acid oligomers. In the second stage, lactic acid is degraded by enzymes. Carbon dioxide, water and biomass are formed in aerobic environment, whereas methane, hydrocarbons and biomass are formed in anaerobic environment (Karamanlioğlu et al., 2017; Tsuji, 2008; Lunt, 1998; Auras, 2004; Kale et al., 2007; Henton, 2005; Torres et al., 1996; Ghorpade et al., 2001; Sangwan and Wu, 2008; Copinet et al., 2009; Longieras et al., 2007; Saadi et al., 2012). There are numerous factors that can influence the biodegradation process.

Hydrolysis initiates the decomposition of PLA in nature. For the hydrolysis reaction, the reaction temperature must be above the ambient temperature and the temperature has a direct effect on the decomposition time.

When the ambient temperature is low, the hydrolysis reaction takes quite a long time to occur (Kolstad et al.; 2012; Itavaara et al., 2002; Massardier-Nageotte et al., 2006; Gartiser et al., 1998; Shogren et al., 2003; Karamanlioglu and Robson, 2013). According to a study, the degradation of PLA by aerobic microorganisms was carried out at 20 °C with 50% relative humidity. According to forced degradation process,

the polymer would still have a molecular weight of 36,000 g/mol after 100 years (Kolstad et al., 2012).

The effect of temperature on biodegradation is similar for the processes conducted in aerobic and anaerobic environment. In an anaerobic study, it was stated that the degradation reaction of PLA was observed above 50 °C, and no degradation occurred at room temperature (Itavaara et al., 2002; Massardier-Nageotte et al., 2006; Gartiser et al., 1998).

In a composting study, as a result of the burial of PLA at 22°C, no change was observed in the physical properties of PLA at the end of one year (Shogren et al., 2003). Similarly, no changes were observed in the polymer structure at the end of one year and no degradation occurred in the composting operations performed at 25 °C and 37°C (Karamanlioglu and Robson, 2013). In addition, since the bacteria such as amycolatopsis and saccharotrix which provide the degradation of PLA are known to be limited, the biological degradation of the polymer occurs in a small number of developing industrial composting facilities (Jarerat et al., 2006; Tokiwa and Jarerat, 2004).

Natureworks, one of the main manufacturers of the polymer, has made it clear that there is a limited number of facilities where the biological recycling of the PLA has been performed and that the degradation of the PLA is not possible unless the conditions for the degradation of the PLA are met (Natureworks, 2019).

The statement of “The degradation of PLA in seas and oceans occurs much shorter time than in commercial polymers” is not valid in all circumstances. The degradation of PLA in seas and oceans is mainly carried out based on hydrolysis reaction. As a result of hydrolysis reaction, PLA is converted to lactic acid; however, water temperature must be high enough to hydrolyze of PLA. Briefly, the hydrolysis reaction is known to be complex, and it is challenging to carry out at ambient temperature. In one of the studies, it was stated that biodegradable polymers such as PLA and polycaprolactone (PCL) also cause microplastic accumulation in seas and

oceans (Bagheri et al., 2017). In this study, as shown in Figure 2.16, it was observed that PLA did not undergo degradation in artificially created sea water and aquatic environment at the end of one year.

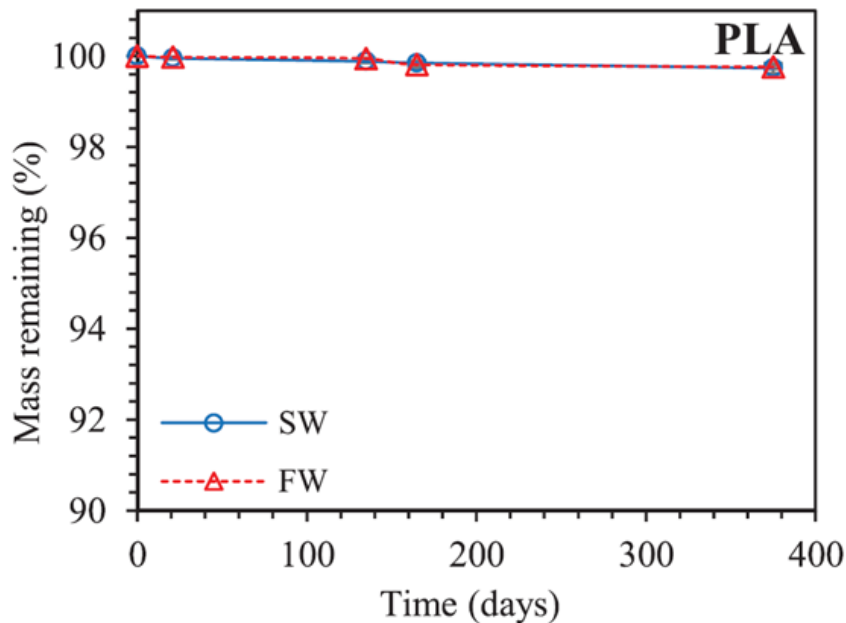


Figure 2.16. Hydrolysis of PLA in artificial seawater (SW) and water (FW) at 25 °C (Bagheri et al., 2017).

For all these reasons, biodegradation is considered to be ineffective in the recycling of PLA. In addition, PLA is produced as composites, blends or PLA containing various additives for use in many fields. Since the additives in the structure of these materials and trace components remained during their production stage remain intact in soil and water, they create negative effects for the living life.

2.9.2 Mechanical Recycling of PLA

Mechanical recycling is frequently used in the recycling of polymers due to its simple and easy applicability. However, since the properties of the recycled

polymers obtained using this technique are generally low, the use of the polymer is limited. Because of the reduction in properties of the polymer as a result of the recycling process, the number of recycling that can be applied to the polymer is limited (Badia and Ribes-Greus, 2016). As in other plastics, mechanical recycling is more applied in the recycling of PLA (Wu and Hakkarainen, 2015; Badia and Ribes-Greus, 2016; Badia et al., 2012; Brüster et al., 2016). As a result of thermal-mechanical recycling of PLA, changes in the molecular weight distribution and rheological structure of the material occur due to the deterioration of the thermal and mechanical properties caused by chain cleavage and intermolecular transesterification in the polymer. According to the research, it is difficult to recycle PLA based materials mechanically because of their recyclability properties. During extrusion, thermomechanical problems occur, which cause negative effects on material properties. As a result, the performance of the recycled polymer decreases and the product value decreases because of the reduction in properties of the material after each mechanical recycling process (Brüster et al., 2016; Badia and Ribes-Greus, 2016). Therefore, various techniques are applied to improve the quality of the recycled product. The main techniques can be summarized as follows: chemical modification of the polymer with the aid of heat annealing, stabilizers, antioxidants or chain linkers, and the mixing or composite of the polymer with other components. In addition to these methods, mechanical and chemical recycling techniques are used to improve the quality of the product to be obtained (Badia and Ribes-Greus, 2016).

2.9.3 Chemical Recycling of PLA

By using chemical recycling technique, the chemical structure of the waste polymer can be changed and new products can be formed as a result of the recycling reaction. Energy, valuable chemicals or raw materials can be attained with chemical technique, which presents an advantage. In addition, the properties of the polymers obtained by mechanical recycling are lower, and the use of the recovered polymer is

limited, and the number of recycled materials makes chemical recycling more feasible.

There are studies in the literature that provide valuable material recovery by chemical recycling of PLA, but industrial recycling of the polymer is still in development. Since this technology has not matured yet, the recycle (resin identification) code of the polymer is classified as “7” in the other plastics category. There are a few pilot plants built for the recycling of PLA waste. These facilities were established by PLA manufacturers. For example, the recovery of low-quality polymers is carried out using hydrolysis technique by Natureworks, the market leader in PLA production, at the company's own plant (Groot and Borén, 2010; Vink et al., 2004). Total Corbion has also stated that it will use chemical recycling technique for PLA polymers that it produces in its own facility and which it does not offer to the market (Jaso, 2019).

When chemical recycling studies of PLA polymer are examined in literature, it is seen that hydrolysis, solvolysis and pyrolysis techniques are widely used. The product resulting from recycling varies depending on the process employed. Lactic acid is typically derived through hydrolysis and solvolysis, whereas lactide is obtained through thermal degradation.

2.9.3.1 Hydrolysis and Solvolysis of PLA

The hydrolysis of polyester occurs when the functional ester groups of the polymer reacts with water. The reaction can be carried out in an acidic, alkaline, or neutral medium, often at high temperature and pressure to obtain lactic acid (Siddiqui et al., 2021). Lactic acid is an essential chemical used extensively in the food, medical and cosmetics industries (Petrus et al., 2019). Thus, chemical recycling of PLA provides the feedstock of PLA by gaining an economical output. Yet, there is a demand for large quantities of water and high pressure due to the insolubility of PLA for the hydrolysis process (Grewell et al., 2014).

The hydrolysis of PLA was investigated at 180 °C and 1.5 MPa for 50 minute to obtain lactic acid (Piemonte et al., 2013a). The hydrolysis of PLA was performed between the temperatures of 160 °C and 180 °C to obtain lactic acid (Piemonte et al., 2013a). The reaction was defined as autocatalytic due to the formation of the carboxyl groups that tends to catalyze the reaction. The studies was further proceed on the kinetic investigation of hydrolysis reaction of PLA. Another work by Piemonte was on the investigation of the hydrolysis of high molecular weight PLA to obtain lactid acid (Piemonto et al., 2013b). PLA pellets were depolymerized in a batch reactor at temperatures close to the melting point of PLA. The experimental runs were conducted at the temperature range of of 160-180 °C as in the previous study, with a constant pressure of 1.5 MPa. The conversion of PLA was only found as 3.39% at 160 °C. For 180 minutes, the conversion of PLA to lactic acid was found to be 98.97%. More than 99% conversion of PLA to lactic acid attained at 180 °C for 90 minutes. An autocatalytic reaction mechanism was fitted for the hyrolysis reaction. It was found that the hydrolysis of PLA is autocatalytic (Henton et al., 2005; Piemonte et al., 2013a). The kinetics of the reaction enhanced by the addition of carboxyl groups that results in the breakage of the ester bonds in the polymer (Piemonte et al., 2013a). Carboxyl groups provide a decrease in the pH of the medium.

In another work, hydrolysis of PLA was performed in the temperature range of 170 °C-200 °C at autogenous pressure without using catalyst (Cristina et al., 2018). The rate constant of the reaction was found to be between 0.102 and 0.263 min⁻¹ in the selected temperature range.

Similar temperature range was seen in the degradation studies of PLA. Lactic acid was obtained from the reaction of PLA in hydrolysis method in the range of 120-190 °C (Tsuji et al., 2008). However, higher reaction temperature was not used in hydrolysis. The temperature above 250 °C leads to decomposition of lactic acid (Mohd-Adnan et al., 2008; Yagihashi et al., 2010; Cristina et al., 2018; Piemonte et al., 2013a, 2013b).

The impact of reaction medium on reaction kinetics was investigated. Lactic acid yield was found to be 94.7% in water at 120 °C for a reaction time of 50.7 hours (Chauliac et al., 2020). The yield was also determined to be 94.2% in NaOH medium at the same temperature for 40.7 hours. The similar yields were attained at higher temperature of 150 °C with a much lower reaction times of 3.7 and 2.5 hours in water and NaOH mediums, respectively. The hydrolysis of PLA in an alkaline solution under microwave irradiation was studied with the objective of chemical recycling of this biodegradable polymer and recovery of the monomer, lactic acid (Siddiqui et al., 2020). To optimize the reaction parameters, the reaction time, temperature, catalyst, use of methanol, and amount of alkaline solution were investigated. With or without catalysts, the depolymerization of PLA was negligible in water at 150 °C.

The hydrolysis of low molecular weight PLA with 50% ethanol, butanol, 1-propanol and 20% 1-butanol was studied at 70 °C up to 140 hours (Iñiguez-Franco et al., 2018). The rate constants demonstrated that the hydrolysis of PLA was slower in the presence of 50% methanol compared to 50% ethanol, 50% 1-propanol, and 20% 1-butanol. In these studies, the decrease in molecular weight was also studied. The hydrolysis of PLA in 50% ethanol was then investigated at 60 °C. In these work, the molecular weight of PLA was significantly decreased after one month.

Due to the slow degradation of PLA in hydrolysis, the effect of ionic liquids on PLA degradation was studied. At moderate temperatures, hydrolysis rate of PLA is slow (Kolstad et al., 2012). Using an ionic liquid catalyst, 1-butyl-3-methylimidazolium acetate [Bmim][OAc], production of calcium lactate from the hydrolysis of poly(lactic acid) was investigated in order to establish a chemical recycling method for waste PLA (Song et al., 2014). The use of ionic liquids provided the catalytic activity and reusability. The highest PLA conversion to calcium lactate was achieved as 93.93% with 76.08% calcium lactate production at 130 °C for 2 hours in hydrolysis. The ionic liquid to PLA mass ratio was decided to be 0.5, whereas the water to PLA mole ratio was chosen 6 in these studies.

The effect of ZnO in the hydrolytic degradation of PLA/ZnO nanocomposites was discussed (Lizundia et al., 2016). The hydrolytic degradation was proceeded at 80 °C in PBS solution up to 25 days. The presence of acidic degradation products in PBS demonstrates that hydrolytic degradation accelerates considerably as ZnO content increases. The abiotic hydrolysis of PLA composites with halloysite nanotubes and a polyacrylic acid copolymer was also studied at 58 °C for 60 days in the presence of microbial growth inhibiting substance (Drohsler et al., 2022).

It has been stated that hydrolysis has not been demonstrated to be a successful depolymerisation approach for post-consumer PLA substrates (Spierling et al., 2018). These restrictions on hydrolysis limit its industrial application significantly.

The alkyl lactate formation can be provided by solvothermal alcoholysis techniques (Petrus et al., 2019). Due to the insolubility of PLA in methanol or water, methanolysis and hydrolysis techniques necessitate higher temperatures (Tsuji et al., 2003) and pressures (Mohd-Adnan et al., 2008) as well as significant amounts of strong acids (Lee et al., 2001) or bases (Tisserat et al., 2011; Yagihashi et al., 2010).

A study has been conducted into the chemical recycling of poly(L-lactic acid) (PLLA) via alcoholysis under microwave irradiation. Under microwave irradiation, the reaction rate in the ranges of 140-180 °C and 130-210 °C was higher than under conventional heating (Hirao et al., 2010). In this study, it was stated that the same reaction mechanism took place in both mediums and lactate formation was observed as a result of the alcoholysis reaction. Microwave assisted alcoholysis of PLA was also done with various diols and tetrabutyl orthotitanate (TBT) (Nim et al., 2020).

Since hydrolysis and solvolysis reactions require the use of significant amounts of energy and solvents, various catalysts are used to lower the reaction temperature and increase yield. Metal and ionic liquid based catalysts were used to enhance the yield and depolymerize of PLA by solvolysis. The effect of Zn on the degradation of PLA was studied (Lamberti et al., 2022; Santulli et al., 2022; Fuchs et al., 2022; Lamberti et al., 2021). The effect of Mg (Lamberti et al., 2022; Santulli et al., 2022), Y, Ti, Zr,

Hf (Santulli et al., 2022) on the PLA degradation were also investigated. There are few studies using ionic liquids in the hydrolysis and solvolysis reaction of PLA (Song et al., 2013, 2014; Liu et al., 2019). In these works, 1-butyl-3-methylimidazolium acetate [Bmim][OAc] (Song et al., 2014) and DBU-based protic ionic liquids (diazabicyclo[5.4.0]undec-7-ene) (Liu et al., 2019) were used. The details of the studies are given below:

PLA was degraded in ethanol between 180 °C and 260 °C for an hour in a pressurized reactor without catalyst (Petrus et al., 2016, 2019). Lactic acid based esters such as ethyl lactyl lactate, and ethyl lactate were produced. The experimental findings indicate that high temperature and an excess of ethanol are required for the effective production of ethyl lactate. The conversion of PLA to ethyl lactate was 5% at 180 °C. At 260 °C, the conversion was enhanced from 50% to 99% when the amount of ethanol increased by tenfold. The temperature range for the alcoholysis process with magnesium ethoxide catalyst was 80 and 200 °C. This process was facilitated by magnesium ethoxide, which allows 90% conversion at temperatures lower than 100 °C and at six times lower pressures compared to the findings reported for catalyst-free reactions.

The alcoholysis of PLA produces value-added compounds such as alkyl lactate; which contributes to the circular economy (Lamberti et al., 2022). The methanolysis of PLA was studied in the presence of commercially available catalysts such as zinc acetate dihydrate ($\text{Zn}(\text{OAc})_2$), magnesium acetate tetrahydrate ($\text{Mg}(\text{OAc})_4$), 4-(dimethylamino)pyridine (DMAP), and triazabicyclodecene (TBD) to obtain methyl lactate. Among these catalysts, $\text{Zn}(\text{OAc})_2$ demonstrated the highest catalytic activity between the temperature of 90-130 °C.

PLA was chemically recycled in this study using either methanol or ethanol to produce the value-added products such as methyl lactate and ethyl lactate at the reaction temperature of 100-130 °C (Lamberti et al., 2021). Zinc acetate dihydrate (ZnAc) and 4-(dimethylamino)pyridine (DMAP) were used. When both catalysts

were utilized in the same proportion, a synergistic impact on the reaction rate was seen. At 130 °C, 99% conversion of PLA to methyl lactate was attained for 120 minutes with DMAP and ZnAc catalysts. The 99% conversion of PLA to ethyl lactate was provided in ethanol for 180 minutes at the same reaction condition. It was found that alcoholysis of PLA proceeds more rapidly in methanol than in ethanol due to the stronger nucleophilicity of methanol. The shorter chains of carbons tends to reduce steric hindrance. Ethyl lactate has higher demand than methyl lactate; however, the reaction rate of methanolysis was higher than that of ethanolysis and methyl lactate is still a value added product.

The solvolysis of PLA was performed in methanol and ethanol with zinc catalysts at the boiling point of the solvent utilized (Carné Sánchez et al., 2011). Without a catalyst, neither methanol nor ethanol were able to convert PLA to monomer; however, zinc acetate increased the yield of monomer to 21% and 70% in ethanol and methanol, respectively. Methanolysis of PLA was also performed to produce methyl lactate with tetramethylammonium fluoride, tetraethylammonium fluoride, tetramethylammonium chloride, tetraethylammonium chloride, tetramethylammonium bromide, tetraethylammonium bromide, tetramethylammonium iodide, tetraethylammonium iodide (Xie et al., 2021). Only the fluoride salts were found to efficiently catalyze the reaction. Methyl lactate yield was found as 59.3 % in methanol solution at 90 °C for an hour with tetramethylammonium fluoride.

The methanolysis of PLA was investigated in the temperature range of 40 °C-110 °C with Zn (II) catalysts to produce methyl lactate (Román-Ramírez et al., 2020).

The methanolysis of PLA was achieved with high methyl lactate yield in the presence of metal halides (KI, KF, KBr, KCl, NaCl, LiCl, and NaF) by utilizing microwave heating (Alberti et al., 2020). The degradation temperature was chosen between 120 and 180 °C in the reaction time of 5-20 minutes. At 180 °C for 10 minutes, no

formation of methyl lactate was observed; however, the maximum 99% methyl lactate yield was achieved with catalysts.

Metal amides were investigated for the alcoholysis of PLA with methanol and ethanol (Santulli et al., 2022). A wide range of metals such as Zn, Mg, Y, Ti, Zr, Hf, and Zn have used in the methanolysis and ethanolysis of PLA at different reaction times and reaction temperatures. Mg catalyst presented the most optimal selectivity and yield value at 25 °C for 2 hours. The polymer undergoes a random scission of polymer chains into oligomeric species, which are subsequently transformed into methyl lactate, in a two-step process.

The degradation of PLA was studied with chloroform at 57 °C in the presence of stannous (II) octoate catalyst for seven hours to produce methyl lactate (Anneaux et al., 2018). The use of chlorinated solvents did not meet the demands of environmentally friendly procedures. The activities of the three types of non toxic and robust carboxy Zn chloride catalysts were investigated in the alcoholysis of PLA (Fuchs et al., 2022). The degradation was performed at 60 °C with THF and the catalyst up to 24 hours.

1-butyl-3-methylimidazolium acetate ([Bmim] [Ac]) and Lewis acidic ionic liquid [Bmim] FeCl₄ materials are among the studied ionic liquids. In the study conducted by Song et al., (2013), the degradation of PLA was performed using methanol and [Bmim][Ac]. In this study, ionic liquid acts as catalyst. In other studies, using ionic liquids, it was concluded that the efficiency of the process was quite high (Song et al., 2013, 2014). DBU-based protic ionic liquids (diazabicyclo[5.4.0]undec-7-ene) was used as both solvents and catalysts for the alcoholysis of PLA to produce lactate esters (Liu et al., 2019). Using DBU-based ionic liquids, PLA could be effectively depolymerized with a 91% yield of methyl lactate at 100 °C for 5 hours.

However, the separation techniques (filtration, vacuum filtration etc.) to purify solvent, product and ionic liquid increases the process cost. In the literature, the degradation of PLA was studied in different ionic liquid medium (Li et al., 2014).

[Bmim] [Ac] ionic fluid has been reported to play a role in the degradation of PLA. Furthermore, the activity of the thermal decomposition reaction of PLA is increased by increasing the alkyl side chain length of imidazolium cations. For anions, the moderate basicity of the acetate ion leads to high activity of imidazolium acetate ionic liquids on the degradation of PLA.

It is likely that the degradation of PLA by hydrolysis and solvolysis methods have negative effects on the environment. In hydrolysis and solvolysis, various separation processes need to be carried out to separate the product from the solvent used in the reaction and purify the solvent so that it can be reused. Efficient use and recovery of water in industrial processes has become more important due to the decrease in water resources in recent years. Therefore, the water used during the reaction needs to be treated. These processes also increase the cost of the process.

In addition to that ring opening polymerization process allows the production of high molecular weight PLA with organometal catalysts (Stefaniak and Mazek, 2021). The method consists of several steps such as condensation of lactic acid, production of lactide that is a cyclic dimer of lactic acid and ring opening polymerization. Lactic acid and alkyl lactate should be transformed into lactide in the production route of PLA that is increasing the cost compared to thermal degradation of PLA (Jaso, 2019).

2.10 Thermal Degradation of PLA

2.10.1 Thermal Degradation of PLA using Thermogravimetric Technique

Thermal degradation of PLA was studied in the literature to determine the material properties of the PLA based composites and blends. The primary aim of these experiments was the determination of thermal properties of PLA during processing and performance of composite in use. In these studies, the product distribution was

not obtained, and the major aim was not related to upcycling or recycling of the polymer.

2.10.2 Determination of the Kinetic Parameters of Degradation Reaction of PLA

In these works, activation energies and kinetic relations were developed based on the thermal gravimetric analysis (TGA) (Palmay et al., 2021; Lv et al., 2019; Das et al., 2017; Huang et al., 2015; Li et al., 2012). Palmay et al., (2021) determined the activation energy of the polymer based on isoconversional kinetic models such as Friedman method, Kissinger-Akahira-Sunose method and Flynn-Wall-Ozawa method. Lv et al., (2019) studied the determination of the activation energy using the Flynn-Wall-Ozawa iso-conversion technique for thermal and thermo-oxidative degradation kinetics. Additionally, four temperature integral models, including the distributed activation energy model (DAEM), Flynn–Wall–Ozawa, Coats–Redfern, and Tang models, have been used to undertake kinetic assessments of mass loss vs temperature data (Huang et al., 2015). In another work, a numerical pyrolysis model known as ThermaKin was utilized to evaluate TGA and DSC observations to generate a quantitative description of the kinetics and thermodynamics of polymer degradation (Li et al., 2013).

In these works, the average activation energy for the degradation process of PLA was found between 91 and 192 kJ/mol. In these works, there has been differences on the kinetic parameters due to the polymer preparation technique, molecular weight of the polymer, operational conditions, the weight of polymer, particle size, heating rate, mass flow rate of the inert gas (Carrasco et al., 2013). A standard power law model was used to obtain the kinetic parameters of high molecular weight PLA 2003D (Sivri et al., 2019). The activation energy for the degradation was found as 262 kJ/mol. This model was also applied for the degradation analysis of propylene and polyethylene (Obalı et al., 2011; Aydemir et al., 2016). The activation energy of

PLA-2003D degradation was found to be 178 kJ/mol based on Kissinger method (Chakraborty et al., 2018). In another study, activation energy of PLA 2003D was obtained between 181-202 kJ/mol according to the modified Coats-Redfern method (Zhao et al., 2016). Behera et al., (2017) found the activation energy of PLA degradation reaction to be 186 kJ/mol. In another study, the activation energy for the degradation of PLA was calculated between 254 kJ/mol and 260 kJ/mol based on Kissinger, Augis and Bennett, Flynn-Wall-Ozawa and Kissinger-Akahira-Sunose methods (Tripathi et al., 2017).

2.10.3 The Influence of Agents on the Thermal Behaviour of PLA

The effects of reinforcements, stabilizers, additives, fillers, functional groups and metals on thermal degradation of PLA were also investigated in kinetic studies. The influence of lignin on thermal degradation behaviour of PLA were discussed. In these studies, it was found that the thermal stability of PLA biocomposites were enhanced with lignin based modifier (Tanjung et al., 2021). In another study, the thermal stability of the PLA-lignin cellulose nanofibrils composite was found to be superior to that of PLA and PLA-lignin cellulose nanofibrils (Liu et al., 2019). Additionally, molybdenum disulfide (MoS₂) and carbon nanotubes (Homa et al., 2020), amide ammonium acetate organic vermiculite (Li et al., 2019), organoclay (Ozdemir et al., 2018a), nanoclay (Ozdemir et al., 2018b), magnesium dihydroxide and magnesium oxide (Viretto et al., 2016), beta zeolite (Ye et al., 2016), metal organic precursors (Roura et al., 2011) and organically modified vermiculite (Fernandez et al., 2013) were analyzed using thermogravimetric analysis to obtain the changes in the thermal properties of PLA.

2.10.4 Thermal Degradation of PLA Composites and Blends

TGA was also used to evaluate the thermal degradation behavior of PLA with blends and copolymers. Thermal gravimetric analyses were performed for PLA blends or

composites with poly(butylene adipate-co-terephthalate) (Ponce et al., 2022), poly(hexylene succinate) (Chrysafi et al., 2021), chitosan biocomposites (Tanjung et al., 2022) and poly(ethylene glycol) (Ozdemir et al., 2018), polypropylene (Rajan et al., 2018), polyethylene terephthalate (Tai et al., 2016), poly[di(carboxylatophenoxy)phosphazene] (Lin et al., 2014), oligomers of 3-hydroxybutyrate or dendrimers of hydroxyalkanoic acids (Ni et al., 2009).

2.10.5 The Influence of Biomass on the Thermal Behaviour of PLA

The influences of biomasses such as banana peel powder (Kong et al., 2022), quinoa husk (Ponce et al., 2022), rice residues (Sun et al., 2022), biochar (Hernandez-Charpak et al., 2022), paper sludge (Gigante et al., 2021), bamboo particles (Zhang et al., 2020), sisal (Moliner et al., 2018), rice straw (Tai et al., 2016) kudzu biomass (Salak et al., 2015), wood flour and rice bran filler (Azwar et al., 2012) on the thermal properties of PLA were studied.

In some studies, products were identified and degradation mechanisms were speculated using a thermogravimetric technique with a few amount of polymer. Lv et al., (2019) studied thermal and thermo-oxidative degradation kinetics and characteristics of poly (lactic acid) and its composites (Lv et al., 2019). Kinetic studies revealed that the apparent activation energy of compounds degrading in oxygen was less than that of materials degrading in nitrogen, suggesting that materials breakdown more easily in the presence of oxygen. The gaseous products were lactide, cyclic oligomers, aldehydes, CO₂, CO, and H₂O, according to the TG-FTIR analysis.

2.10.6 Molecular Simulations on the Degradation of PLA

The reactive force field molecular dynamics (ReaxFF-MD) simulations were done for the first time on polylactic acid to provide a theoretical insight about the thermal

and thermo-oxidative breakdown processes of PLA (Li et al., 2022). In these studies, cook-off simulations at high temperatures in the 1800-2400 K range were done to get perspective into the thermal degradation of PLA (Li et al., 2022).

The findings revealed that the PLA's initial thermal breakdown process was homolytic cleavage of the C-O bond close to the ester group, followed by C-O bond breaking in the ester group and C-C bond cleavage (Li et al., 2022). Following the homolytic scission, thermal breakdown mostly produced carbon monoxide, carbon dioxide, and acetaldehyde as volatile byproducts (Li et al., 2022). On the other hand, in simulations of thermo-oxidative degradation, alkyl peroxide and hydroperoxide were produced, which decomposed into alkoxy and hydroxyl radicals, leading to an increase in the proportion of lower carbon (C₁-C₄) (Li et al., 2022).

Reactive molecular dynamics was also used to examine the effect of density and environmental variables on the degradation kinetics of amorphous polylactide (Mlyniec et al., 2016). Simulations of PLA decomposition with oxygen and water have demonstrated that higher temperatures accelerate the rate of decomposition. The reaction products were found as carbon monoxide at initial stages of the degradation while carbon monoxide and methylketene were seen at higher temperatures. Temperature significantly affected the rate of breakdown of PLA in oxygen rather than in water. This is consistent with the experimental finding that the presence of oxidizing agents promotes the polymer scission process (Valles et al., 2000, Chaudhry et al., 2000). Hydrolytic reactions, radical degradation, and transesterification all occur simultaneously, resulting in the release of gas products such as acetaldehyde, ketene, carbon monoxide, and carbon dioxide (McNeill et al., 1985, Kopinke et al., 1996). Acetaldehyde and carbon monoxide were also produced from homolytic reactions (Mlyniec et al., 2016).

2.10.7 Reaction Mechanism and Products in the Degradation of PLA Composites and Blends

The effect of the reduced graphene oxide was investigated on the PLA-reduced graphene oxide composites (Usachev et al., 2022). The formation of acrylic acid, vinylacetic acid, dioxolanes, meso-lactide, D,L-lactide, trimer, tetramer and pentamer was observed for both PLA and PLA composites at 400 °C. A reduction in the segmental mobility of PLA chains inhibits the production of dioxolanones via the intramolecular nonradical ester exchange process.

In another work, lignin has increased the thermal stability of PLA nanocomposites, while tannin demonstrated relatively low catalytic effect on the degradation of PLA based composite (Ainali et al., 2022). At temperatures above 200 °C, intramolecular transesterification dominates the generation of lactide with the formation of cyclic oligomers resulting from cis elimination. The production of acrylic acid and other oligomers was attained due to β scission reactions. Further breakdown results in the eventual synthesis of acetaldehyde and carbon dioxide (Ainali et al., 2022; Aoyagi et al., 2002). The gaseous products comprised lactide, cyclic oligomers, aldehydes, carbon dioxide, carbon monoxide, and water, according to the TG-FTIR study on the thermal degradation of PLA composites containing starch in an inert and oxygen atmosphere (Lv et al., 2019).

2.10.8 Pyrolysis System

Although most of these studies are intended to obtain the thermal behaviour of PLA based blends and composites, a few studies are directly related to pyrolysis. Yet, the degradation experiments were carried out using TGA or Py-GC/MS with a few milligrams of polymer (Arrieta et al., 2013). The products were determined by heating the reactor to 600 °C within 0.6 s. This fast heating prevented the racemization of D and L lactide to meso lactide and further cracking. Yet, in

industrial applications, extreme heating is not preferred due to economical reasons. The product distribution could also be differ in real life applications from that in fast pyrolysis systems. In some studies, the degradation of PLA was studied in reaction systems rather than TGA. These works are summarized below:

Thermal degradation of high molecular weight PLA (10 mg) was studied in the batch system in the range of 250-290 °C for 15 hours under a reduced pressure below 3 mm Hg (Tsuji et al., 2003). The maximum yield of lactides was found as 14%. Thermal degradation of PLA were studied in the same reaction system under vacuum for the synthesis of meso lactide (Tsuji et al., 2017). Thermal degradation was conducted at 250 °C and 300 °C up to 750 minute. Maximum meso lactide yields were found to be 30% and 40% by moles at 250 °C and 350 °C, respectively.

For the pilot scale applications, the degradation of oligolactic acid with number average molecular weights in the range of 780-2900 g/mol was investigated for batch operations (Mulyashov et al., 2011). The main focus is to simulate the lactide production plant with tin catalysts in vacuum environment. Methyl lactate, methyl ester of dimeryc lactic acid, meso-lactide, 1,1-lactide, methyl ester of trimeryc lactic acid, methyl ester of tetrameryc lactic acid were reaction products along with lower molecular weight oligomers.

Apart from these studies, the effect of catalysts and side groups, additives in PLA were investigated in PLA degradation reaction. 1 g PLA was pyrolyzed in two-stage bed in the range of 500-700 °C with Ni/MgAl₂O₄ catalysts to obtain hydrogen and carbon nanotubes (Prabu et al., 2022). The first bed contained PLA, whereas the catalyst placed into the second bed. The products were mostly composed of H₂ and CH₄. In the fixed bed reactor, the catalytic pyrolysis of PLA and petroleum based plastics such as high-density polyethylene, low-density polyethylene, and polypropylene was studied with zeolite, spent FCC and MgO catalysts in the range of 400 °C-600 °C (Saeung et al., 2021). From the pyrolysis of PLA, lactic acid, lactide, and propanoic acid were obtained. Similarly, co-pyrolysis of PLA was

studied with HDPE between 400 °C and 500 °C in the batch system (Miskolczi, 2013). The products were gas, pyrolytic oil, water and residue. Although different products were attained based on temperature and the ratio of PLA to willow, monomers of PLA were not seen. Lastly, flash co-pyrolysis of PLA with biomass was investigated at 500 °C in semi-batch reaction system to obtain energy (Cornelissen et al., 2009). Energy recuperation was found to be 51.5% for 1:1 PLA/willow blend.

In another aspect, the pyrolysis of PLA was performed with various microwave absorbers such as tire, carbon and Fe (Undri et al., 2014). Lactide was produced to a maximum of 27.7% based on the amount of PLA used. Acetic acid, propionic acid and carbonyl compounds were detected in liquids. In addition, When Fe was used as microwave absorber, the solid formation increased, the amount of lactide increased with carbon microwave absorber.

Isothermal pyrolysis was done for obtaining the thermal behaviour of only 50 mg PLA complexes with different end structures at 250 °C for 2 hours (Fan et al., 2004a). It was found that the degradation starts approximately 220 °C. The formation of lactide isomers was detected. The same reaction mechanism was seen in all type of end groups. The effect of end groups of PLA (PLLA-Ca and PLLA-H) in degradation was also studied in both Py-GC/MS and glass tube oven (Fan et al., 2003a). The pyrolysis of 200 mg polymer was performed at 350 °C for 20 minutes. The reaction products were analyzed by using ¹H-NMR and GC. The major reaction products were composed of lactide isomers, cyclic and linear oligomers, acetaldehyde and acrylic acid. The racemization properties of 200 mg PLLA-Ca was also investigated in glass tube oven at 250 °C for the reaction times of 60, 120, and 240 minutes (Fan et al., 2003b). The yield of the L,L lactide was found approximately as 96.3%.

Lastly, the effect of the Sn based residual catalyst remained structure in the structure of PLA was further investigated on the decomposition of PLA using TGA (Fan et

al., 2004b). Sn was found to be effective on the degradation of PLA and the formation of lactide. The effect of MgO and CaO on the degradation of PLA was also investigated for PLA composites (Fan et al., 2004c). Metals tended to a decrease in degradation temperature and an enhancement on the production of lactide isomers rather than oligomers.

2.11 Chemical Recycling of Plastics with Supercritical Carbon Dioxide

The effective use and recovery of water in industrial processes have gained greater significance in recent years due to depleting water resources. In addition, it has been determined that the annual production of organic solvents widely used in the industry is 20 million tons, and these solvents pose a significant threat to the environment (Clark et al., 2015). Hence, governments and environmental organizations stress the importance and necessity of developing sustainable processes and technologies for the use of "green" solvents in industry.

In this context, supercritical fluids are solvents that mimic liquids in terms of density and gases in terms of diffusion and viscosity, and possess tunable resolving power and transport qualities by adjusting temperature and pressure (Knez et al., 2014). Carbon dioxide is one of the most widely used supercritical fluids in many diverse applications (Nalawade, 2006; Cooper et al., 2001; Leitner et al., 2002). The fluid is affordable, safe, easily accessible, non-toxic, non-explosive and non-flammable (Knez et al., 2014). Due to its low viscosity and surface tension properties, the critical temperature of supercritical carbon dioxide, which accelerates mass transfer, is quite low compared to many solvents (Cooper et al., 2001). In this way, the transition of matter to the critical phase requires less energy and provides advantages in applications.

In materials processing, supercritical carbon dioxide can serve as a solvent, anti-solvent, solute, and reaction medium (Zhang et al., 2014). Due to improved mass transfer of the reactants, reactions conducted in a supercritical fluid medium proceed

at a faster rate than those utilizing liquid organic solvents (Fan et al., 1999; Ramsey et al., 2009; York et al., 2004). By eliminating the requirement for separation operations, the use of supercritical fluids enables the development of environmentally friendly industrial alternatives. On the other hand, it has been found that the transition of a reaction from an organic solvent to supercritical carbon dioxide induces considerable changes in the chemo-, regio-, and stereoselectivity of a variety of processes (Leitner et al., 2002).

Supercritical carbon dioxide involved barely in a few degradation studies of polymers. Depolymerization of PET was studied with supercritical carbon dioxide at 500–650 °C by pyrolyzing (Wei et al., 2011). Supercritical carbon dioxide promoted the dissociation of the PET precursor into aromatic hydrocarbons, which then degrade into carbon. Carbon were produced with a 47.5% yield at 650 °C for 9 hours.

Degradation of PVC was controlled in supercritical carbon dioxide medium to achieve maximum debromination (Zhang and Zhang, 2020). With the use of supercritical carbon dioxide, solid, oil, and gas products were obtained. Carbon dioxide, hydrogen, methane, and ethane were value-added gas products in the decomposition of electronic display housing plastic containing halogen.

Lastly, enzymatic degradation of poly(ϵ -caprolactone) was studied using supercritical carbon dioxide (Kondo et al., 2002). Poly(ϵ -caprolactone) could be converted into repolymerizable cyclic dicaprolactone (DCL) in ScCO₂ at 18 MPa and 40 °C in the presence of low amount of water and lipase. Maximum 91% DCL yield was obtained.

In this work, the degradation of PLA was carried out under supercritical carbon dioxide for the first time. The development of recycling and recovery technologies of PLA-based materials is important in terms of preventing waste accumulation of the polymer and supporting the production and use of the polymer; however, there

is a limited work in the literature when compared to commodity plastics and the recycling technology of PLA has not matured yet.

2.12 Aim of the Study

The production rate of PLA has increased with the expanded usage areas of the polymer over the past decade. Even though PLA was launched in the market as a solution to the accumulation of plastic waste, misconceptions about the biodegradability of the polymer on the market may soon lead to a waste issue resulting from PLA. Yet, current recycling techniques are insufficient for the industrial PLA waste. Compared to commodity plastics, PLA recycling has received less attention in the literature as well.

In a wide range of environmental conditions, including landfills, seas, and oceans, it is known that PLA is not entirely biodegradable. Unless pH, temperature, nutrient, and water concentrations are optimal, the biological breakdown of PLA wastes will be insufficient, and waste will continue to accumulate. In mechanical recycling, polymer can be processed only to a certain extent, and the contribution of mechanical recycling to the sustainability can be deemed to be comparatively low.

Since valuable chemicals and energy may be recovered from waste, chemical recycling of PLA is superior to these techniques; nevertheless, PLA recycling technology has not yet matured. Chemical recycling of PLA was done following mainly hydrolysis, solvolysis and thermal decomposition techniques. Hydrolysis and solvolysis reactions require the use of significant amounts of energy and solvents.

Lactide was produced as reaction product from the thermal decomposition of PLA. Obtaining the lactide monomer would also be advantageous over hydrolysis and solvolysis methods by shortening the production process of PLA. Yet, in the literature, most of these studies aim to determine the thermal behavior of PLA mixtures and composites, a small proportion is directly related to pyrolysis. In these

works, TGA or Py-GC/MS instruments were used with a little amount of polymer, typically a few milligrams. The temperature was high and reaction time was fairly short, even in seconds. However, for economic reasons, excessive temperature cannot be achieved in industrial applications. In practical uses, the product distribution may also differ from that of fast pyrolysis systems.

In the literature, the effect of metals on degradation of PLA was evaluated mainly in composites of PLA by pyrolysis technique. Pyrolysis of PLA was studied with metals on a few studies, and these metals were not loaded to any support. The effect of tin, which is frequently used as a synthesis catalyst in the polymerization reaction of PLA and remaining in the structure of the synthesized polymer, on the degradation reaction of PLA was studied in a few works.

Lastly, there are few studies on the degradation of polymers in supercritical CO₂, while there is not any study on degradation of PLA in supercritical CO₂.

As a summary of this study is:

- A comprehensive evaluation of the degradation of PLA was provided using various strategies in order to prevent waste accumulation and degrade waste into chemicals with added value. Within this scope, the degradation of PLA was performed using thermal gravimetric analyzer (TGA), pyrolysis system and high-pressure reaction system. The degradation of PLA was carried out with and without mesoporous catalysts designed specifically for the PLA degradation (Figure 2.17).

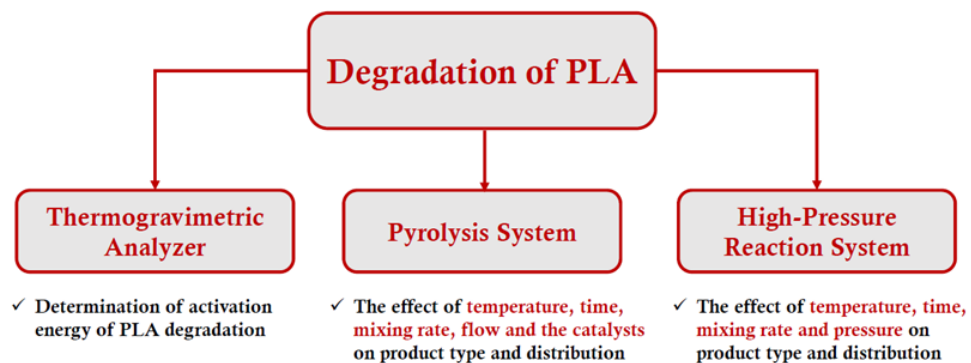


Figure 2.17. The degradation of PLA with different techniques.

- Thermal degradation of PLA was investigated in these systems with different reaction parameters to observe the effect of these reaction parameters on product type and distribution.
- In this study, Al, Fe and Mg silica aerogel catalysts were synthesized and characterized with different techniques to determine the the most active catalysts in the pyrolysis system. The activation energy of PLA degradation was determined with and without catalysts.
- A pyrolysis system for the non-catalytic and catalytic degradation of PLA was designed and installed including the reaction vessel and separation units for the reaction products.
- The effects of metal loaded mesoporous catalysts on the degradation of PLA were investigated for the first time in the pyrolysis system to be installed. Product distribution depending on the reaction temperature, time, mixing rate, flow rate and catalyst type was evaluated by pyrolysis technique comprehensively.
- The decomposition of PLA was also carried out in supercritical CO₂ medium for the first time.

- The effects of reaction pressure, temperature, time and mixing rate on the degradation of PLA and product distribution were investigated.

With the development of effective and environmentally benign techniques, negative impacts of waste PLA-based materials on the environment will be eliminated and the waste will be evaluated economically. The mentioned efforts are to ensure that waste materials will not negatively affect the natural life cycle and will be converted into feedstock and value-added products for economic efficiency. The outputs of the work will contribute to polymer recycling studies and introduce a novel approach.

CHAPTER 3

EXPERIMENTAL

The experimental studies are represented in four parts.

1. Synthesis and Characterization of Silica Aerogel Based Catalysts
2. Thermal Degradation of PLA using Thermogravimetric Method
3. PLA Degradation Experiments
4. Analyses of the Products

3.1 Synthesis and Characterization of Silica Aerogel Based Catalysts

3.1.1 Synthesis of Silica Aerogel Support

Silica aerogel catalysts are synthesized with the following Değirmencioğlu's procedure (Değirmencioğlu, 2018). Değirmencioğlu (2018) modified the synthesis procedure of silica aerogel based on several works (Davis et al., 1992; Deshpande, Smith, and Brinker 1992). Silica aerogel, which acts as a support for catalytic material, was synthesized by following the sol-gel technique. Tetraethyl orthosilicate (TEOS, $\text{SiC}_8\text{H}_{20}\text{O}_4$, Merck Millipore, 10.01 g) was added drop by drop to the ethanol mixture. Afterward, hydrochloric acid (HCl, Merck Millipore) was added into the solution, which was mixed for two hours using a magnetic stirrer at room temperature. The ethanol mixture and the base catalyst, first ammonia (NH_3 , Merck Millipore) and then ammonium fluoride (NH_4F , Merck Millipore), were added to the solution. Gel formation occurred within minutes with the addition of the catalyst and was waited for eight hours for aging. After the completion of the aging stage, ethanol was drained, hexane (Sigma-Aldrich) was added over the gel and the system was

kept at 45 °C for two hours. The solvent exchange was done with further addition of hexane. Trimethylchlorosilane (TMCS, C₃H₉SiCl, Merck Millipore) was then added dropwise over the gel. The gel was then kept at 45 °C for five hours. At the end of the duration, the solvent exchange was repeated in the same manner as explained above. Finally, the gel was dried at 125 °C for two hours to obtain the silica aerogel. This sample was named “SAU”. Some of the silica aerogel materials were calcined at 500 °C with a heating rate of 1 °C/min for at least 12 hours under helium atmosphere with a flow rate of 50 mL/min. This sample was named as “SA”.

3.1.2 Impregnation of Metal into Silica Aerogel Support

Metal loading into SAU or SA support was carried out using the wet impregnation method. One gram of silica aerogel was added to ethanol. Meanwhile, the metal precursor was also dissolved in ethanol with different weight ratios. After dissolution, the metal precursor solution (2.5-15 wt.%) was added into the silica aerogel solution and the solution was mixed at room temperature for 24 hours. The mixture was then dried in an oven at 60 °C overnight. The same procedure was applied for the different metal loadings. Within the scope of the thesis, Al (Al(NO₃)₃·9H₂O, Sigma Aldrich), Fe (Fe(NO₃)₃·9H₂O, Sigma Aldrich) and Mg (Mg(NO₃)₂·6H₂O, Sigma Aldrich) were loaded into silica aerogel support. The dried metal loaded samples were calcined at 500 °C for 12 hours under helium gas to obtain metal loaded silica aerogel catalyst. The sample codes are named as SAUXY or SAXY based on the support material. In metal loaded catalysts, X and Y present the metal type and the percentage of the metal loading into support, respectively. The synthesized catalysts were given in Table 3.1.

Table 3.1. Metal loaded silica aerogel-based catalysts.

Sample Code	Metal	Support	Metal Amount (wt. %)
SAAl2.5	Aluminum	Calcined Silica Aerogel (SA)	2.5
SAAl10			10
SAAl15			15
SAUAl15	Aluminum	Uncalcined Silica Aerogel (SAU)	15
SAUFe15	Iron		
SAUMg15	Magnesium		

3.1.3 Characterization of Silica Aerogel Based Catalysts

The synthesized silica aerogel-based catalysts were characterized using several techniques. The surface areas and the porosities of the silica aerogel support and metal loaded silica aerogel catalysts were determined using Micromeritics Tristar II 3020 device. The samples were degassed for 4 hours at 200 °C. N₂ sorption analysis was carried out at the relative pressure (P/P₀) range of 0.0001 and 0.99.

Fourier Transform Infrared Spectroscopy (FTIR) analysis was mainly used for obtaining the structure of silica aerogel. Perkin Elmer Spectrum Two Model FTIR spectroscopy with Attenuated Total Reflection (ATR) was used in the analysis. The analysis was performed in the wavenumber range of 500 cm⁻¹ and 4000 cm⁻¹ accumulated of 64 scans with 4 cm⁻¹ resolutions.

Acid sites on the catalysts were obtained using Diffuse Reflectance Fourier Transform Infrared Spectroscopy. The samples and pyridine were placed into a desiccator. At room temperature, the samples were exposed to pyridine for 3 weeks. Perkin Elmer Spectrum One Model FTIR spectroscopy with Diffuse Reflectance

(DRIFTS) was used in the analysis. The analysis was performed in the wavenumber range of 500 cm^{-1} and 4000 cm^{-1} accumulated of 100 scans with 4 cm^{-1} resolutions.

Total acidic capacity of the metal loaded catalyst was determined using Temperature Programmed Desorption of Ammonia (NH_3 -TPD). The NH_3 -TPD analysis was carried out using Micromeritics Chemisorb 2720 with temperature programmed controller. Sample (0.05 g) was firstly heated up to $200\text{ }^\circ\text{C}$ under argon atmosphere with a flow rate of 50 mL/min . Sample was then saturated with 5 vol% ammonia in helium with the same flow rate for an hour. After the adsorption stage, the sample was heated up to $700\text{ }^\circ\text{C}$ under helium atmosphere (30 mL/min) with two step heating: from ambient air to $125\text{ }^\circ\text{C}$ with a heating rate of $30\text{ }^\circ\text{C/min}$ and from $125\text{ }^\circ\text{C}$ to $700\text{ }^\circ\text{C}$ with a heating rate of $10\text{ }^\circ\text{C/min}$.

3.2 Thermal Degradation of PLA using Thermogravimetric Method

PLA used in the degradation reaction was provided from NatureWorks. The product code of the polymer is 2003D, and it has the following properties: specific gravity: 1.24, melt flow rate: 6 g/10 min , melting point: $145\text{--}160\text{ }^\circ\text{C}$. Degradation of PLA was studied using thermogravimetric analyzer with or without metal loaded silica aerogel catalyst. The performance of the catalysts was tested using Shimadzu TGA-DTG-60/60H device. Degradation experiments were carried out under nitrogen atmosphere with a flow rate of 50 mL/min from ambient temperature to $500\text{ }^\circ\text{C}$ with a heating ramp of $5\text{ }^\circ\text{C/min}$ to determine the activation energy of thermal degradation reaction of PLA.

3.3 PLA Degradation Experiments

3.3.1 PLA Pyrolysis System

Degradation of PLA is carried out under the argon atmosphere at different reaction temperatures and times at atmospheric pressure. PLA pyrolysis system was designed and installed. The system is operated as a semi-batch. The system and its components are given in Figure 3.1 and Table 3.2.

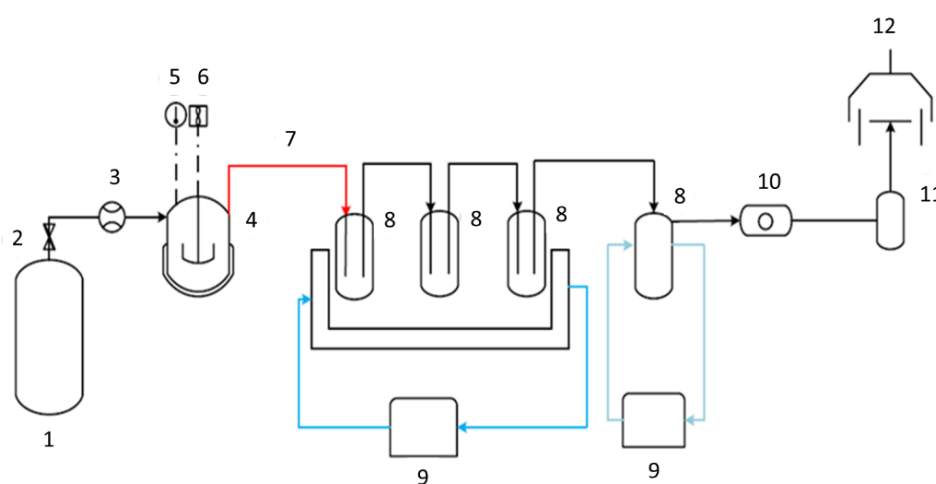


Figure 3.1. Installed pyrolysis system.

Table 3.2. The components of the pyrolysis system.

Code	Equipment	Code	Equipment
1	Argon Tank	7	Heating Tape with a Thermocouple and a Controller
2	Exit Valve of the Argon Tank	8	Condenser Vessels
3	Mass Flow Controller	9	Cooling Fluid Circulators
4	Reactor with Furnace	10	Gas Sampling Bulb
5	Temperature Reader and Controller	11	Soap Bulb Meter
6	Reactor Mixer	12	Ventilation System

The pyrolysis system and its components are described below:

An argon gas tank (1) is present in the system to provide an inert medium in the reactor and remove the gas products from the reactor. The flow rate of the argon gas entering the reactor is adjusted with the mass flow controller (3). The pyrolysis system has a 100 ml stainless steel reactor (4) with the dimensions of 4 cm inlet diameter and 8 cm height. To adjust the reactor temperature, a tube furnace is placed outside of the reactor. The temperature of the reactor is measured using a thermocouple connected to the controller (5). The outlet line of the reactor is wrapped with a heating tape (7) to prevent the condensation of the products in the line. The temperature of this heating tape is controlled with a temperature controller. There have been three condenser vessels (8) that are kept at 20 °C with the circulated water bath (9) to collect the condensable products. Following, another condenser is installed, cooled with the circulated water bath at a temperature of -5 °C, to collect the condensable products.

A gas sampling bulb (10) on the set-up is used to collect the gas products during the reaction. Condensable products are collected in the condenser vessels. All condensable and non-condensable compounds are analyzed using GC.

3.3.1.1 Experimental Procedure for the Non-catalytic Degradation of PLA in Pyrolysis System

The selected amount of PLA pellets (Natureworks, 2003D, 2.0 g) is placed into the reactor. Argon gas is fed to the system with the selected range of flow rate (25-100 ml/min). The heating rate is adjusted as 5 °C/min. When the reactor temperature reaches the desired temperature, the reaction time is started. The reactor effluent gas composition is analyzed continuously at certain time intervals using GC. When the reaction time is completed, the heating of the reactor is turned off and the system is allowed to cool. At the end of the reaction, solid remained in the reactor, the condensable product collected in the condenser vessels are weighted. Each

experiment was repeated minimum two times, and at the optimal reaction set, three runs were done to obtain standard deviation. The parameter range is given in Table 3.3.

Table 3.3. Reaction parameters of the non-catalytic degradation of PLA.

Reaction Parameter	Value
Reaction Temperature (°C)	200-375
Reaction Time (min)	15-240
Flow Rate (ml/min)	25-100
Mixing Rate (rpm)	45-140

3.3.1.2 Experimental Procedure for Degradation of PLA with Metal Loaded Silica Aerogel Catalysts:

The selected amount of PLA pellets (Natureworks, 2003D, 2.0 g) and 1 g catalyst are placed into the reactor. Argon gas is fed to the system with a flow rate of 50 ml/min. The heating rate is adjusted as 5 °C/min. When the reactor temperature reaches the desired set temperature, the reaction time is started. The reaction time is 60 min, and the reaction temperature is in the range of 200 °C-275 °C for all catalytic degradation of PLA. The reactor effluent gas composition is analyzed continuously using GC. When the reaction time is completed, the heating of the reactor is turned off and the system is allowed to cool. At the end of the reaction, the condensable product collected in the condenser vessels, and the solid product are weighted. The condensable and non-condensable compounds are analyzed with GC.

3.3.2 Supercritical PLA Degradation System

The degradation of PLA was carried out in the supercritical CO₂ environment in a high-pressure batch reactor at different reaction conditions such as pressure, temperature, and reaction time. The supercritical reaction system and its components are given in Figure 3.2 and Table 3.4. The components of the supercritical reaction system.

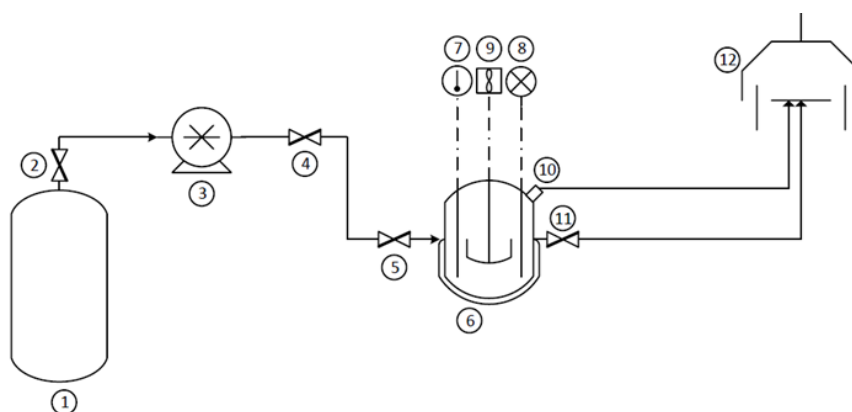


Figure 3.2. Supercritical reaction system.

Table 3.4. The components of the supercritical reaction system.

Code	Equipment	Code	Equipment
1	Liquid CO ₂ Tank	7	Temperature Gauge and Controller
2	Exit Valve of Liquid CO ₂	8	Pressure Gauge and Reader
3	Syringe Pump	9	Reactor Mixer
4	Exit Valve of Syringe Pump	10	Rupture Disk
5	Inlet Valve of Reactor	11	Exit Valve of Reactor
6	Reactor with Heating Jacket	12	Ventilation System

The supercritical reaction system has a 50 ml high-pressure stainless-steel reactor (6), with a pressure gauge and indicator (8), a rupture disc (10), thermocouple and

controller (7), inlet (5) and outlet (11) valves, heating jacket, and a mixer (9). The pressure of the system is monitored with a pressure gauge (8) and the temperature of the system is adjusted with a thermocouple and a controller. A rupture disc (10) is for prevention of undesired levels of pressure in the reactor exceeding the pressure limit of the reactor. The mixing rate can be adjusted (9). A syringe pump (3) is used to supply liquid carbon dioxide to the reactor inlet (5) at the desired flow rate or pressure. The maximum working pressure in the reactor is 345 bar in the supercritical reaction system.

3.3.2.1 The Experimental Procedure for the Degradation Reaction of PLA in the Supercritical CO₂ Environment

The selected amount of PLA pellets (Natureworks, 2003D, 1 g) is placed into the high-pressure reactor, then mixer is started. Then, CO₂ is pre-charged to the high-pressure reactor at the pressure and temperature where CO₂ is in the gas phase. The reactor temperature is gradually increased with the controller while CO₂ is transferred to the system with the high-pressure syringe-pump. When the pressure and temperature of the system reach the desired values, the reaction time is started. The temperature of the system is kept constant during the reaction while the reactor was continuously mixed at a certain mixing rate if mixing was introduced. When the reaction time is completed, heating of the reactor is stopped, and the reactor is allowed to cool naturally under room temperature. After the pressurized reactor has cooled down, the gas is discharged from the reactor in a controlled manner. At the end of the reaction, solid product is weighted. At a selected reaction set, three runs were performed to obtain the standard deviation of the system. The analysis of the solid product is carried out using GC. The range of the reaction parameters is tabulated in Table 3.5.

Table 3.5. Reaction Parameters of Thermal Degradation of PLA in Supercritical CO₂.

Reaction Parameters	Range
Reaction Temperature (°C)	190-220
Reaction Pressure (bar)	103-206
Reaction Time (min)	30-480
Mixing Rate (rpm)	0-140

3.4 Analyses of the Products

3.4.1 GC Analyses of the Condensable, Gas and Solid Products

The analyses of the condensable product and solid product in the supercritical reactor were carried out by using Varian CP 3800 GC equipped with an FID detector and TRB-1 (Teknokroma) capillary column (30 m x 0.25 mm x 0.25µm). The capillary column is made of 100% dimethylpolysiloxane. A method has been developed to analyze the products. The method is as follows:

The temperatures of the injector and FID detector are 275 °C. Column pressure is 5 psia. The column oven is programmed to heat the oven from 125 °C (Hold: 20 min) to 150 °C with a 5 °C/min heating rate (Hold: 5 min) and 200 °C with a 5 °C/min heating rate (Hold: 5 min). The split ratio is chosen as 100. 1 µl sample is injected into the column. Relative response factor values of lactide isomers (C₆H₈O₄, Sigma Aldrich), lactic acid (C₃H₆O₃, Sigma Aldrich) and propionic acid (C₃H₆O₂, Sigma Aldrich) were obtained based on reference acetone.

The analysis of the non-condensable product was done using Shimadzu GC-2010 Plus CP 3800 GC equipped with a TCD detector and Supelco capillary column (30 m x 0.53 mm). The temperatures of the injector and TCD detector were 200 °C and 250 °C, respectively. Linear velocity of argon carrier gas is set as 26.6 cm/sec. The

column oven was programmed to heat the oven from 40 °C (Hold: 7.5 min) to 250 °C with a 23 °C/min heating rate (Hold: 14 min). 0.25 ml sample was injected into the column. The calibration gas contains hydrogen, carbon monoxide, carbon dioxide, methane and ethylene with 1 mol%. The balance gas was argon. Acetaldehyde (CH₃CHO, Merck) was also calibrated. By analyzing the calibration gas, beta factors, and retention times of the components were determined.

3.4.2 Analyses of the Solid in the Pyrolysis Reactor

The solid residue, which is the solid remaining in the reactor of the pyrolysis system, was analyzed using TGA and Ubbelohde viscometer.

Thermal properties of the solid residue and PLA were studied using Shimadzu TGA-DTG-60/60H Thermogravimetric Analyzer. Tests were performed under a nitrogen atmosphere with a flow rate of 50 mL/min from ambient temperature to 500 °C with a heating ramp of 5 °C/min.

PLA was dissolved in chloroform in the range of 0.25-1.0 g/dL. Solid in the pyrolysis reactor was also dissolved in chloroform. Using an Ubbelohde viscometer, the time for the flow of the polymer solution were determined at 25°C. The viscosity average molecular weight of the solid was calculated.

CHAPTER 4

RESULTS AND DISCUSSION

The results and discussion of the study will be provided in two major segments throughout this section. These sections are listed below:

1. Degradation of PLA with Different Techniques
2. Catalytic Degradation of PLA

In this work, the degradation of polylactic acid (PLA) was investigated comprehensively using diverse techniques and approaches in different reaction systems. Within this scope, the degradation of PLA was performed using various systems including a thermogravimetric analyzer (TGA), a pyrolysis system, and a high-pressure reaction system.

To determine the reaction kinetics of the polymer, PLA was firstly degraded by following thermogravimetric method. The degradation of PLA was mainly accomplished using a custom-designed pyrolysis system and a high-pressure reaction system operating under different reaction parameters. The comparison of the reaction systems and effective reaction parameters was also discussed.

In addition, as another approach, catalytic pyrolysis has the potential to be used for PLA feedstock recycling and production of value-added chemicals from the PLA. Al, Fe and Mg loaded silica aerogel catalysts were synthesized and characterized for the degradation reaction of PLA. Then, catalytic pyrolysis of the polymer was performed using these catalysts. Lastly, the effect of the catalysts on the product type and distribution was evaluated. The outputs of the studies are reported sequentially throughout this section.

4.1 Degradation of PLA with Different Techniques

4.1.1 Thermal Degradation of PLA using Thermogravimetric Method

A model study was conducted to observe the degradation behaviour of PLA using thermogravimetric analyzer (TGA). To stimulate the pyrolysis system, a degradation study was done under a nitrogen atmosphere with a 50 ml/min flow rate and a heating rate of 5 °C/min. Weight loss of polymer as a function of temperature is given in Figure 4.1. Thermal degradation of PLA by thermogravimetric method.

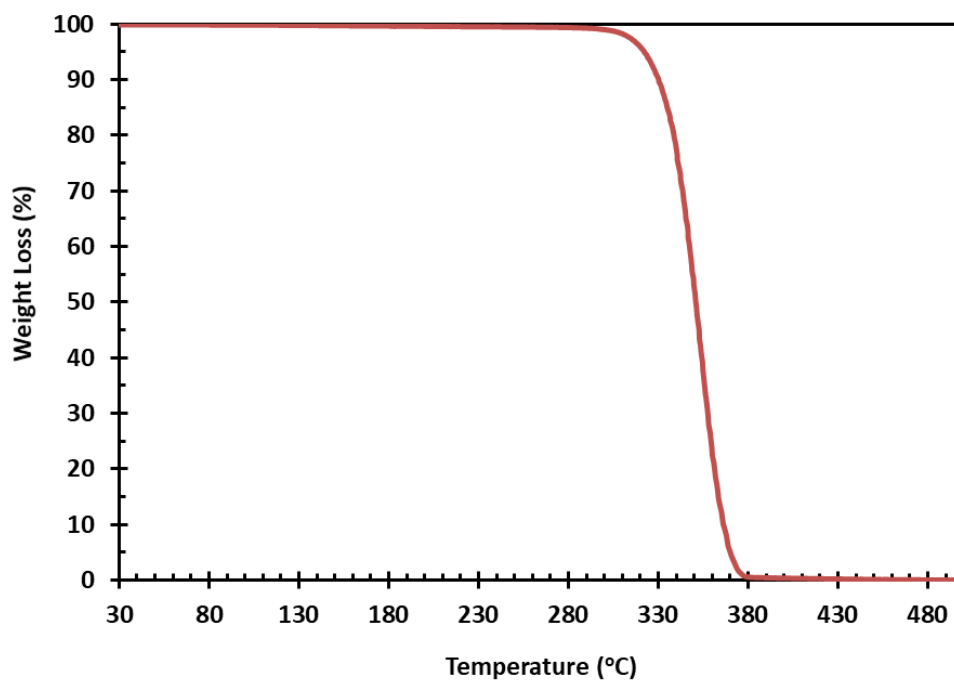


Figure 4.1. Thermal degradation of PLA by thermogravimetric method.

As seen in Figure 4.1, only 5% of the polymer was degraded at 322 °C. Similarly, the degradation temperature of the 30% weight loss was obtained at 344 °C. The

degradation of PLA was completed at 378 °C. The sharp decrease in weight of the polymer was seen in the temperature range of 331-371 °C due to chain scission.

The kinetic parameters of the PLA degradation reaction were evaluated based on a standard power law model. The activation energy calculation is given in Appendix A. The activation energy of the PLA degradation reaction was found to be 262 kJ/mol (Sivri et al., 2019). In the literature, the activation energy of the PLA (2003D) degradation reaction was in a broad range from 178 to 260 kJ/mol (Chakraborty et al., 2018; Zhao et al., 2016; Behera et al., 2017; Tripathi et al., 2017). The calculated activation energy is in good agreement with the literature.

4.1.2 Degradation of PLA by Pyrolysis

4.1.2.1 Design and Operation of the Pyrolysis System for the Degradation Reaction of PLA

In this study, the reaction temperature, reaction time, mixing rate, and flow rate were the four parameters investigated to construct a basis for PLA recycling. The effect of reaction parameters on the actual product type and distribution was systematically evaluated to contribute the studies in the literature. Within this scope, a pyrolysis system was tailor-made designed to study the degradation of PLA isothermally in a semi-batch reactor under argon atmosphere.

PLA degradation was performed using the pyrolysis system under different reaction parameters such as mixing rate, reaction temperature, reaction time and flow rate of argon. In the experiments, the polymer was put into the reactor before the system was turned on. Later, the inert gas flow was continuously fed to the reactor and the pyrolysis system was heated up to the desired reaction temperature.

During the reaction, the condensable product accumulated in the condenser vessel and non-condensable product were removed from the reactor simultaneously. The

solid product could remain inside the reactor while condensable products that were in slurry or waxy form collected in the condensers at the end of the reaction. The gas products were also named as non-condensable products.

The amounts of the solid and condensable products were determined by measuring the weight of the products in the reactor and condensers. The amount of the non-condensable products was calculated by subtracting the amount of the solid and condensable products from the initial weight of PLA and the yields of solid, condensable, and non-condensable products were calculated based on the amount of the initial PLA (Appendix B).

The composition of the condensable products was determined from GC analyses. The mole numbers of the condensable products were calculated using relative response factor (RRF). The weight fractions of the condensable products were subsequently determined. The calculation procedure is given in Appendix C. GC was also used to determine the composition of the non-condensable products at certain time intervals. Using the beta factor (β), the mol numbers of the non-condensable products were computed. Afterward, the mole fractions of the non-condensable products were calculated (Appendix D).

4.1.2.2 The Effect of the Mixing Rate on the Product Type and Distribution

Mass transfer limitation can be minimized by mixing the reaction mixture throughout the reaction time. The reaction kinetics can be improved by boosting the mass transfer, ensuring homogeneity of the mixture by mixing. In addition, mixing might enhance the collision between molecules. The temperature of the reactor would be maintained uniformly throughout.

Thus, the optimal degree of mixing was determined by investigating the PLA degradation process at 225 °C and 250 °C for 60 minutes while mixing the mixture at 45, 70, and 140 rpm in an argon atmosphere of 50 ml/min.

Based on the thermogravimetric analysis, 1% weight loss was seen approximately at 300 °C in the degradation reaction of PLA. The melting point of the polymer was determined approximately 150 °C with differential scanning calorimetry (DSC) (Appendix E). Since the temperatures of 225 °C and 250 °C were lower than the effective degradation temperature range detected by TGA. For the PLA degradation conducted at 225 °C, the yields of the solid, condensable and non-condensable products are given in Figure 4.2 with error bars. Most of the products were found to be solid in the reactor. These solid products could include the lower molecular weight compounds and oligomers. In addition, the condensable product yield was low.

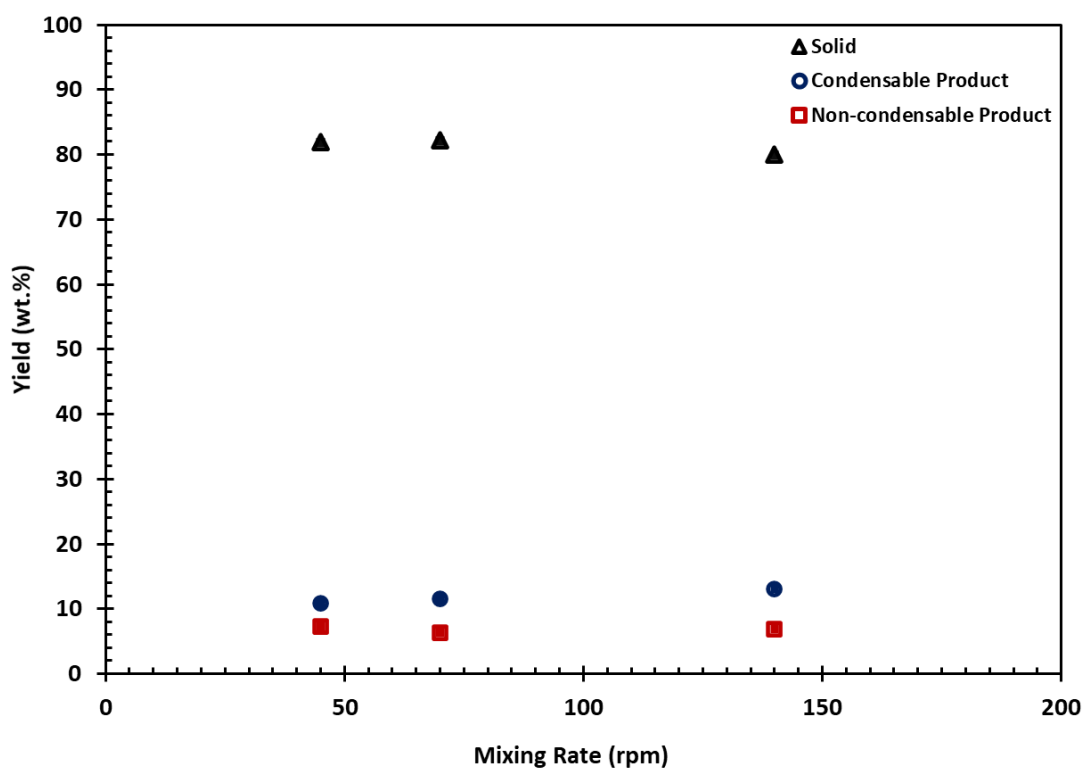


Figure 4.2. The effect of mixing rate on the yield of the products (225 °C, 60 min, 70 rpm, 50 ml/min).

At 70 rpm, the yields of the solid, condensable and non-condensable products were found to be 82%, 12%, and 6%, respectively. There was not seen significant alteration in the yield at the studied mixing rate range.

GC analysis was used to determine the compositions of the condensable and non-condensable products. In the studied mixing rate range, The condensable products were composed of 73 % D, L lactide and 27 % meso lactide by weight (Figure 4.3). The standard deviation of each product were determined in the condensable products. All product distribution figures were drawn with the error bars.

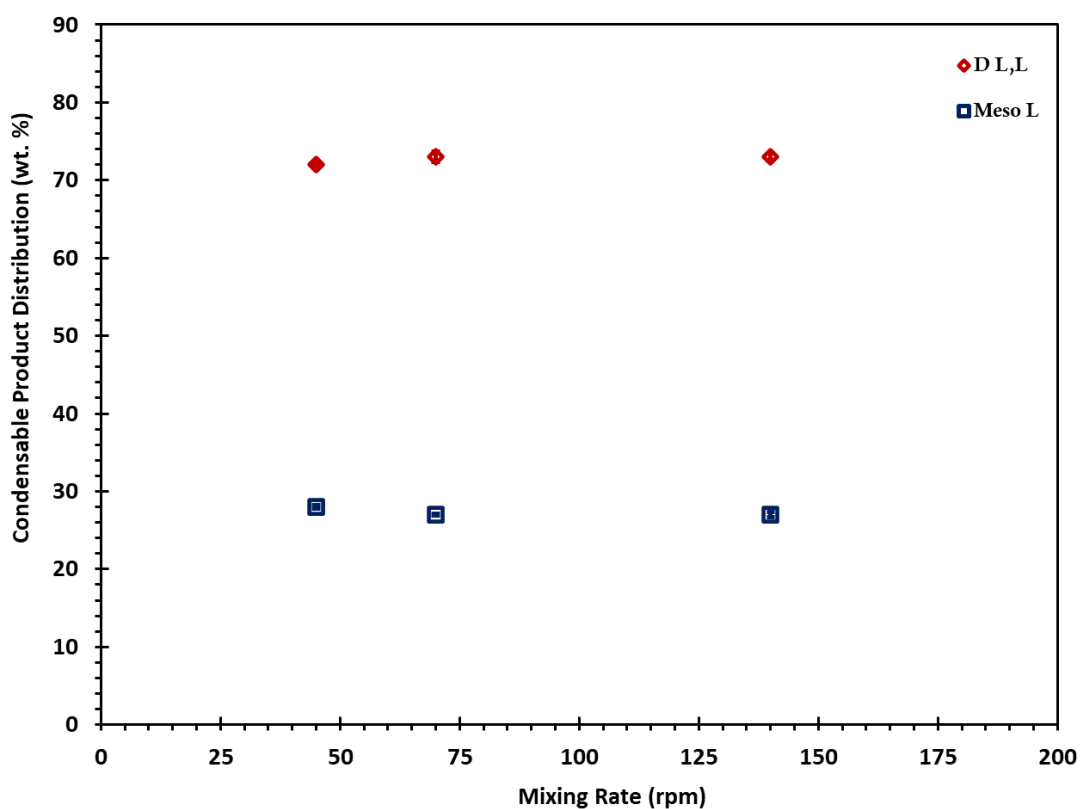


Figure 4.3. The effect of mixing rate on the condensable product distribution (225 °C, 60 min, 50 ml/min).

Lactide is used in the production of PLA by ring opening polymerization (Stefaniak & Masek, 2021). Lactide contains two stereocenters, which might be same in L,L-lactide and D,D-lactide and different in meso-lactide. Three isomers of the lactide is illustrated in Figure 4.4.

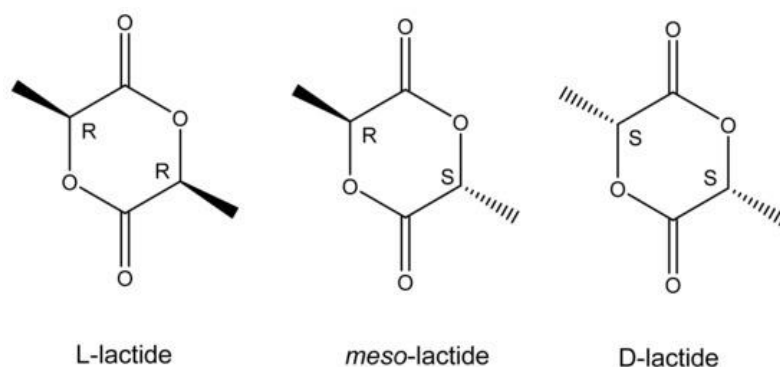


Figure 4.4. The isomers of lactide (Meimoun et al., 2022).

D-lactide and L-lactide have comparable physical properties, whereas meso lactide is different from the other two due to its lower melting point (De França et al., 2022). L lactide and D lactide could not be separated in gas chromatography due to their comparable properties as discussed in the literature (Feng et al., 2017).

L lactide and D lactide are generally preferred in the industrial production of PLA (de França et al., 2022). However, there have been some efforts for the production of PLA via meso lactide (Buffet & Okuda, 2011; Hador et al., 2022). Therefore, the production of lactide isomers contributes to the circular economy by pyrolysis. D and L lactide isomers might be formed by both transesterification and free radical reaction mechanisms of PLA (Sun et al., 2022). However, meso lactide can only be formed by free radical reaction mechanism (Kopinke et al., 1996; Sun et al., 2022).

The composition of non-condensable products was also detected using GC. The formation of acetaldehyde and carbon monoxide was observed at the reaction time of 15 minute at all mixing rates (Figure 4.5). The gas products were confirmed to have the same chemical composition regardless of the mixing rate.

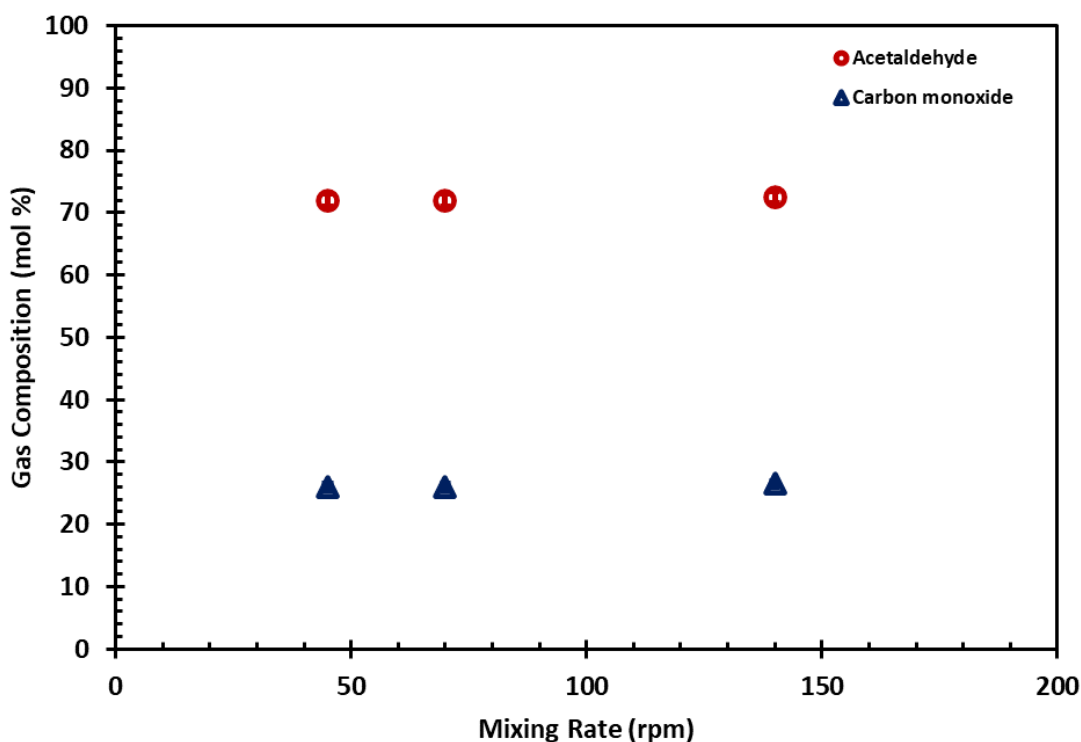


Figure 4.5. The effect of mixing rate on the non-condensable product distribution at the 15th min. (225 °C, 60 min, 50 ml/min).

At the 50th minute, carbon dioxide formation was observed in addition to acetaldehyde and carbon monoxide (Figure 4.6). The formation of acetaldehyde, carbon monoxide and carbon dioxide was also seen in the literature studies in the degradation of PLA (Kopinke et al., 1996, Sun et al., 2022). Gas composition did not change with the mixing rate at the 50th minute as well.

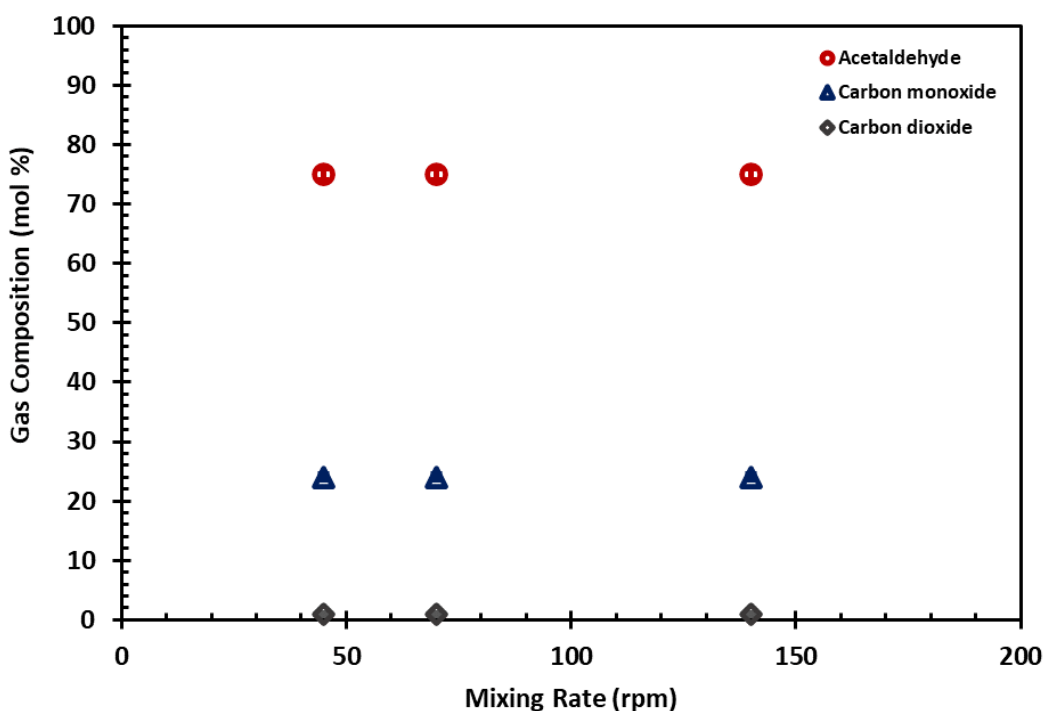


Figure 4.6. The effect of mixing rate on the non-condensable product distribution at the 50th min. (225 °C, 60 min, 50 ml/min).

The effect of the mixing rate was also studied at a higher temperature of 250 °C where the degradation reaction rate was higher. Similarly, the yield and product distribution were investigated with respect to mixing rate. In all mixing rates, the yields of the solid, condensable, and non-condensable products were found to be 11%, 40%, and 49% by weight, respectively.

The same composition was detected for the condensable and non-condensable products. The formation of lactide isomers and lactic acid was detected with a minor unidentified product at all mixing rates. 63% D L,L, 31% Meso L and 5% LA was produced with 1% U1, very small amount of unidentified product, by weight. Thus, increasing the mixing rate from 45 rpm to 140 rpm did not have a significant effect on the products. At both 15 and 50 minute, acetaldehyde, carbon monoxide, and

carbon dioxide were identified in the non-condensable products. By weight, acetaldehyde increased from 76% to 80% whereas carbon monoxide decreased from 23% to 19%. The carbon dioxide mole fraction remained unchanged. It was observed that the mixing rate in the studied range had no effect on the yield, product type and distribution. The effects of the other reaction parameters were investigated by selecting the mixing rate of 70 rpm.

4.1.2.3 The Effect of the Reaction Temperature on the Product Type and Distribution

To test repeatability, the experiment was performed at three times at 275 °C, 70 rpm for 60 minutes under 50 ml/min argon flow (Figure 4.7). There was not seen any solid product at the given reaction condition. The yields of the condensable and non-condensable products were found to be 38 % and 62 %, respectively. The error bars given in the figures represent the standard deviation. The standard deviation was determined to be 0.33. There were minor fluctuations in the yields of condensable and non-condensable products between the runs.

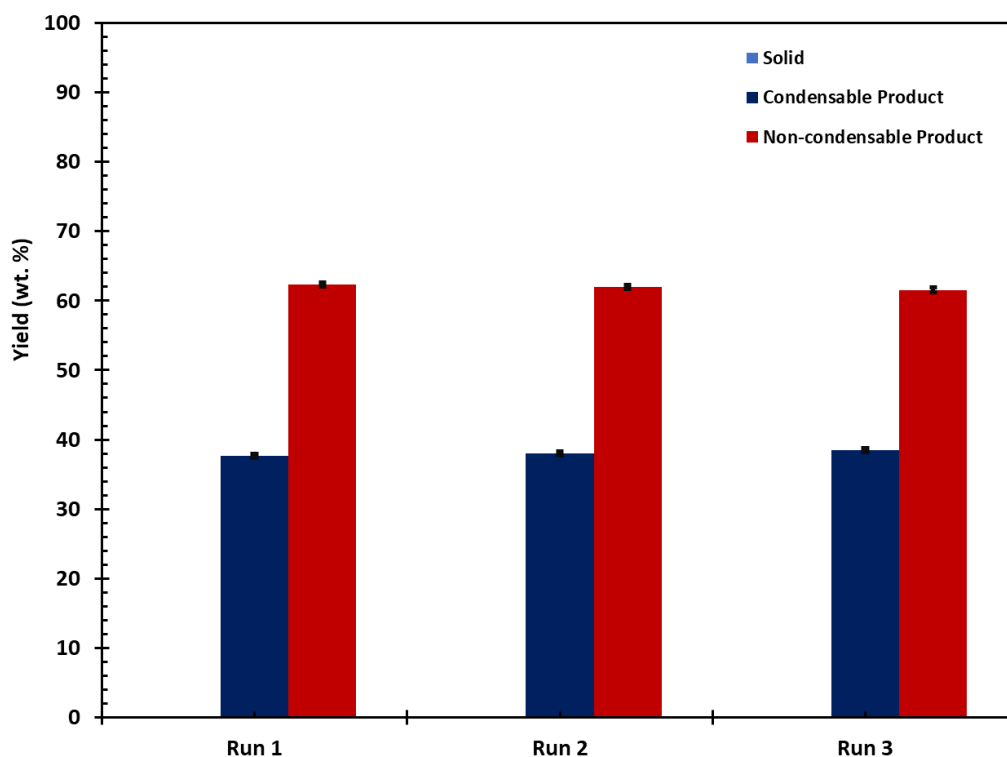


Figure 4.7. The yields of products obtained from three runs at different times (275 °C, 60 min, 70 rpm, 50 ml/min).

The composition of the condensable products is given in Figure 4.8. The formation of lactide isomers with lactic acid and propionic acid was detected. An unidentified product (U1) was seen at the retention time of 12.1 min. The majority of the products were lactide isomers with 48.7 wt.% D,L L and 33.0 wt.% Meso L. The amounts of LA, PA and U1 were determined to be 11.7 wt. %, 2 wt.% and 4.6 wt.%, respectively. In addition, the standard deviations of D,L L, Meso L, LA, PA, and U1 were found to be 0.47, 0, 0.47, 0, and 0.94, respectively.

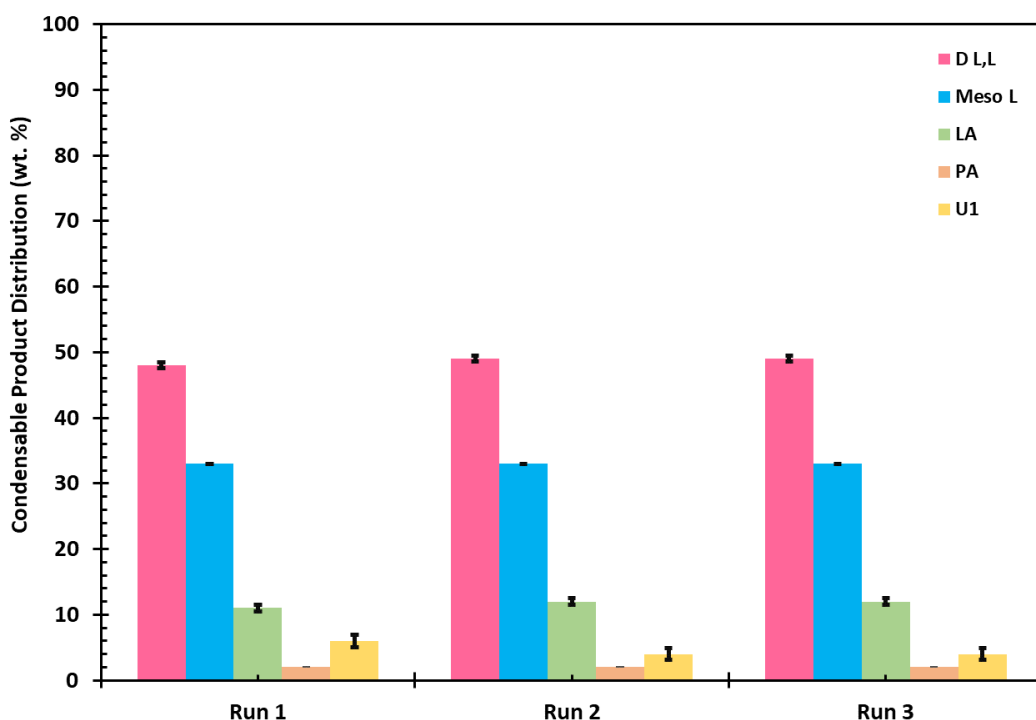


Figure 4.8. Product distribution of the condensable product obtained from three runs at different times (275 °C, 60 min, 70 rpm, 50 ml/min).

Lastly, the gas compositions of three runs were compared at the 15th min and 50th min (Figures 4.9 and 4.10). The main gas product was acetaldehyde in three runs. Carbon monoxide formation was also observed at the 15th min and 50th min. 5.3 mol% of carbon monoxide formed at the 15th minute while the production of carbon monoxide was determined to be 19 mol% at the 50th minute. Small quantity of carbon dioxide (1 mol%) was also detected. The results confirmed the reliability and repeatability of the experiments.

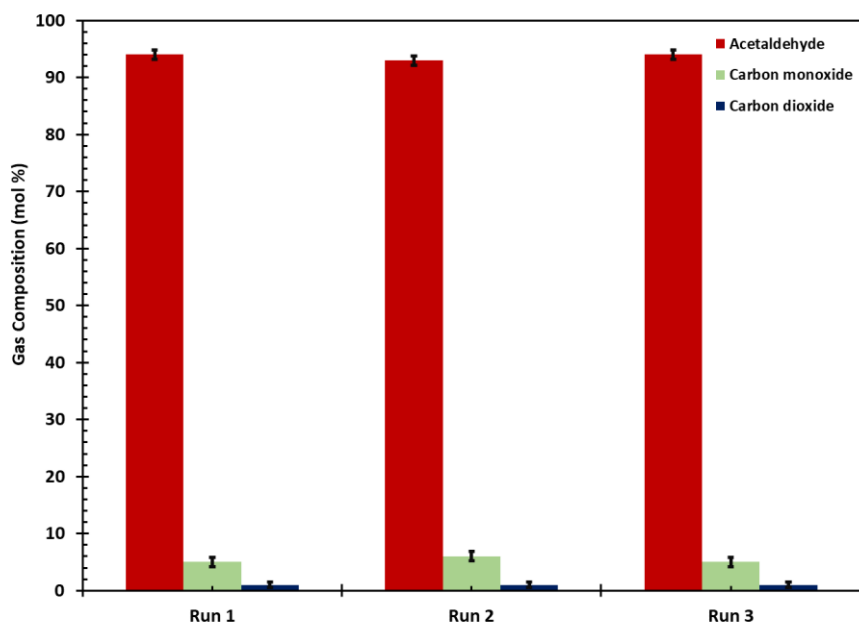


Figure 4.9. The gas composition obtained from three runs at the 15th min (275 °C, 60 min, 70 rpm, 50 ml/min).

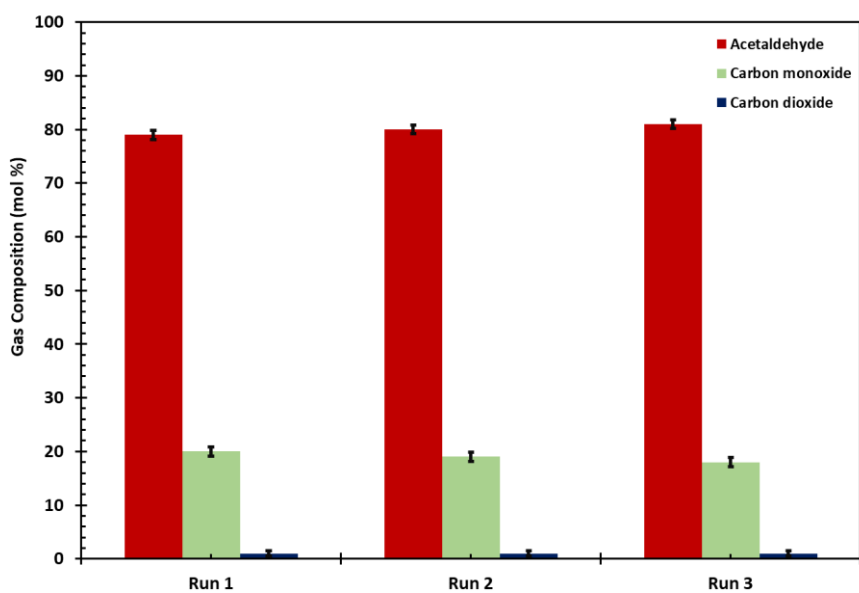


Figure 4.10. The gas composition obtained from three runs at the 50th min (275 °C, 60 min, 70 rpm, 50 ml/min).

To investigate the influence of temperature on product yield and distribution, the degradation of PLA was carried out at temperature range from 200 to 375 °C with an increment of 25 °C for 60 minutes while stirring the mixture at 70 rpm under the argon atmosphere (50 ml/min). The yield of the products at different temperatures is illustrated in Figure 4.11.

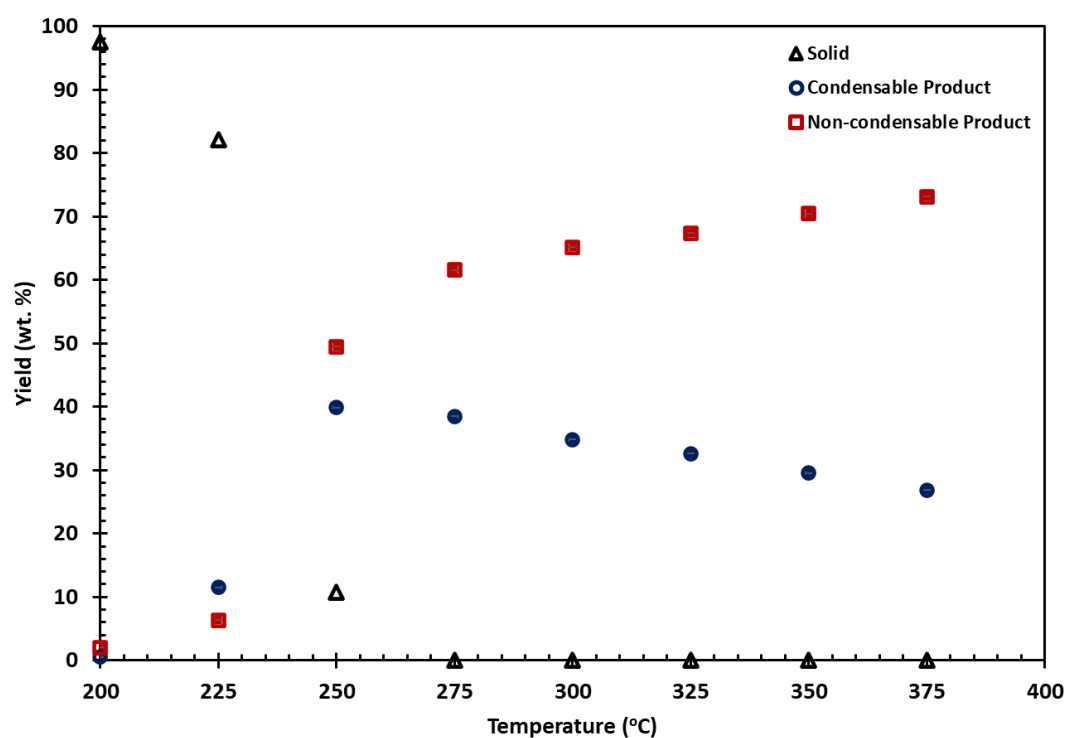


Figure 4.11. The effect of reaction temperature on the yield of products (60 min, 70 rpm, 50 ml/min).

At 200 °C, most of the reaction products were attained in the reactor and the solid yield was found to be 97.5 wt. %. The condensable and non-condensable products were determined to be 0.5 wt.% and 2 wt.%, respectively. Increasing the reaction time from 60 to 480 minutes at this temperature changed the amount of solid very

slightly from 94 to 92 wt.%. The high solid yield indicates the presence of higher molecular weight fragmentations.

By increasing the temperature from 225 °C to 250 °C, the solid yield declined from 82% to 11%. No solid was observed when the temperature reached 275 °C. Since the optimal reaction temperature was found to be 275 °C due to no solid formation and higher amount of condensable products.

The yield of non-condensable products steadily increased from 6% to 73% in the range of 225 °C and 375 °C. The yield of condensable products was increased from 12% to 40% between 225 °C to 250 °C, then was decreased from 40 % to 27 %.

TGA analysis of the solid products was performed in the temperature range of 30-500 °C at a heating rate of 5 °C/min under nitrogen atmosphere for the solid remaining in the reactor. The weight loss of the solid with respect to temperature is given in Figure 4.12.

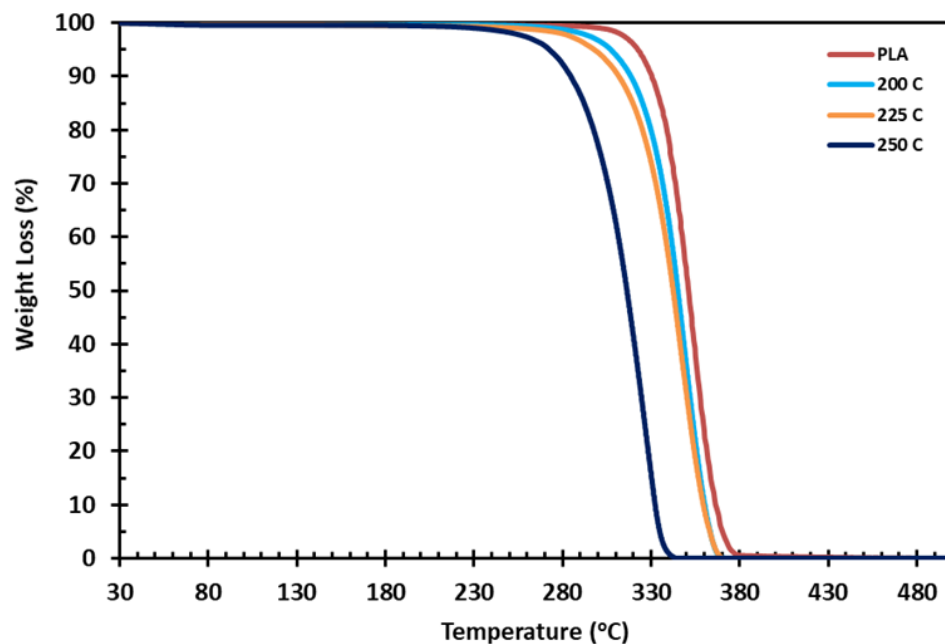


Figure 4.12. Degradation profiles of the solid products obtained at reaction temperature range of 200 °C and 250 °C.

As seen in Figure 4.12, increasing the reaction temperature tends to shift the degradation profile to the left. This shift indicates a decrease in degradation temperature. The decrease in degradation temperatures of the solid products became more remarkable with the increase of the reaction temperature from 225 °C to 250 °C. The degradation temperatures of PLA and solid products at 5% and 60% weight losses are given in Table 4.1.

Table 4.1. Degradation temperatures of solid products at 5% and 60% weight losses.

Sample	Degradation Temperature (°C)	
	At 5% Weight Loss	At 60% Weight Loss
PLA	322	354
Solid Products at 200 °C	306	348
Solid Products at 225 °C	297	346
Solid Products at 250 °C	272	320

While 5% weight loss for the PLA was observed at 322 °C, the same weight loss was seen at 306 °C, 297 °C and 272 °C for the solid products obtained at the reaction temperatures of 200 °C, 225 °C, and 250 °C, respectively. The degradation reaction of PLA initiates by altering the structure and breaking down the longer polymer chains and the molecular weight of solids could be less than PLA. Random chain scissions lead to a reduction of molecular weight of the polymer (Taubner and Shishoo, 2001; Chen et al., 2023).

The viscosity average molecular weights of the solids were determined using intrinsic viscosities. Calculation of the viscosity average molecular weight is given in Appendix F. Figure 4.13 shows the changes in the viscosity average molecular weight of the solid products obtained at 200 °C, 225 °C, and 250 °C.

The viscosity average molecular weight of PLA was found to be 169,098 g/mol. With increasing reaction temperature, the molecular weight of solid products decreased to 6,893 g/mol.

The decrease in the viscosity average weight of the solids with temperature indicated that PLA degraded to lower molecular weight compounds. This results are good agreement with both yield and TGA results.

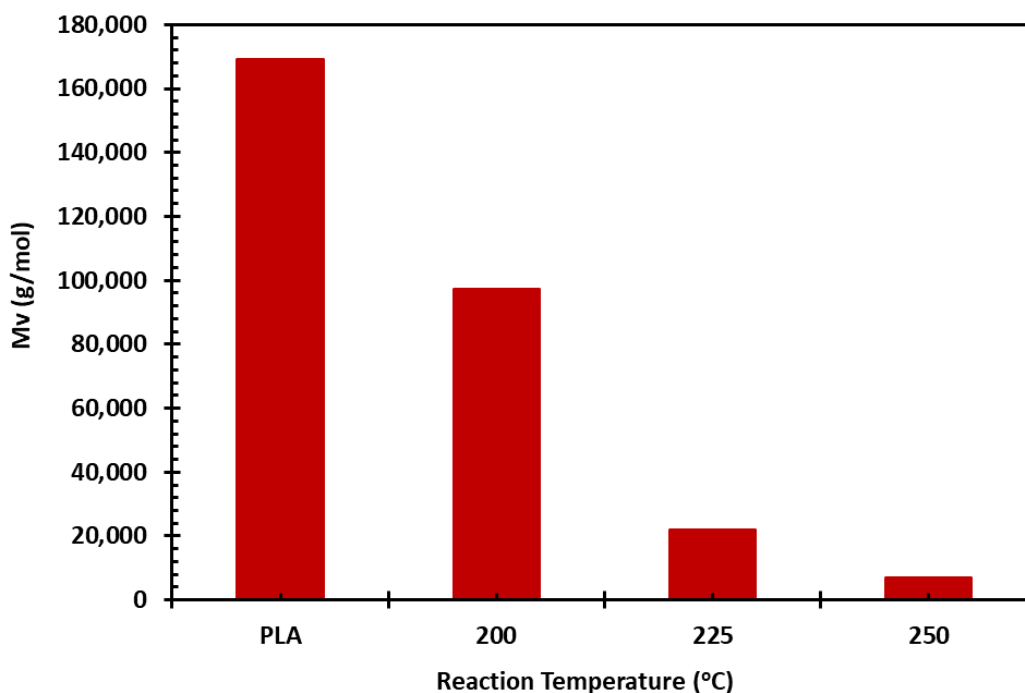


Figure 4.13. The viscosity average molecular weight of the solid product with respect to reaction temperature (60 min, 70 rpm, 50 ml/min).

The composition of the condensable products is illustrated in Figure 4.14. Composition of each condensable product was analyzed with GC at least four times. The standard deviations of each product were determined in the condensable products. All product distribution figures were drawn with the error bars.

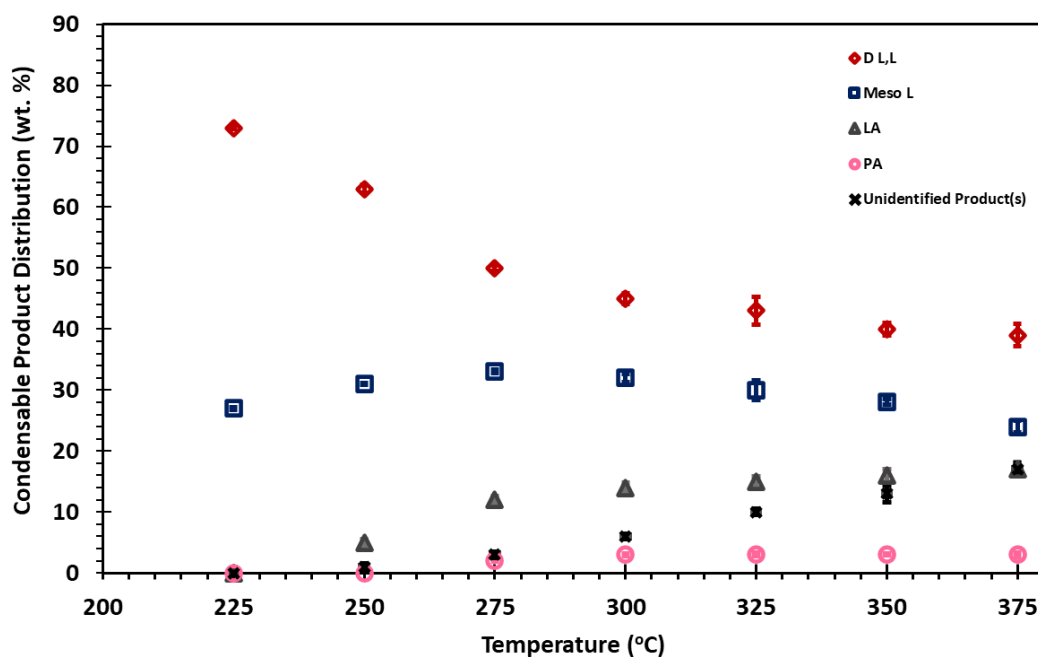


Figure 4.14. The effect of reaction temperature on condensable product distribution (60 min, 70 rpm, 50 ml/min).

D,L lactide (D L,L), meso lactide (Meso L), lactic acid (LA) were the major condensable reaction products, as shown in Figure 4.14. In addition to these products, propionic acid (PA) was detected. In some experimental sets, the presence of the unidentified products (U1 and U2) was observed. Increasing the reaction temperature tends a certain decrease in the amount of the D,L lactide while the change in the meso lactide was comparably low. Between the temperatures of 225 °C and 275 °C, there was a slight increase in the amount of meso lactide. Temperature was also found to accelerate the conversion of L, L lactide to meso lactide (Tsukegi et al., 2007). After 300 °C, there was seen a decrease in both isomers.

Lactic acid formation was started at 250 °C, and became significant at higher reaction temperature. The reason of the rise could be explained by the dominance of

intermolecular transesterification and cis elimination. Propionic acid formation was firstly observed at 275 °C.

Propionic acid was remained nearly the same in regardless of an increase in reaction temperature. Propionic acid formation could be related to the radical reactions through an alkyl-oxygen or acyl-oxygen homolytic breaking (Undri et al., 2014), and the decomposition of lactic acid (Komesu et al., 2017).

The changes in the areas of the unidentified products (U1 and U2) as a function of temperature are given in Figure 4.15. The formation of unidentified product (U1) was seen firstly at 250 °C with 1 wt.%. The amount of U1 was risen with increasing reaction temperature in the range of 250 °C-350 °C. The area of U1 increased approximately threefold in these temperature range. Another unidentified product (U2) was seen at the temperatures of 350 °C and 375 °C with U1. The area of U1 was reduced by half in this temperature range. Similarly, the area of U2 increased more than threefold. As seen from Figure 4.15, there was an increase in the areas of the unidentified products with temperature.

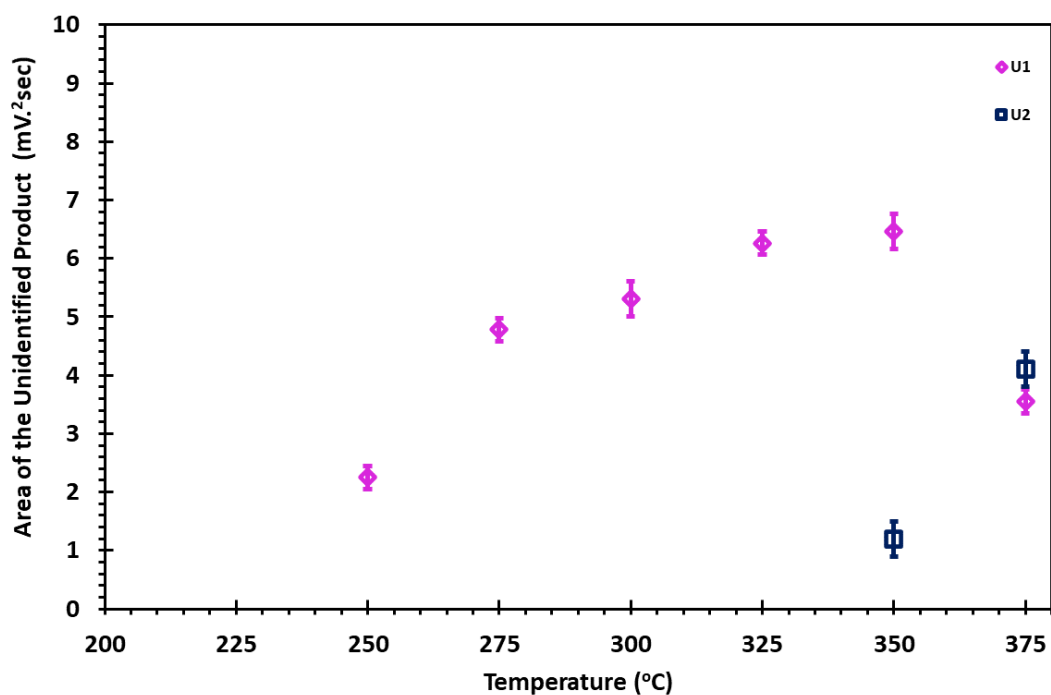


Figure 4.15. The effect of reaction temperature on the area of unidentified product.

The experimental studies continued to investigate the effect of reaction temperature on the non-condensable products. The degradation reaction of PLA was carried out at the temperature range of 225-375 °C for 60 min.

Gas products were analyzed during the degradation reaction of PLA. In the first analyses, the composition of gas products was obtained at the 15th min. The composition of gas products depending on reaction temperature is presented in Figure 4.16. The effect of reaction temperature on non-condensable product distribution at the 15th min. (60 min, 70 rpm, 50 ml/min).

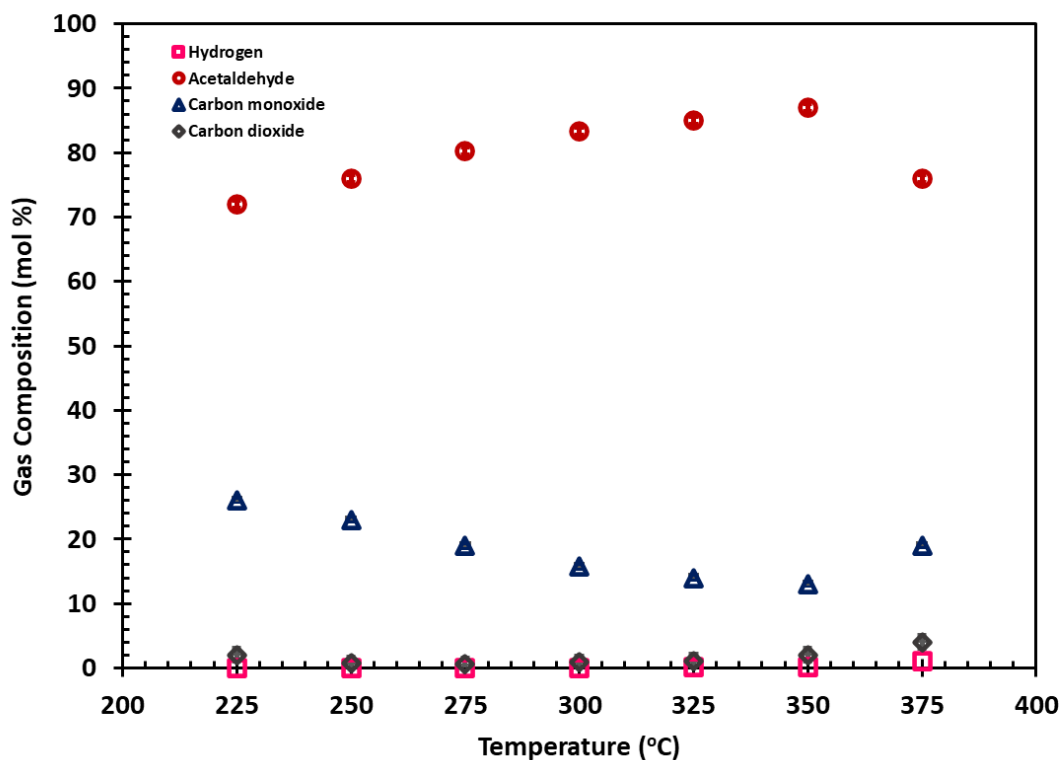


Figure 4.16. The effect of reaction temperature on non-condensable product distribution at the 15th min. (60 min, 70 rpm, 50 ml/min).

In the studied temperature range, carbon monoxide, carbon dioxide and acetaldehyde were observed. Thermal degradation of PLA was initiated by the homolytic cleavage of the C-O bond close to the ester group, followed by C-O bond breaking in the ester group and C-C bond cleavage. (Li et al., 2022). Following the homolytic scission, thermal breakdown mostly produced carbon monoxide, carbon dioxide, and acetaldehyde as volatile by-products (Li et al., 2022).

Most of the gas products was composed of acetaldehyde. Increasing reaction temperature tends to an increase in the formation of acetaldehyde. On the other hand, carbon monoxide decreased with temperature. It was also noted that higher temperatures accelerate the rate of decomposition of PLA (Mlyniec et al., 2016).

Carbon monoxide formation was seen at initial stages of the degradation while carbon dioxide were formed at higher temperatures (Mlyniec et al., 2016). The outputs of the study are coherent with literature.

After 275 °C, ethylene formation was observed in a trace amount. Hydrogen formation was also detected at 325 °C and 350 °C with a mole fraction lower than 1%. Acetaldehyde was maximized at the temperature of 350 °C whereas the maximum carbon monoxide was attained at 225 °C. The formation of acetaldehyde, carbon dioxide and hydrogen were also seen in the decomposition process of lactic acid (Komesu et al., 2017). Acetaldehyde was also formed by depending on the radical degradation reactions of PLA (Undri et al., 2014).

At the 50 minute of the reaction, gas composition was also analyzed (Figure 4.17). There was seen a remarkable similarity in gas composition profiles between the reaction times of 15 minute and 50 minute. The amount of acetaldehyde increased up to 325 °C. After 325 °C, it started decreasing. At 350 °C, hydrogen production was seen with 1% by moles.

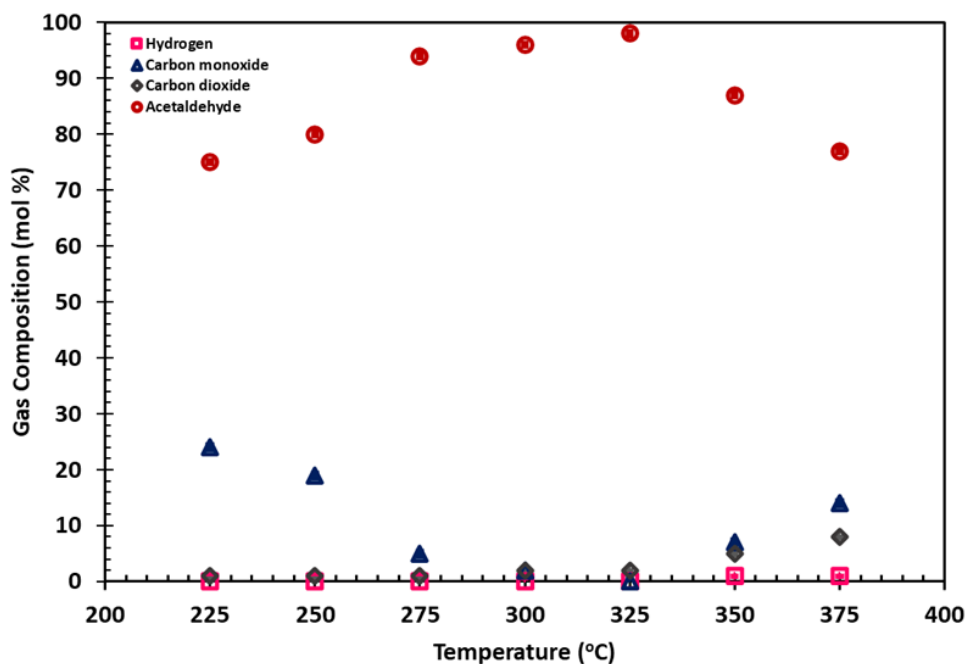


Figure 4.17 The effect of reaction temperature on non-condensable product distribution at the 50th min. (60 min, 70 rpm, 50 ml/min).

4.1.2.4 The Effect of the Reaction Time on the Product Type and Distribution

The effect of reaction time on yield and product distribution was investigated at two different reaction temperatures, 225 °C and 300 °C. PLA degradation reaction was carried out at 225 °C, 70 rpm under 50 ml/min flow at different reaction times. The reaction time was chosen between 60 and 480 min in this temperature. After the reaction was completed, similarly, the reaction products were obtained as solid, condensable, and non-condensable. The effect of the reaction time on product yield is illustrated in Figure 4.18 with the error bars.

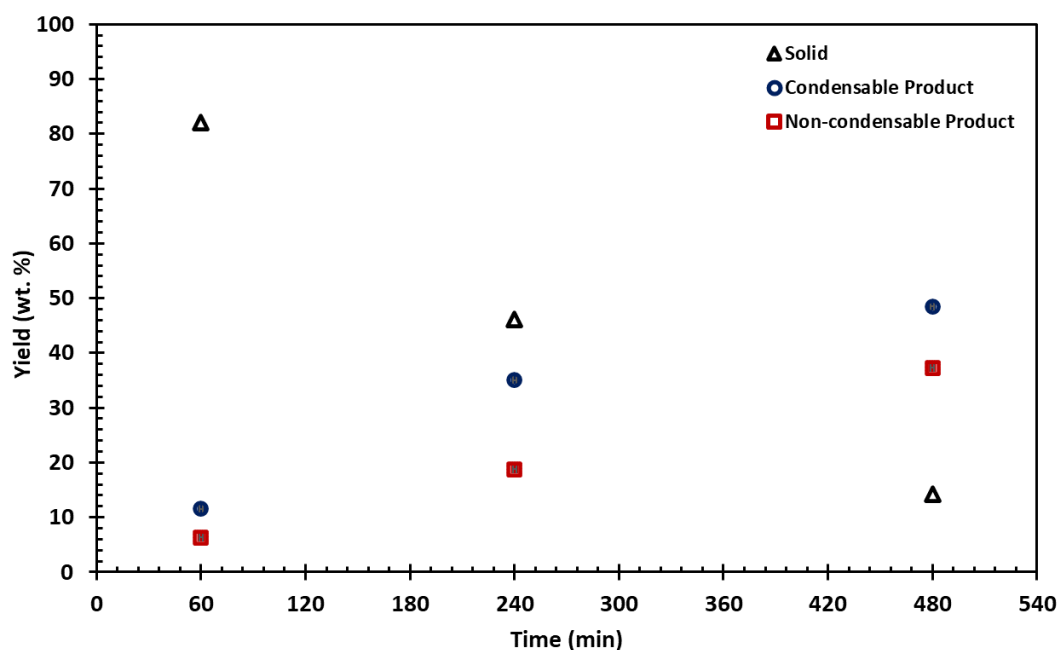


Figure 4.18. The effect of reaction time on the yield of product (225 °C, 70 rpm, 50 ml/min).

When the reaction time increased from 60 min to 480 minutes, the yield of the non-condensable products increased gradually from 6% to 37%, corresponding to a gradual decrease in the solid products in the reactor from 82% to 14%. This behavior was due to the degradation of PLA to lower molecular weight products.

Although the reaction time was extended up to 480 minutes, there was still solid in the reactor that was not degraded into condensable and non-condensable products. The thermal degradation of the solid products at different reaction times was investigated using TGA (Figure 4.19).

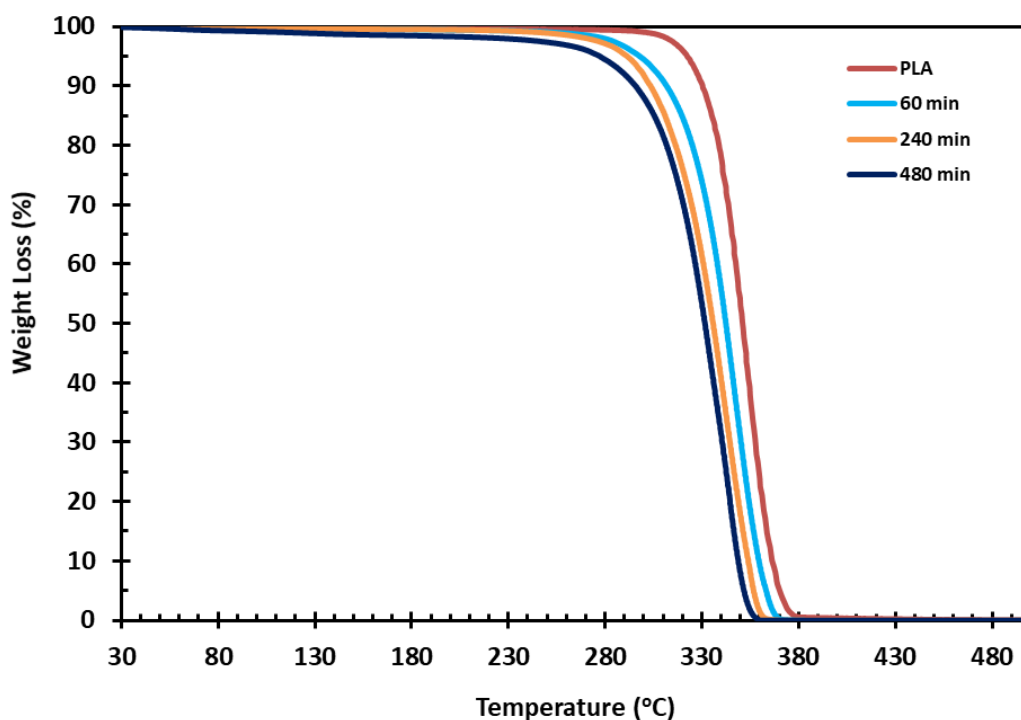


Figure 4.19. Degradation profile of the solid reaction products obtained at different reaction times.

As seen in the figure, an increase in reaction time shifts the degradation temperature to the left. This indicates that the PLA degradation reaction proceeds and reaction products can be generated through the breakdown of the chains. The decrease in degradation temperature of solid products with an increase in the reaction time was similar to the effect of temperature as in Figure 4.19. Degradation temperatures of solid products at 5% and 60% weight loss is given in Table 4.2. With an increase in reaction time, the degradation temperature was decreased at the point where 5% and 60% weight losses occur.

Table 4.2. Degradation temperatures of solid products at 5% and 60% weight losses.

Sample	Degradation Temperature (°C)	
	At 5% Weight Loss	At 60% Weight Loss
PLA	322	354
Solid Products at 60 min	306	346
Solid Products at 240 min	297	337
Solid Products at 480 min	272	336

The viscosity average molecular weight of the solids as a function of reaction time is given in Figure 4.20. With an increase in reaction time, the viscosity average molecular weight decreased from 169,098 g/mol to 5,561 g/mol after 480 minutes, which indicates that PLA degraded to lower molecular weight products.

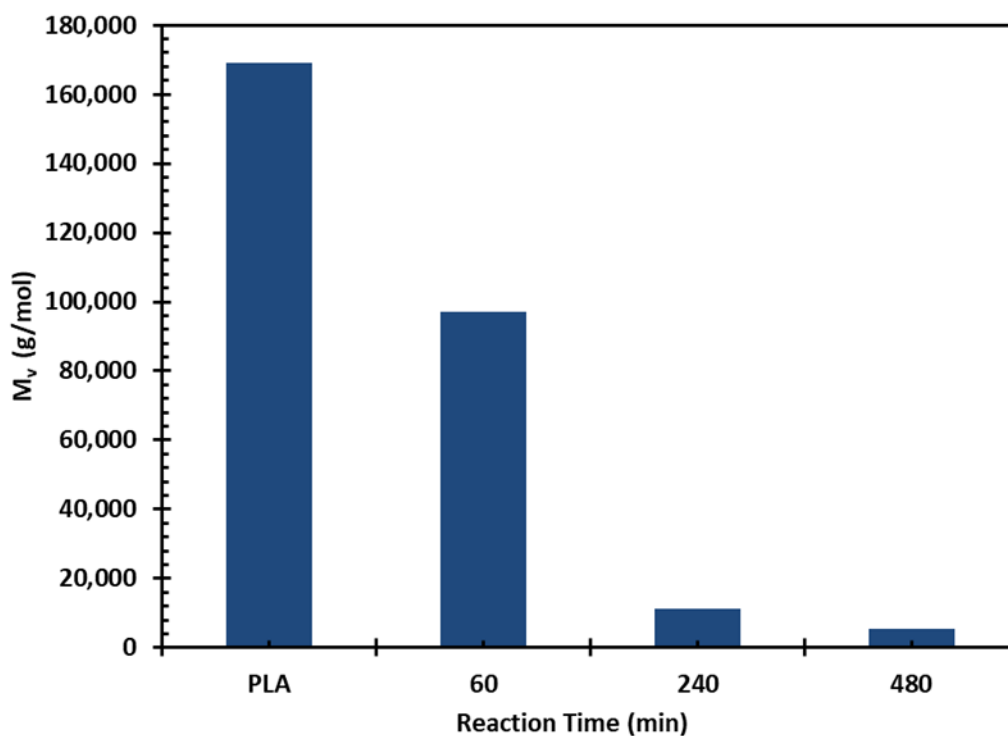


Figure 4.20 The viscosity average molecular weight of the solid products with respect to reaction time (225 °C, 70 rpm, 50 ml/min).

Figure 4.21 demonstrates the composition of the condensable products as a function of reaction time. At this reaction temperature, only the formation of D,L lactide (D L,L), meso lactide (Meso L) were observed. The linear decrease of D L,L and the linear increase of Meso L were observed in the experiments with increasing reaction time. The degradation of D L,L was also solely studied in the pyrolysis system at 300 °C for 60 minutes with the same mixing rate and flow rate. 14% of the D L,L was converted into Meso L.

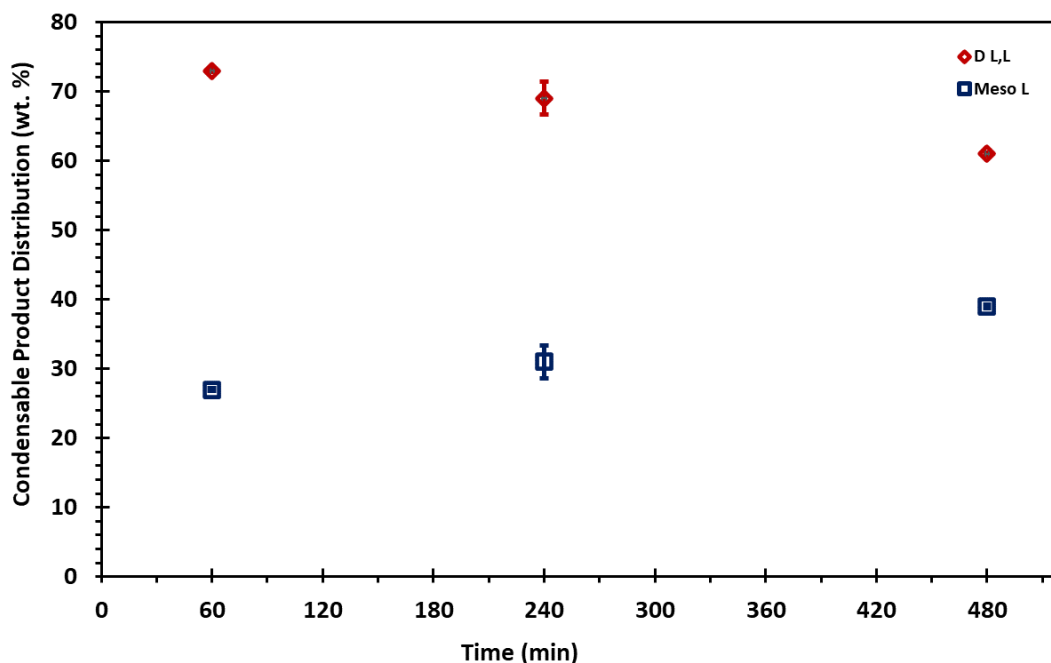


Figure 4.21. The effect of reaction time on condensable product distribution (225 °C, 70 rpm, 50 ml/min).

When reaction time extends up to 480 min, the amount of the meso lactide was risen from 27% to 39%. The composition of gas products was analyzed at selected time intervals for the experiments conducted 60, 240, and 480 minutes. The composition of gas products depending on reaction time is presented in Figure 4.22.

The formation of the acetaldehyde, carbon monoxide and carbon dioxide were seen in the studied reaction time range. A similar pattern was observed for the non-condensable products obtained at the reaction times of 60 and 240 minutes.

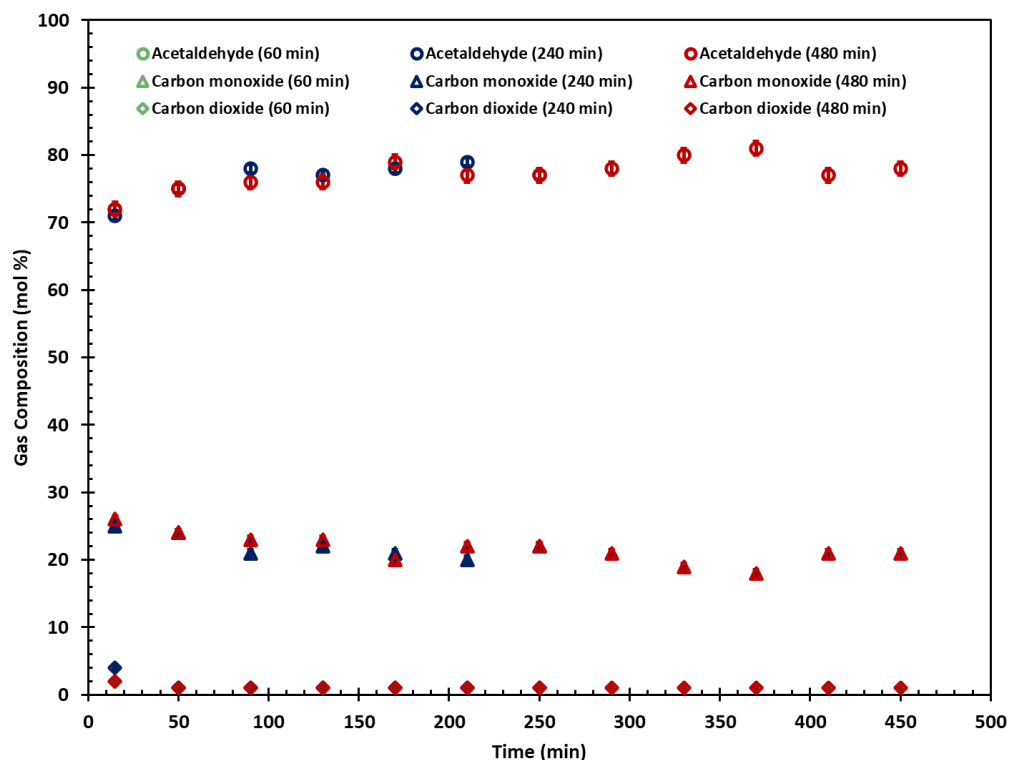


Figure 4.22. The effect of reaction time on non-condensable product distribution (225 °C, 70 rpm, 50 ml/min).

In addition, the effect of reaction time was further studied at 300 °C in the range of 15 minute and 60 minute at the same flow and mixing rate. The yield of the solid, condensable, and non-condensable products remained constant with increasing reaction time (Figure 4.23). There was not found any solid products in the reactor in the studied reaction time range. Condensable products were determined to be roughly 34%, while non-condensable products were 66% by weight .

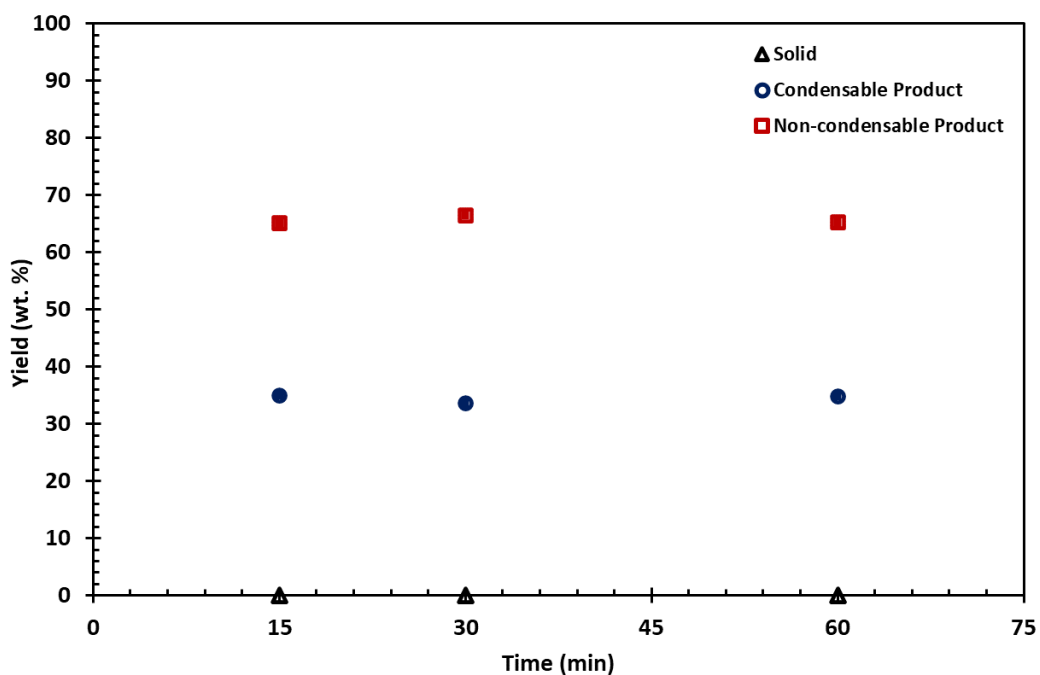


Figure 4.23. The effect of reaction time on the yield of products (300 °C, 70 rpm, 50 ml/min).

The composition of the condensable products was revealed to be remarkably similar for all reaction times. The amount of D,L lactide was slightly reduced from 49% to 45% by increasing reaction time from 15 minute to 30 minute and then remained constant. This was due to the higher reaction rate at 300 °C. The condensable product distribution was also quite similar for the experimental sets of 30 and 60 minutes (Figure 4.24).

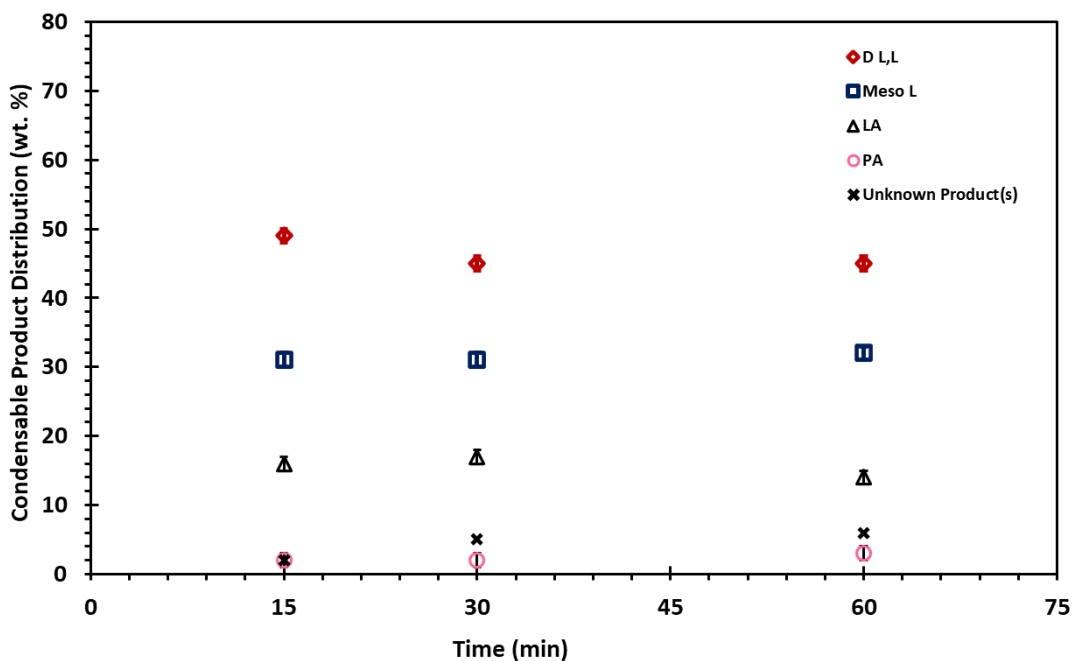


Figure 4.24. The effect of reaction time on condensable product distribution (300 °C, 70 rpm, 50 ml/min).

The formation of unidentified product (U1) was seen firstly at 15 minute with 2 wt.%. Change in the areas of the unidentified products (U1) as a function of temperature is given in Figure 4.25. The amount of U1 was increased with increasing reaction time The area of U1 increased by increasing reaction time up to 30 min. Then, both the area and the composition remained constant at the reaction times of 30 and 60 minutes.

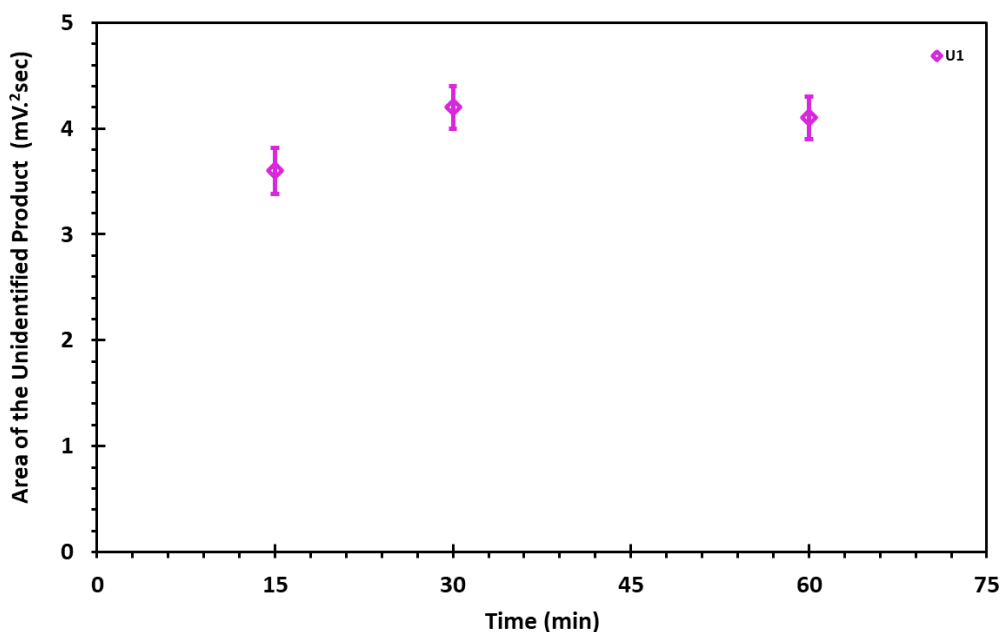


Figure 4.25. The effect of reaction time on the area of unidentified product (U1).

The non-condensable product distribution is shown in Figure 4.26. Acetaldehyde was the major reaction product at all reaction times. The mole percentage of acetaldehyde rose from 79% to 83% within the first 15 minute of the reaction. Carbon monoxide was decreased from 20% to 16% at given time interval. A small quantity of carbon dioxide was in the gas stream. The gas composition was found the same for the reaction times of 30 minute and 50 minute.

At 30 min, acetaldehyde increased up to 96% when the reaction time reached up to 30 minutes. Carbon monoxide was only 3% of the non-condensable products. After that time, the composition of the non-condensable products remained the same. This was an indication of the degradation reaction of PLA was completed before 30 minutes due to better reaction kinetics assured at 300 °C.

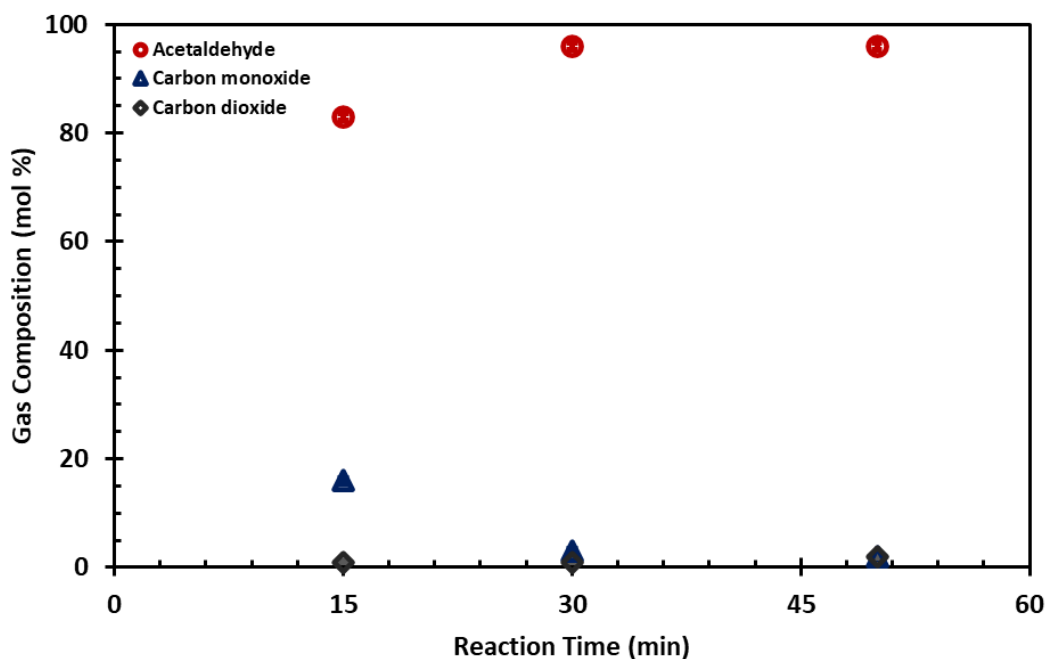


Figure 4.26. The effect of reaction time on non-condensable product distribution (300 °C, 70 rpm, 50 ml/min).

4.1.2.5 The Effect of the Flow Rate on the Product Type and Distribution

Lastly, the effect of the flow rate was evaluated at 225 °C. PLA degradation experiments were performed by stirring the mixture with a mixing rate of 70 rpm for 60 minutes under the argon flow between 25 ml/min and 100 ml/min. The effect of the flow rate on the yield is given in Figure 4.27.

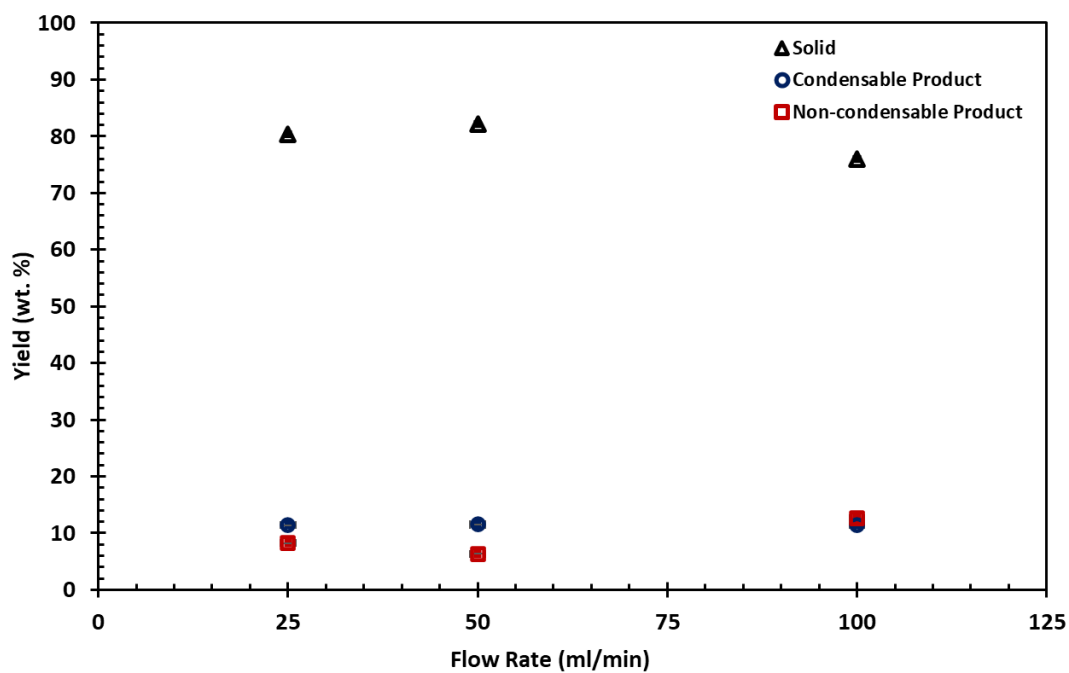


Figure 4.27. The effect of flow rate on the yield of products (225 °C, 70 rpm, 60 min).

Due to the lower reaction rate, the effect of the flow rate on yield and product distribution was not much significant at 225 °C between 25 ml/min and 50 ml/min. The solid yield was reduced from 82% to 76% when the flow rate raised from 50 ml/min to 100 ml/min. There was not observed a significant change on the yield. The composition of the condensable products is illustrated in Figure 4.28.

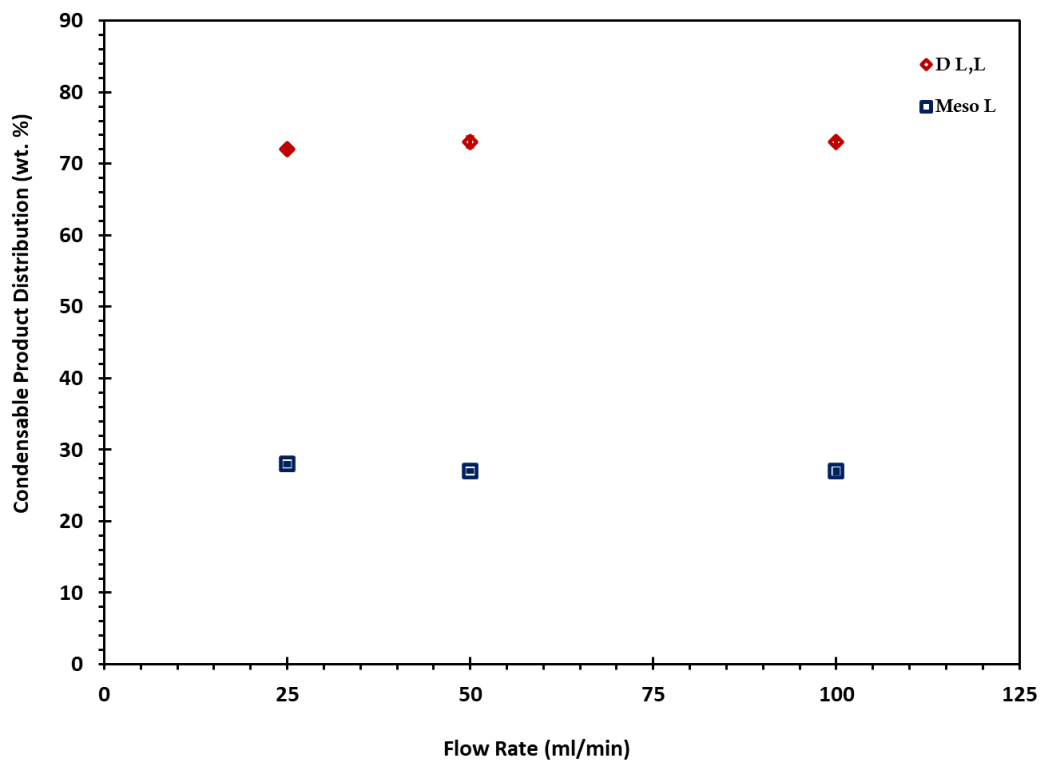


Figure 4.28. The effect of flow rate on condensable product distribution (225 °C, 70 rpm, 60 min).

It is interesting to note that this reduction in solid tends to an increase in non-condensable products while the amount of the condensable products remained approximately constant with 73% D L lactide and 27% meso lactide. The contents of the gas products are presented in Figure 4.29. At the reaction temperature of 15 minute, the maximum amount of acetaldehyde was obtained as 72% at 50 ml/min; however, there was not found remarkable discrepancies by depending on flow rate.

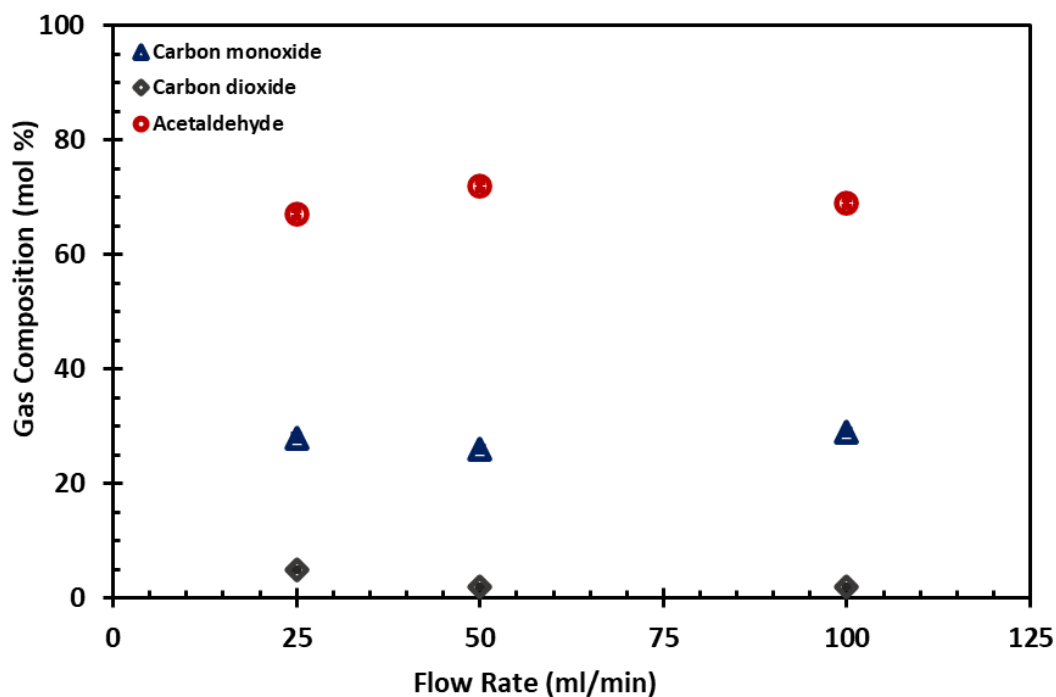


Figure 4.29. The effect of flow rate on non-condensable product distribution at the 15th minute (225 °C, 70 rpm, 60 min).

A similar observation was done at ongoing reaction time of 50 minute (Figure 4.30). The rapid removal of the gas products tends to increase in acetaldehyde formation. The amount of acetaldehyde was risen from 74% to 78% with an increase of 25 ml/min flow rate, then all non-condensable products was composed of acetaldehyde & carbon monoxide.

Within the investigated flow rate range, these results demonstrated that flow rate had no substantial influence on the yield and composition of the product. The reaction temperature and reaction time had highly important in product yield and composition.

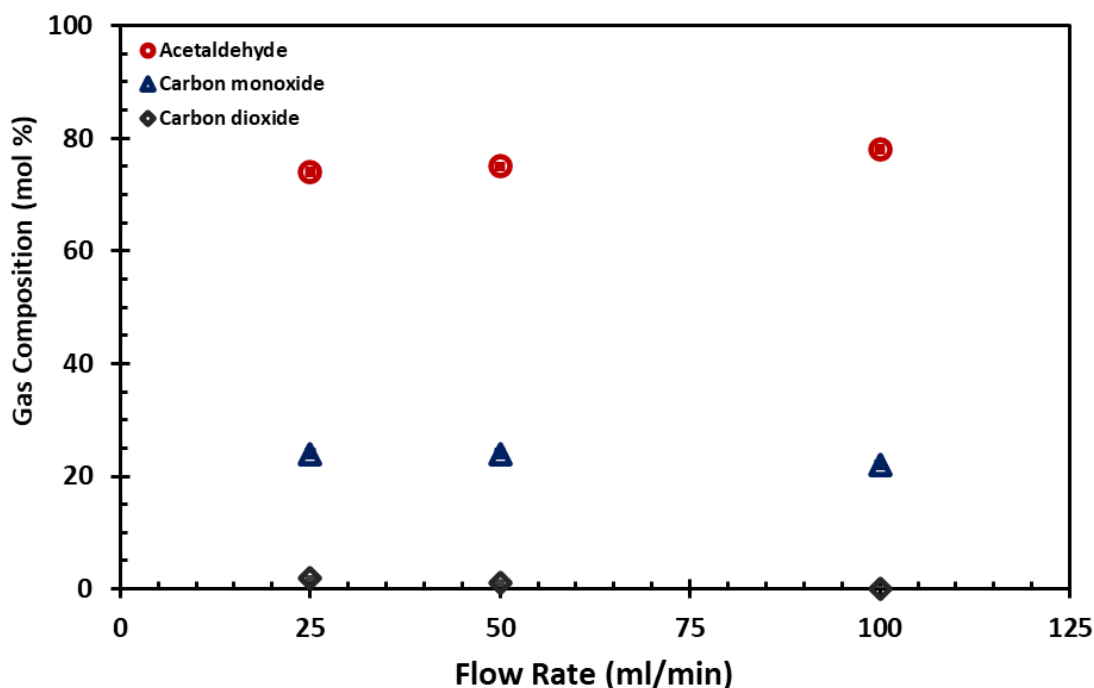


Figure 4.30. The effect of flow rate on non-condensable products distribution at the 50th minute (225 °C, 70 rpm, 60 min).

4.1.3 Degradation of PLA in Supercritical Carbon Dioxide

PLA depolymerization was conducted in a batch reactor under supercritical CO₂ medium to evaluate the influence of four major parameters, namely reaction temperature, pressure, time and mixing rate on the yield and product distribution of PLA depolymerization. At the end of the reaction, both solid and gas products formed. Depending on the reaction conditions, the solid products, which were collected in the reactor, were either in tar or wax form. The weight of the solid products was measured, and the amount of the gas products was calculated by subtracting the weight of the solid products from the weight of PLA loaded to the reactor (Appendix G). The composition of the solid product was determined from GC analyses. The mole numbers of the condensable products were calculated with

relative response factor (RRF). The weight fractions of the solid product were subsequently determined. The calculation procedure is given in Appendix C.

4.1.3.1 The Effect of Mixing Rate on the Product Type and Distribution

In the PLA depolymerization reactions carried out in supercritical CO₂, PLA was in the molten state at applied temperatures while no cosolvent was used. The solubility of low molecular weight PLA in supercritical carbon dioxide was low (Gregorowicz and Bernatowicz, 2009). Due to its high molecular weight, PLA used in this study is not soluble in supercritical carbon dioxide. However, it was expected that supercritical CO₂ could dissolve the possible decomposition products such as lactide isomers or lactic acid (Stassin et al., 2005, Gregorowicz and Bernatowicz, 2009). This could facilitate the mass transfer of the products from the polymer, thus could contribute to isolation of the depolymerization products. In this regard, the mixing rate was important as it could affect the rate of dissolution of the depolymerization products into the supercritical CO₂ phase. Therefore, the effect of mixing rate was evaluated by carrying out the degradation reaction of PLA at 200 °C, 103 bar for 120 minutes at three different mixing rates (0, 70 and 140 rpm). The reaction temperature was set at 200 °C so that the polymer was above its normal melting temperature and below the starting point of its thermal degradation, which is around 300 °C (Sivri et al. 2019). The pressure of 103 bar provides a sufficiently higher pressure than the critical pressure of CO₂, yet it is relatively low for supercritical fluid processes. The effect of the mixing rate on product yield is illustrated in Figure 4.31. To test the repeatability of the system, the experiment was performed three times at 200 °C, 103 bar and 70 rpm for 120 minutes. The standard deviation of the solid yield was determined to be 0.32, which is represented with the error bars in Figure 4.31.

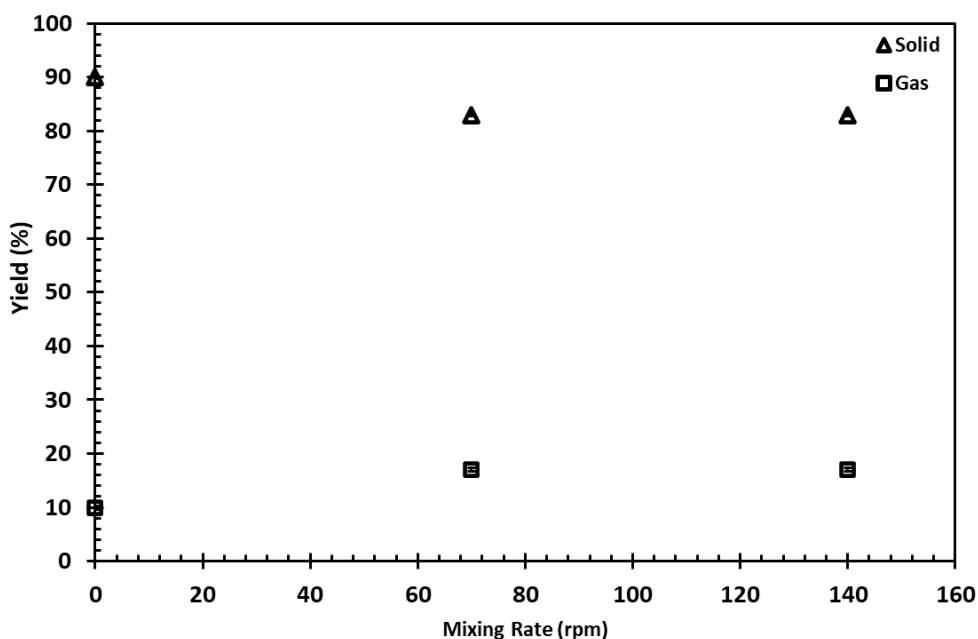


Figure 4.31. The effect of the mixing rate on the yield of the products (200 °C, 103 bar, 120 min).

The gas formation in all mixing rates supports that PLA decomposed into low molecular weight components. The yield of solid products decreased approximately from 90 to 83 percent by mass as the mixing rate increased to 70 rpm, which corresponds to an increase in the gas products with mixing rate. It was found that further increase in the mixing rate from 70 rpm to 140 rpm did not have any effect on the yield of the solid products. The solid products were analyzed using GC, and the distribution of components in the solid products are given in Figure 4.32. The standard deviation of each component was calculated after all sample measurements were performed at least four times.

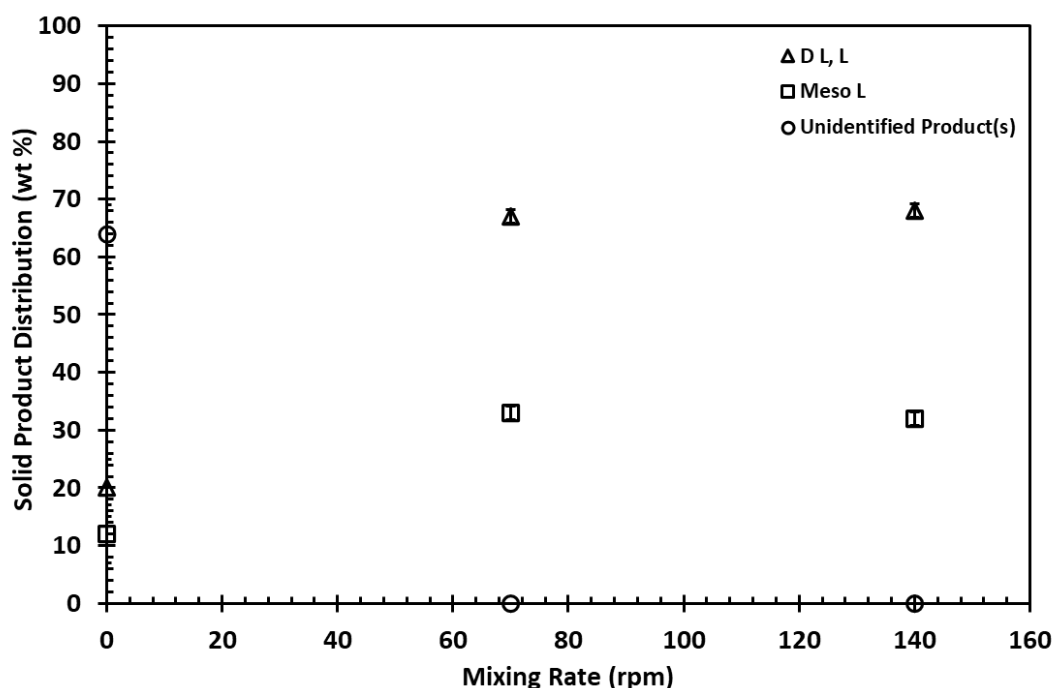


Figure 4.32. The effect of the mixing rate on the solid product distribution (200 °C, 103 bar, 120 min).

GC analysis of the solid products of the reaction carried out at 200 °C, 103 bar for 120 minutes without mixing, showed two peaks, which were D,L lactide (D L, L) and meso lactide (Meso L). However, it was found that only 32% of the solid products were composed of these components. Some other products, low molecular weight PLA and oligomers were observed. Those products that were undetectable by GC constituted the remaining of the solid products, which is represented as unidentified products in Figure 4.32. By increasing the mixing rate, the conversion of PLA to lactide isomers was sharply improved. Solid products of the reactions conducted at the same conditions but 70 rpm and 140 rpm composed of the lactide isomers, which consisted 67 % of D,L lactide and the balance was meso lactide. Lactide formation via thermal degradation of PLA was seen in many reaction pathways such as the reactions of transesterification, free radical and cis elimination

(Kopinke et al., 1996; Yi et al. 2017; Cailloux, 2015). These experiments showed that lactide formation also occurred in supercritical CO₂ medium at relatively low temperatures compared to degradation studies of PLA in the literature. PLA depolymerization was effectively realized at remarkably lower temperatures in supercritical CO₂ medium. Carbon dioxide serves primarily as a solvent when it is in direct contact with a polymer (Nalawade et al., 2004). In polymerization studies conducted with carbon dioxide, the viscosity of the produced polymer is decreased by dissolved carbon dioxide and, as a result, conversion is boosted through greater mass transfer (Kendall et al., 1999; Leitner et al., 2002). It is possible that in PLA degradation, supercritical carbon dioxide decreased the viscosity of the molten polymer and enhanced mass transfer in the reaction medium, which was further improved with mixing. The striking increase in the lactide yield with mixing is due to the enhanced the rate of dissolution and diffusion of the lactide isomers into the supercritical phase, increasing the lactide yield of the reaction.

The effects of temperature, time, and pressure on the performance of PLA depolymerization in supercritical CO₂ in terms of product yield and composition were subsequently evaluated at 70 rpm as identical solid yield and lactide isomer distribution were obtained at both 70 rpm and 140 rpm of mixing rate. The effects of the other parameters were investigated by selecting the mixing rate of 70 rpm.

4.1.3.2 The Effect of Reaction Time on the Product Type and Distribution

The effect of reaction time on the PLA degradation product distribution and yield was investigated in two independent experimental sets. The first set was carried out at 200°C, 103 bar, 70 rpm of mixing rate for different reaction times between 60 and 240 min. After the reaction was completed, similarly, the reaction products were obtained as solid and gas. The effect of the reaction time on their yields is illustrated in Figure 4.33. The yield of gas products increased, and solid products decreased slightly with reaction time.

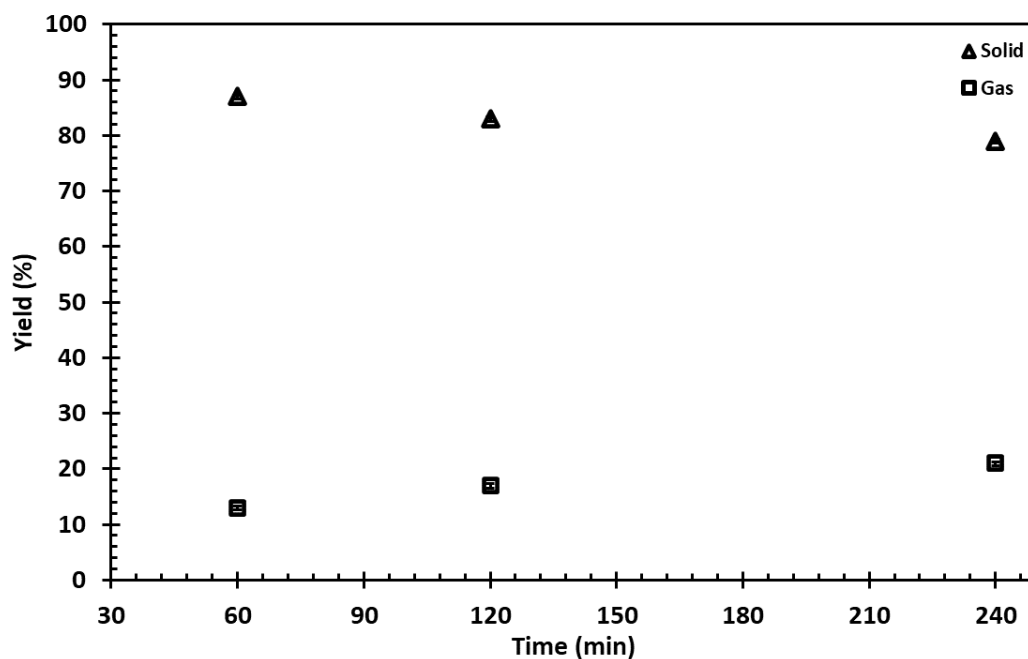


Figure 4.33. The effect of reaction time on the yield of products (200 °C, 103 bar, 70 rpm).

When the reaction was carried out for 60 min, the solid products detected by GC were composed of D, L lactide and meso lactide, while they occupied 67 % of the solid products (Figure 4.34). The balance was the unidentified products such as oligomers or lower molecular weight compounds. Increasing the reaction time to 120 min leads to a higher conversion of PLA to lactide isomers, which constitute the entire solid products. Increasing the reaction time further to 240 min results in formation of lactic acid thus decreasing the weight fraction of lactide isomers in solid products. Increasing the reaction time causes the conversion of PLA to low molecular weight products. The lactic acid production indicates that in depolymerization of PLA in supercritical CO₂, transesterification, free radical or cis elimination reactions become more effective at longer reaction time.

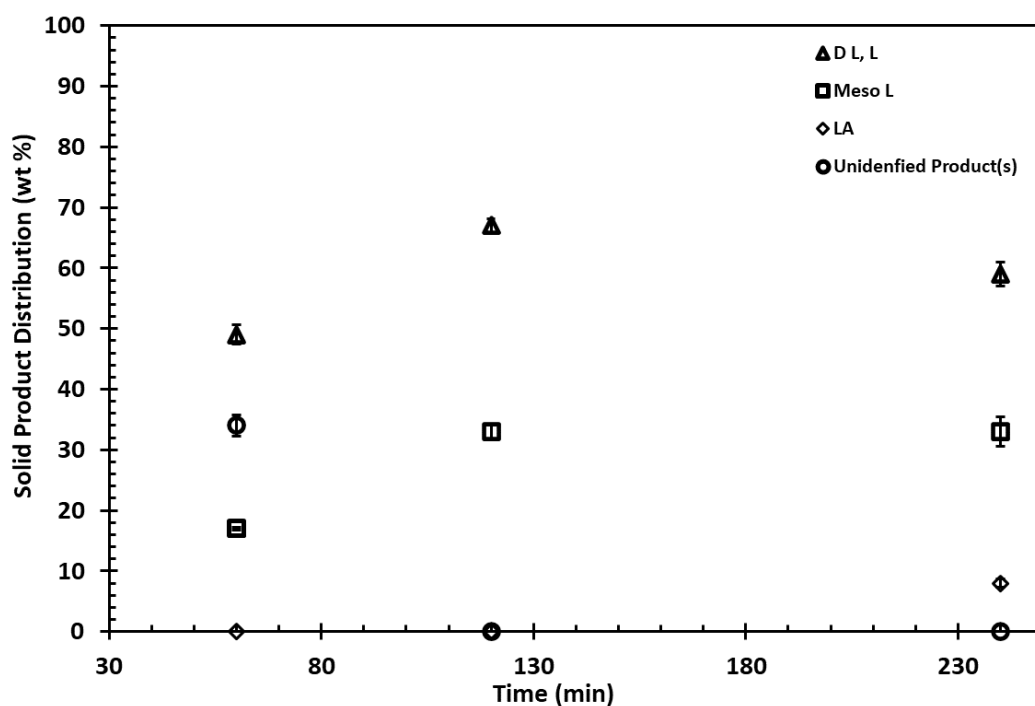


Figure 4.34. The effect of reaction time on the solid product distribution (200 °C, 103 bar, 70 rpm).

The influence of reaction time on PLA degradation carried out at a higher temperature, 220 °C, was evaluated with reaction runs for 30, 60, and 120 min at the same pressure and mixing rate. The solid and gas product yields had a similar trend with those at the lower temperature; i.e., a slight decrease in the yield of solid products and the slight increase in the yield of gas products were observed (Figure 4.35). However, the GC analysis of the solid products showed that at 220 °C, in 30 min, the solid products were entirely composed of D, L and meso lactide isomers and lactic acid in Figure 4.36. Lactic acid was produced in the depolymerization reaction carried out for 240 min at 200 °C, while a 20 °C increase in the reaction temperature led to formation of lactic acid only in 30 min of reaction time. The amount of lactic acid increased by about three folds with time increasing to 120 min, which could be attributed to the greater influence of transesterification, free radical

and cis elimination reactions during the depolymerization of PLA at the higher temperature. As a consequence, the amount of D L, lactide was reduced from 59% to 52%.

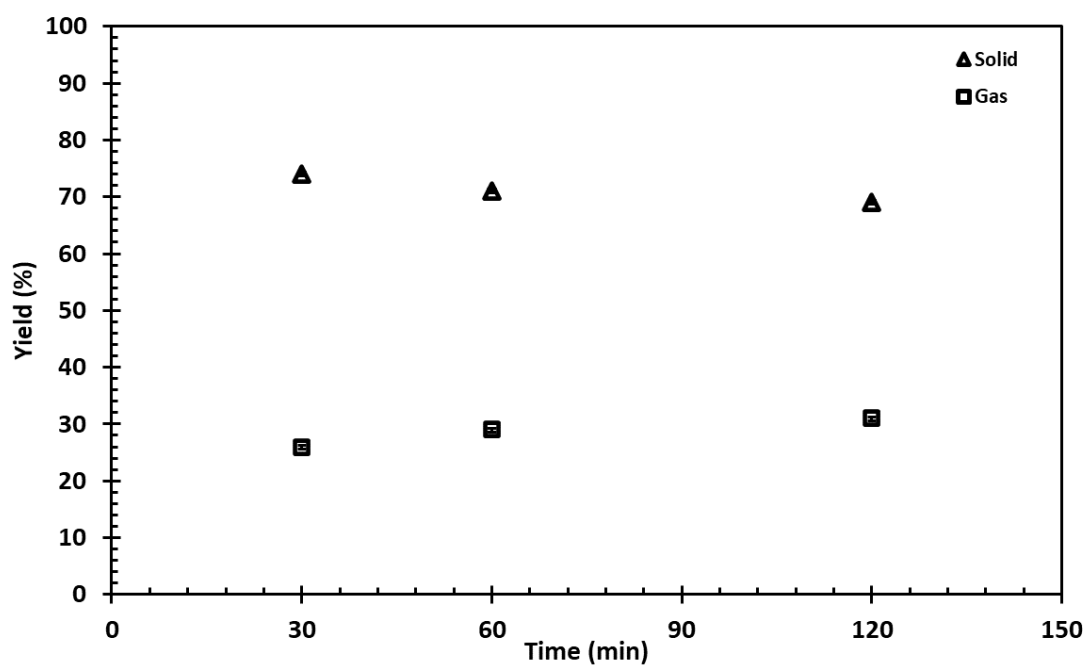


Figure 4.35. The effect of reaction time on the yield of products (220 °C, 103 bar, 70 rpm).

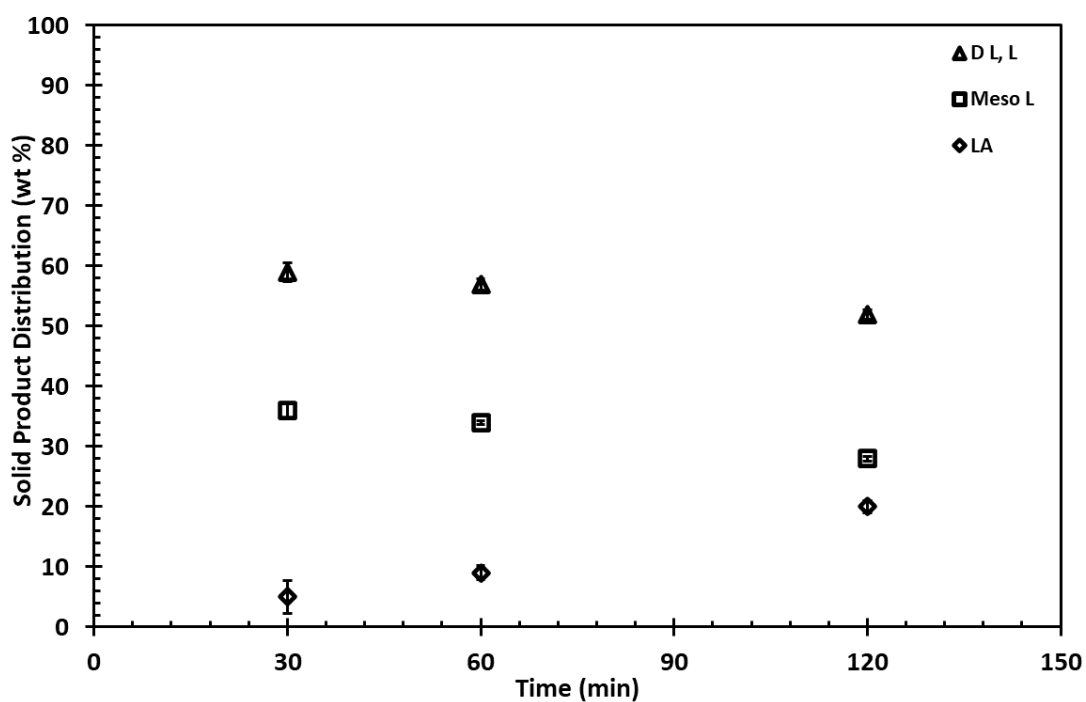


Figure 4.36. The effect of reaction time on the solid product distribution (220 °C, 103 bar, 70 rpm).

4.1.3.3 The Effect of Reaction Temperature on the Product Type and Distribution

The degradation reaction of PLA was carried out at five different temperatures in the range of 190 °C and 230 °C at 103 bar, 70 rpm for 120 min. When the temperature increased from 190 °C to 230 °C, the yield of the gas products increased gradually from 6% to 36%, corresponding to a gradual decrease in the solid products obtained in the reactor from 94% to 64% (Figure 4.37). When PLA degraded at 190 °C, about 80 % of the solid products by weight was composed of D,L lactide and meso lactide, while balance were similarly unidentified products (Figure 4.38). About three quarters of the lactide isomers was D,L lactide type. As the temperature was increased to 200 °C, the entire solid products were composed of D,L lactide and meso

lactide, and no unidentified products remained, which was also valid at the higher studied temperatures. The formation of lactic acid began at 210 °C and became more pronounced as temperature increases, which was evidence for the occurrence of transesterification, free radical and cis elimination reactions in depolymerization of PLA at these conditions. As the composition of lactic acid in the solid products increased from 8 % to 32 % by weight, the composition of D,L lactide and meso lactide decreased to 47 % and 21 % by weight, relatively.

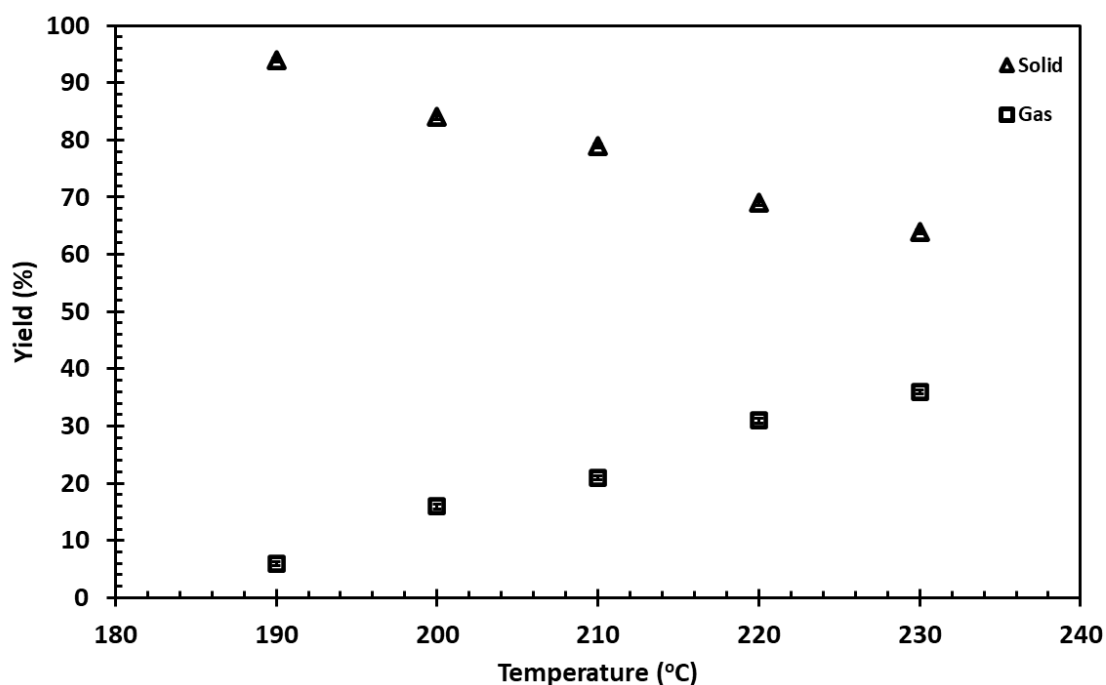


Figure 4.37. The effect of reaction temperature on the yield of products (103 bar, 120 min., 70 rpm).

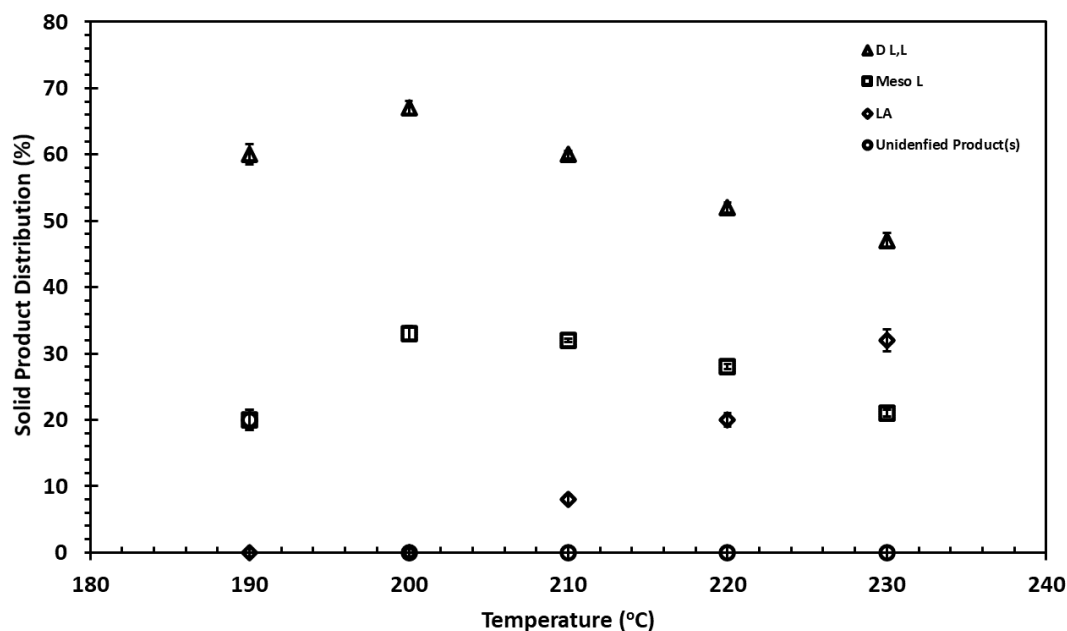


Figure 4.38. The effect of reaction temperature on the solid product distribution (103 bar, 120 min, 70 rpm).

Carbon dioxide mainly serves as an inert reaction medium, in some applications, it can interact with some functional groups (Leitner et al., 2002). Supercritical carbon dioxide with an increase in temperature may dissolve the decomposition products. Dissolution of the decomposition products may ensure the mass transfer of the products from reaction medium.

4.1.3.4 The Effect of Reaction Pressure on the Product Type and Distribution

The impact of the reaction pressure was investigated at two different temperatures of 200 and 220 °C. As first, the experiments were carried out at 200 °C for 120 minutes between 103 and 206 bar. As an alternative experimental set, degradation of

PLA was realized at 220 °C for 30 minutes between 103 and 206 bar. The product yield obtained at 200 °C was seen in Figure 4.39.

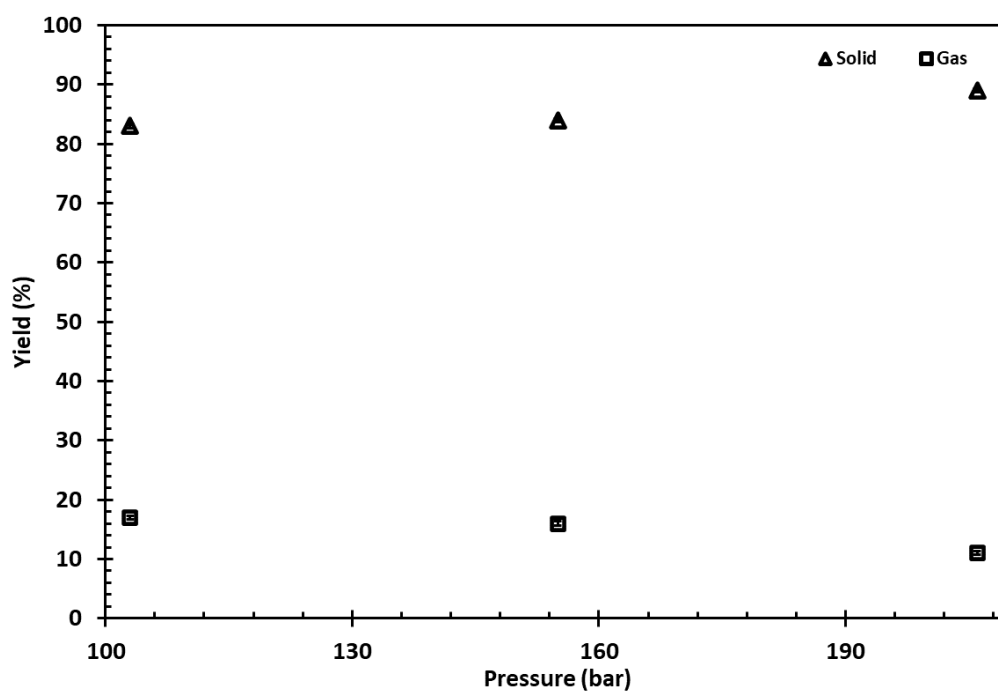


Figure 4.39. The effect of reaction pressure on the yield of products (200 °C, 120 min, 70 rpm).

In contrast to reaction time and temperature, an increase in reaction pressure tends to a slight increase in solid product yield. The maximum yield for the product in the reactor was attained at 206 bar. The yield of the product presented in the reactor increased from 83% to 89% as the pressure was increased from 103 bar to 206 bar. Dissolution of carbon dioxide in a polymer matrix enhances chain mobility and induces chain relaxation due to its plasticizing impact (Çulhacıoğlu et al., 2019). Enhanced mass transfer properties and reaction rates can be observed with supercritical carbon dioxide in multiphase reactions (Leitner et al., 2002).

It is interesting to note that although there is a tendency to increase the solid yield, the solid product composition stays the same with the alteration of the pressure (Figure 4.40).

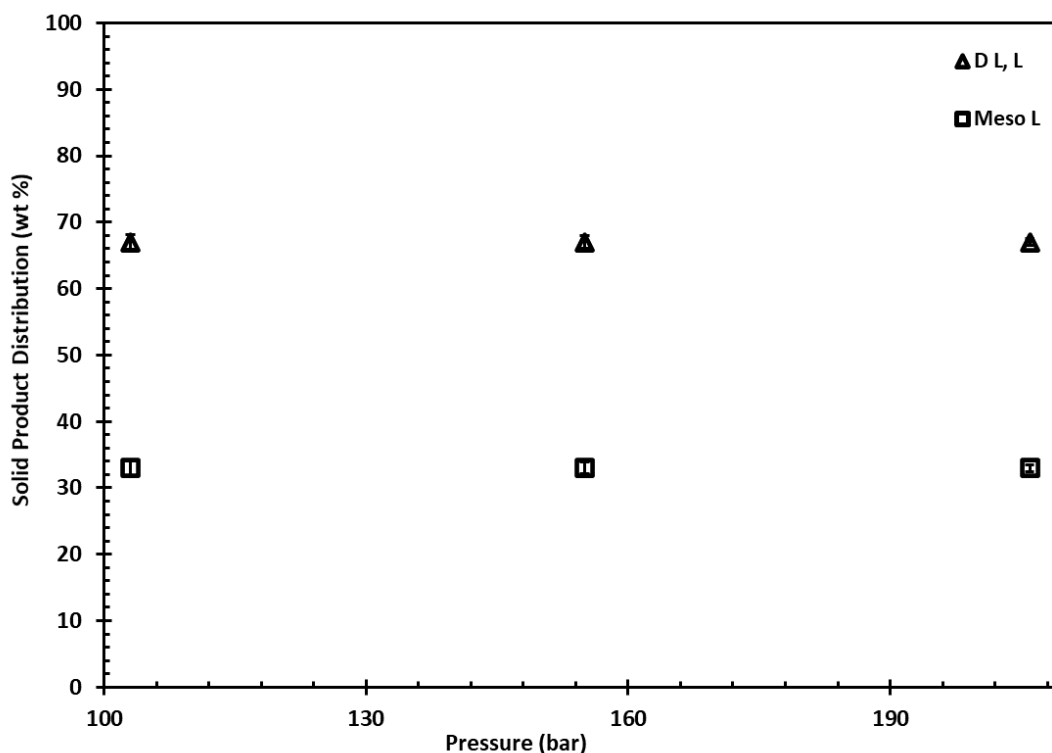


Figure 4.40. The effect of reaction pressure on the solid product distribution (200 °C, 120 min, 70 rpm).

Only lactide isomers were detected as degradation products in this experimental set. The quantity of D L lactide was approximately double that of meso lactide. The influence of pressure on solid yield was also evaluated at higher temperature, 220 °C, with the reaction time of 30 min. A similar behaviour was observed with previous experimental set that have lower reaction temperature and higher reaction time (Figure 4.41).

Similarly, the maximum solid yield was obtained at 206 bar. The solid yield increased from 74% to 79% in the pressure range of 103-206 bar. The content of the product was investigated. D L, L, Meso L, and LA were formed. Substantial alterations in the amount of the products were not observed depending on the pressure as given in Figure 4.42. Particularly, there was no discernible difference in the amount of D L lactide and meso lactide and lactic acid dependent on pressure.

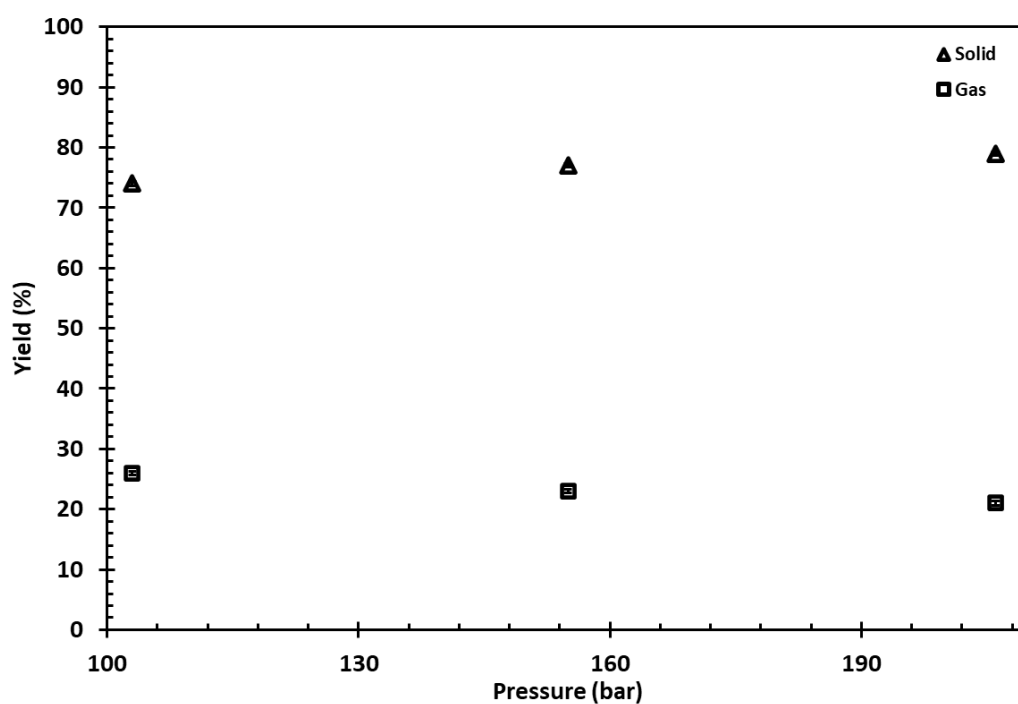


Figure 4.41. The effect of reaction pressure on the yield of products (220 °C, 30 min, 70 rpm).

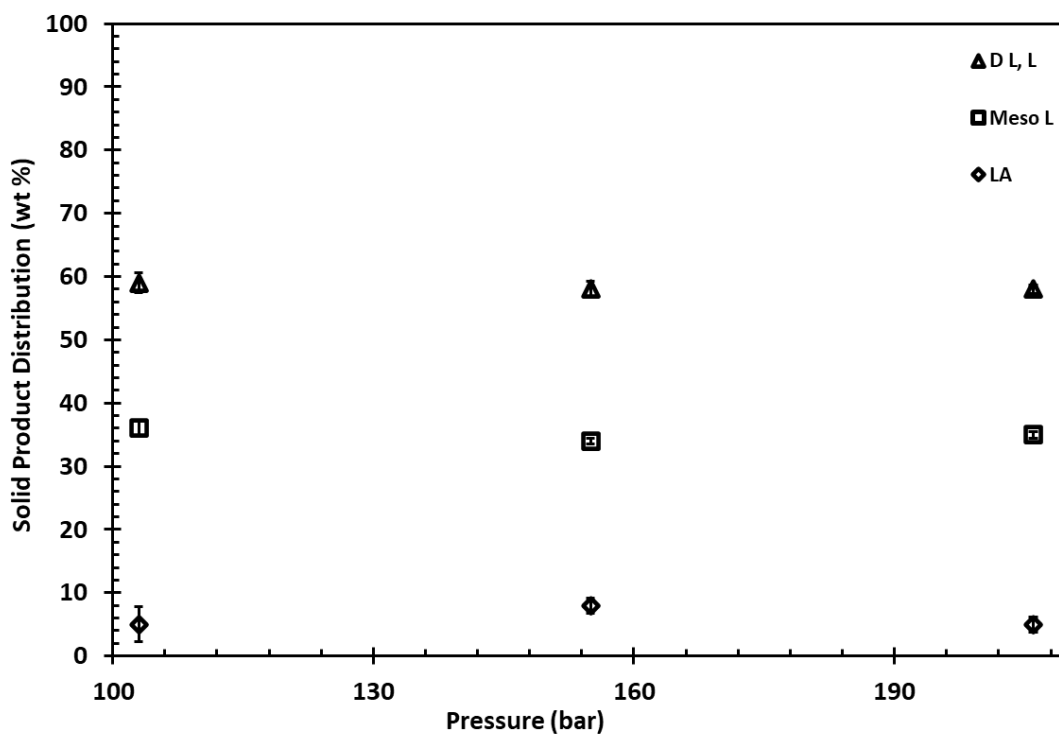


Figure 4.42. The effect of reaction pressure on the solid product distribution (220 °C, 30 min, 70 rpm).

4.1.4 Comparison of PLA Degradation Techniques

Degradation of PLA was performed utilizing a thermal gravimetric analyzer (TGA), a pyrolysis system, and a supercritical reaction system. Thermogravimetric technique was solely used to determine the degradation temperature range and activation energy for the thermal degradation of PLA. The degradation temperature range was determined to be between 322 and 378 °C.

Although the majority of current studies in the literature were aimed to determine the thermal behavior of PLA-based mixtures and composites, pyrolysis plays a limited role. These experiments were carried out utilizing TGA or Py-GC/MS

instruments with very small quantity of polymer, typically a few milligrams. In these systems, mass transfer limitation and isomerization of lactide were reduced with instantaneous reaction times. Thus, the type and distribution of the products do not represent the actual content. Due to financial constraints, heating the system to high temperature cannot be preferred in industrial applications. Thus, a pyrolysis system designed and installed for the degradation of PLA. The effect of reaction parameters on degradation products is studied extensively in installed pyrolysis system to provide an insight on recycling applications of the polymer. Despite the fact that reaction temperature and time had a substantial impact on product type and composition, mixing rate and flow rate did not have a higher impact on degradation of PLA within the parameter range studied.

On the basis of the initial quantity of PLA, the yield of the compounds was determined. The calculation is given in Appendix B. The yield value of the compounds in condensable product is illustrated in Figure 4.43.

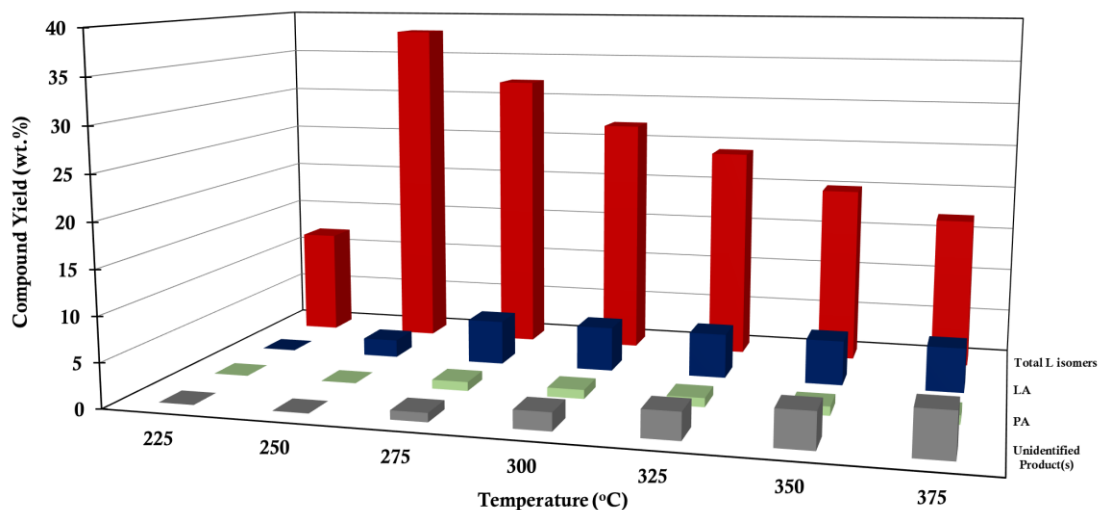


Figure 4.43. The effect of reaction temperature on the yield of compounds in condensable products (60 min, 70 rpm, 50 ml/min).

The yield of D, L L varied between 8% and 25%, by weight while the yield of Meso L was in the range of 3-13 wt.%. The total yield of lactide isomers was found to be 38% at 250 °C. The highest yield of lactic acid was 5% while the yield of propionic acid was only 1%. The yield of both lactic acid and propionic acid remained constant at the reaction temperature of 275 °C and 375 °C. The yield of unidentified products increased gradually up to 5 wt.% at 375 °C.

Secondly, the effect of reaction time on yield of compounds in condensable products is given in Figure 4.44.

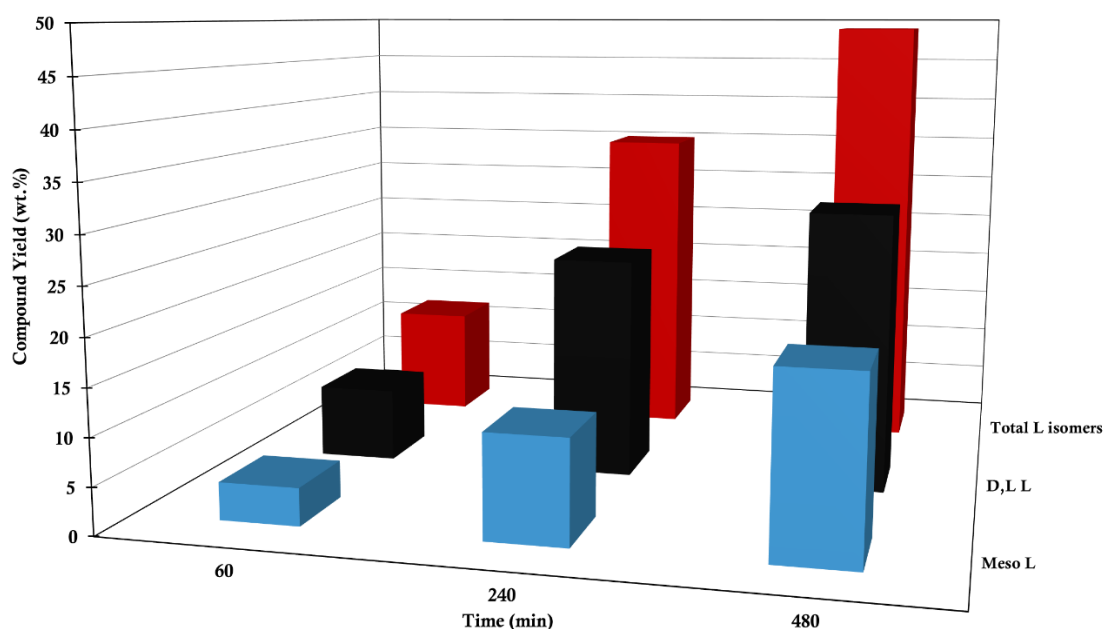


Figure 4.44. The effect of reaction time on the yield of compounds in condensable products (225 °C, 70 rpm, 50 ml/min).

With increasing reaction time, both D L,L and meso lactide yields increased. By weight, the yield of D, L L ranged from a minimum of 8 to a high of 30. The yield

of Meso L was increased from 3 to 19 wt.%. For 480 minutes, the total yield of lactide isomers was determined to be maximum 49 wt. %. When evaluating the yield of gas components, there was dominance of acetaldehyde nearly all in studied parameters.

As a second system, PLA degradation was studied in supercritical carbon dioxide medium.

The most effective parameter was reaction temperature for the PLA degradation with supercritical carbon dioxide. A similar pattern was observed for the yield of the compounds with the pyrolysis (Figure 4.43). Yet, the highest yield was obtained with 83% total yield of lactide isomers at 200 C, 103 bar, 70 rpm and 120 minutes.

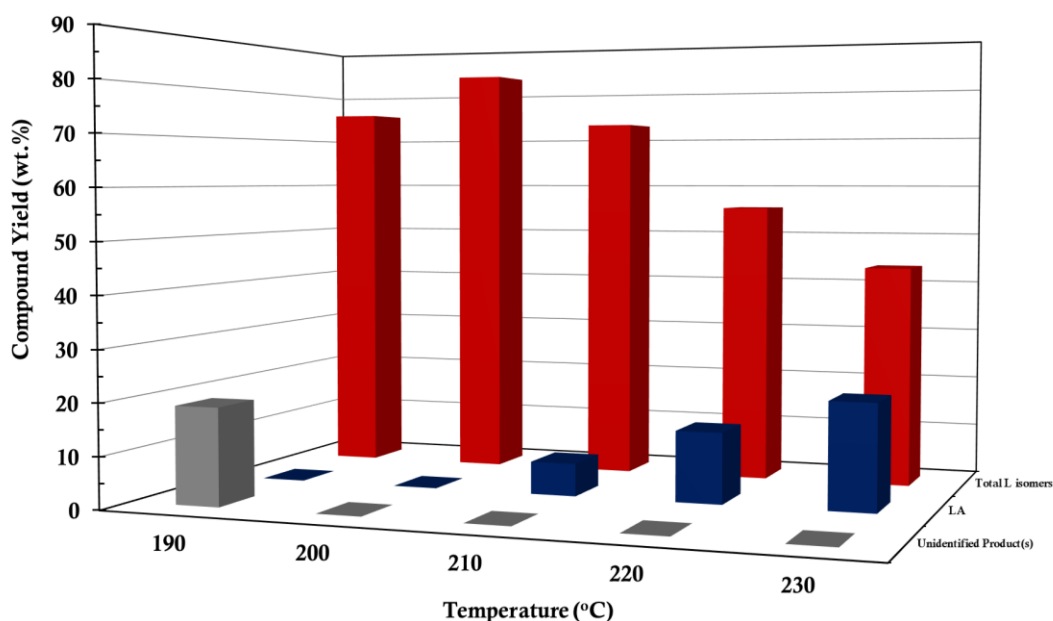


Figure 4.45. The effect of reaction temperature on the yield of compounds in solid products (120 min, 103 bar, 70 rpm).

The total yield of lactide isomers was raised to a maximum 83 wt.%. The yield of lactic acid was increased with time to 21 wt.% at 230 °C. The yield of unidentified product was 19 wt.% at 190 °C. With increasing reaction temperature, there was not seen any unidentified product in the reactor. The yield of the components was investigated with the reaction time parameter at 200 °C (Figure 4.46).

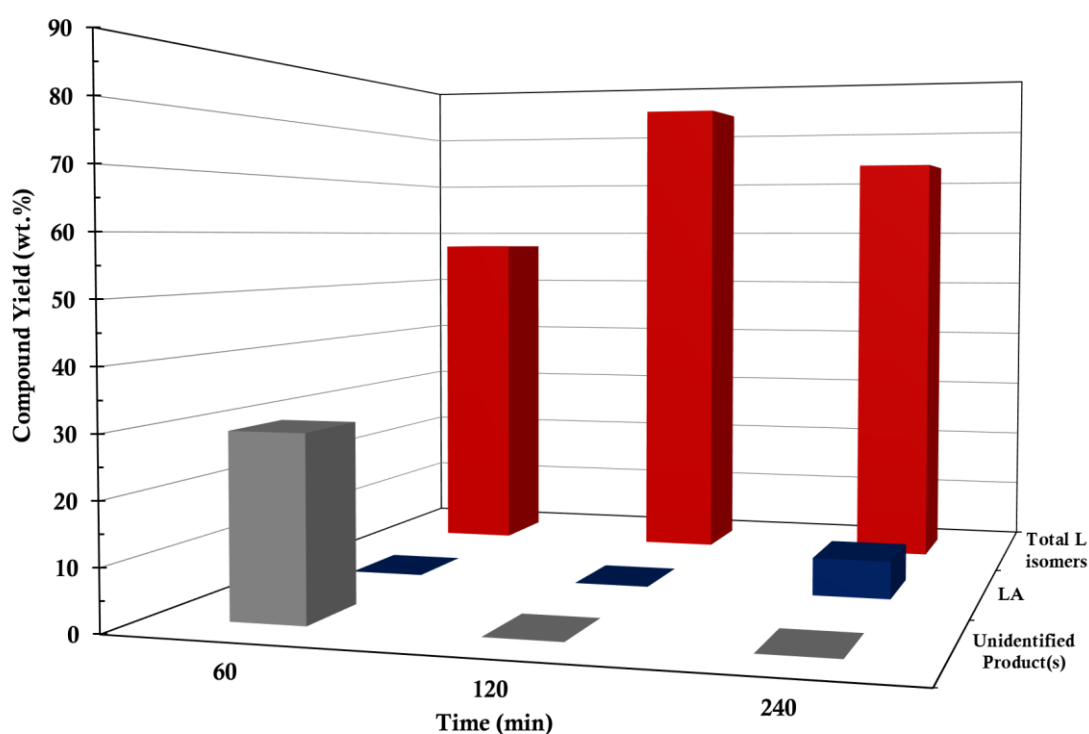


Figure 4.46. The effect of reaction time on the yield of compounds in solid products (200 °C, 103 bar, 70 rpm).

The total yield of lactide isomers was increased from 57 wt.% to 83 wt.% when increasing the reaction time up to 120 min. The total yield of lactide isomers then reduced to 73 wt.% at the reaction time of 240 min. The yield of lactic acid became remarkable with a value of 6 wt.% at 240 minutes.

Lastly, although reaction pressure has a limited effect on product type and distribution, maximum total yield of lactide isomers (89%) were reached at 200 °C, 206 bar, and 70 rpm for 120 minutes.

When comparing the reaction systems, it was evident that pyrolysis system offers a tunable production of value-added products in a wide range. The most of condensable compounds were lactide isomers, while the most prevalent non-condensable product was acetaldehyde. In the experiments performed at 225 °C, 70 rpm, 50 ml/min in the reaction time between 60 min and 480 min, the yield of D L,L ranged between 8% and 30% by weight. In the same reaction conditions, the yield of meso L changed from 3 to 19%. In all experiments, the highest yield of lactic acid was 5% while propionic acid has a 1% yield, which is quite low. Additionally, the maximum yield of unidentified compounds rose to 5%. It is apparent that the yield of acetaldehyde was quite high in all studied parameters.

The highest total yield of lactide isomers were achieved as 49% at 225 °C, 70 rpm, 50 ml/min for 480 minutes. Lactide isomers were produced in a controlled manner with slower degradation reaction rate. Yet, the reaction time was substantially long. The closest total yield result to the highest total yield was attained at 250 °C, 70 rpm, 50 ml/min for 60 minutes. The yields of D L,L and meso L were found to be 25% and 12%, respectively. To ensure economic efficiency, the working range can be adjusted within this range for lactide production by pyrolysis.

The degradation of PLA was also carried out in the batch-mode high pressure reaction system. The results demonstrated that when applied as a reaction medium, supercritical carbon dioxide has a remarkable effect on the degradation of PLA providing high yield production of lactide isomers. Low yield values had acquired without stirring the mixture. The conversion of PLA to lactide isomers was relatively low without mixing. The yield of D L,L was found to be between 18 and 60% by weight. The yield of Meso L was in the total yield range of 11% to 28%. At 200 °C, 206 bar and 120 minutes, the highest total lactide isomer yield was attained with

89%, by weight. Producing lactide isomers was also achieved in supercritical carbon dioxide medium. Yet, the high-pressure applications increase the operation cost. Thus, the optimal yield (83%) was achieved at a lower pressure of 103 bar at 200 °C, 70 rpm for 120 minutes. The maximum lactic acid yield was found to be 21 wt.% at 230 °C, 103 bar and 120 minutes.

In both systems, lactide isomers were effectively produced. In addition, the production of lactic acid was provided by adjusting the reaction parameters. The production of PLA involves a number of chemical reactions. Lactic acid and lactide production account for a considerable portion of the production cost. The share of lactide production on the cost is more than 80% (Jaso et al., 2019). By shortening the production route of PLA, economic efficiency can be attained, and the production of these chemicals contributes to the closed loop production of PLA.

4.2 Catalytic Degradation of PLA

Catalytic pyrolysis is a viable technique for producing value-added products and feedstocks with lower energy demand and higher conversion and selectivity. Since the degradation of PLA includes a series of complex solid-liquid-gas reactions, accelerated mass transfer of the components contributes to achieve a better reaction kinetic. Due to their inherent pore properties, mesoporous catalysts exhibit exceptional reaction kinetics in thermal degradation processes of commodity plastics (Aydemir et al., 2013, 2016; Obalı et al., 2009, 2011). Thus, in this work, Al, Fe and Mg loaded silica aerogel catalysts were loaded into silica aerogel support, and characterized using several techniques. These catalysts were used in the degradation of PLA in the reaction temperature of 200-275 °C. The effects of metal loaded silica aerogel catalysts on the degradation of PLA were investigated for the first time in the pyrolysis system. The actual product type and distribution were obtained with these catalysts under different reaction temperatures.

4.2.1 Degradation of PLA with Aluminum Loaded Catalyst

Within the scope of this study, aluminum was loaded into silica aerogel support. The catalyst was investigated in terms of textural properties, morphology, acidity, and its activity in PLA degradation. The degradation of PLA was studied with aluminum loaded silica aerogel catalyst at different reaction temperatures. The effect of the catalyst on product type and distribution was evaluated in the pyrolysis system comprehensively.

4.2.1.1 Characterization of Aluminum Loaded Catalyst

4.2.1.1.1 Characterization of Silica Aerogel Material

Silica aerogel-based catalysts were rarely investigated only in a few degradation studies of polymeric waste (Sivri et al., 2019; Habib, 2019). In this work, due to high surface area and inherent thermal stability properties of the aerogel, silica aerogel was used as the support of the catalyst in the degradation of PLA. A representative image for the synthesized silica aerogel material (SAU) is given in Figure 4.47. The produced silica aerogel material.



Figure 4.47. The produced silica aerogel material.

As seen from Figure 4.47, silica aerogel has cloudy appearance and color. The physical properties of silica aerogel materials were obtained by physisorption studies. Figure 4.48 presents nitrogen adsorption/desorption isotherms of SAU materials. The adsorption/desorption isotherms of silica aerogel materials belong to different batches which are produced at different times.

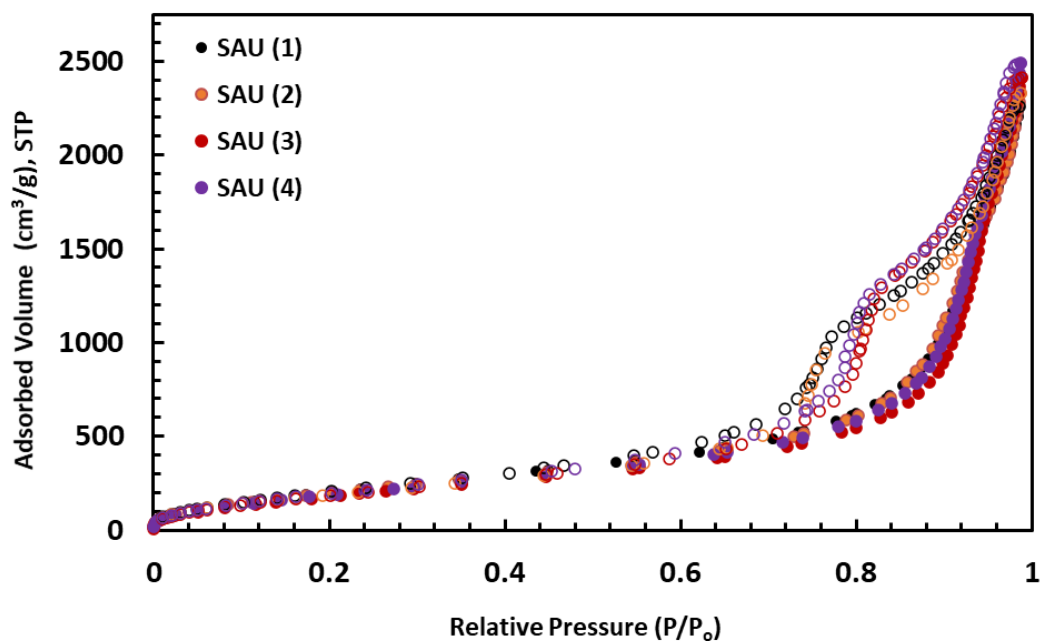


Figure 4.48. Nitrogen adsorption/desorption isotherms of different uncalcined (SAU) silica aerogel material batches (filled and empty symbols represent adsorption and desorption branches, respectively).

From adsorbed nitrogen volume-relative pressure curve, Type IV isotherm was seen which is an indication of mesoporous material. At lower pressure ranges, monolayer adsorption occurred, then it followed multilayer adsorption. At higher pressure ranges or near saturation point, capillary condensation took place, and the amount of adsorbed volume reached a limit in adsorption amount.

Hysteresis 3 was obtained for silica aerogel materials, which is an indication of non-rigid aggregation of plate like particles forming slit like pores. The isotherm and hysteresis types of the batches were found to be the same.

A calcination procedure was also applied to tailor or enhance the material properties of the support (SA). Nitrogen adsorption/desorption isotherms of uncalcined (SAU) and calcined (SA) silica aerogel materials are illustrated in Figure 4.49.

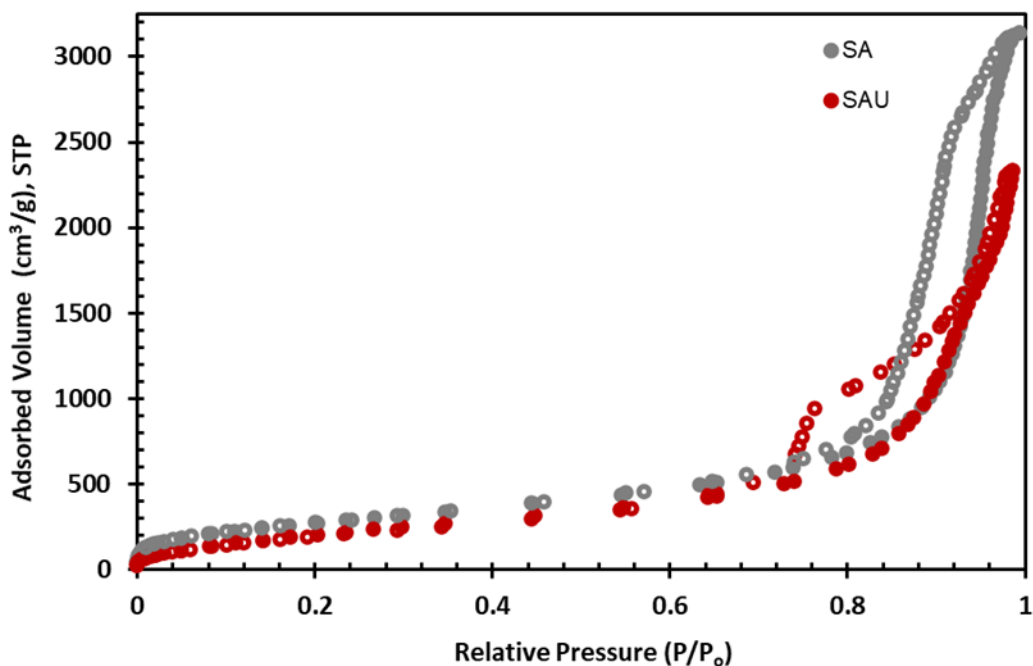


Figure 4.49. Nitrogen adsorption/desorption isotherms of uncalcined (SAU) and calcined (SA) silica aerogel materials (filled and empty symbols represent adsorption and desorption branches, respectively).

Based on the physisorption of SAU and SA, Type IV isotherm was seen for both support materials, which points out mesoporous material. H1 type hysteresis was observed for the SA support at a relative pressure range of 0.74–0.98 due to the capillary condensation of nitrogen in the mesopores of the structure, which shows uniform, narrow pore size distribution; however, SAU revealed H3 hysteresis at a relative pressure between 0.74 and 0.99 which is the indication of non-rigid aggregates of plate-like particles with slit-shaped pores (Lowell et al., 2006).

Pore size distributions of SAU and SA were also given in Figure 4.50. Despite the presence of micropores and macropores, there was a predominance of mesoporous regions within the structure of both support materials. It was revealed that SA has a higher pore size than that of SAU. TMCS modification has largely contributed to the

increase in pore size by removing adsorbed water, entrapped solvent, and organic groups inside the pores of support. An extra calcination procedure provided an enhancement on surface and pore properties of the produced silica aerogel.

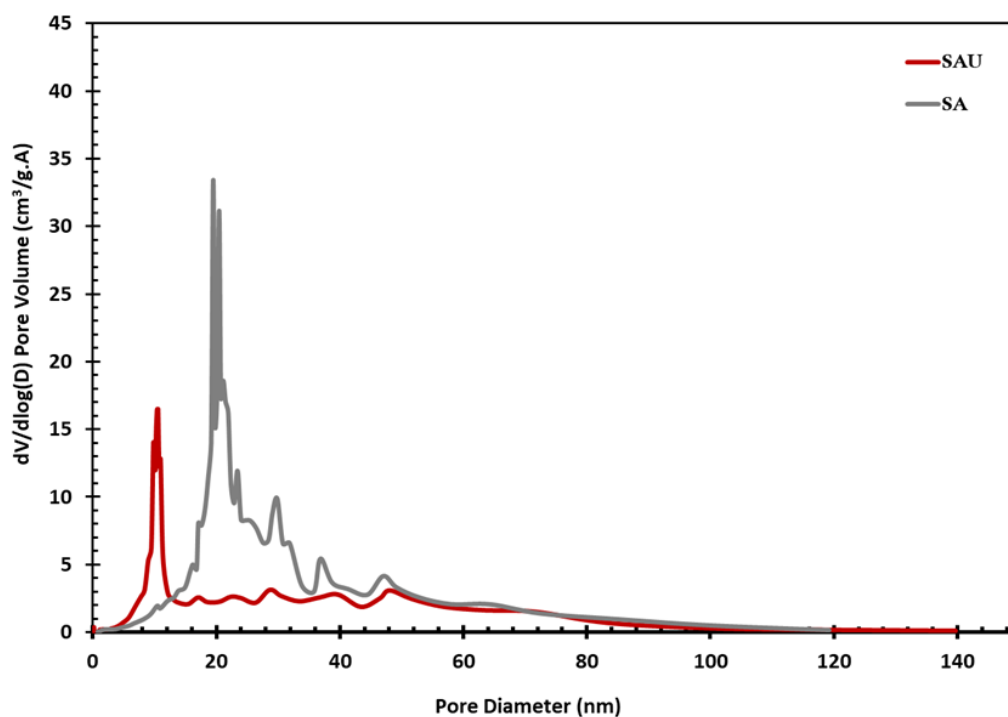


Figure 4.50. Comparison of the pore size distributions of uncalcined (SAU) and calcined (SA) silica aerogels.

Pore size distribution results are in good agreement with the isotherm results. The physical properties of uncalcined (SAU) and calcined silica aerogels (SA) produced from four different batches produced at different times are summarized in Table 4.3. The physical properties of uncalcined and calcined silica aerogels. Standard deviations of surface area, pore volume, and pore diameter indicated the reproducible silica aerogel production.

Table 4.3. The physical properties of uncalcined and calcined silica aerogels.

Support Material	Surface Area (m²/g)	Pore Volume (cm³/g)	Pore Diameter (nm)	Microporosity (%)
SAU	806±35	3.67±0.14	11.06±0.67	4.59±0.16
SA	900±69	4.83±0.27	14.36±1.91	4.75±0.67

SEM image of uncalcined silica aerogel is presented in Figure 4.51. SEM images of the uncalcined silica aerogel (SAU) with 100kX magnification. The porous and sponge-like morphology of the silica aerogel is seen in the image. Although the mesopores were dominantly found in the structure, there were also different pore sizes in the structure of the support (pink squares in Figure 4.51). These results are in good agreement with the pore size distribution results of SAU provided by physisorption analyses.

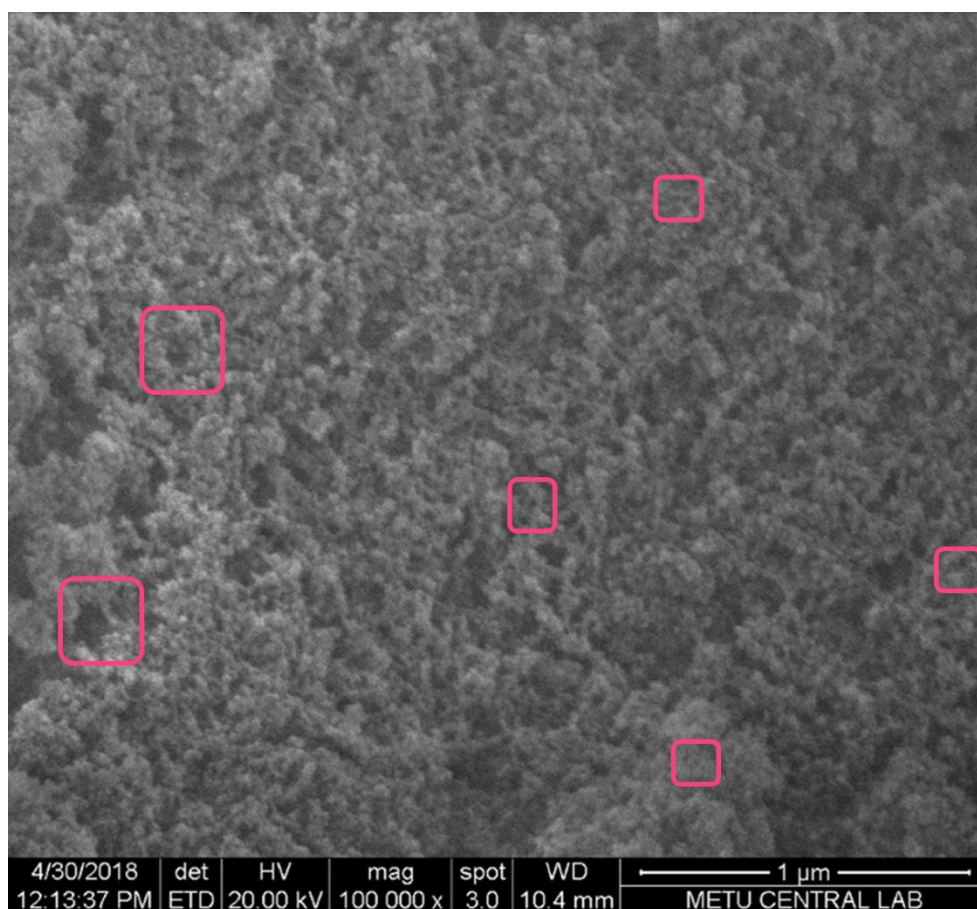


Figure 4.51. SEM images of the uncalcined silica aerogel (SAU) with 100kX magnification.

FTIR spectra of SAU and SA are given in Figure 4.52. In the spectrum of SA-U material peaks obtained at 548 cm^{-1} , 798 cm^{-1} , and 955 cm^{-1} are due to Si-O stretching vibration. The peaks at 691 cm^{-1} , 757 cm^{-1} , and 811 cm^{-1} were related to Si-O-Si stretching. C-H stretching was detected at the wavenumber of 2963 cm^{-1} due to the TMCS modification. Peaks at 845 cm^{-1} and 1256 cm^{-1} correspond to Si-C stretching. The sharp peak around 1066 cm^{-1} with a shoulder around 1168 cm^{-1} belongs to Si-O-Si stretching. FTIR results revealed that SAU has the characteristic peaks of silica aerogel (Al-Oweini and El-Rassy, 2009; Wu et al., 2018; Habib,

2019). In other words, these results matched well with the FTIR spectrum given in the literature.

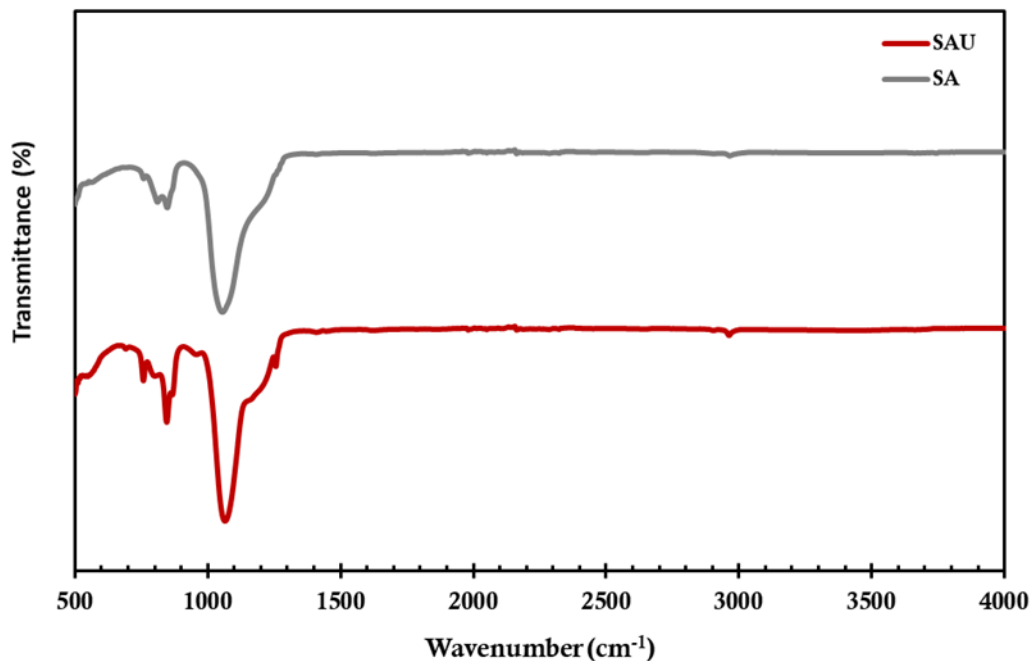


Figure 4.52. FTIR spectra of uncalcined (SAU) and calcined (SA) silica aerogels.

In the SA material, the intensities of the C-H stretching peak at 2963 cm⁻¹ and the Si-C stretching peaks at 845 cm⁻¹ and 1256 cm⁻¹ decreased due to the removal of methyl groups with the calcination process. On the other hand, the intensity of the peak presented at 811 cm⁻¹ increased. The same behavior was also observed in the other calcined silica aerogel studies in the literature (Nayak and Bera, 2009; Wu et al., 2018). This might be due to the transformation of Si-CH₃ bonds to Si-OH to make the Si-O-Si structure more stable (Nayak and Bera, 2009). SAU has mainly a hydrophobic character. The hydrophobicity of the aerogel arises from the nonpolar groups in the structure; however, a hydrophilic character becomes more pronounced with calcination. Within the scope of this study, aluminum loaded silica aerogel

catalysts are investigated in terms of pore characteristics, surface and textural properties, structural analysis, acidity, and degradation ability of PLA.

4.2.1.1.2 Characterization of Aluminum Loaded Silica Aerogel Catalyst

By mass, aluminum makes up about 8% of the Earth's crust, where it is the third most abundant element and the most abundant metal in the world (Sciencing, 2020). It was presumed that aluminum could be an effective catalyst for the degradation of PLA due to its high affinity for hydrogen atoms in the structure of PLA. It was known that aluminum can promote the cracking of plastics such as PE and PP (Obalı et al., 2009, Aydemir and Sezgi, 2013, 2016). In these processes, large hydrocarbon molecules are broken down into smaller segments. Due to these features, aluminum was loaded into SA support with different weight ratios. Effect of aluminum loading on adsorption/desorption isotherms are given in Figure 4.53.

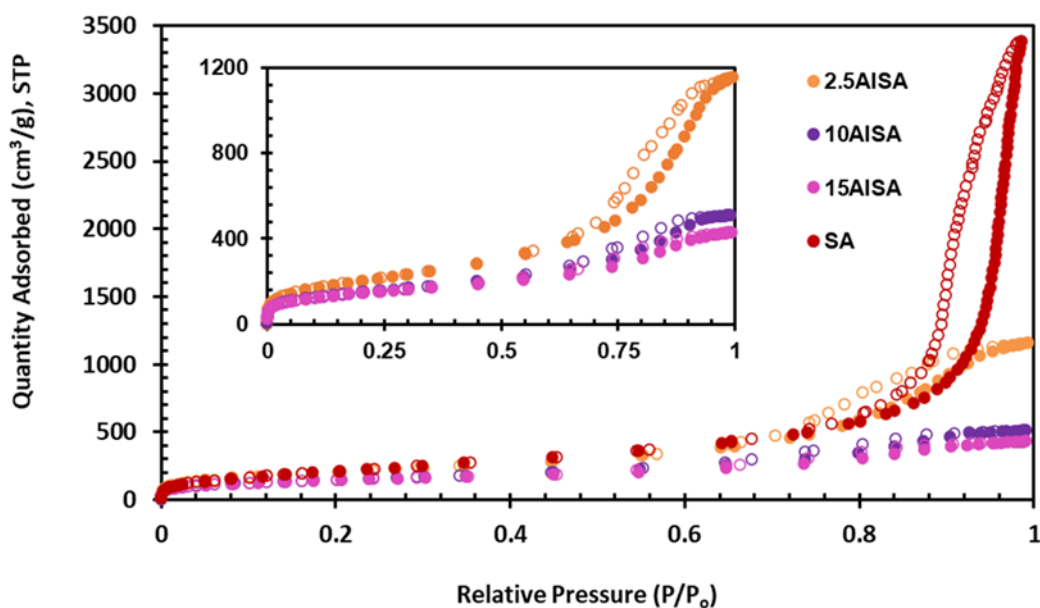


Figure 4.53. Nitrogen adsorption/desorption isotherms of aluminum loaded silica aerogel catalysts with different weight ratios (filled and empty symbols represent adsorption and desorption branches, respectively).

The aluminum loaded silica aerogel catalysts also exhibited Type IV isotherm and the mesoporous structure is conserved at all studied metal loading amounts. Hysteresis loop of the metal loaded catalysts were determined to be H1.

Pore sizes of the aluminum loaded silica aerogel catalysts decreased with an increase in metal loading amount (Figure 4.54). Pore size distributions of the catalytic materials shifted to lower pore diameter values due to blockage of the meso and macro pores with metals. It was found that increase of aluminum loading amount led to a decrease in pore size distribution.

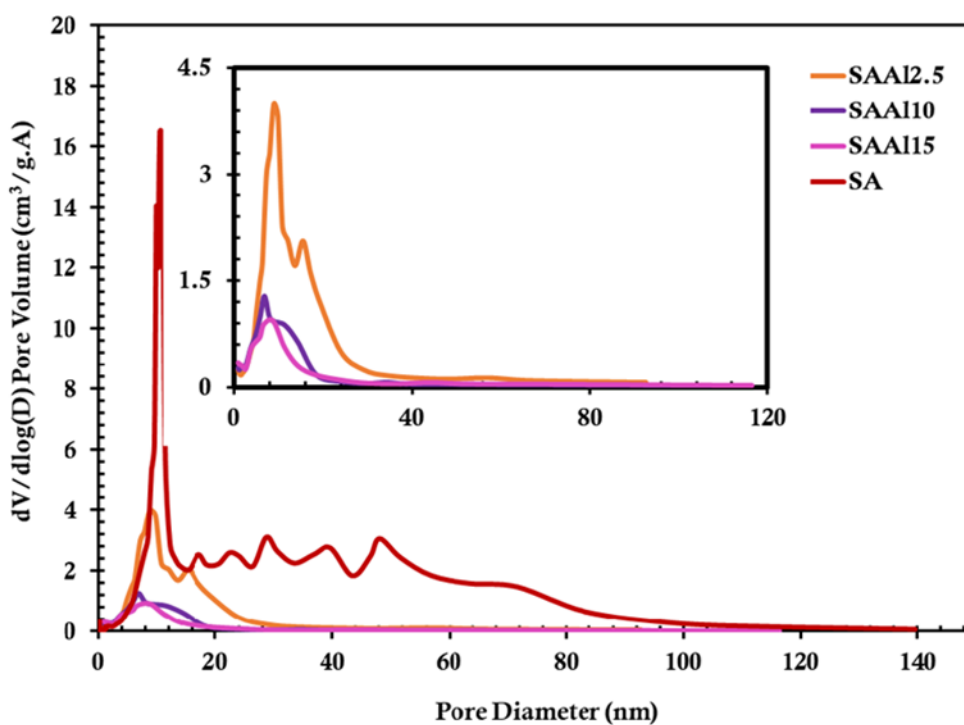


Figure 4.54. The pore size distributions of aluminum loaded silica aerogel materials.

The physical properties of aluminum loaded silica aerogels are given in Table 4.4.

Table 4.4. The physical properties of aluminum loaded silica aerogel catalysts.

Support Material	Surface Area (m ² /g)	Pore Volume (cm ³ /g)	Pore Diameter (nm)	Microporosity (%)
SAA12.5	743	1.79	6.38	10.61
SAA110	537	0.81	4.10	18.42
SAA115	510	0.69	3.60	21.74

With an increase in aluminum loading amount a decrease in the surface area, pore volume and pore diameter of the catalysts was observed, which is possibly due to the blockage of the pores with the loaded metal. It is also seen that microporosity was highly increased with the increasing amount of metal loading due to the blockage of the pores. The morphologies of the aluminum loaded silica aerogel materials were also analyzed for the SAA110 and SAA115 catalysts (Figure 4.55).

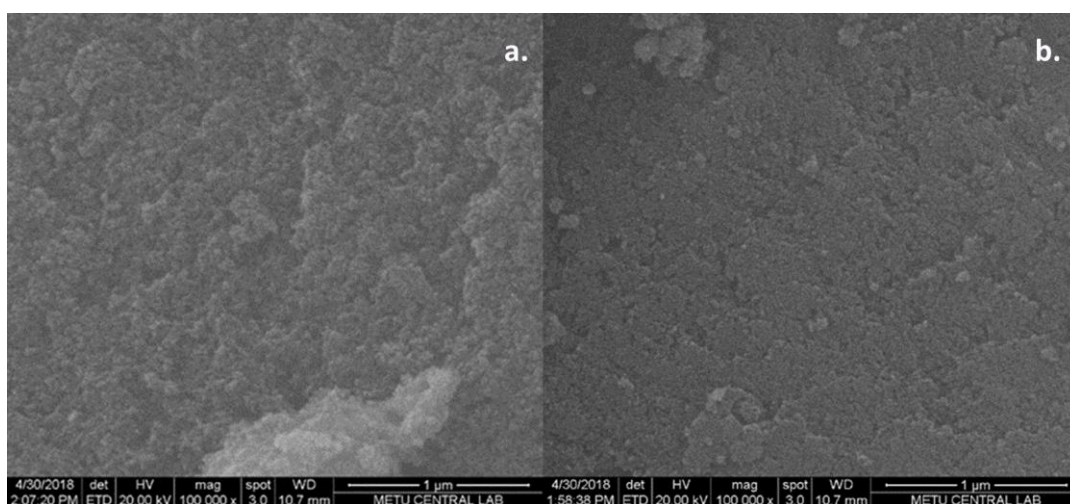


Figure 4.55. SEM images of the aluminum loaded silica aerogel catalysts: a. SAA110, b. SAA115 with 100kX magnification.

With aluminum loading, the mesoporous structure was conserved in the SAA110 catalyst. Yet, a change in the morphology of the support was observed for the SAA115 catalyst. EDX analyses were done by selecting more than 5 different regions of the sample to take the average of aluminium content. A representative EDX graph is presented in Figure 4.56. EDX analyses revealed that the average aluminum contents in the SAA110 and SAA115 catalysts were 8 and 10 wt. %, respectively. Metal loading becomes compelling with the increase in aluminum amount in the support. Due to the coating of the sample with Au and Pd, there were signals of Au and Pd in the EDX results. These metals were excluded calculating the weight ratio of Al. Si and O were observed due to the structure of aerogel. The weight ratio of Al was calculated as 11% for SAA115 at this sample point.

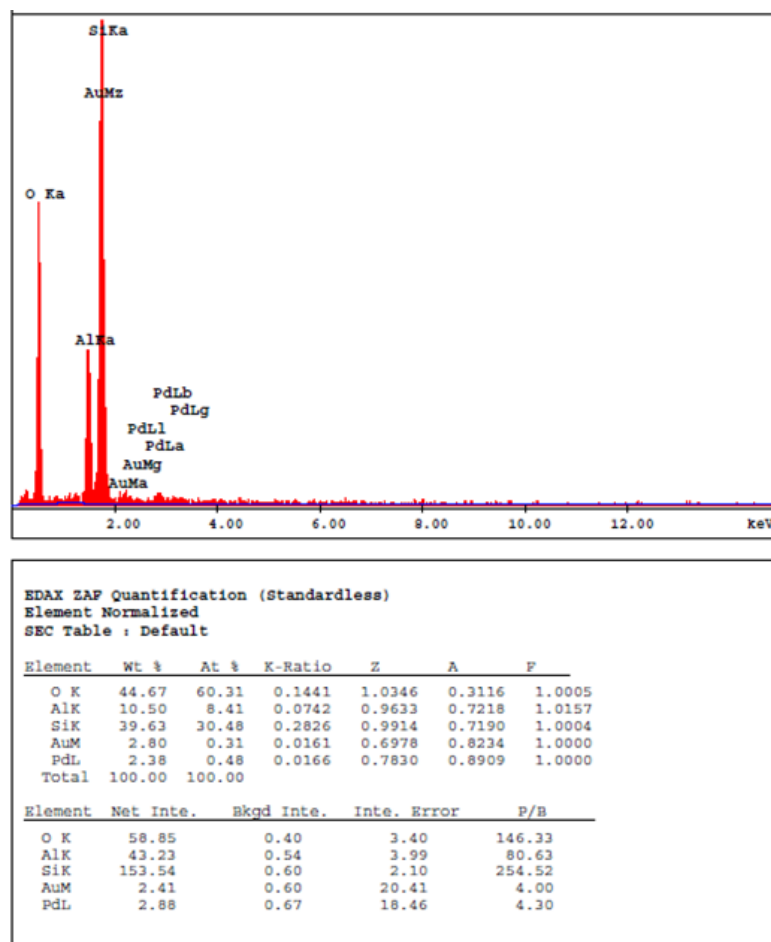


Figure 4.56. EDX analysis of the SAA15 catalyst.

Lastly, acidic catalyst is required for breaking the polymer chains. Therefore, TPD analysis of the synthesized catalyst was performed to get information about their acidity. NH_3 -TPD curves of Al loaded catalysts are given in Figure 4.57. The sharp peak at around seventies is the physisorption peak of NH_3 indicating weak acidity. The peak starting from 120°C shows chemically desorbed NH_3 . There are two peaks around 277°C and 364°C showing moderate acidity. Total acidic capacities of the catalysts are tabulated in Table 4.5

It was observed that with an increase in metal loading their total acidic capacity increased. In other words, loading of metal into the support makes the support material more acidic.

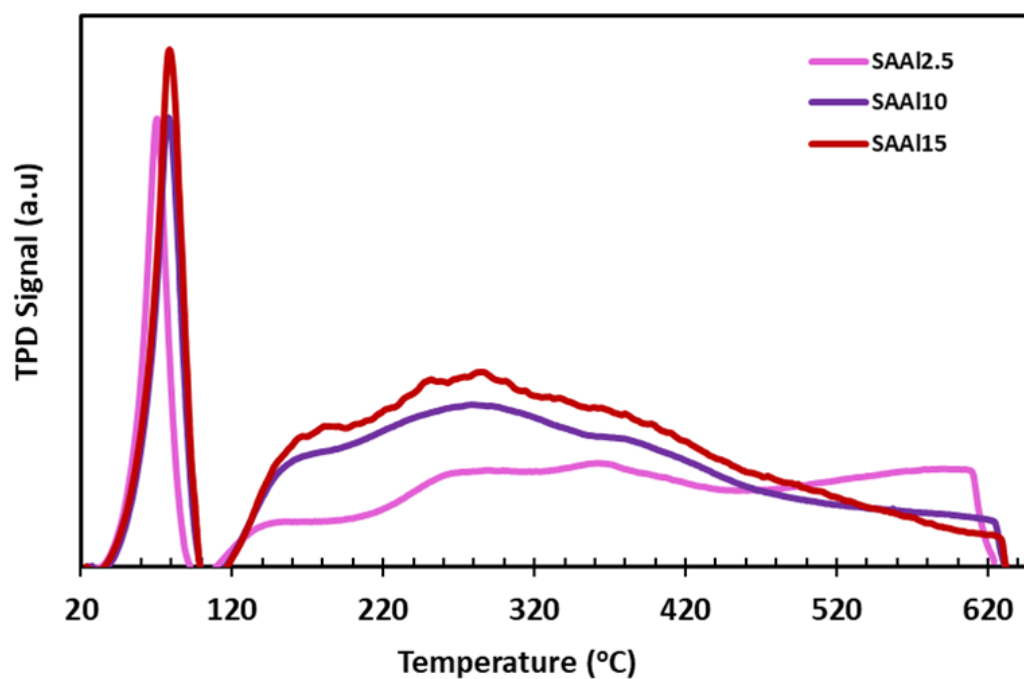


Figure 4.57. NH₃-TPD curves of aluminum loaded silica aerogel catalysts.

Table 4.5. Total acidic capacities of aluminum loaded silica aerogel catalysts.

Catalyst	Total Acidic Capacity (mmol/g)
SAAI2.5	1.20
SAAI10	1.54
SAAI15	1.91

15 wt.% aluminum loading was then done into uncalcined silica aerogel to synthesize SAUA115 catalyst. The alterations in the physical properties was compared with SAA115. The nitrogen adsorption/desorption isotherms of 15 wt.% aluminum loaded catalysts materials are given in Figure 4.58.

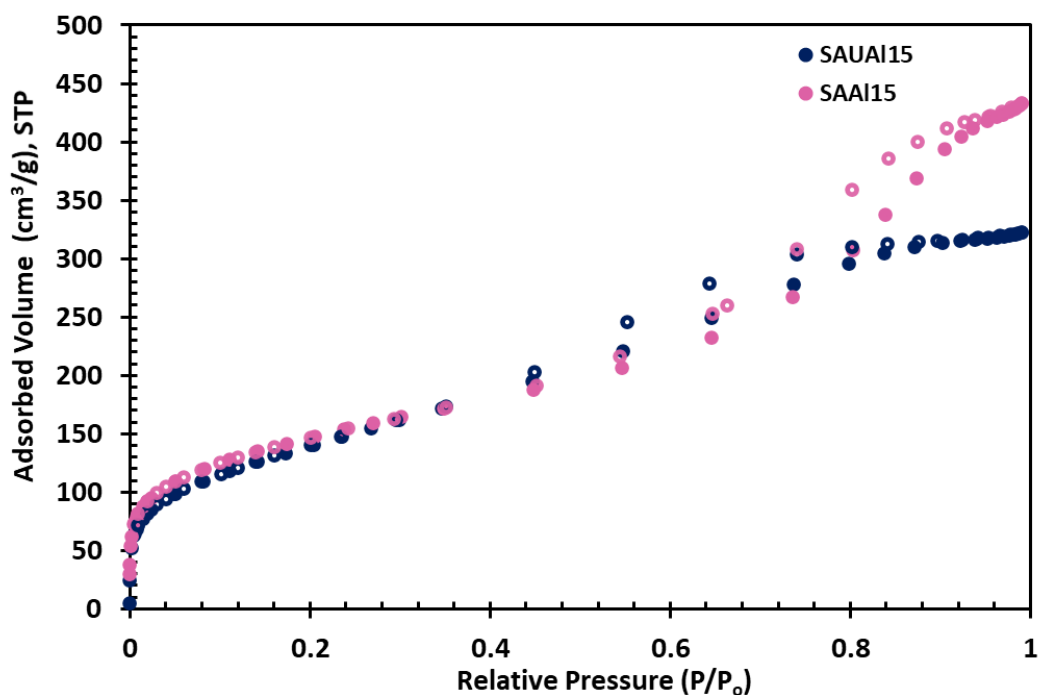


Figure 4.58. Nitrogen adsorption/desorption isotherms of 15 wt.% aluminum loaded silica aerogel catalysts (filled and empty symbols represent adsorption and desorption branches, respectively).

The aluminum loaded silica aerogel catalysts also exhibited an isotherm of Type IV, and the mesoporous structure was retained at the highest metal loading to the both uncalcined and calcined silica aerogel support. H1 was revealed to be hysteresis loop for both SAUA115 and SAA115 catalysts. The hysteresis started at the relative pressure of 0.45 for SAUA115 while the hysteresis was observed at 0.55 for SAA115. The hysteresis shifted to the left for SAA115 catalyst, which is an indication of larger pore size in the structure.

The pore size distributions of the catalysts were given in Figure 4.59. The pore size distribution of 15% aluminum loaded silica aerogel materials.

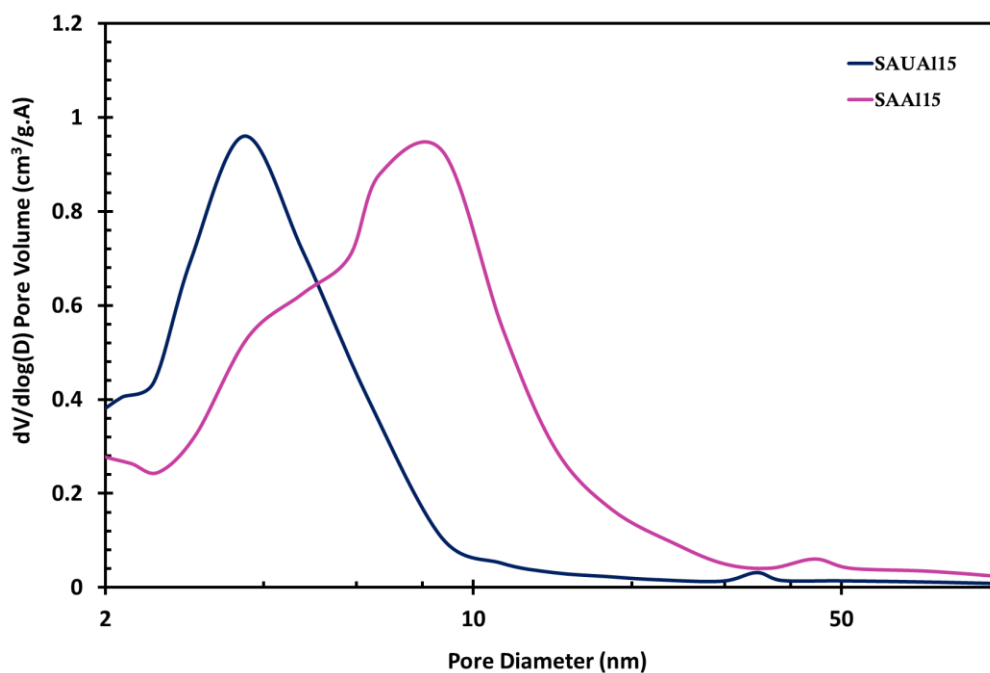


Figure 4.59. The pore size distribution of 15% aluminum loaded silica aerogel materials.

Pore sizes of the aluminum loaded silica aerogel catalysts decreased with aluminum loading into uncalcined silica aerogel support. SAUA115 has lower pore size than SAA115. These results are consistent with the adsorption/desorption isotherms. The physical properties of the 15 wt.% aluminum loaded catalysts are given in Table 4.6.

Table 4.6. The physical properties of 15 (wt.%) aluminum loaded silica aerogel catalysts.

Support Material	Surface Area (m ² /g)	Pore Volume (cm ³ /g)	Pore Diameter (nm)	Microporosity (%)
SAUA115	510	0.51	2.67	27
SAA115	510	0.69	3.60	21.74

Although nearly the same surface area were attained for the SAUA115 and SAA115 catalysts, the microporosity was increased with aluminum loading to the uncalcined silica aerogel support. The SEM images of SAUA115 in Figure 4.60. The porous structure was conserved with Al loading.

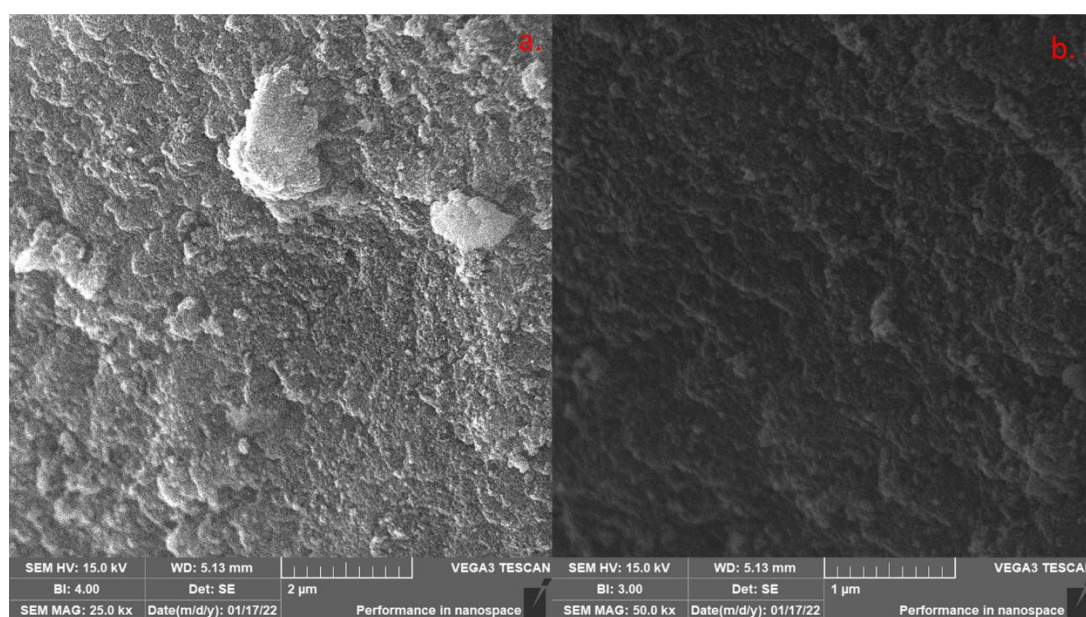


Figure 4.60. SEM images of 15 wt.% aluminum loaded uncalcined silica aerogel catalyst: a. 25kX magnification b. 50 kX magnification.

EDX analysis revealed that the average aluminum contents in the SAUA15 were 12 wt. %, respectively. The aluminum content of the SAUA15 (12 wt.%) was higher than that of SAA15 (15 wt.%). The surface acidities of 15 wt.% aluminum loaded into uncalcined and calcined silica aerogel supports were compared in Figure 4.61.

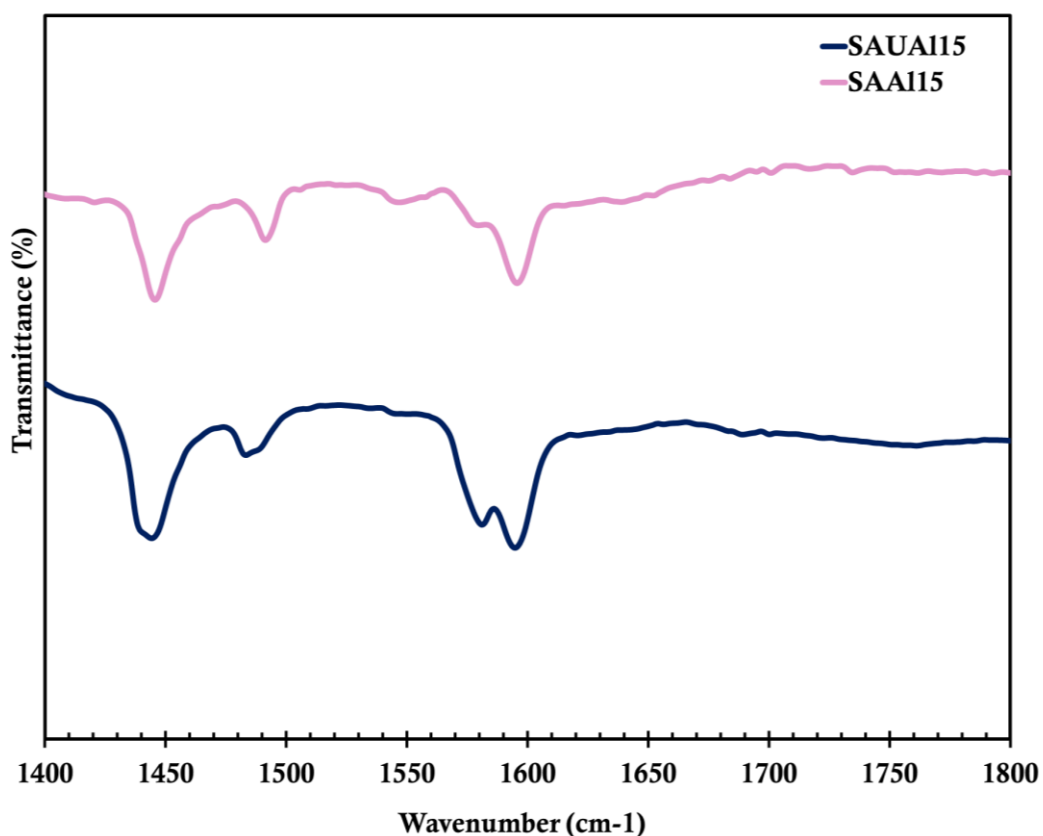


Figure 4.61. DRIFTS spectra of the pyridine adsorbed 15 wt.% aluminum loaded into uncalcined & calcined silica aerogels.

The Lewis and Brønsted acid site peaks were observed in the wavenumber range of 1400-1700 cm⁻¹. It was found that from the literature Brønsted acid site peaks were detected at the wavenumbers of 1540 cm⁻¹, 1608 cm⁻¹, and 1640 cm⁻¹ (Busca et al., 1998). The presence of Lewis acid regions was in the wavenumbers of 1438 cm⁻¹,

1455 cm^{-1} , 1575 cm^{-1} , and 1580 cm^{-1} -1632 cm^{-1} (Gokturk, 2021; Kooli et al., 2000; Chen et al., 2017; Busca et al., 1998). Moreover, the band around 1490 cm^{-1} correlates to both Lewis and Bronsted acid sites (Gokturk, 2021; Khalil et al., 2020; Güner, 2007; Dinçer, 2019; Obalı et al., 2011). The peaks at 1445 cm^{-1} , 1580 cm^{-1} , and 1596 cm^{-1} on both catalysts showed the Lewis acid sites (Aydemir, 2013). The peak intensity at 1580 cm^{-1} was much higher in SAUA15 (12 wt.%) than that in SAA15 (11 wt.%). The peak between 1483 cm^{-1} and 1492 cm^{-1} indicated both Lewis and Brønsted acid sites for the SAUA15 and SAA15 catalysts.

4.2.1.2 Determination of Activation Energy of PLA Degradation Reaction in the Presence of Aluminum Loaded Silica Aerogel Catalyst

The performance of the aluminum loaded catalysts was tested using thermogravimetric analyzer. A kinetic model study was also done to observe the effect of aluminum loaded silica aerogel-based catalysts on the degradation of PLA. PLA was degraded under a nitrogen atmosphere with a 50 ml/min flow rate for a catalyst to PLA weight ratio of 0.5. The kinetic parameters of the PLA degradation reaction were evaluated based on a standard power law model and following the procedure reported in the study of Coats and Redfern (1964). The method is provided in Appendix A.

Figure 4.62 illustrates thermogravimetric plots of thermal degradation of PLA with synthesized catalysts. As seen in the figure, silica aerogel slightly improved the thermal stability of PLA shifting curve to a slightly higher temperature range. On the contrary, loading aluminum into silica aerogel support shifted the degradation profile to the left. This shift became more significant with the increase of aluminum loading in the reaction medium. Shift of degradation profile to the left is an indication of a significant decrease in the degradation temperature of PLA. Increase of acidity caused such a decrease in the PLA degradation reaction temperature. Among

different amounts of Al loaded silica aerogel catalysts, the best degradation profile was attained in the presence of the SAUA115 catalyst.

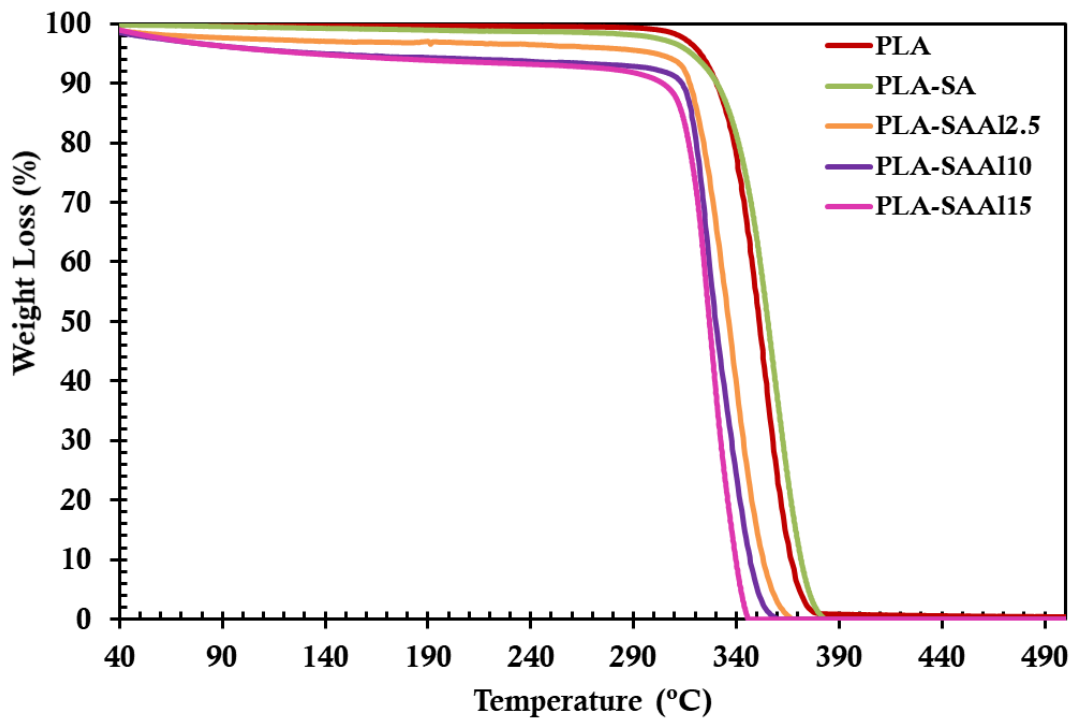


Figure 4.62. Degradation profile of PLA in the presence of the aluminum loaded catalyst.

The activation energies of the synthesized catalysts are tabulated in Table 4.7. With the addition of metal into catalyst the activation energy of the reaction reduced from 262 kJ/mol to 189 kJ/mol.

Table 4.7. Activation energies of PLA degradation reaction in the presence of Al loaded silica aerogels.

Sample	Activation Energy (kJ/mol)
PLA	262
PLA-SAAI2.5	223
PLA-SAAI10	196
PLA-SAAI15	190
PLA-SAUAI15	189

With an increase in metal loading, the activation energy further reduced to 190 kJ/mol due to the presence of more acidic sites in the structure of the catalyst. This result showed that there is a close relationship between the aluminum content and the degradation of PLA in terms of catalytic activity. The degradation of PLA was also studied with SAUAI15. The activation energy required for the degradation of PLA was found to be 189 kJ/mol. With 15 wt.% aluminum loaded silica aerogel catalysts, the degradation of PLA was reduced by roughly 27%. SAUAI15 was used in catalytic degradation of PLA due to better metal dispersion, higher acidity and lower activation energy attained in TGA.

4.2.1.3 Degradation of PLA in the presence of Aluminum Loaded Silica Aerogel Catalyst

The degradation of PLA was studied in the presence of Al loaded silica aerogel catalyst (SAUAI15) in the pyrolysis system. Since reaction temperature was found to be the most effective parameter in product yield and distribution, the experiments conducted at different reaction temperatures varying from 200 °C to 275 °C with

25 °C increments. The effect of catalyst on the product yield is illustrated in Figure 4.63.

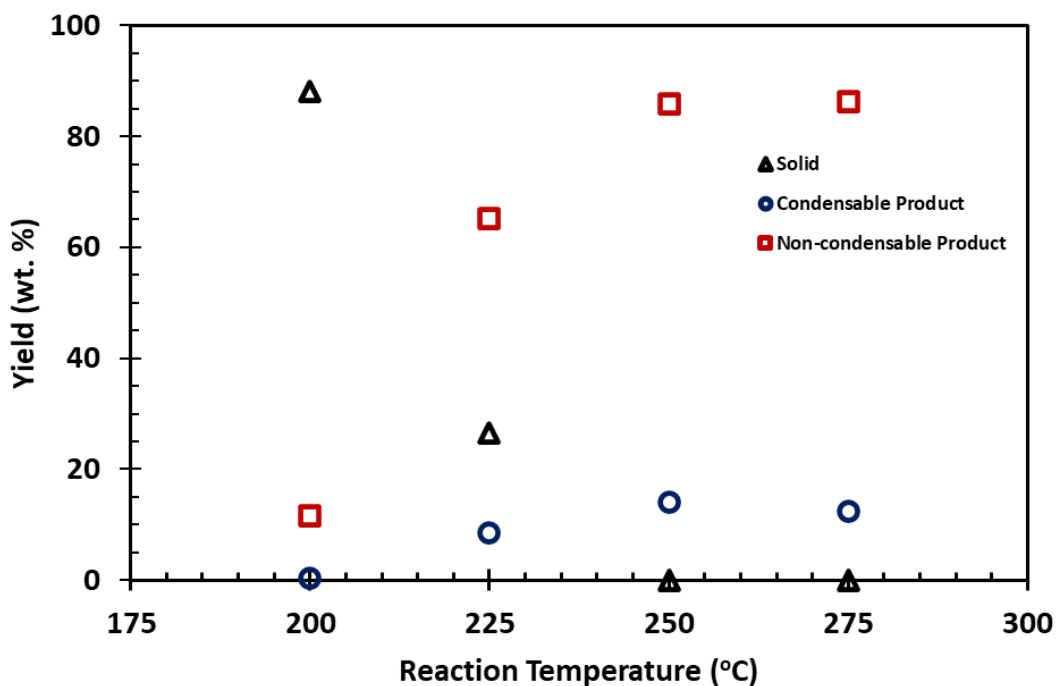


Figure 4.63. The effect of reaction temperature on the yield of products (SAUA115, 60 min, 70 rpm, 50 ml/min).

In the non-catalytic degradation of PLA, the decomposition of PLA was started at 200 °C with 0.5 wt.% of condensable product, 2 wt.% of non-condensable product and 97.5 wt.% of solid product. In the catalytic degradation, the decomposition of PLA started at the same temperature but with different yield weight percentage values. With increasing reaction temperature, a decrease in solid yield and increase in both condensable and non-condensable product yields were observed between the temperature of 200 and 250 °C. At 200 C, the solid yield was found to be 88.14 wt.%

in the reactor. The solid yield was then significantly decreased to a value of 26.47 wt.% at the reaction temperature of 225 °C. The solid product includes low molecular weight compounds and coke formation at the temperature range of 200 and 225 °C. After the temperature of 250 °C, there was not seen any low molecular weight compounds and coke in the reactor. However, coke formation was observed on the surfaces of the catalyst up to a maximum level of 1.29 wt.% at 275 °C. The SAUA115 catalyst tends to a significant increase in the production of non-condensable products with increasing reaction temperature. The effect of the catalyst was also discussed by comparing with the non-catalytic degradation experiments conducted at the same reaction conditions (Figure 4.64).

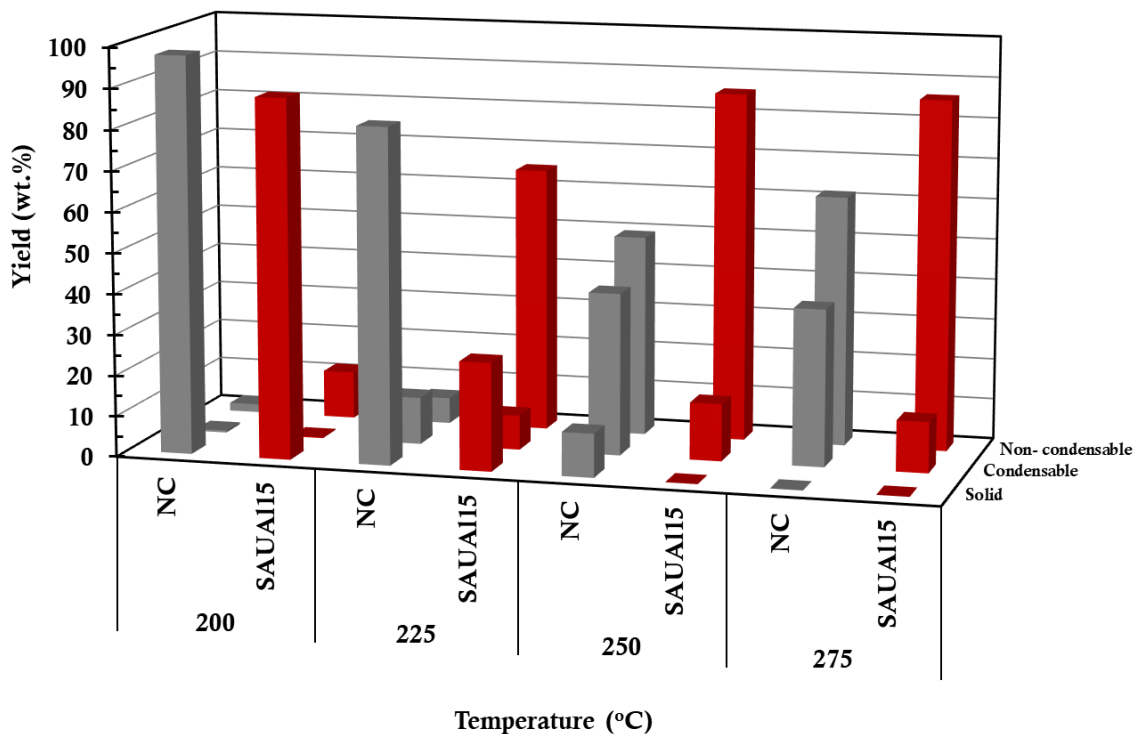


Figure 4.64. Comparison of the catalytic degradation of PLA with the the non-catalytic degradation of PLA in terms of reaction temperature and product yield (60 min, 70 rpm, 50 ml/min).

When the results of the non-catalytic and catalytic degradation of PLA were compared , the solid yield was decreased from 97.5 to 88.14 wt. % in the presence of aluminum loaded catalyst at 200 °C. Although there was not seen a remarkable increase in condensable products, the non-condensable product amount increased from 2 to 11.62 wt.% with the use of SAUAl15 catalyst. The increase in the non-condensable product amount indicates that the catalyst is active in the PLA degradation reaction.

In the non-catalytic degradation of PLA, the yields of solid, condensable and non-condensable products were 82.14 wt.%, 11.52 wt.% and 6.33 wt.% at 225 °C, respectively. The yield of solid product significantly decreased to 26.47 wt.% and the non-condensable product yield increased from 6.33 wt.% to 65.10 wt.% with the use of the SAUA115 catalyst.

At 250 °C, the decrease in solid yield led to an increase in non-condensable products with the catalyst. The non-condensable product yield was found to be 85.94 wt. %. However, the amount of condensable products was reduced from 39.84 wt.% to 14.06 wt.% in the presence of SAUA115 catalyst.

The same trend was observed for the reaction temperature of 275 °C. A slight decrease decrease in condensable products was followed by a slight increase in non-condensable products with SAUA115. The SAUA115 catalyst allowed the formation of more non-condensable product compared to the other product yield (Figure 4.64). The compositions of the condensable and non-condensable products were investigated. The effect of reaction temperature on condensable product distribution in the presence of the SAUA115 catalyst is illustrated in Figure 4.65.

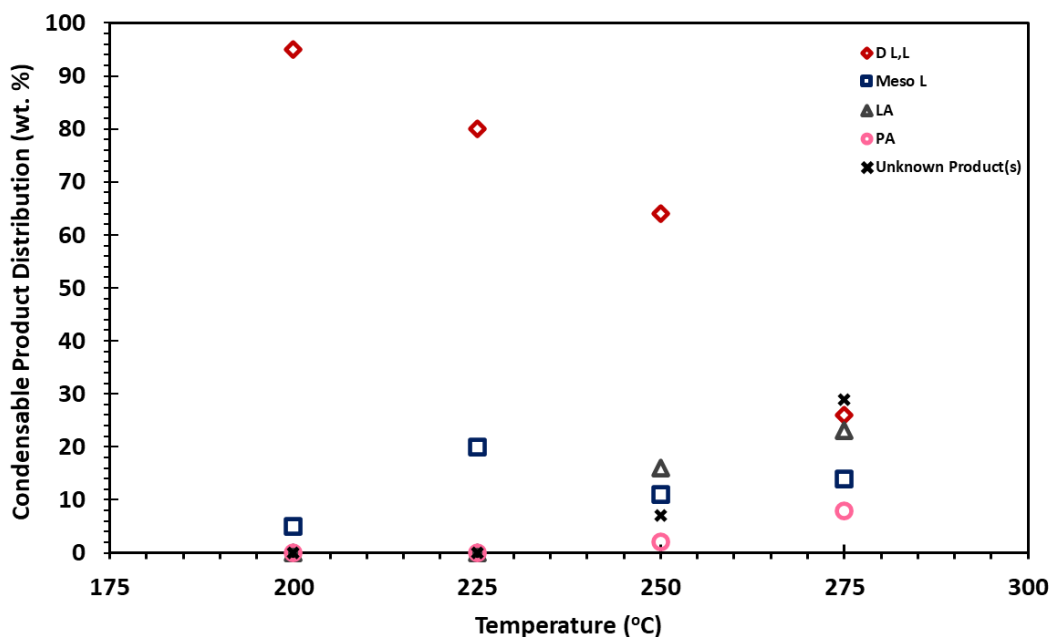


Figure 4.65. The effect of reaction temperature on condensable product distribution (SAUA115, 200-275 °C, 60 min, 70 rpm, 50 ml/min).

With an increase in reaction temperature, D,L,L decreased and LA increased. The amount of Meso L increased from 200 °C to 225 °C, then started to decrease. Beginning from 250 °C, unidentified products were formed at the retention times of 9.3 (U3), 13.4 (U4), 15.9 (U5) and 22.1 min (U2). The formation of unidentified products may result from the conversion of higher molecular weight products to lower molecular weight products due to the acidic nature of the catalyst or from a change in the degradation reaction mechanism. The amounts of propionic acid and unidentified products were increased with increasing the reaction temperature. Figure 4.66 illustrates comparison of the catalytic degradation of PLA with the non-catalytic degradation of PLA in terms of reaction temperature and product distribution in condensable product.

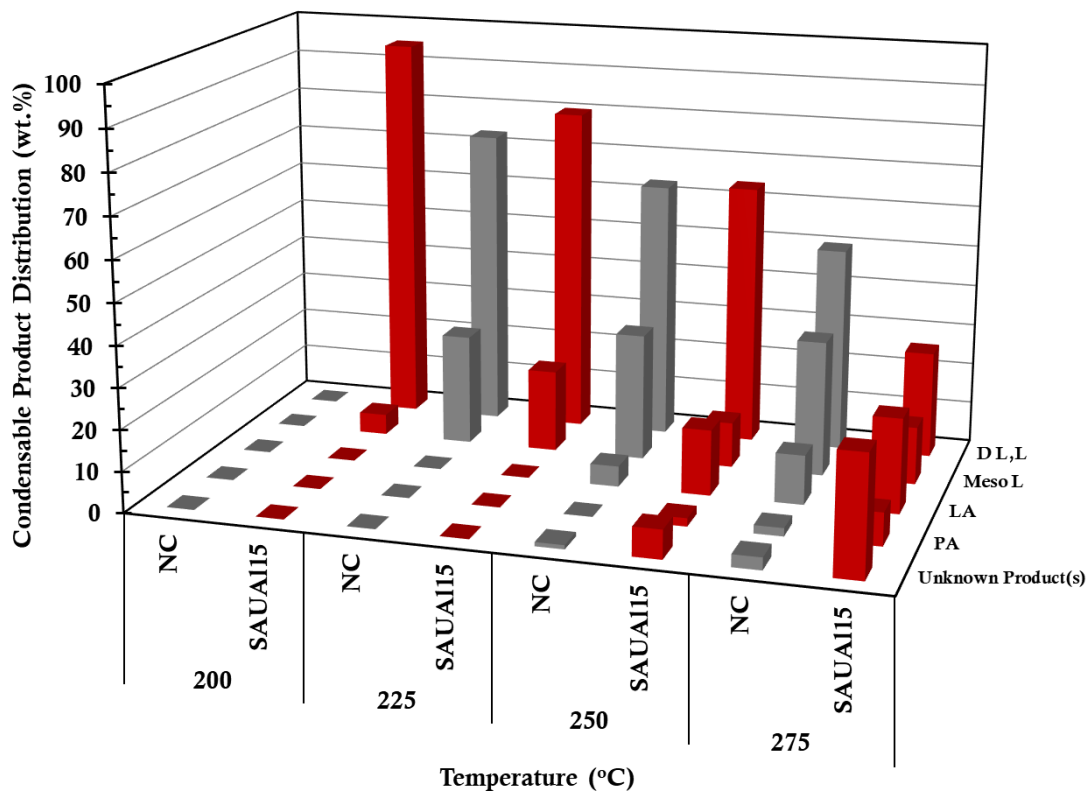


Figure 4.66. Comparison of the catalytic degradation of PLA with the the non-catalytic degradation of PLA in terms of reaction temperature and product distribution in condensable product (60 min, 70 rpm, 50 ml/min).

In non-catalytic degradation studies at 200 °C, only a few mg of condensable products were obtained. With SAUAI15, the formation of lactide isomers was observed. Only 5 wt.% of the condensable products was Meso L. The increase in the formation of lactide isomers was also provided with SAUAI15 for the temperatures of 225 °C and 250 °C.

At 250 °C, the formation of lactide isomers, lactic acid, propionic acid was seen with some unidentified products. Unidentified products were detected at the retention times of 9.3 (U3), 13.4 (U4), 15.9 (U5) and 22.1 min (U2). For the non-catalytic

degradation of PLA, only one peak at 12 minutes (U1) was observed. Due to the acidic nature of the catalyst or a change in the degradation reaction mechanism, the production of unidentified products may result from the conversion of higher molecular weight products to lower molecular weight products.

At 275 °C, the same components were observed for both non-catalytic and catalytic degradation of PLA. The amounts of propionic acid and unidentified components were remarkably increased compared to non-catalytic degradation of PLA at this temperature.

The effect of reaction temperature on non-condensable products was also studied. The non-condensable products were analyzed during the catalytic degradation reaction of PLA. The composition of gas products was firstly analyzed at 15 minute. The composition of gas products with respect to reaction temperature is presented in Figure 4.67.

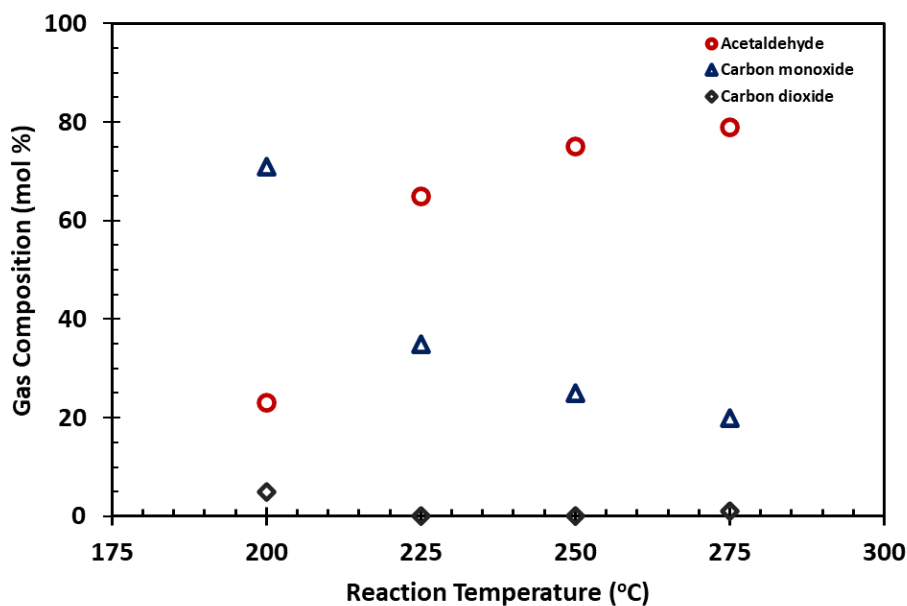


Figure 4.67. The effect of reaction temperature on non-condensable product distribution at the 15th minute (SAUA115, 60 min, 70 rpm, 50 ml/min).

In the studied temperature range, carbon monoxide, carbon dioxide and acetaldehyde were formed. Thermal breakdown process of PLA may be initiated by the homolytic cleavage of the C-O bond close to the ester group, followed by C-O bond breaking in the ester group and C-C bond cleavage. (Li et al., 2022). Following the homolytic scission, thermal breakdown may mostly produce carbon monoxide, carbon dioxide, and acetaldehyde as volatile byproducts (Li et al., 2022).

The main gas product was acetaldehyde in the studied temperature range. In the literature, the amount of CO was higher than that of CO₂ (Kopinke et al., 1996). Increasing reaction temperature tends to an increase in the formation of acetaldehyde. On the other hand, carbon monoxide decreased with temperature. Carbon monoxide was observed at initial stage of the degradation while carbon dioxide was seen (Mlyniec et al., 2016).

Gas composition was also analyzed at 50 minute of the reaction (Figure 4.68). There was seen slight differences in gas composition profiles between the reaction times of 15 minute and 50 minute. The amount of acetaldehyde increased up to 225 °C. After 225 °C, it started dropping up to 250 °C and nearly remained the same between the temperatures of 225 °C and 250 °C. It was known that acetaldehyde degraded into carbon monoxide and methane (Winkler et al., 1934); however, methane formation was not detected. Due to the higher reaction rate in the temperature of 250 °C compared to 225 °C, the degradation reaction was about to be completed at the 50th minute. Therefore, the decrease in acetaldehyde was observed with the increase of temperature from 225 °C to 250 °C.

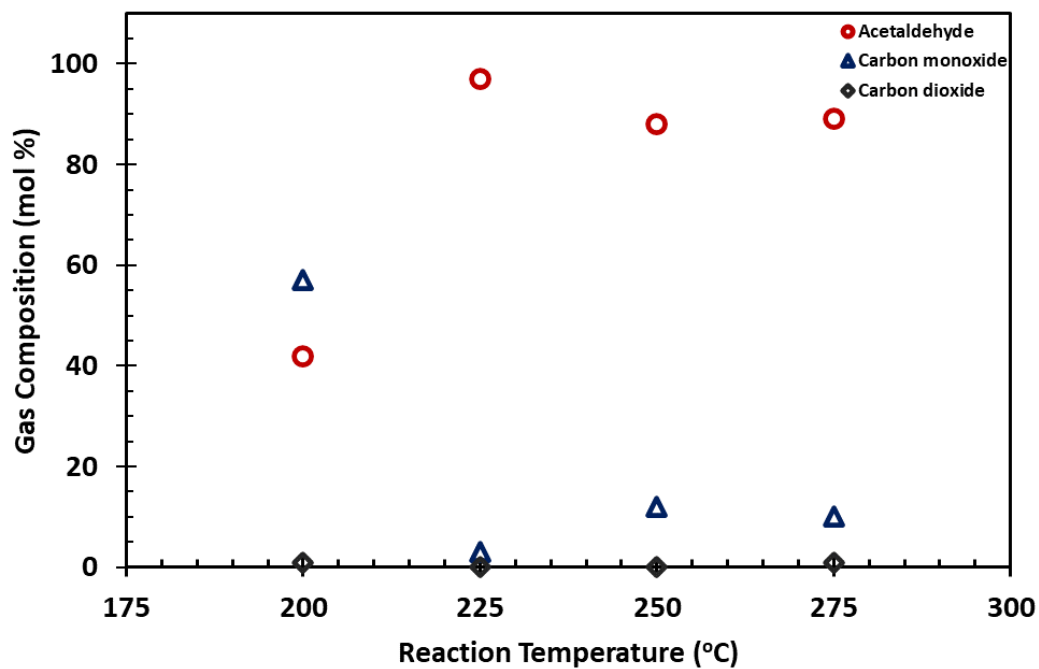


Figure 4.68. The effect of reaction temperature on non-condensable product distribution at the 50th minute (SAUA115, 60 min, 70 rpm, 50 ml/min).

Figure 4.69 presents comparison of the catalytic degradation of PLA with the non-catalytic degradation of PLA in terms of reaction temperature and product distribution in the non-condensable product at the 15th min.

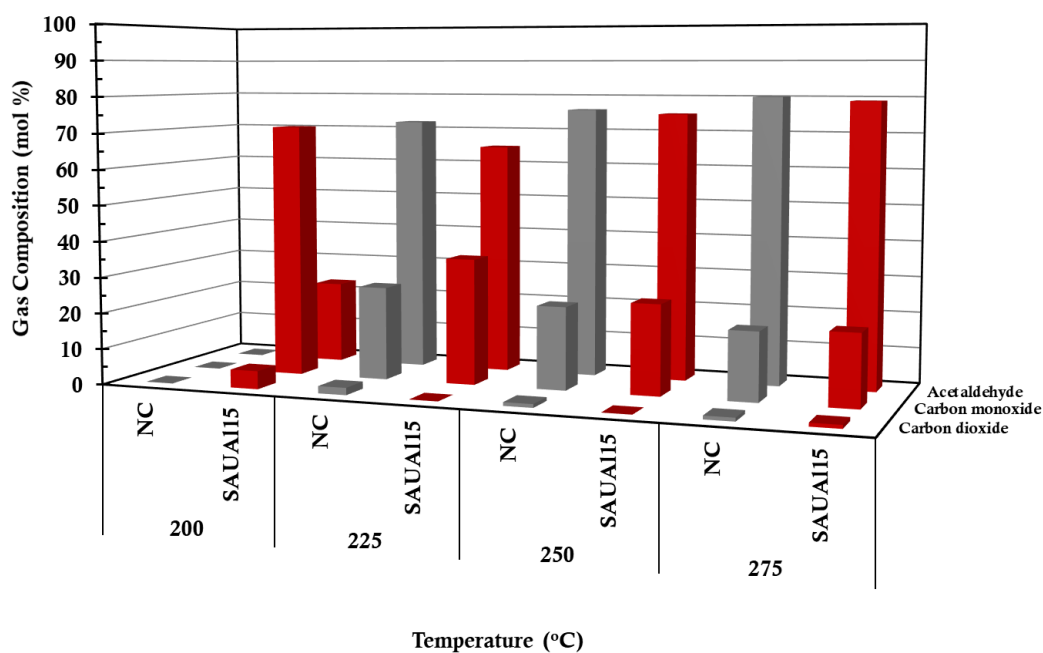


Figure 4.69. Comparison of the catalytic degradation of PLA with the the non-catalytic degradation of PLA in terms of reaction temperature and product distribution in non-condensable product at the 15th min (60 min, 70 rpm, 50 ml/min).

In non-catalytic degradation of PLA, there was not detected any gas formation at 15 minute. The catalytic degradation reaction initiated with the formation of acetaldehyde, carbon monoxide and carbon dioxide. A great portion of the gas products was composed of carbon monoxide at 15 minute with the SAUAI15 catalyst. Increasing reaction temperature tends to a rise in the formation of acetaldehyde for both non-catalytic and catalytic degradation experiments. On the other hand, carbon monoxide decreased with reaction temperature. The reaction products were found as carbon monoxide at initial stages of the degradation while carbon dioxide were seen (Mlyniec et al., 2016).

Comparison of the catalytic degradation of PLA with the the non-catalytic degradation of PLA was done in terms of reaction temperature and product distribution in non-condensable product at the 50th min (Figure 4.70).

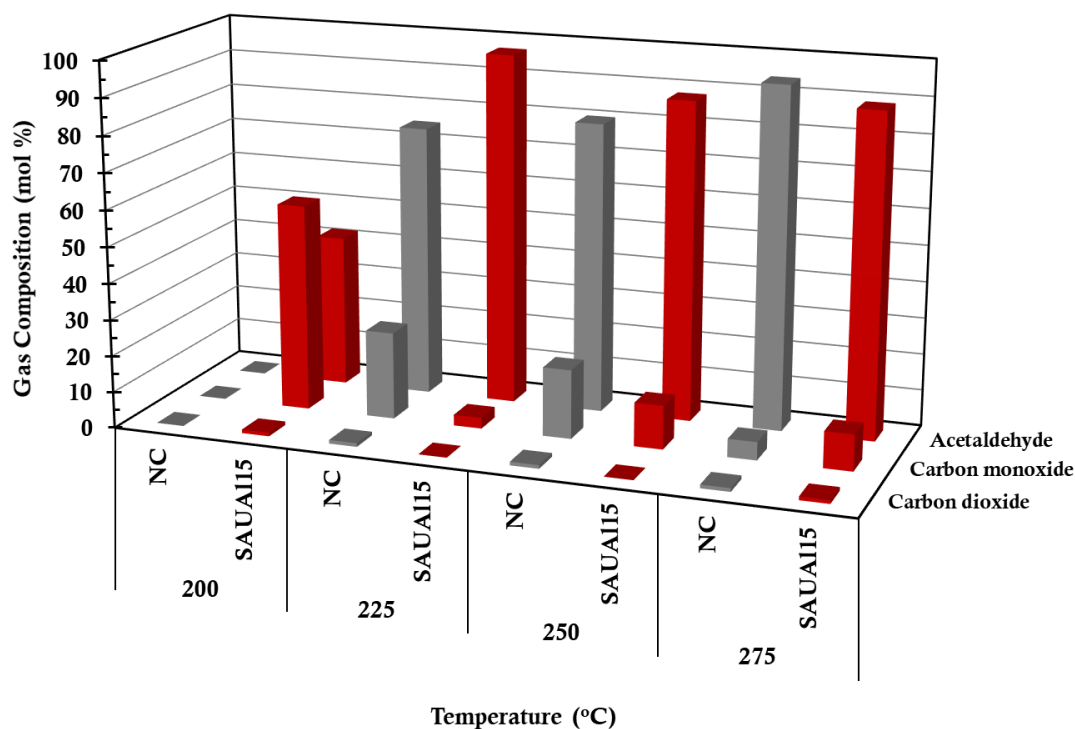


Figure 4.70. Comparison of the catalytic degradation of PLA with the the non-catalytic degradation of PLA in terms of reaction temperature and product distribution in non-condensable product at the 50th min (60 min, 70 rpm, 50 ml/min).

At 200 °C, the amount of acetaldehyde was sharply increased in the presence of SAUAI15 for 50 minute compared to non-catalytic degradation of PLA. Generally, an increase in the amount of acetaldehyde and a decrease in the amount of CO were observed compared to non-catalytic degradation of PLA.

4.2.1.4 Characterization of the Used Catalysts

The nitrogen adsorption/desorption isotherms of the used aluminum loaded catalysts materials are given in Figure 4.71.

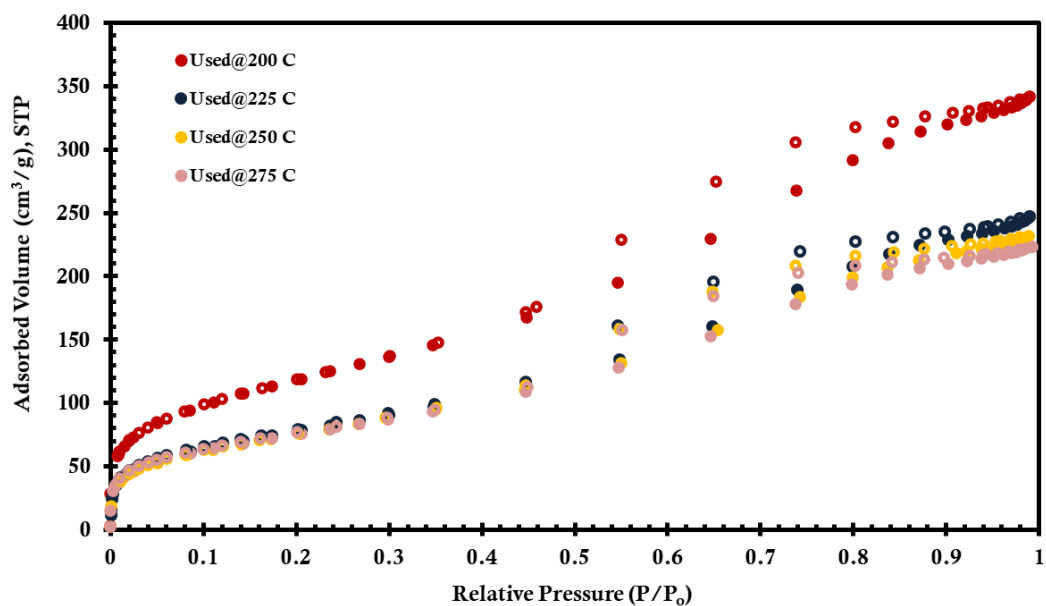


Figure 4.71. Nitrogen adsorption/desorption isotherms of used aluminum loaded silica aerogel catalysts (filled and empty symbols represent adsorption and desorption branches, respectively).

With an increase in reaction temperature, there was seen a decrease in adsorbed nitrogen volume with an exception of the used SAUA115 catalyst at 200 °C. The reduction in adsorbed nitrogen volume might be resulted from the carbon deposition in the catalyst. The pore size distribution of the catalysts are given in Figure 4.72.

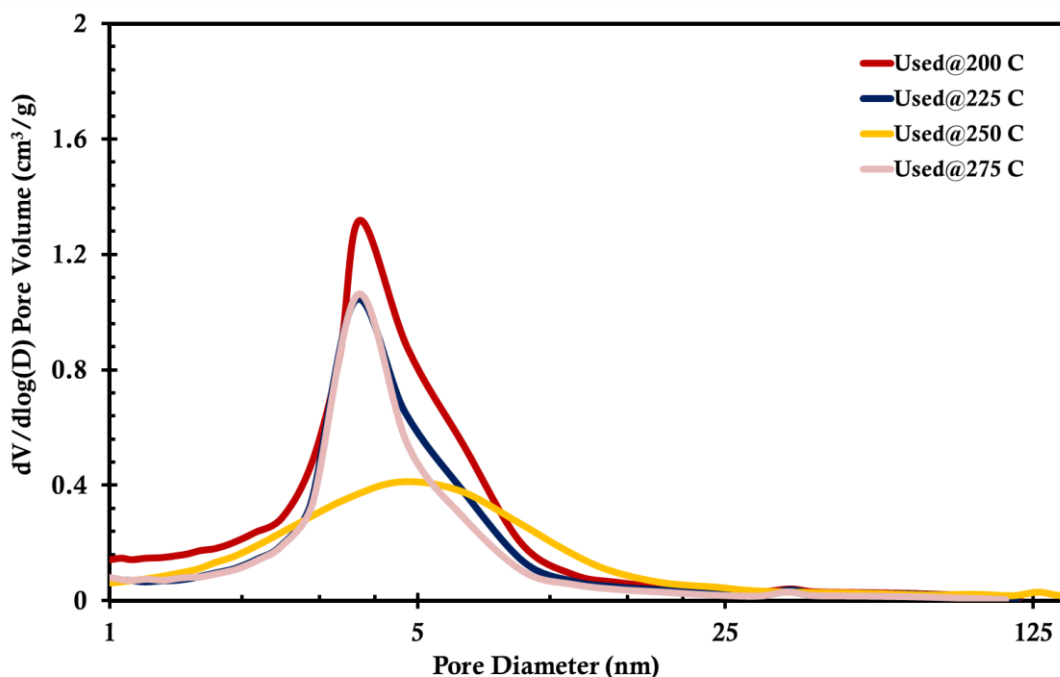


Figure 4.72. Comparison of the pore size distributions of used aluminum loaded silica aerogel catalysts.

The pore volume of the catalyst was decreased with reaction temperature except for the SAUA115 catalysts used at 200 °C. The adsorption/desorption results are consistent with the pore size distribution result of the used SAUA115 catalysts. Shift of the pore size distribution to the lower pore diameter region can be resulted from the coke formation in the catalyst. The physical properties of the used catalysts are given in Table 4.8. The physical properties of used aluminum loaded silica aerogel catalysts.

Table 4.8. The physical properties of used aluminum loaded silica aerogel catalysts.

Catalyst	Surface Area (m²/g)	Pore Volume (cm³/g)	Pore Diameter (nm)	Microporosity (%)
Used@200 °C	429	0.54	3.26	25.2
Used@225 °C	285	0.39	3.52	23.6
Used@250 °C	277	0.36	3.41	23.4
Used@275 °C	273	0.35	3.34	25.2

There was seen a decrease in surface area and pore diameter in the used catalyst at higher temperatures due to the deposition of carbon in the pores of the catalyst.

4.2.2 Degradation of PLA with Iron Loaded Catalyst

Within the scope of this study, iron was the second metal loaded into silica aerogel support. The catalyst was investigated in terms of surface and textural properties, acidity, and degradation ability of PLA as in aluminum loaded catalysts. The degradation of PLA was studied with iron loaded silica aerogel catalysts at the same reaction temperature range as the degradation of PLA with the SAUA115 catalyst. The effect of the iron catalyst on product type and distribution was evaluated in the pyrolysis system comprehensively.

4.2.2.1 Characterization of Iron Loaded Silica Aerogel Catalyst

In addition to aluminum metal, iron was loaded into silica aerogel with 15 wt. %. The physical properties of iron loaded catalyst was investigated with the nitrogen physisorption. Nitrogen adsorption/desorption isotherms of uncalcined silica aerogel material (SAU) and iron loaded silica aerogel catalyst (SAUFe15) are illustrated in Figure 4.73.

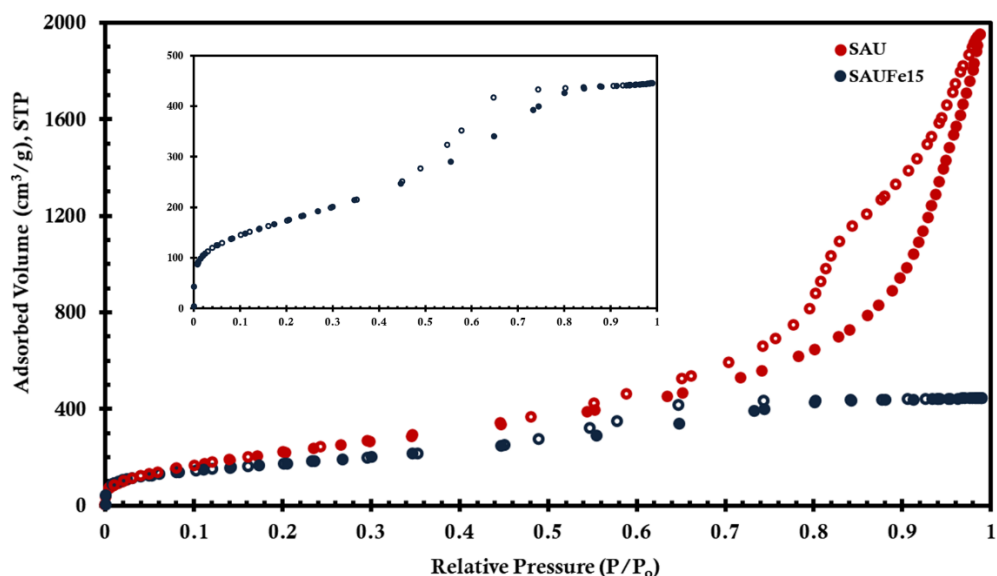


Figure 4.73. Nitrogen adsorption/desorption isotherms of 15 wt.% iron loaded silica aerogel catalyst (filled and empty symbols represent adsorption and desorption branches, respectively).

Iron loaded silica aerogel catalysts also exhibited an isotherm of type IV with H1 hysteresis loop. Iron loading into silica aerogel support causes a decrease in nitrogen adsorption volume. This decrease might be resulted from the blockage of the pores. Furthermore, the pore size distributions of 15 wt.% iron loaded catalyst was provided in Figure 4.74. There has been a certain decrease in pore volume and pore diameter due to the pore blockage. Iron metal was placed into the meso and macropores in the support. The pore size distribution result of the SAUFe15 catalyst was consistent with the adsorption/desorption isotherm result of the catalyst. The physical properties of 15 wt.% iron loaded silica aerogel catalysts was determined. BET surface area was $449 \text{ m}^2/\text{g}$. Pore volume and pore diameter were found to be $1.5 \text{ cm}^3/\text{g}$ and 9.31 nm , respectively. The microporosity of the catalyst was 11.4%.

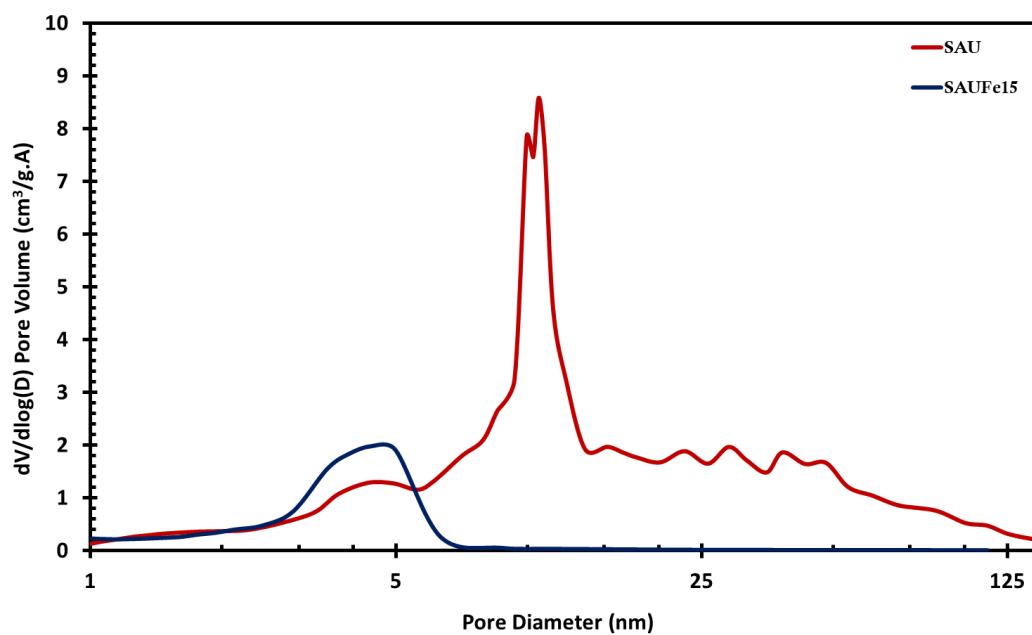


Figure 4.74. The pore size distribution of 15% iron loaded silica aerogel material.

SEM image of SAUFe15 is presented in Figure 4.75. The porous and sponge-like morphology of the silica aerogel is seen. This image is in good agreement with SAU. The metal loadings into supports were found approximately 15 wt.% from EDX analysis of the SAUFe15 catalysts.

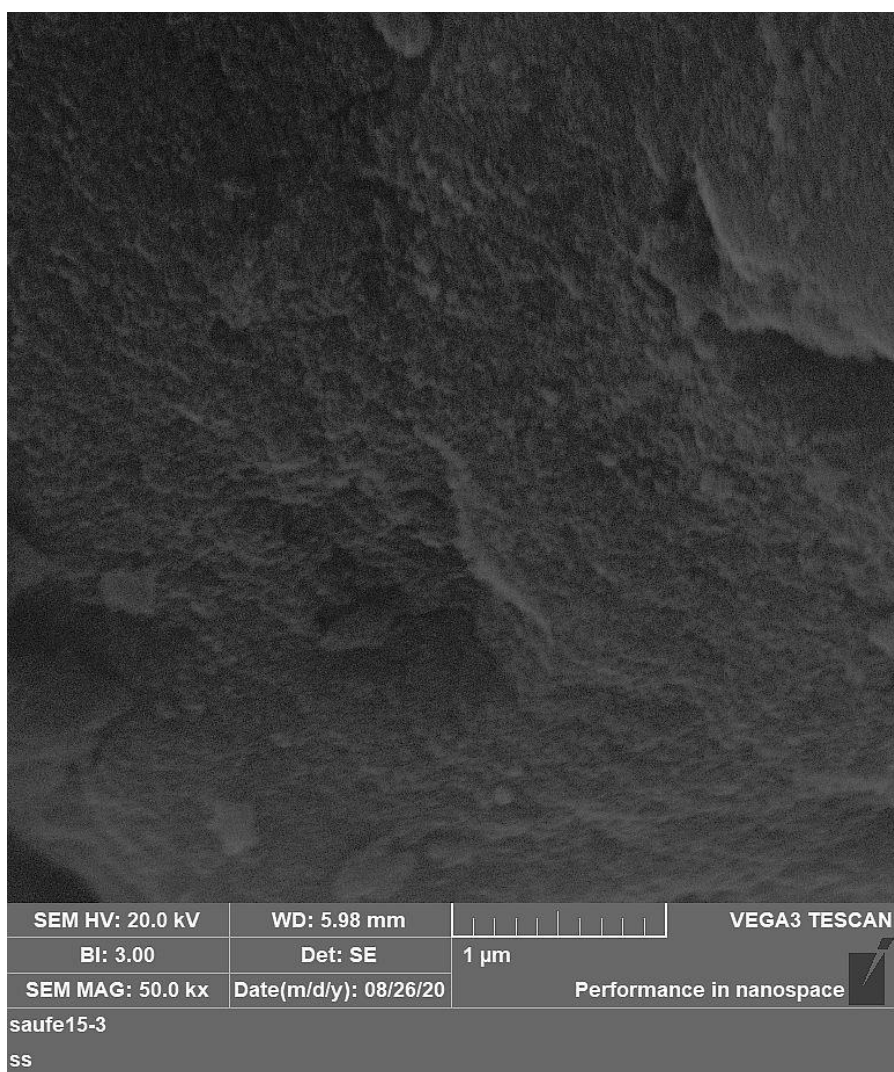


Figure 4.75. SEM image of 15 wt.% iron loaded silica aerogel catalyst with 50kX magnification.

Finally, the DRIFTS spectrum of the pyridine adsorbed SAUFe15 catalyst is shown in Figure 4.76. 15 wt.% iron loaded catalyst exhibited peaks at 1445 cm^{-1} , 1580 cm^{-1} , and 1596 cm^{-1} . These peaks indicated the existence of Lewis acid sites on the catalyst (Aydemir, 2013).

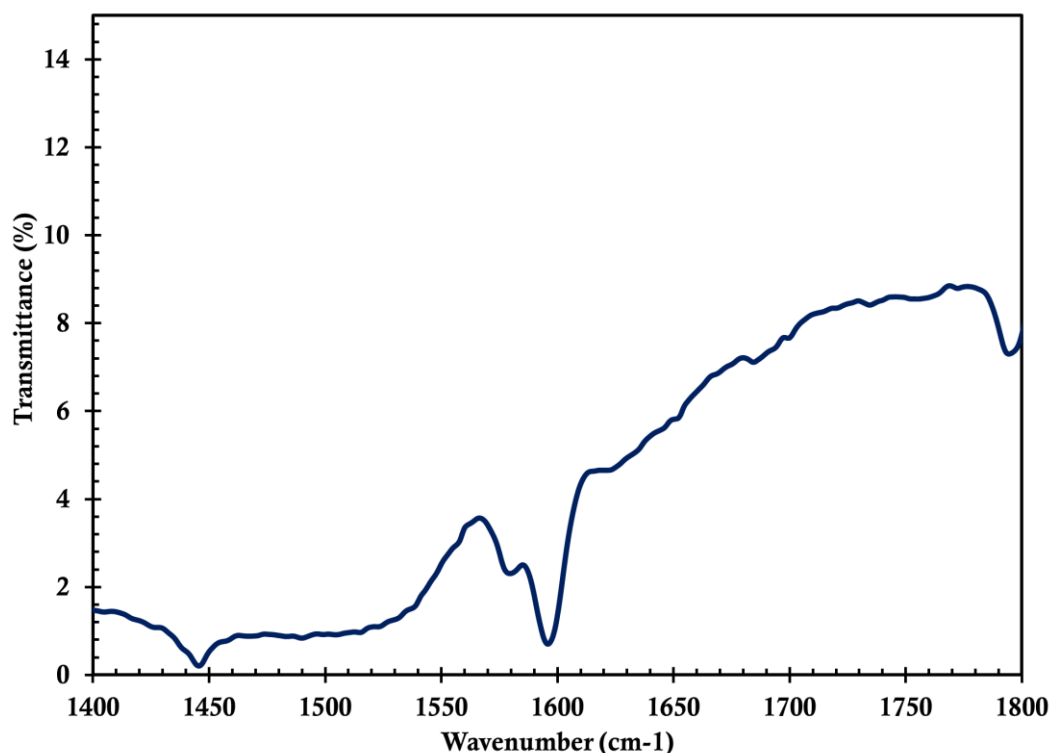


Figure 4.76. DRIFTS spectrum of the pyridine adsorbed 15 wt.% iron loaded silica aerogel catalyst.

4.2.2.2 Determination of Activation Energy of PLA Degradation Reaction in the Presence of Iron Loaded Silica Aerogel Catalyst

Activation energy of PLA degradation in the presence of the iron loaded catalyst was determined using TGA. PLA was degraded under a nitrogen atmosphere with a 50 ml/min flow rate and a 0.5 catalyst to PLA weight ratio. The kinetic parameters of the PLA degradation reaction were evaluated based on a standard power law model. The calculations are given in Appendix A. Figure 4.77 presents thermogravimetric plots of thermal degradation of PLA with iron catalyst.

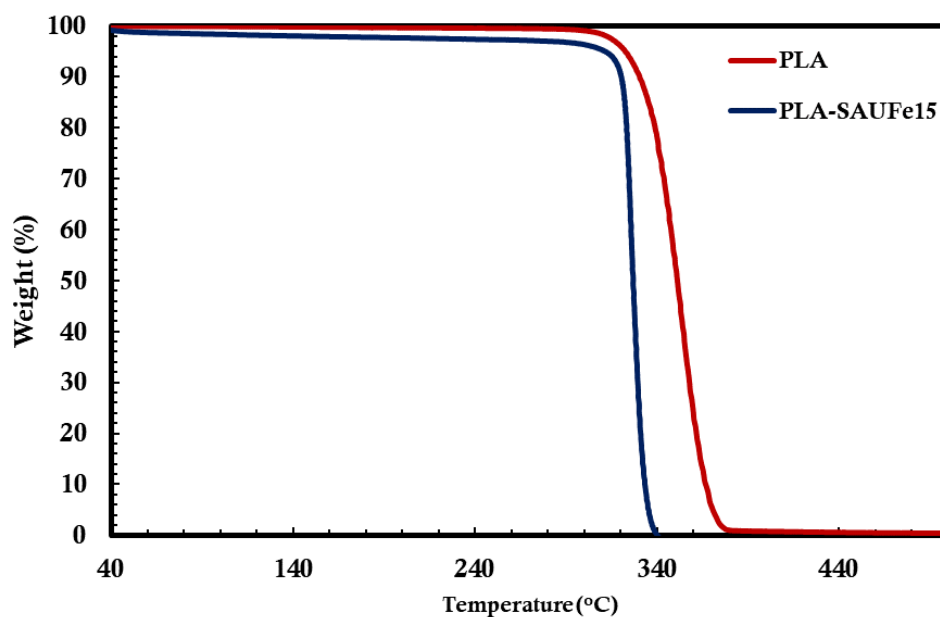


Figure 4.77. Degradation profile of PLA in the presence of the iron loaded catalyst.

As seen in the figure, the use of iron loaded silica aerogel catalyst in the degradation of PLA shifted the degradation profile to the left. This is an indication of a significant decrease in the degradation temperature of PLA. Temperature differences in the degradation of PLA in the presence of SAUF15 catalyst is given in Table 4.9. The highest temperature difference was observed at 60% weight loss.

Table 4.9. Degradation temperature values at 5%, 30%, and 60% weight losses with the SAUFe15 catalyst.

Sample	Degradation Temperature (°C)		
	At 5% Weight Loss	At 30% Weight Loss	At 60% Weight Loss
PLA	322	344	354
PLA-SAUFe15	311	325	328

The activation energy required for the degradation of PLA was calculated as 193 kJ/mol.

4.2.2.3 Degradation of PLA in the presence of Iron Loaded Silica Aerogel Catalyst

In the pyrolysis system, the degradation of PLA was investigated in the presence of an iron loaded silica aerogel catalyst (SAUFe15). PLA degradation was performed at various reaction temperatures ranging from 200 °C to 275 °C. The effect of catalyst on the product yield is illustrated in Figure 4.78.

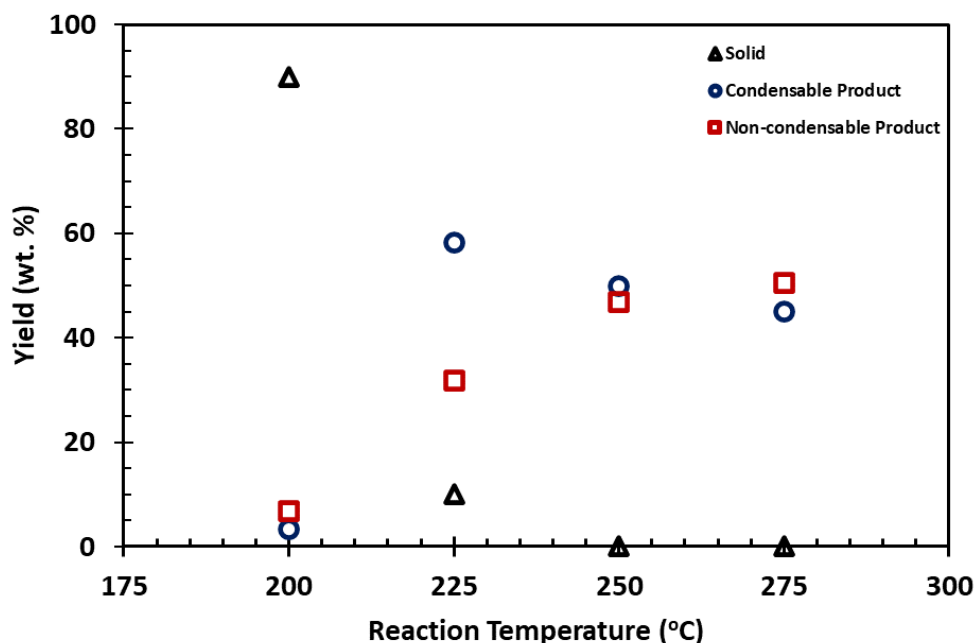


Figure 4.78. The effect of reaction temperature on the yield of products (SAUFe15, 60 min, 70 rpm, 50 ml/min,)

With increasing reaction temperature between 200 and 275 °C, there was shown a decrease in solid product yield with an increase in both condensable and non-condensable product yield. The condensable products increased from 200 °C to 225 °C and then decreased up to 275 °C. At the reaction temperatures of 250 °C and 275 °C, there was not seen any solid product formation; however, coke formation was observed up to 4.5%.

Figure 4.79 demonstrates the comparison of the degradation of PLA in the presence of the SAUFe15 catalyst with the non-catalytic degradation of PLA in terms of reaction temperature and product yield.

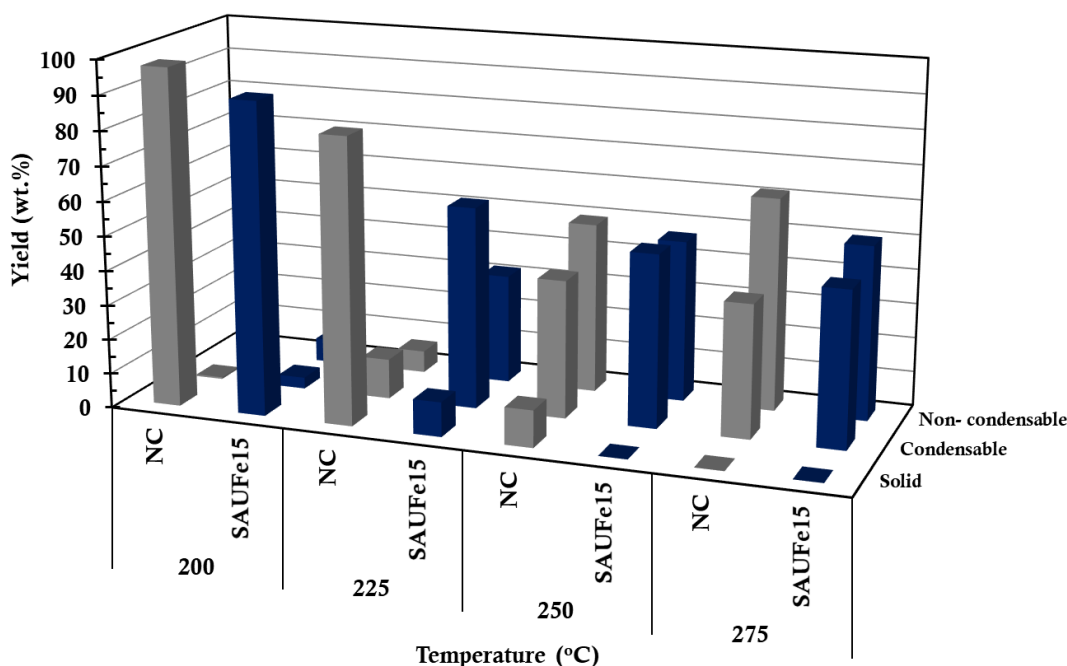


Figure 4.79. Comparison of the catalytic degradation of PLA with the the non-catalytic degradation of PLA in terms of reaction temperature and product yield (60 min, 70 rpm, 50 ml/min).

In the presence of iron-loaded catalyst at 200 °C, the solid yield reduced from 97.5 to 89.94 wt.%. While condensable products increased by 6.5 fold, non-condensable products increased up to 3.5 fold.

For non-catalytic degradation of PLA, the yields of solid, condensable, and non-condensable products were 82.14 wt%, 11.52 wt.%, and 6.33 wt.%, respectively at 225 °C. At 225 °C, the solid yield was found to be 9.97% with the SAUFe15. The solid yield was nearly reduced ninefold. At this temperature, chain scission mechanisms tends to the breakage of the chains by proving lower molecular weight components in the reactor. In addition, there was seen coke formation with lower

molecular weight components in the reactor. The condensable product yield was significantly increased from 11.52 % to 58.3 %, by weight with the SAUFe15 catalyst. The non-condensable product yield was reached to 31.74 wt.%.

At 250 °C, no solid product was observed. The yield of the condensable product was 49.88 wt% with SAUFe15. The amount of non-condensable products decreased slightly compared to non-catalytic degradation. The coke formation was found to be 3.3 wt.% at this reaction temperature with the SAUFe15 catalyst.

At 275 °C, the yield of condensable products decreased to 45.07 wt.%. With SAUFe15 catalyst, there was a trend towards the production of condensable products. The coke formation was risen up to 4.5 wt.% at 275 °C with the SAUFe15 catalyst.

It was determined the composition of condensable and non-condensable products. Figure 4.80 illustrates the influence of reaction temperature on the distribution of condensable products.

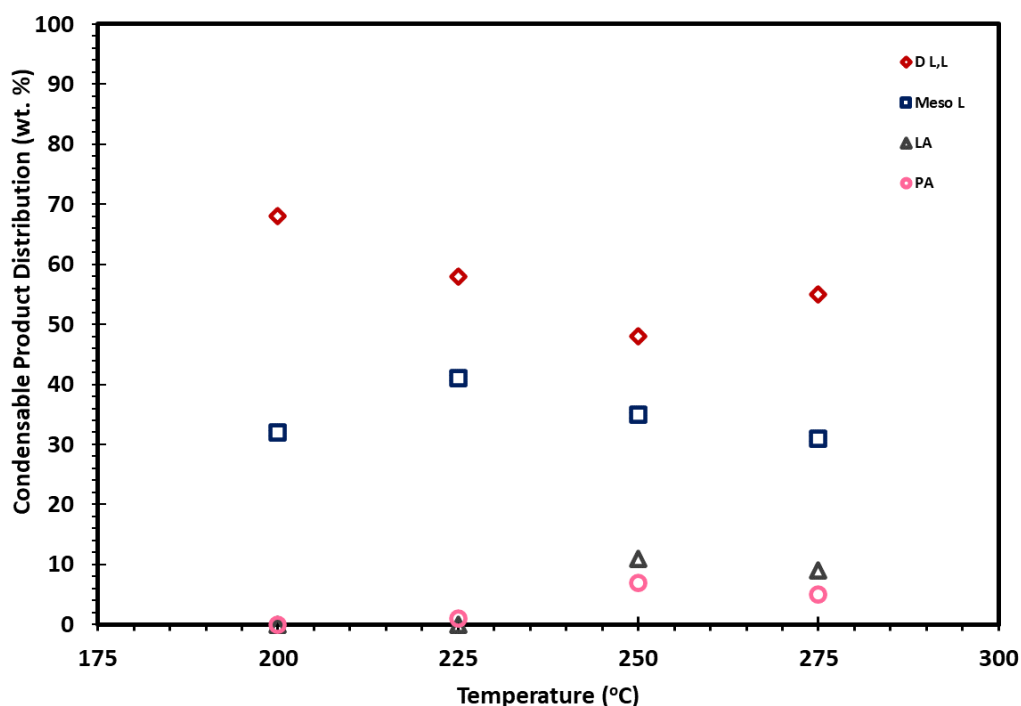


Figure 4.80. The effect of SAUFe15 on condensable product distribution (200-275 °C, 60 min, 70 rpm, 50 ml/min).

With regard to an increase in reaction temperature, D,L,L linearly decreased from 200 °C to 250 °C, then the amount of D,L,L was then increased. The decrease in D,L,L resulted in a rise in Meso L up to 225 °C. The presence of meso lactide was an indication of the radical reactions. The lactic acid formation between the temperatures of 250 °C and 275 °C shows the cis elimination degradation mechanism. Propionic acid can be formed from both radical degradation reaction and the degradation of lactic acid. In addition, catalytic degradation results were compared with non-catalytic degradation results. Figure 4.81 gives the comparison of the catalytic PLA degradation results with the the non-catalytic PLA degradation

results in terms of reaction temperature and product distribution in condensable product.

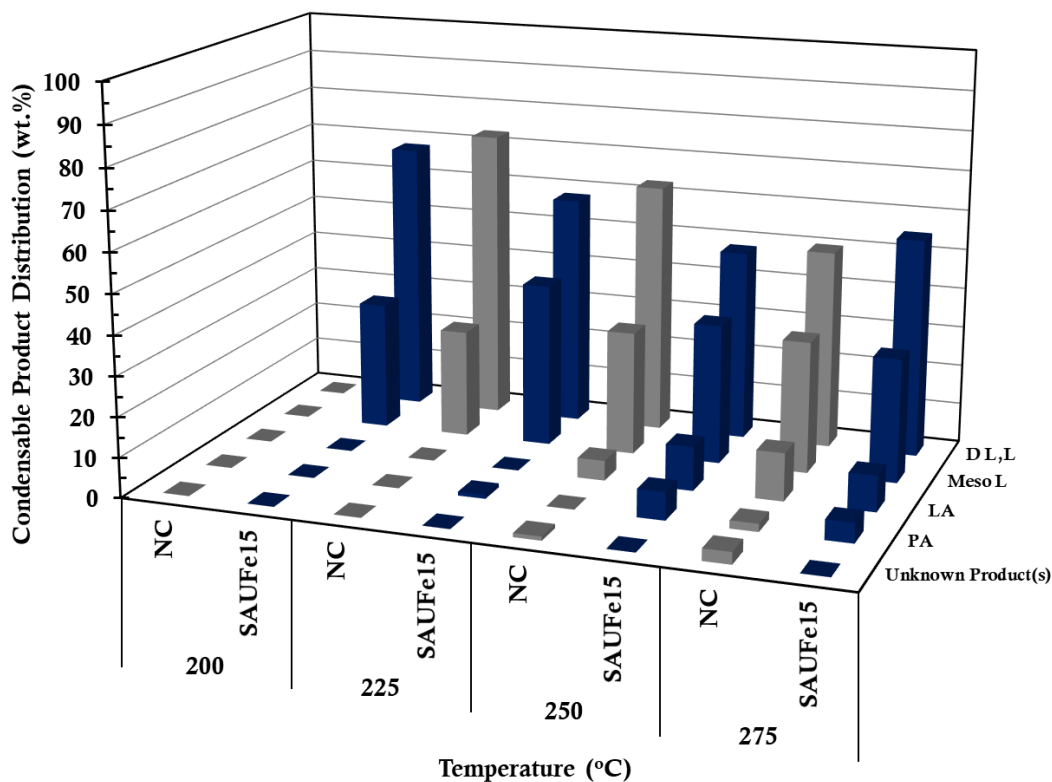


Figure 4.81. Comparison of the PLA degradation of PLA in the presence of SAUFe15 with the non-catalytic degradation of PLA in terms of reaction temperature and product distribution in condensable product (60 min, 70 rpm, 50 ml/min).

In the temperature range of 200 °C and 250 °C, the same degradation behaviour was observed for the non-catalytic and catalytic degradation of PLA.

At 250 °C, the formation of lactic acid and propionic acid became significant with a total of 18 wt.%. It is interesting to note that D L,L was shown a slight increase at 275 °C. This causes a decline in the compositions of Meso L, LA and PA.

The experimental studies on the impact of reaction temperature on non-condensable products proceeded. During the catalytic degradation process of PLA, the non-condensable products were analyzed. The composition of gas products was analyzed at the 15th minutes. Figure 4.82 demonstrates the composition of gas products based on the reaction temperature.

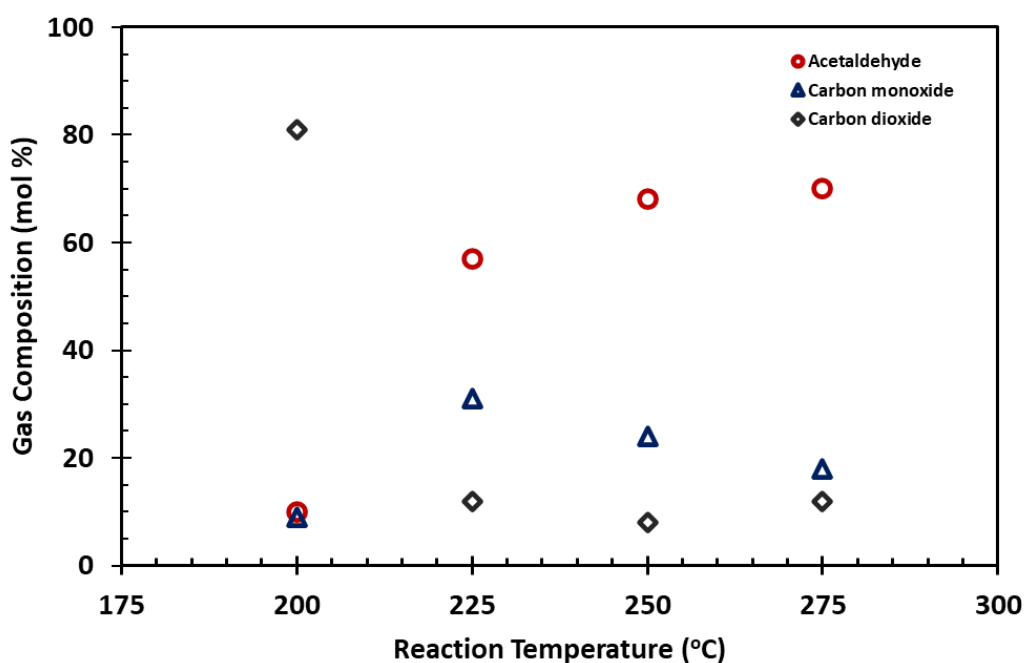


Figure 4.82. The effect of reaction temperature on non-condensable product distribution at the 15th min (SAUFe15, 60 min, 70 rpm, 50 ml/min).

In the studied temperature range, carbon monoxide, carbon dioxide and acetaldehyde were identified. It was interesting to note that the reaction initiated by carbon dioxide formation at 200 °C, then significantly reduced from 81% to 12%, by moles at 225 °C. The concentration of carbon dioxide shifted between 8 and 12 mol% between the temperatures of 250 °C and 275 °C. Acetaldehyde was increased with an increase

in reaction temperature. Gas composition was also analyzed at the 50th minute of the reaction (Figure 4.83).

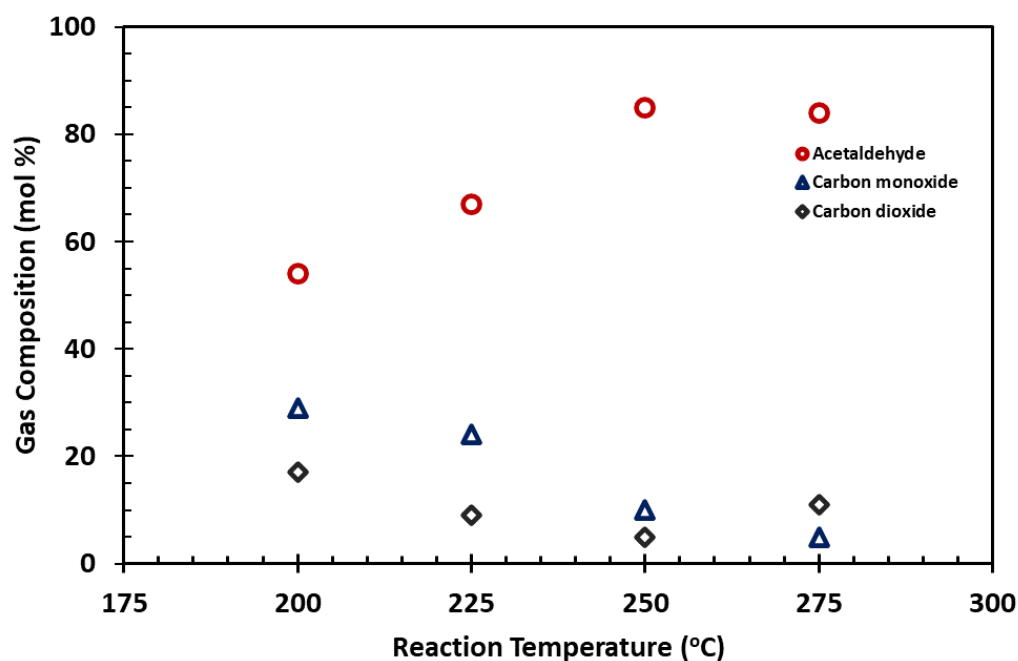


Figure 4.83. The effect of reaction temperature on non-condensable product distribution at the 50th min (SAUFe15, 60 min, 70 rpm, 50 ml/min).

In the studied temperature range, acetaldehyde constituted the majority of the gaseous products. Increasing reaction temperature tends to a rise in the formation of acetaldehyde. On the other hand, carbon monoxide linearly decreased between the temperatures of 200 °C and 275 °C. Figure 4.84 presents the comparison of the catalytic degradation of PLA with the non-catalytic degradation of PLA in terms of reaction temperature and product distribution in non-condensable product at the 15th min

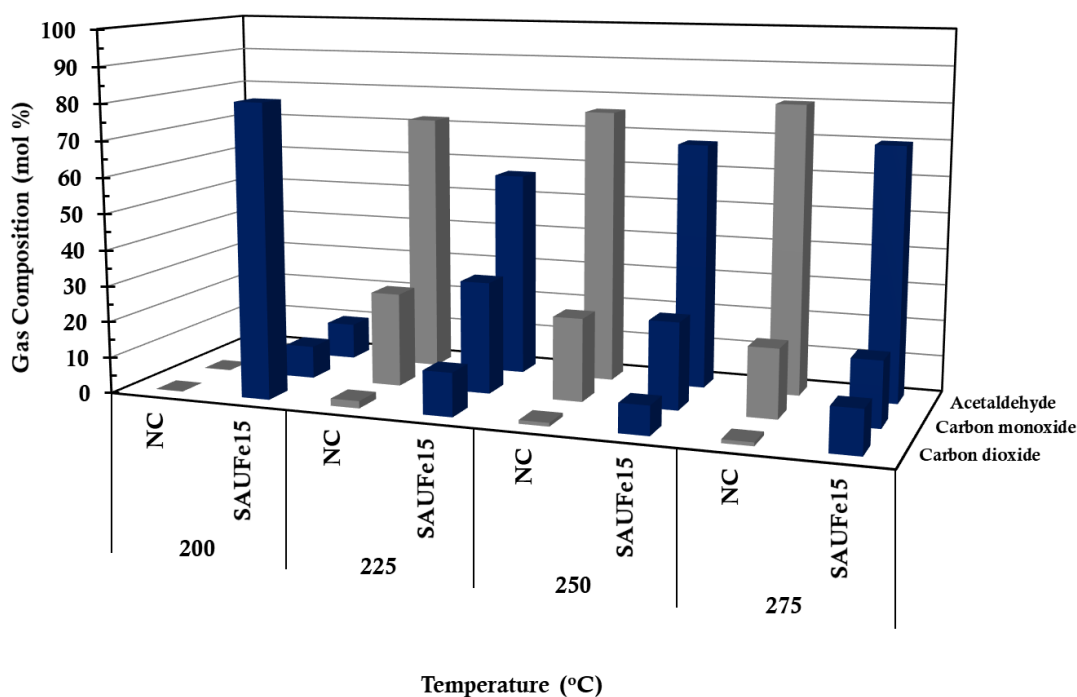


Figure 4.84. Comparison of the catalytic degradation of PLA with the the non-catalytic degradation of PLA in terms of reaction temperature and product distribution in non-condensable product at the 15th min (60 min, 70 rpm, 50 ml/min).

In the temperature range of 225-275 °C, a similar degradation trend was seen with a decrease in acetaldehyde concentration and an increase in carbon dioxide concentration in contrast to non-catalytic degradation of PLA. Figure 4.85 presents the effect of SAUFe15 on gas composition at the 50th minute by comparing the non-catalytic degradation reaction of PLA between the temperature range of 200-275 °C.

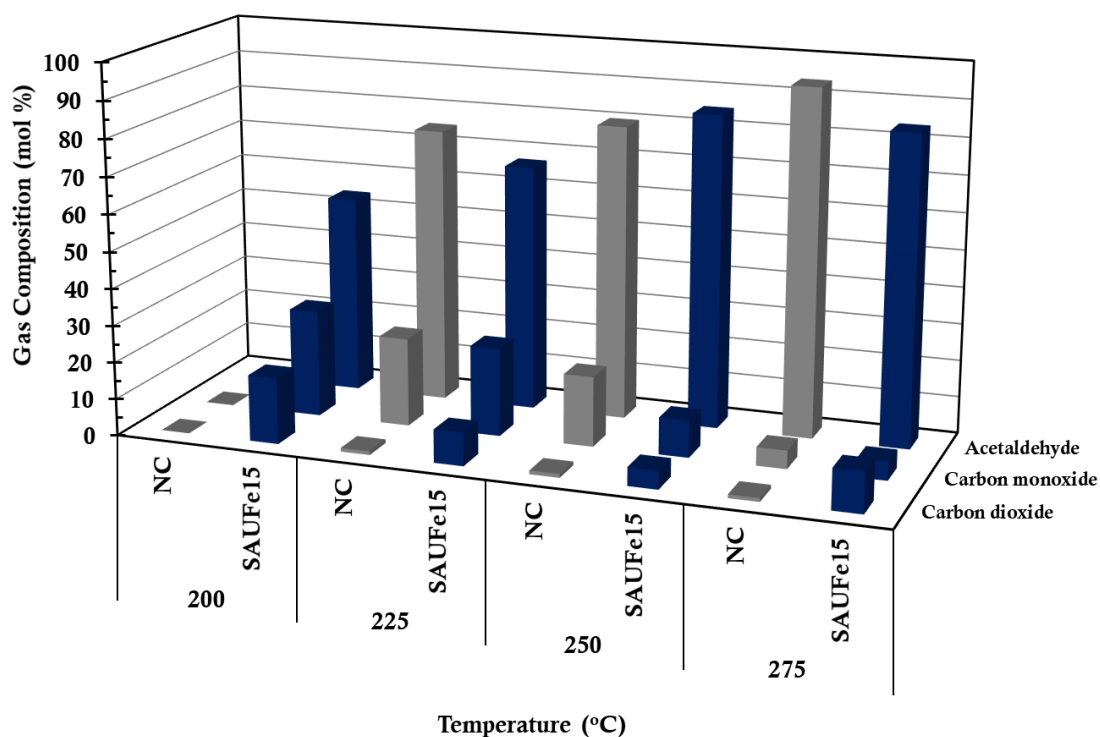


Figure 4.85. Comparison of the degradation of PLA in the presence of SAUFe15 with the the non-catalytic degradation of PLA in terms of reaction temperature and product distribution in non-condensable product at the 50th min (60 min, 70 rpm, 50 ml/min).

An increase in the production of carbon dioxide was mainly provided with the SAUFe15 catalyst at the both reaction time.

4.2.2.4 Characterization of the Used Iron Loaded Silica Aerogel Catalysts

Physisorption studies were carried out to investigate variations in the physical properties of the SAUFe15 catalysts. The nitrogen adsorption/desorption isotherms of 15 wt.% iron loaded catalysts are given in Figure 4.86.

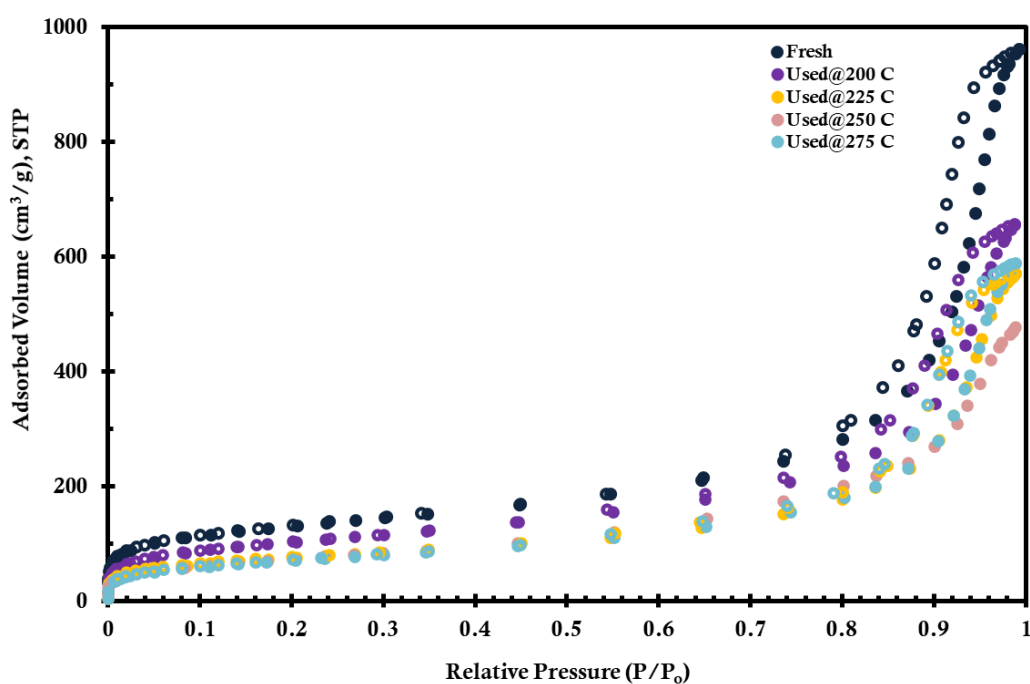


Figure 4.86. Nitrogen adsorption/desorption isotherms of the used iron loaded silica aerogel catalysts (filled and empty symbols represent adsorption and desorption branches, respectively).

All used catalysts exhibited Type IV isotherm with H1 hysteresis. With an increase in reaction temperature, a decrease in nitrogen adsorbed volume was observed. This decrease in adsorbed volume may be due to the formation of coke within the pores of the catalyst. Figure 4.87 demonstrates the pore size distribution of the catalyst.

Pore size distribution results of the used catalysts were consistent with the isotherm results of the catalysts.

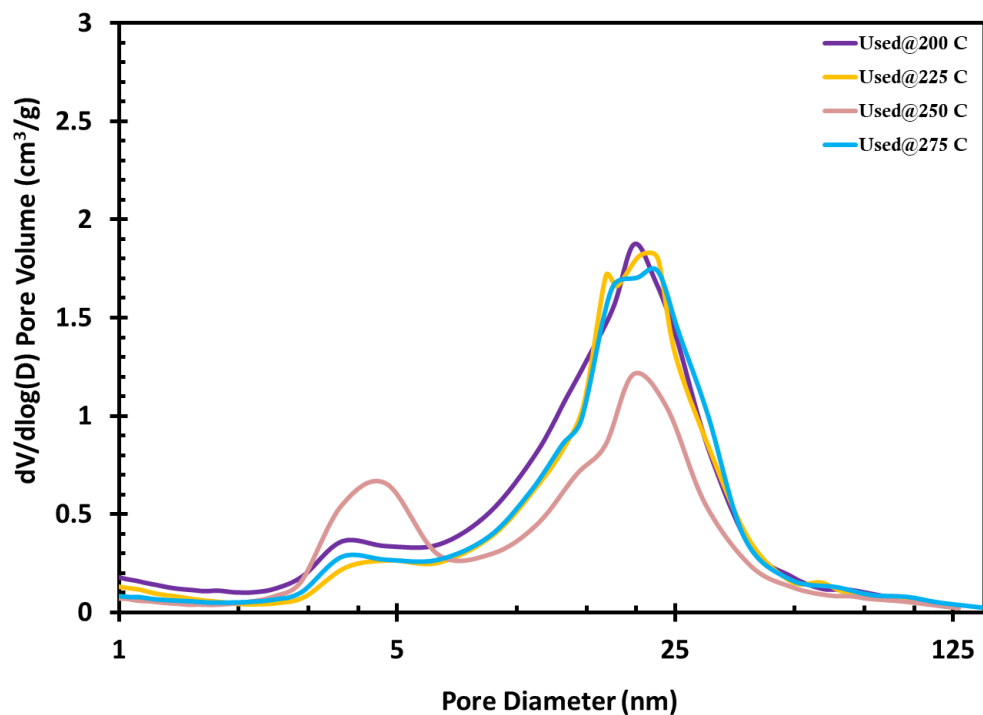


Figure 4.87. Comparison of the pore size distributions of the used iron loaded silica aerogel catalysts.

Table 4.10 summarizes the physical properties of the used iron loaded silica aerogel catalysts.

Table 4.10. The physical properties of the used iron loaded silica aerogel catalysts.

Catalyst	Surface Area (m ² /g)	Pore Volume (cm ³ /g)	Pore Diameter (nm)	Microporosity (%)
Used@200 °C	358	1.02	7.60	12.5
Used@225 °C	259	0.89	9.18	10.5
Used@250 °C	258	0.74	7.41	11.5
Used@275 °C	249	0.91	9.62	9.2

A decrease in surface area and pore volume were seen when the catalyst was utilized at higher temperatures. This decrease may be due to the formation of coke in the pores of the catalyst. At 250 °C, the coke formation was obtained 3.3 wt.% while the coke formation was risen up to 4.5%, by weight. A coke formation was found approximately 90 mg at 275 °C.

The XRD patterns of the fresh and used catalysts are given in Figure 4.88. XRD patterns of fresh and used SAUFe15 catalysts.

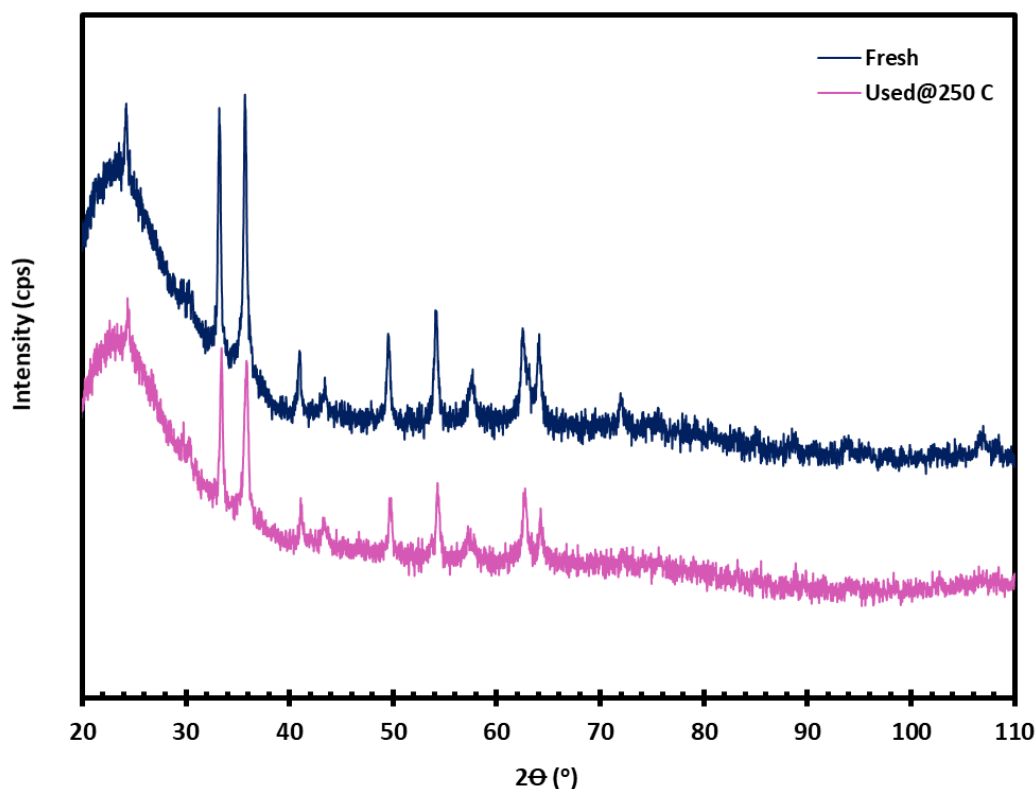


Figure 4.88. XRD patterns of fresh and used SAUFe15 catalysts.

The XRD pattern of the used catalyst is the same as the XRD pattern of the catalyst. It was found that the catalyst have the peaks of Fe_2O_3 . There was seen peak at 26.38° . This peak could be related to carbon formation in the catalyst.

4.2.3 Degradation of PLA with Magnesium Loaded Catalyst

Magnesium was the last metal loaded into silica aerogel support. Performance of the catalyst was studied in the degradation of PLA. In the pyrolysis system, the effect of the catalyst on the product type and distribution was investigated.

4.2.3.1 Characterization of Magnesium Loaded Catalyst

Characterization of magnesium loaded silica aerogel catalysts were done by using several techniques. Figure 4.89 shows the nitrogen adsorption/desorption isotherm of SAUMg15.

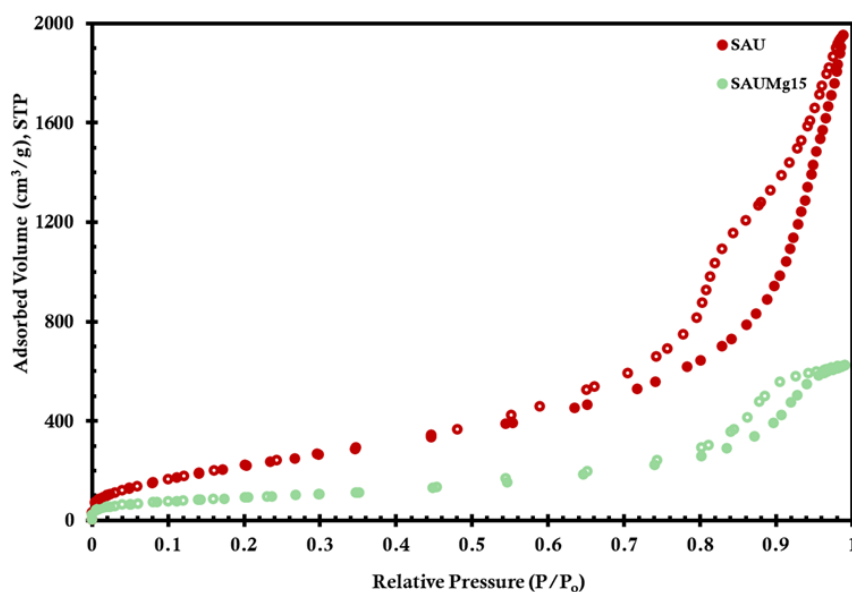


Figure 4.89. Nitrogen adsorption/desorption isotherms of magnesium loaded silica aerogel catalyst (filled and empty symbols represent adsorption and desorption branches, respectively).

The magnesium loaded silica aerogel catalyst exhibited an isotherm of type IV, and the mesoporous structure is retained at all synthesized Mg loaded catalysts. Hysteresis loop was revealed to be H1 for magnesium loaded silica aerogel.

Figure 4.90 illustrates the pore size distributions of the 15 wt.% magnesium loaded catalyst. Due to the pore blockage, there has been a drop in pore volume.

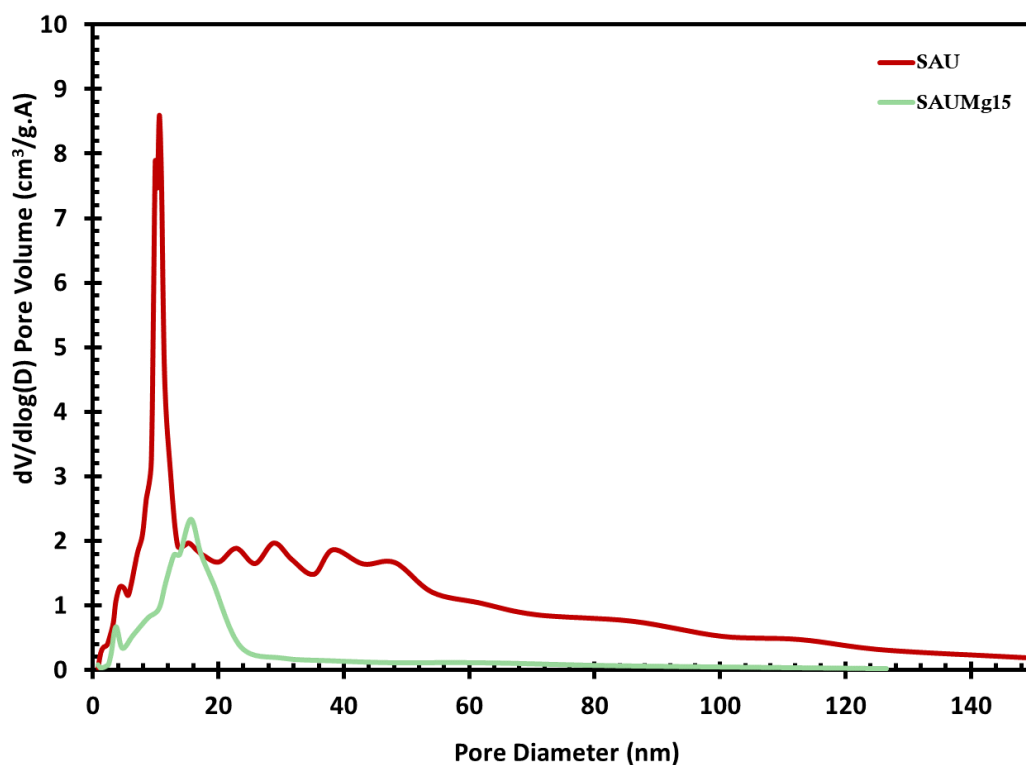


Figure 4.90. The pore size distribution of magnesium loaded silica aerogel catalyst.

Multi-point BET surface area of the SAUMg15 catalyst was determined to 331 m²/g. The average pore volume and pore diameter of the catalyst were found to be 0.97 cm³/g and 7.90 nm, respectively. The microporosity of the catalyst was obtained as 10.84 %.

Lastly, the pyridine was adsorbed on the catalyst to assess the surface acidity of the catalyst (Figure 4.91). Catalyst containing 15% magnesium displayed peaks at 1445 cm⁻¹, 1580 cm⁻¹, and 1596 cm⁻¹. These peaks belong to Lewis acid sites on the catalyst (Aydemir, 2013).

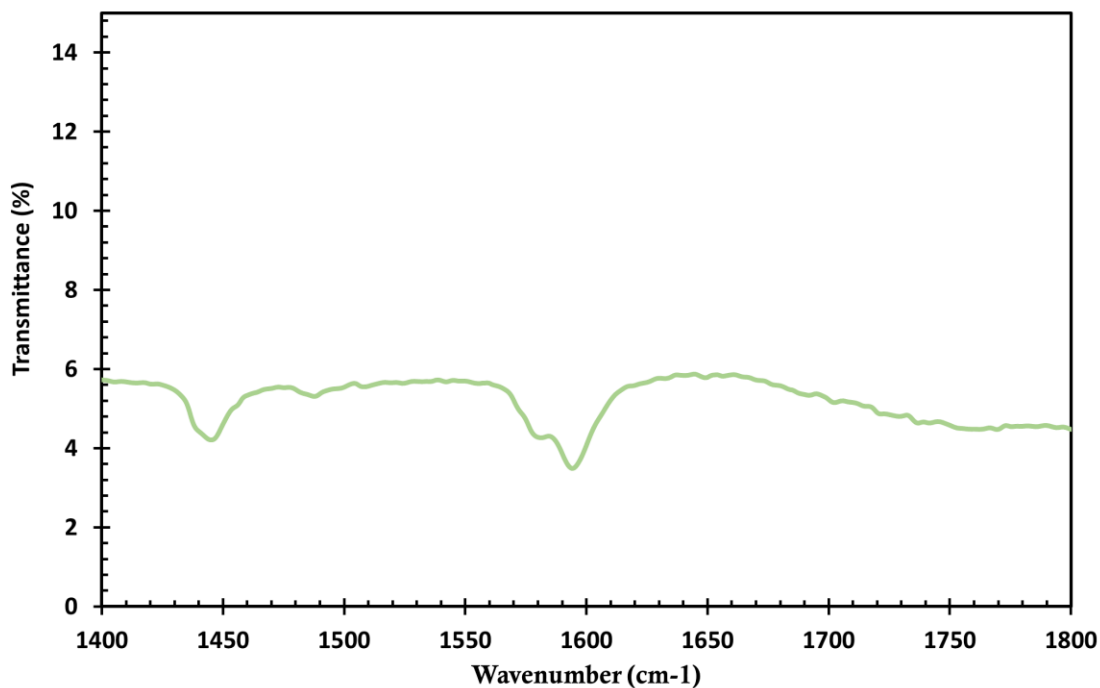


Figure 4.91. DRIFTS spectrum of the pyridine adsorbed 15 wt.% magnesium loaded silica aerogel catalyst.

4.2.3.2 Determination of Activation Energy of PLA Degradation Reaction in the Presence of Magnesium Loaded Silica Aerogel Catalyst

Activation energy of PLA degradation in the presence of magnesium loaded catalysts was determined using TGA. PLA was degraded under a nitrogen atmosphere with a 50 ml/min flow rate and the catalyst to PLA weight ratio of 0.5. The kinetic parameters of the PLA degradation reaction were evaluated based on a power law model. Activation energy calculation is given in Appendix A. Figure 4.92 presents thermogravimetric plots of thermal degradation of PLA with magnesium catalyst.

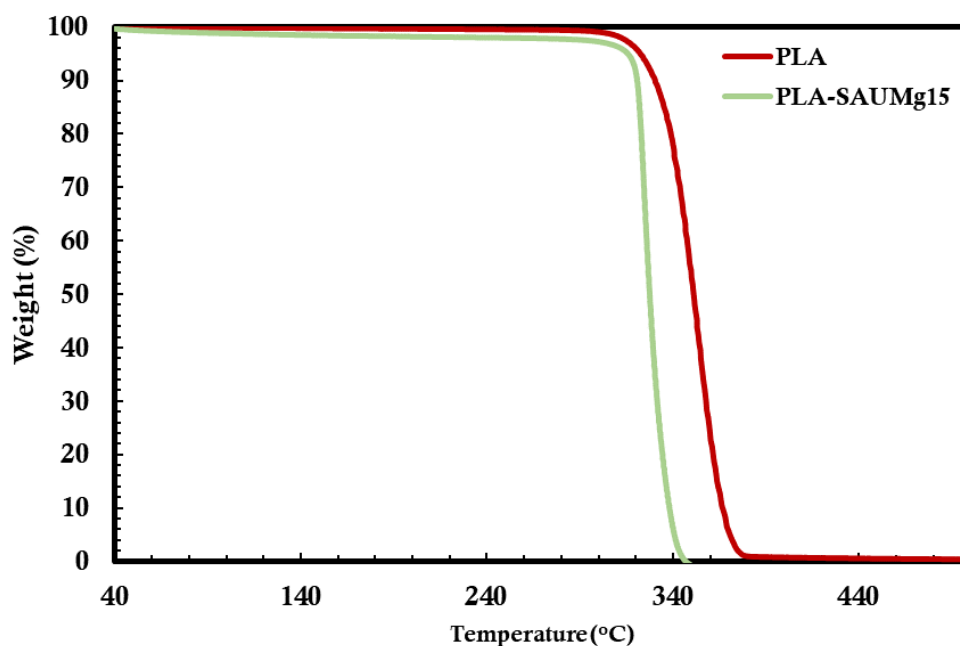


Figure 4.92. Degradation profile of PLA in the presence of the magnesium loaded catalyst.

Magnesium loaded silica aerogel catalyst shifted the degradation curve to the left, as seen in the figure. This indicates a considerable reduction in the PLA degradation temperature. 208 kJ/mol was determined to be the activation energy of PLA degradation reaction.

Temperature differences in the degradation of PLA in the presence of the SAUMg15 catalyst is given in Table 4.11. The highest temperature difference (25 °C) was observed at 60% weight loss.

Table 4.11. Degradation temperature values at 5%, 30%, and 60% weight losses with the SAUMg15 catalyst.

Sample	Degradation Temperature (°C)		
	At 5% Weight Loss	At 30% Weight Loss	At 60% Weight Loss
PLA	322	344	354
PLA-SAUMg15	316	324	329

4.2.3.3 Degradation of PLA in the presence of Magnesium Loaded Silica Aerogel Catalyst

In the pyrolysis system, the degradation of PLA with magnesium loaded silica aerogel catalyst (SAUMg15) was investigated at reaction temperatures ranging from 200 to 275 °C. Figure 4.93 shows the influence of the catalyst on the product yield

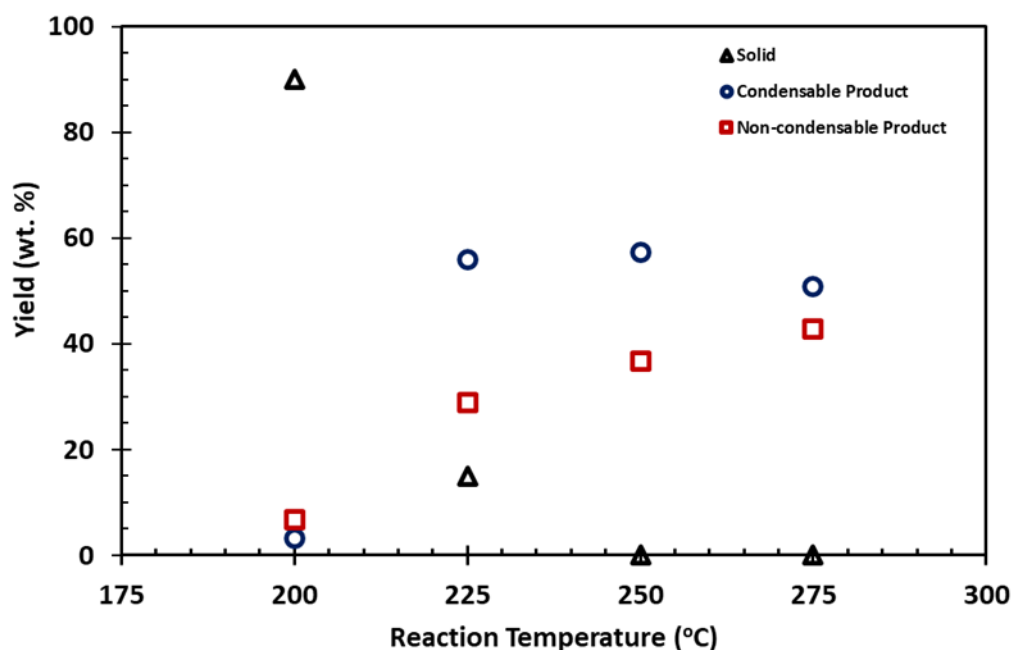


Figure 4.93. The effect of reaction temperature on the yield of products (SAUMg15, 60 min, 70 rpm, 50 ml/min)

With increasing reaction temperature from 200 to 275 °C, a decrease in solid product yield and an increase in non-condensable product yield were observed. The condensable products firstly rose from 200 °C to 225 °C, then continued to slightly decrease up to 275 °C. At 200 °C, the solid yield was 90.29 wt.%. At the reaction temperature of 225 °C, the solid yield decreased significantly to 15.22 wt.%. Coke formation was observed in the solid products in all studied temperature. At 250 °C, the coke formation was found to be 5.9 wt% whereas 6.5 wt.% coke formation was seen at 275 °C.

Figure 4.95 shows the comparison of the degradation of PLA in the presence of the SAUMg15 catalyst with the non-catalytic degradation of PLA in terms of reaction temperature and product yield.

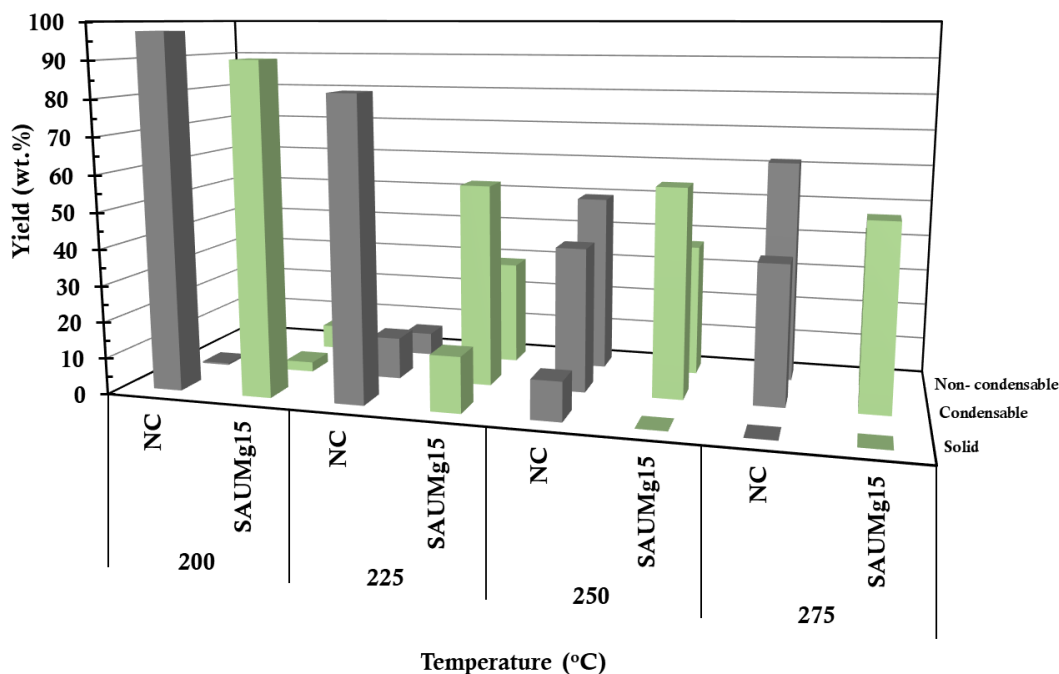


Figure 4.94. Comparison of the degradation of PLA in the presence of SAUMg15 with the the non-catalytic degradation of PLA in terms of reaction temperature and product yield (60 min, 70 rpm, 50 ml/min).

In the presence of magnesium loaded catalyst at 200 °C, the solid yield reduced from 97.5 to 90.29 wt.%. While condensable product increased 5 times at 200 °C, non-condensable product increased 3 times at this temperature compared to non-catalytic degradation of PLA. The increase in condensable and non-condensable products revealed that SAUMg15 is an active catalyst for the degradation of PLA.

In the non-catalytic degradation of PLA at 225 °C, the calculated yields of solid, condensable, and non-condensable products were 82.14 wt%, 11.52 wt.%, and 6.33 wt.%, respectively.

At 225 °C, the solid products were converted into condensable and non-condensable products with the catalyst. The solid yield was found to be 15.52 % with SAUMg15. The solid yield was nearly reduced ninefold. At this temperature, chain scission mechanisms tends to the breakage of the chains by proving lower molecular weight components in the reactor. In addition, there was seen coke formation with lower molecular weight components in the reactor. The condensable product yield was significantly increased from 11.52 % to 55.89 %, by weight. The non-condensable product yield was reached to 28.89 wt.%.

The decline in solid yield led to an increase in condensable products at 250 °C with the catalyst. The yield of the condensable product was 57.36 wt%. The amount of non-condensable products decreased slightly.

In contrast to non-catalytic degradation, the rise in condensable products was followed by a fall in non-condensable products. Figure 4.95 illustrates the influence of the SAUMg15 catalyst on the distribution of condensable product.

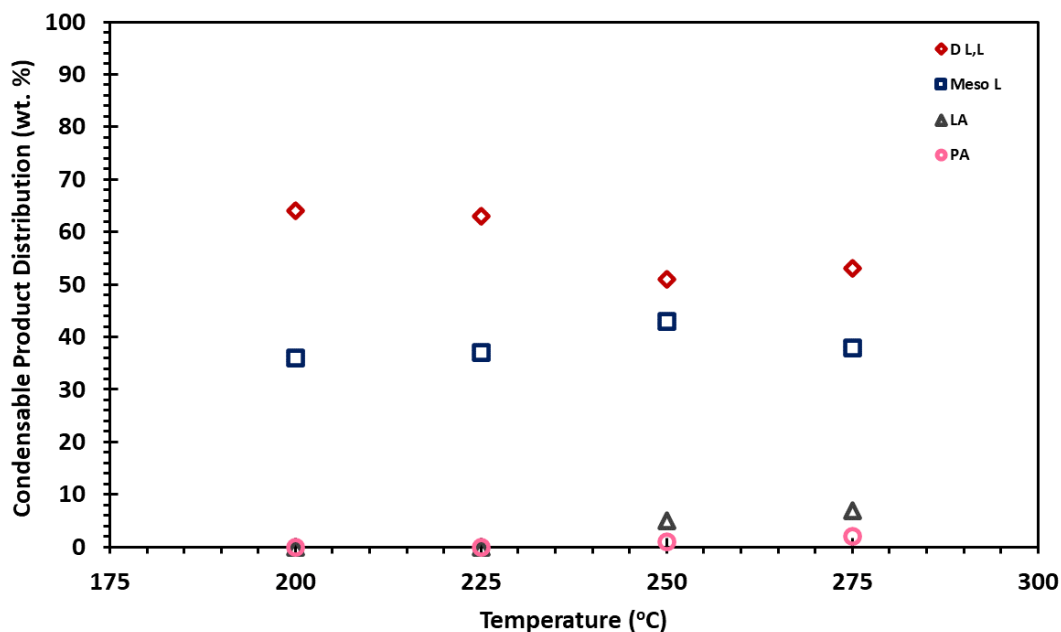


Figure 4.95. The effect of SAUMg15 on condensable product distribution (60 min, 70 rpm, 50 ml/min).

With regard to an increase in reaction temperature, D L,L and Meso L remained nearly constant between 200 °C and 225 °C. Then, a reduction in meso L was observed in the temperature range of 250 °C and 275 °C. The decrease in D L,L resulted in a rise in Meso L. The presence of meso lactide was an indication of the radical reactions. The lactic acid formation in the temperature range of 250-275 °C shows the cis elimination reaction. Propionic acid can be formed from both radical degradation reaction and the degradation of lactic acid. Figure 4.96 gives comparison of the catalytic degradation PLA degradation with the non-catalytic PLA degradation in terms of reaction temperature and condensable product distribution.

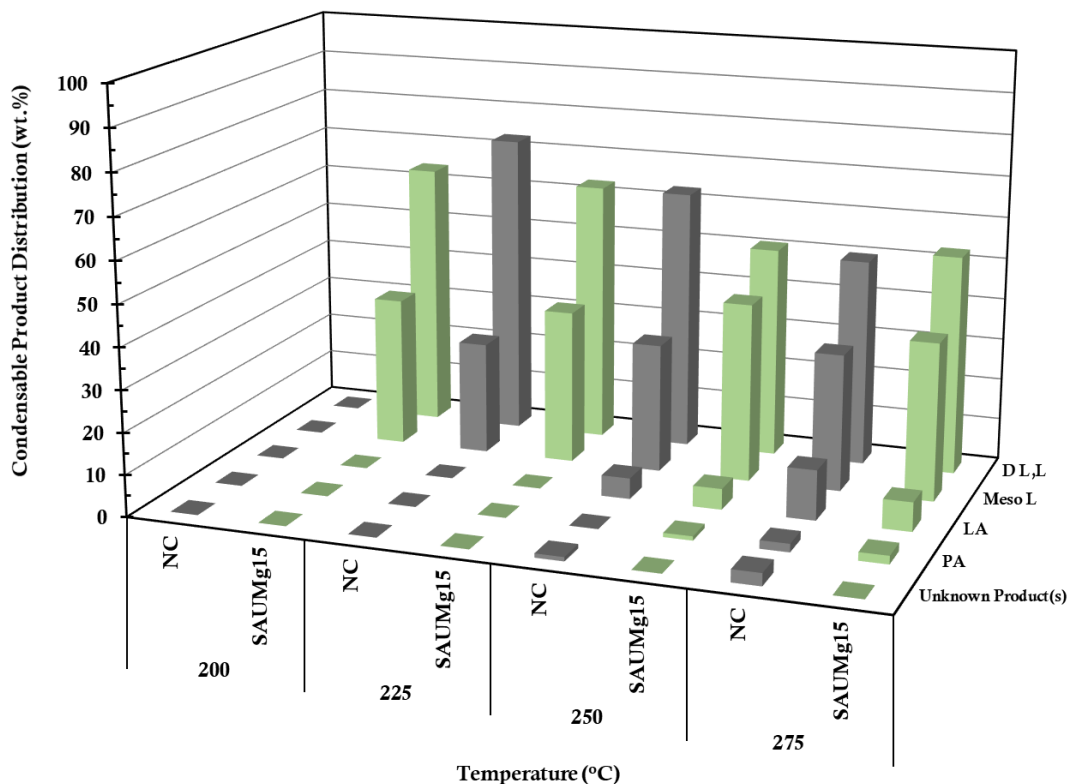


Figure 4.96. Comparison of the degradation of PLA in the presence of SAUMg15 with the the non-catalytic degradation of PLA in terms of reaction temperature and product distribution in condensable product (60 min, 70 rpm, 50 ml/min).

The production of lactide isomers was observed in the studied temperature range. Amounts of Meso L in the catalytic degradation was higher than that in the non-catalytic degradation in the studied temperature range. There were one unidentified product (U1) in the non-catalytic PLA degradation. On the other hand, there was not any unidentified product in the catalytic degradation of PLA. At 275 °C, the formation of lactic acid and propionic acid was only a total of 9 wt.%. D L,L was shown a slight increase at 275 °C.

The composition of gas products in the first 15 minute was analyzed. Figure 4.97 demonstrates the composition of gas products based on the reaction temperature. Carbon monoxide, carbon dioxide, and acetaldehyde were gas products.

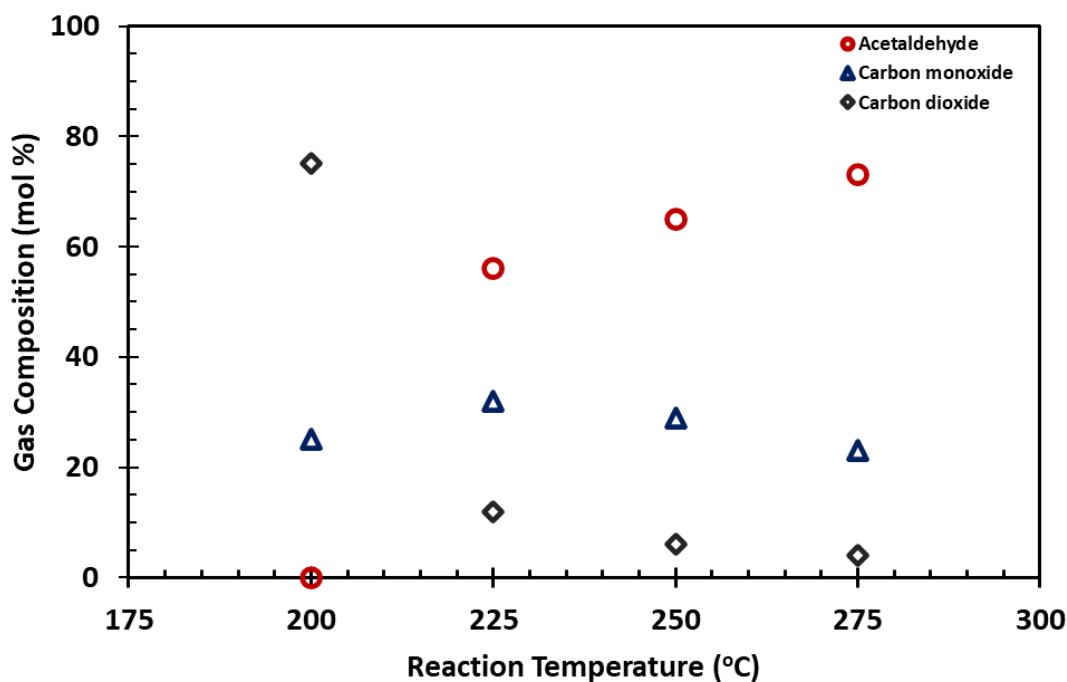


Figure 4.97. The effect of reaction temperature on non-condensable product distribution at 15 minute (SAUMg15, 60 min, 70 rpm, 50 ml/min).

At 200 °C, the main product was carbon dioxide (75 mol%). The rest was carbon monoxide, and acetaldehyde was not observed at this temperature. Acetaldehyde increased with a decrease in both carbon dioxide and carbon monoxide with increasing reaction temperature. In addition, the gas composition was also analyzed at the 50th minute (Figure 4.98).

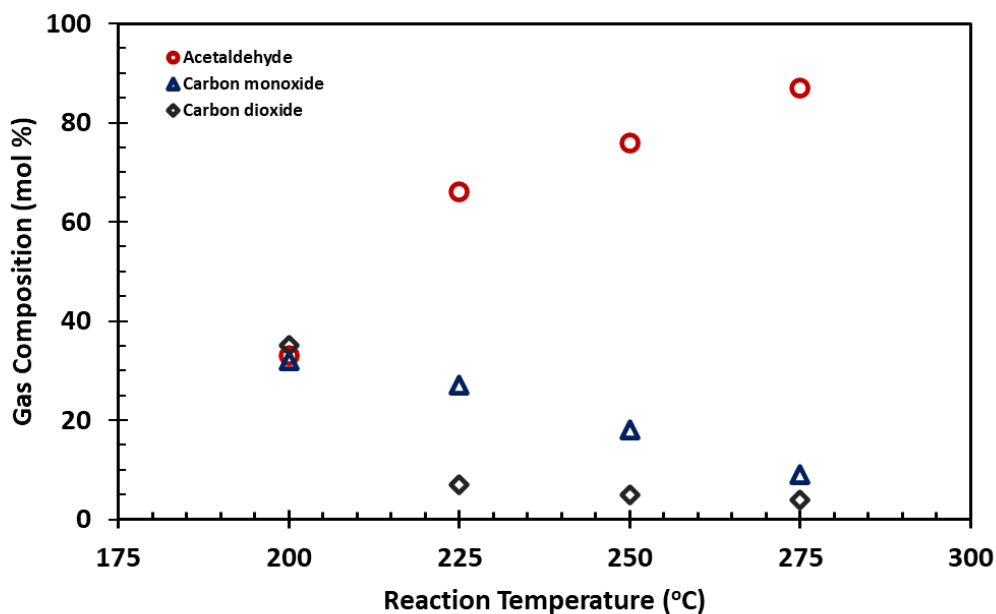


Figure 4.98. The effect of reaction temperature on non-condensable product distribution at 50 minute (SAUMg15, 60 min, 70 rpm, 50 ml/min).

In all temperature range, acetaldehyde constituted the majority of the gaseous products. Increasing reaction temperature tends to a rise in the formation of acetaldehyde as in the 15th minute. On the other hand, carbon monoxide and carbon dioxide linearly decreased between 200 °C and 275 °C. Figure 4.99 presents comparison of the degradation of PLA in the presence of SAUMg15 with the non-catalytic degradation of PLA in terms of reaction temperature and product distribution in non-condensable product at the 15th minute.

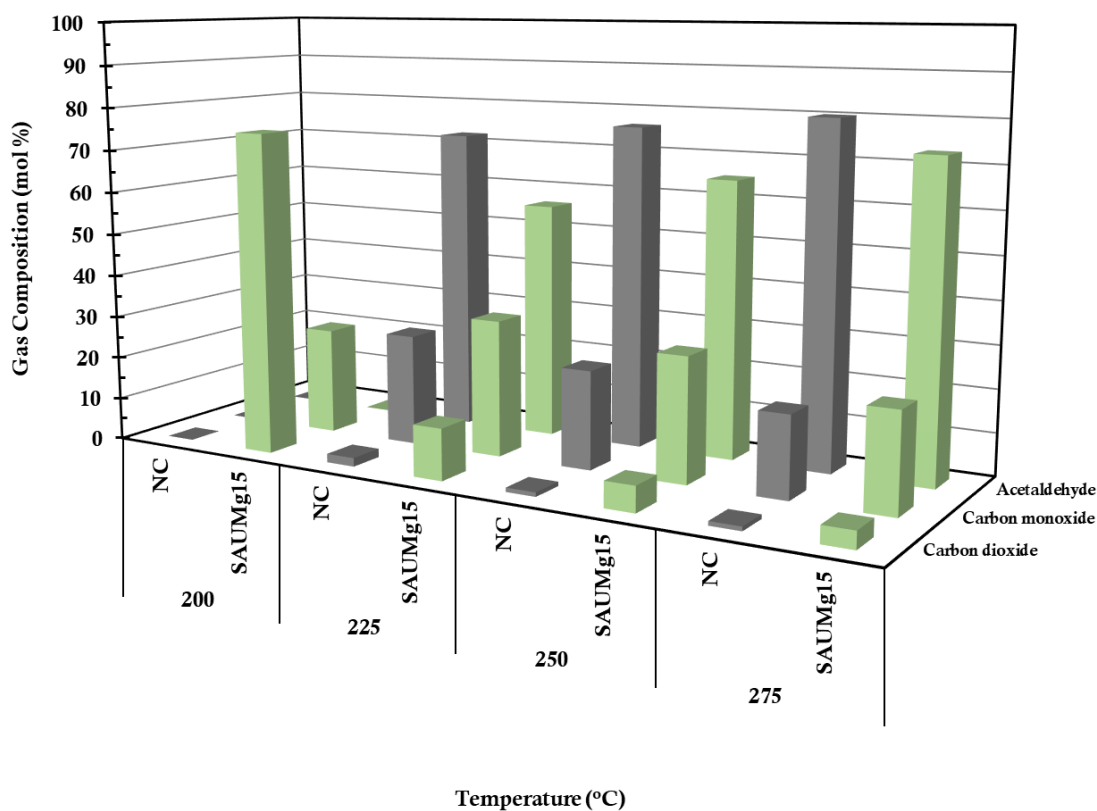


Figure 4.99. Comparison of the degradation of PLA in the presence of SAUMg15 with the non-catalytic degradation of PLA in terms of reaction temperature and product distribution in non-condensable product at the 15th minute (60 min, 70 rpm, 50 ml/min).

Concentrations of carbon monoxide and carbon dioxide in the catalytic decomposition of PLA were higher than that in the non-catalytic decomposition of PLA. Figure 4.100 presents the comparison of the catalytic degradation of PLA with the the non-catalytic degradation of PLA in terms of reaction temperature and product distribution in non-condensable product at the 50th minute.

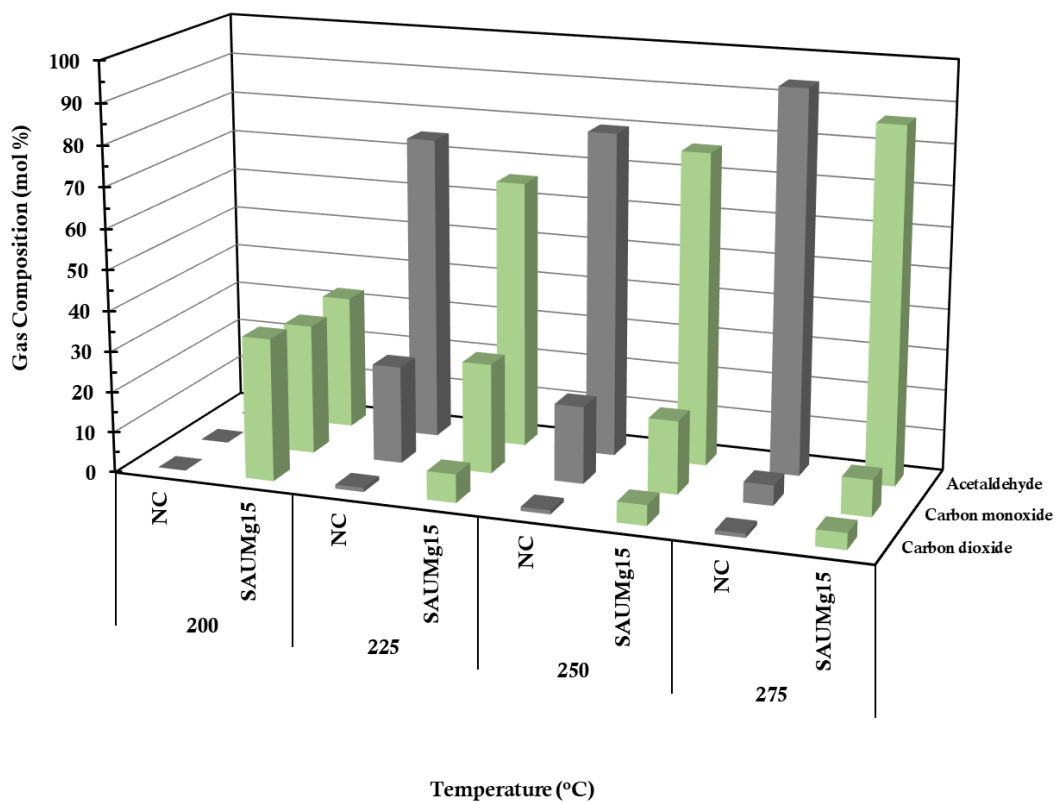


Figure 4.100. Comparison of the degradation of PLA in the presence of SAUMg15 with the the non-catalytic degradation of PLA in terms of reaction temperature and product distribution in non-condensable product at the 50th minute (60 min, 70 rpm, 50 ml/min).

At 200 °C, the concentrations of acetaldehyde, CO and CO₂ were higher than that in the non-catalytic degradation of PLA. The amount of carbon monoxide was slightly increased in the presence of SAUMg15 for 50 minute. The increase in the production of carbon dioxide was mainly provided with the SAUMg15 catalyst.

4.2.3.4 Characterization of the Used Magnesium Loaded Silica Aerogel Catalysts

The physical properties of the used SAUMg15 catalysts were investigated using nitrogen physisorption techniques. Figure 4.101 represents the nitrogen adsorption/desorption isotherms of the used 15 wt.% magnesium-loaded catalysts.

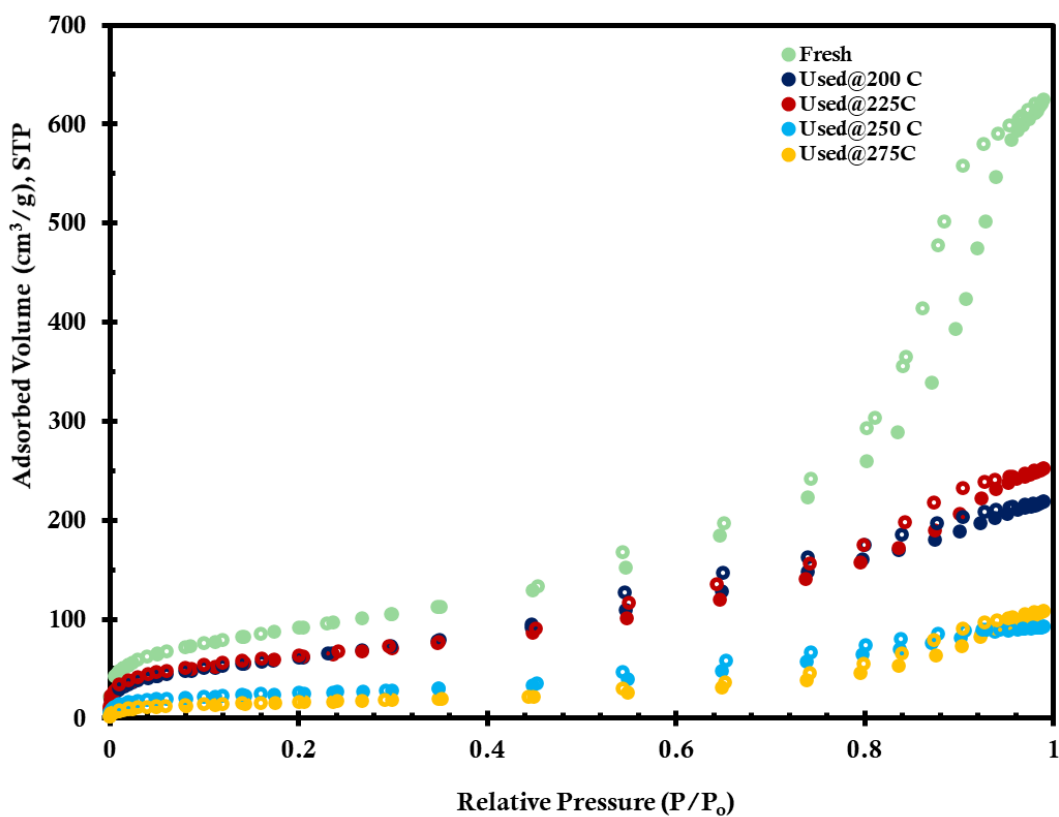


Figure 4.101. Nitrogen adsorption/desorption isotherms of the used magnesium loaded silica aerogel catalysts (filled and empty symbols represent adsorption and desorption branches, respectively).

The used magnesium loaded silica aerogel catalysts maintained their mesoporous structure after the degradation reactions. With an increase in reaction temperature,

nitrogen adsorbed volume decreased, which indicates the formation of coke in the pores of the catalyst. The pore size distributions of the used magnesium loaded silica aerogel catalysts are given Figure 4.102.

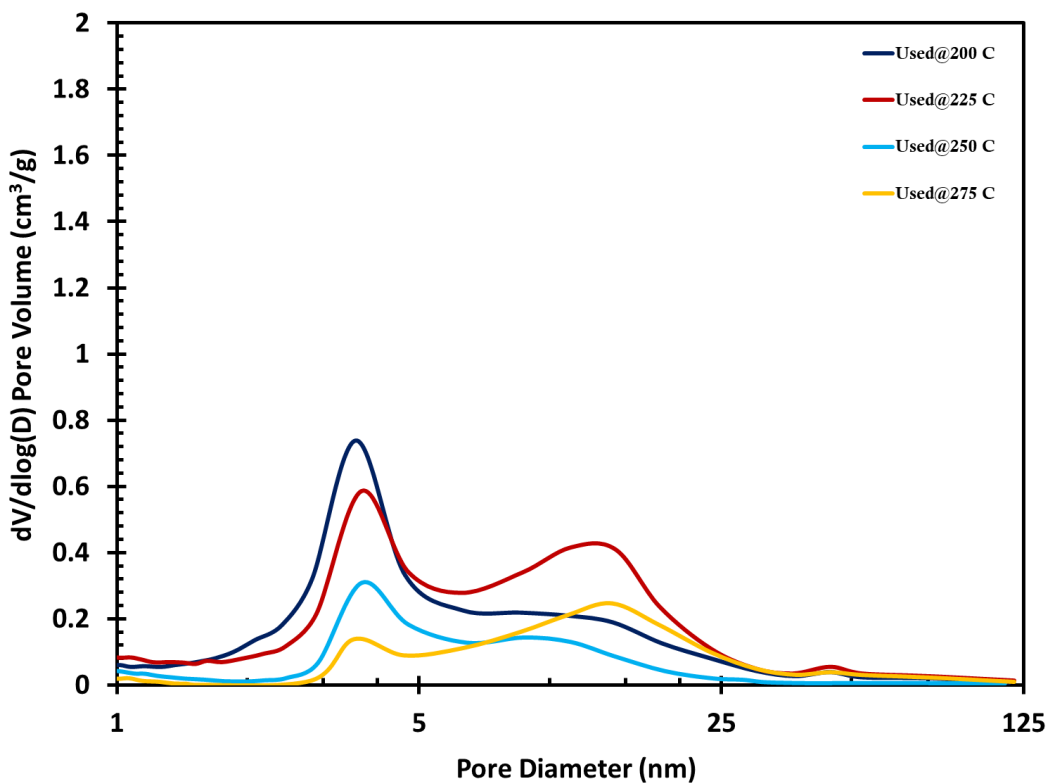


Figure 4.102. The pore size distributions of the used magnesium loaded silica aerogel catalysts.

With the coke formation, there was seen a decrease in pore volume. This is consistent with the adsorption/desorption isotherms of the used catalyst. Table 4.12 summarizes the physical properties of the used magnesium loaded silica aerogel catalysts.

Table 4.12. The physical properties of used aluminum loaded silica aerogel catalysts.

Catalyst	Surface Area (m²/g)	Pore Volume (cm³/g)	Pore Diameter (nm)	Microporosity (%)
Used@200 °C	228	0.34	3.82	20
Used@225 °C	221	0.40	4.57	19
Used@250 °C	86.5	0.14	4.2	21
Used@275 °C	56.5	0.17	6.7	12

When the catalyst was used at higher temperatures, both surface area and pore volume reduced due to coke deposition. 6.5 wt.% coke formation was observed at 275 °C.

4.2.4 Comparison of Activities of Different Metal Loaded Catalysts in PLA Degradation

Degradation of PLA was studied with three different metals. Al, Fe and Mg metals were loaded into silica aerogel support and the degradation of PLA was performed with these catalysts at the reaction temperature range of 200-275 °C. These catalysts were compared in terms of product yield, condensable and non-condensable product distribution. Figure 4.103 illustrates the effect of metal type in the catalyst on the product yield.

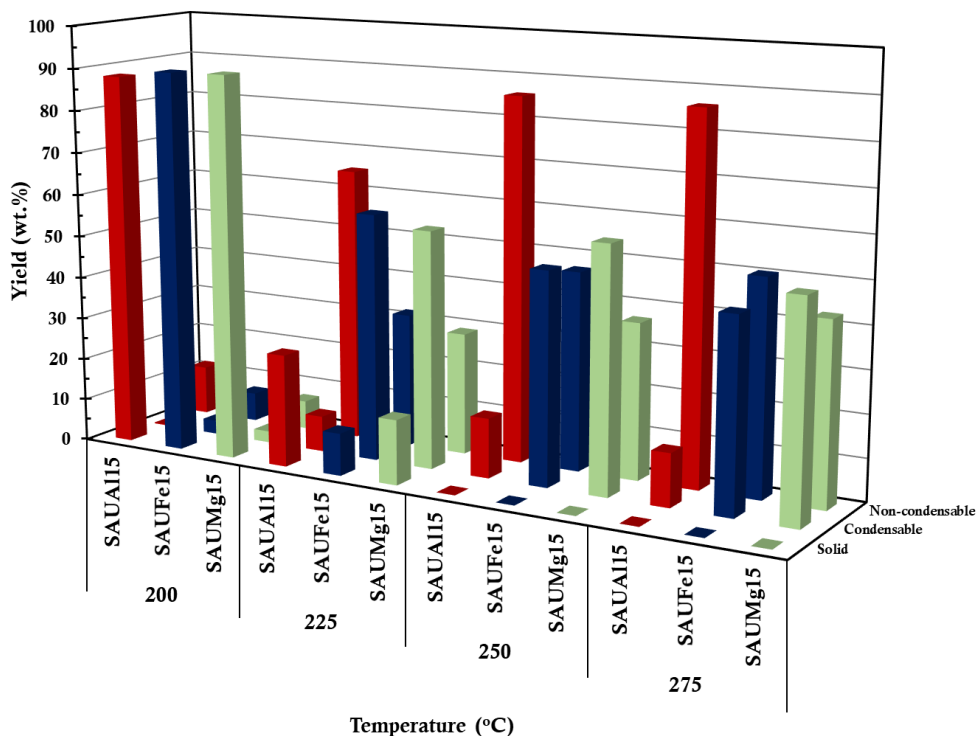


Figure 4.103. The effect of the type of metal in the catalyst on the yield of products (200-275 °C, 60 min, 70 rpm, 50 ml/min).

At 200 °C, PLA demonstrated similar degradation behavior in the presence of all catalysts. Catalysts provided a decline in the solid yield to a range between 88.14 and 90.29 wt% depending on metal type. The condensable products were in the range of 0.25-3.25 wt.% while the non-condensable products were found to be between 0.25 wt.% and 11.25%. The increase in condensable and non-condensable product and the decrease in solid product at 200 °C indicated that Al, Fe, and Mg loaded catalysts were active catalyst for degradation of PLA.

SAUA115 resulted in the formation of non-condensable products, whereas SAUFe15 and SAUMg15 yielded more condensable products.

The solid yield was significantly decreased with the catalysts at 225 °C where PLA degradation became much more apparent. With catalysts, the solid yield reduced from 82.14 wt.% to a range of 9.97-26.47 wt.%. Degradation of PLA in the presence of SAUA115 catalyst produced more non-condensable products than degradation of PLA with SAUFe15 and SAUMg15 in the studied temperature range. With the use of the SAUFe15 and SAUMg15 catalyst, more condensable products were produced. No solid formation was observed after 225 °C. In the three catalysts, coke deposited on the pores of silica aerogel support. In the metal loaded silica aerogel catalysts, the highest coke deposition was observed in the SAUMg15 catalyst. The effect of type of metal in the catalyst on condensable product distribution is illustrated in Figure 4.104.

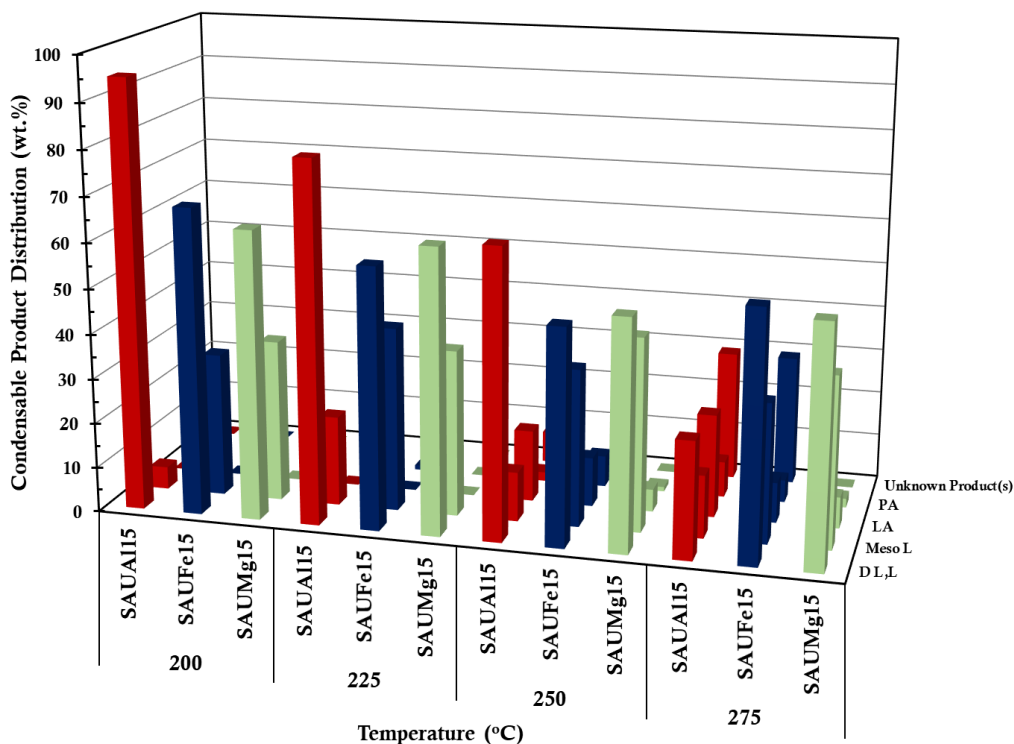


Figure 4.104. The effect of type of metal in the catalyst on condensable product distribution (200-275 °C, 60 min, 70 rpm, 50 ml/min).

D L,L and Meso L were the main products in the condensable products due to non-radical and radical degradation reactions. The same products were obtained with Fe and Mg loaded silica aerogel catalysts; however, different unidentified products were observed with Al loaded catalyst in the temperature range of 250-275 °C. The formation of unidentified products at the retention times of 9.3 (U3), 13.4 (U4), 15.9 (U5) and 22.1 min (U2) may be resulted from the presence of both Lewis and Bronsted acid sites in the catalyst.

In all metal loaded catalysts, the concentration of D L,L decreased with the reaction temperature. On the other hand, Meso L increased up to 225 °C with Fe and Al loaded catalysts. This increase in Meso L was seen up to 250 °C with Mg loaded catalyst. After 250 °C, LA and PA were formed in the presence of all catalysts. The formation of lactic acid in SAUAl15 was much lower than that in the SAUFe15 and SAUMg15 catalysts. On the other hand, the highest propionic acid generation attained with SAUFe15. The same trend in product distribution was seen for all catalyst with temperature.

Acidic sites cause the breakage of C-C bonds. Thus, the cracking of PLA was proceed faster and tended to the formation of lower molecular weight products. Thus, the amount of non-condensable product was higher in the PLA degradation with SAUMg15. Even though SAUFe15 and SAUMg15 have only Lewis acid sites, these catalysts do not have the Brönsted acid site.

Figure 4.105 demonstrates the effect of metal type in the catalysts on non-condensable product distribution at the 15th minute of the reaction.

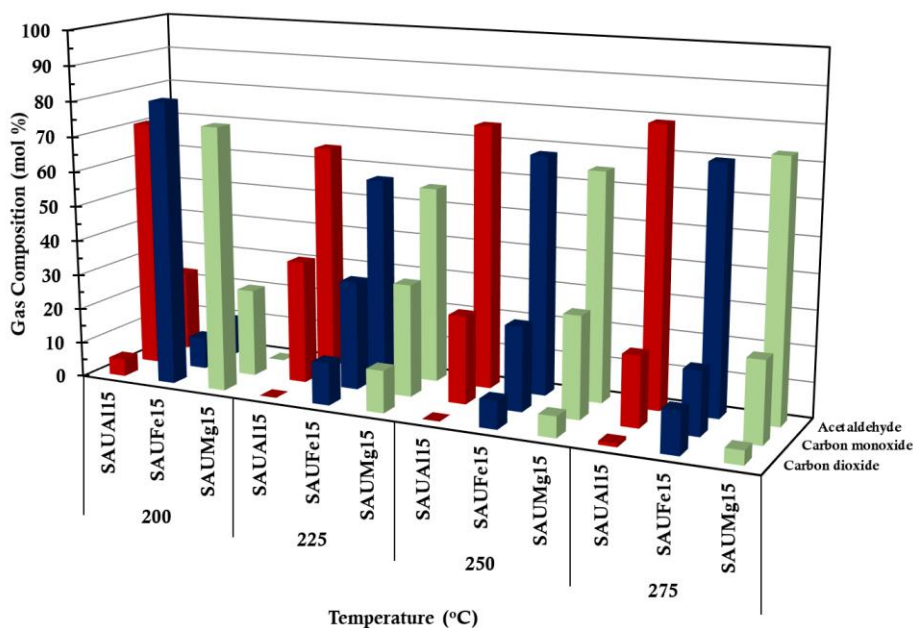


Figure 4.105. The effect of the type of the metal in the catalyst on non-condensable product distribution at the 15th minute of the reaction (60 min, 70 rpm, 50 ml/min).

At 200 °C, the initiation of the reaction was realized differently for all metals. Carbon monoxide was the major degradation product with 71 mol% at this temperature in the presence of SAUAl15. The major degradation product was carbon dioxide for SAUFe15 and SAUMg15. Although there was seen the formation of acetaldehyde with SAUFe15, there was not any acetaldehyde formation with SAUMg15. At a temperature of 225 °C, acetaldehyde was the main degradation product for all catalysts. The gas compositions for the SAUFe15 and SAUMg15 catalysts were nearly the same. The effect of the type of metal in the catalyst on non-condensable product distribution was also evaluated at the 50th min of the reaction (Figure 4.106).

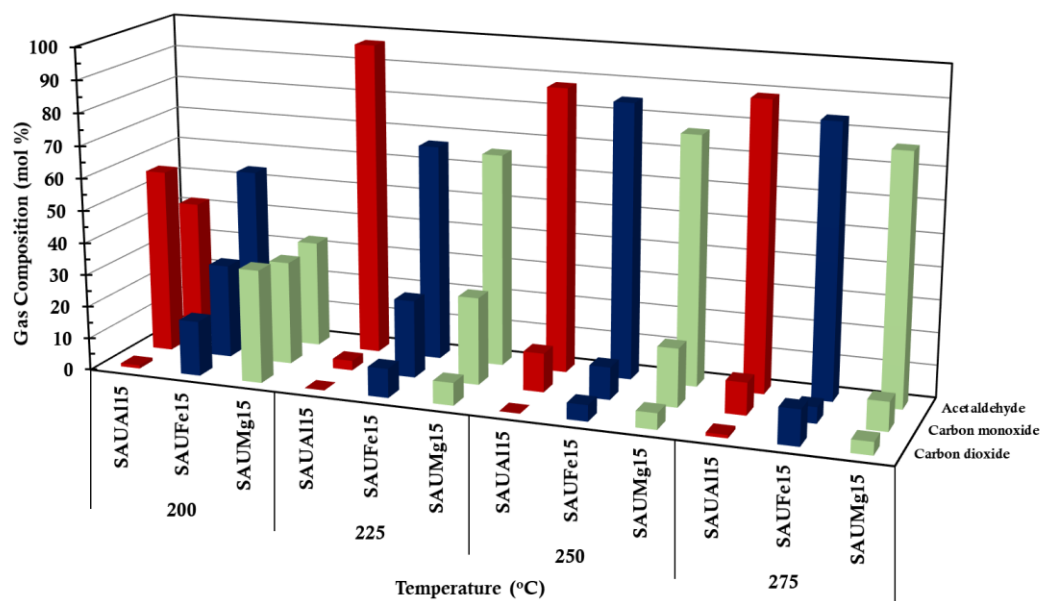


Figure 4.106. The effect of the type of metal in the catalyst on non-condensable product distribution at the 50th minute of the reaction (60 min, 70 rpm, 50 ml/min).

At 200 °C, acetaldehyde increased with SAUAl15, then remained constant. Striking similarities were found in the gas composition for SAUFe15 and SAUMg15 at preceding reaction times.

The highest condensable amount was 58.30 wt.% in SAUFe15 at 225 °C, 60 min, 70 rpm under 50 ml/min argon flow. Maximum 86.23 wt.% non-condensable yield was observed in SAUAl15 at 275 °C. D L,L compound yield was also obtained with SAUFe15 at 225 °C. The best catalyst was SAUFe15 in terms of circular economy approach.

CHAPTER 5

CONCLUSIONS

In this work, the degradation of polylactic acid (PLA) was performed by using different techniques to prevent waste accumulation and convert waste into value-added products and/or feedstocks. Thus, the degradation of PLA was studied under different reaction parameters in the pyrolysis system.

- The most effective parameter was found to be reaction temperature in the studied range while reaction time was the second most effective parameter.
- The formation of lactic isomers and lactic acid was observed with a little amount of propionic acid depending on the reaction parameters.
- The yield of lactide isomers was determined to be maximum 49 wt. % at 225 °C for 480 minutes in the studied reaction parameter range.
- In non-condensable products, acetaldehyde composed of the majority of the products. In addition to acetaldehyde, carbon monoxide and carbon dioxide were detected with low amount of hydrogen.
- Pyrolysis technique has the potential to be utilized for PLA recycling and the production value-added products and/or feedstocks.

As a second approach, degradation of PLA was performed for the first time in supercritical CO₂ medium.

- The most effective parameters were reaction temperature and reaction time, respectively.
- The formation of lactide isomers and lactic acid was provided depending on reaction parameters.
- At 200 °C, 206 bar and 120 minutes, the highest lactide isomer yield was attained with a high value of 89%, by weight in the studied parameter range.

- The second highest lactide isomer yield (83%) was achieved at a lower pressure of 103 bar at 200 °C, 70 rpm for 120 minutes in the studied parameter range.
- It was observed that supercritical carbon dioxide has a remarkable effect on the degradation kinetics of PLA providing high yield of lactide isomers.

Lastly, degradation of PLA was performed with Al, Fe and Mg loaded silica aerogel catalysts at different temperatures.

- With metal loading, Type IV isotherm was conserved in the silica aerogel support, which indicates mesoporous structure; however, hysteresis type changed from III to I.
- TGA results showed that Al, Fe and Mg loaded silica aerogel catalysts were found to be effective in decreasing the activation energy and degradation temperature.
- DRIFTS results revealed that Al has both Lewis and Bronsted acid sites whereas Fe and Mg have only Lewis acid sites.
- Although the reaction rate was slow at 200 °C, more condensable and non-condensable products were formed when the catalyst used at this temperature. The three metal loaded silica aerogels are active catalysts for the degradation of PLA.
- Al loaded catalysts lead to a significant increase in non-condensable product amount.
- Fe and Mg loaded catalysts causes a rise in condensable product amount.
- The highest lactide isomer yield was 11 wt.% with SAUAl15 catalyst at 250 °C.
- In the presence of SAUFe15 catalyst, the highest lactide isomer yield was 58 wt.% at 225 °C while the highest lactide was 56 wt.% with SAUMg15 at the same temperature.

The mentioned efforts are to ensure that waste materials will not negatively affect the natural life cycle and will be converted into feedstock and value-added products for economic efficiency. The outputs of the work will contribute to industrial and research-oriented polymer recycling studies.

CHAPTER 6

RECOMMENDATIONS

- Due to the formation of coke, bimetallic catalysts are offered to enhance the reaction kinetics.
- The number of cycle can be investigated for the synthesized catalysts.
- Carbon dioxide atmosphere can be applied in the pyrolysis system.
- The composition of gases can be obtained in supercritical reaction system.

REFERENCES

- Ainali, N. M., Tarani, E., Zamboulis, A., Črešnar, K. P., Zemljič, L. F., Chrissafis, K., Lambropoulou, D. A., & Bikiaris, D. N. (2021). Thermal Stability and Decomposition Mechanism of PLA Nanocomposites with Kraft Lignin and Tannin. *Polymers*, *13*(16). <https://doi.org/10.3390/polym13162818>
- Åkesson, D., Vrignaud, T., Tissot, C., & Skrifvars, M. (2016). Mechanical Recycling of PLA Filled with a High Level of Cellulose Fibres. *Journal of Polymers and the Environment*, *24*(3), 185–195. <https://doi.org/10.1007/s10924-016-0760-0>
- Alberti, C., Damps, N., Meißner, R. R. R., Hofmann, M., Rijono, D., & Enthaler, S. (2020). Selective Degradation of End-of-Life Poly(lactide) via Alkali-Metal-Halide Catalysis. *Advanced Sustainable Systems*, *4*(1). <https://doi.org/10.1002/adsu.201900081>
- Almeida, D., & de Fátima Marques, M. (2016). Thermal and catalytic pyrolysis of plastic waste. *Polimeros*, *26*(1), 44–51. <https://doi.org/10.1590/0104-1428.2100>
- Al-Oweini, R., & El-Rassy, H. (2009). Synthesis and characterization by FTIR spectroscopy of silica aerogels prepared using several Si(OR)₄ and R''Si(OR')₃ precursors. *Journal of Molecular Structure*, *919*(1–3), 140–145. <https://doi.org/10.1016/j.molstruc.2008.08.025>
- Álvarez-Chávez, C. R., Edwards, S., Moure-Eraso, R., & Geiser, K. (2012). Sustainability of bio-based plastics: General comparative analysis and recommendations for improvement. *Journal of Cleaner Production*, *23*(1), 47–56. <https://doi.org/10.1016/j.jclepro.2011.10.003>
- Amonette, J. E., & Matyáš, J. (2017). Functionalized silica aerogels for gas-phase purification, sensing, and catalysis: A review. *Microporous and Mesoporous Materials*, *250*, 110–119. <https://doi.org/10.1016/j.micromeso.2017.04.055>

- Anderson, M. L., Stroud, R. M., & Rolison, D. R. (2002). Enhancing the Activity of Fuel-cell Reactions by Designing Three-dimensional Nanostructured Architectures: Catalyst-modified Carbon - Silica Composite Aerogels. *Nano Letters*, 2(3), 235–240. <https://doi.org/10.1021/nl015707d>
- Andrady, A. L., & Neal, M. A. (2009). Applications and societal benefits of plastics. *Philosophical Transactions of the Royal Society B: Biological Sciences*, 364(1526), 1977–1984. <https://doi.org/10.1098/rstb.2008.0304>
- Anneaux, B., Campanelli, J., Foley, E. (2018). Low Temperature Solution Depolymerization of PLA: Paper presented at ANTEC 2018. Orlando.
- Aoyagi, Y., Yamashita, K., & Doi, Y. (2002). Thermal degradation of poly[(R)-3-hydroxybutyrate], poly[ε-caprolactone], and poly[(S)-lactide]. *Polymer Degradation and Stability*, 76(1), 53–59. [https://doi.org/https://doi.org/10.1016/S0141-3910\(01\)00265-8](https://doi.org/https://doi.org/10.1016/S0141-3910(01)00265-8)
- Arrieta, M. P., Parres, F., López, J., & Jiménez, A. (2013). Development of a novel pyrolysis-gas chromatography/mass spectrometry method for the analysis of poly(lactic acid) thermal degradation products. *Journal of Analytical and Applied Pyrolysis*, 101, 150–155. <https://doi.org/https://doi.org/10.1016/j.jaap.2013.01.017>
- Association of Plastic Recyclers. (2022). Recycling rates of post-consumer plastic bottles sourced in the United States in 2019 and 2020, by material type [Graph]. In Statista. Retrieved November 28, 2022, from <https://www.statista.com/statistics/623553/plastic-bottle-recycling-rates-in-the-us-by-material-type/>
- Auras, R., Harte, B., & Selke, S. (2004). An overview of polylactides as packaging materials. In *Macromolecular Bioscience*, 4(9), 835–864. <https://doi.org/10.1002/mabi.200400043>
- Aydemir B., Sezgi N. A. (2013). “Alumina and tungstophosphoric acid loaded mesoporous catalysts for the polyethylene degradation reaction”, *Ind. Eng. Chem. Res.* 52, 15366–15371. <https://doi.org/10.1021/ie400634m>

- Aydemir, B., & Sezgi, N. A. (2016). Pyrolysis of Polyethylene over Aluminum-Incorporated MCM-41 Catalyst. *Chemical Engineering Communications*, 203(5), 635–641. <https://doi.org/10.1080/00986445.2015.1076800>
- Azwar, E., Vuorinen, E., & Hakkarainen, M. (2012). Pyrolysis-GC–MS reveals important differences in hydrolytic degradation process of wood flour and rice bran filled polylactide composites. *Polymer Degradation and Stability*, 97(3), 281–287. <https://doi.org/https://doi.org/10.1016/j.polymdegradstab.2011.12.017>
- Badia, J. D., Strömberg, E., Karlsson, S., & Ribes-Greus, A. (2012). Material valorisation of amorphous polylactide. Influence of thermo-mechanical degradation on the morphology, segmental dynamics, thermal and mechanical performance. *Polymer Degradation and Stability*, 97(4), 670–678. <https://doi.org/10.1016/j.polymdegradstab.2011.12.019>
- Badia, J. D., & Ribes-Greus, A. (2016). Mechanical recycling of polylactide, upgrading trends and combination of valorization techniques. *European Polymer Journal*, 84, 22–39. <https://doi.org/10.1016/j.eurpolymj.2016.09.005>
- Bagheri, A. R., Laforsch, C., Greiner, A., & Agarwal, S. (2017). Fate of So-Called Biodegradable Polymers in Seawater and Freshwater. *Global Challenges*, 1(4), 1700048. <https://doi.org/10.1002/gch2.201700048>
- Basu, A., Langer, R., & Domb, A. J. (2016). Special issue: Polylactide (PLA) Based Biopolymers. *Advanced Drug Delivery Reviews*, 107, 1-2. <https://doi.org/10.1016/j.addr.2016.11.002>
- BBC. (2016). “Will there be more fish or plastic in the sea in 2050?” Retrieved January 28, 2022, from <https://www.bbc.com/news/magazine-35562253>.
- Behera, K., Chang, Y.H., Chiu, F.C., & Yang, J.C. (2017). Characterization of poly(lactic acid)s with reduced molecular weight fabricated through an autoclave process. *Polymer Testing*, 60, 132–139. <https://doi.org/https://doi.org/10.1016/j.polymertesting.2017.03.015>

- Bopp, R. (2012). NatureWorks® Ingeo™ polylactide: past, present and future. *Biopolymers & Biocomposites Workshop*.
- Bozorgmehr, M. R., Morsali, A., Beyramabadi, S. A., Moghaddam, F. K., Pashirepour, J., & Shakeri, M. (2014). All atom molecular dynamics simulation study of polyethylene polymer in supercritical water, supercritical ethanol and supercritical methanol. *Journal of Supercritical Fluids*, 86, 124–128. <https://doi.org/10.1016/j.supflu.2013.12.010>
- Bouzouita, A. (2016). *Elaboration of polylactide-based materials for automotive application : study of structure-process-properties interactions*. <https://theses.hal.science/tel-01417533>
- Brandon, A. M., & Criddle, C. S. (2019). Can biotechnology turn the tide on plastics?. *Current Opinion in Biotechnology*, 57, 160-166. <https://doi.org/10.1016/j.copbio.2019.03.020>
- Brandrup, J., Immergut, E.H., Polymer Handbook, Interscience Publishers, New York, 1966.
- Brockhaus, S., Petersen, M., & Kersten, W. (2016). A crossroads for bioplastics: exploring product developers' challenges to move beyond petroleum-based plastics. *Journal of Cleaner Production*, 127, 84–95. <https://doi.org/10.1016/j.jclepro.2016.04.003>
- Brüster, B., Addiego, F., Hassouna, F., Ruch, D., Raquez, J. M., & Dubois, P. (2016). Thermo-mechanical degradation of plasticized poly(lactide) after multiple reprocessing to simulate recycling: Multi-scale analysis and underlying mechanisms. *Polymer Degradation and Stability*, 131, 132–144. <https://doi.org/10.1016/j.polymdegradstab.2016.07.017>
- Buffet, J.-C., & Okuda, J. (2011). Initiators for the stereoselective ring-opening polymerization of meso-lactide. *Polym. Chem.*, 2(12), 2758–2763. <https://doi.org/10.1039/C1PY00206F>

- Bureau of International Recycling. (2019). "Global Recycling Foundation Announces Recycling Heroes Theme For 2020" Retrieved 7 Nov. 2019, from <https://bir.org/news-press/latest-news/global-recycling-foundation-announces-recycling-heroes-theme-for-2020/>
- Busca, G. (1998). Spectroscopic characterization of the acid properties of metal oxide catalysts. *Catalysis Today*, 41(1–3), 191–206. [https://doi.org/10.1016/S0920-5861\(98\)00049-2](https://doi.org/10.1016/S0920-5861(98)00049-2)
- Cameron, D. J. A., & Shaver, M. P. (2011). Aliphatic polyester polymer stars: Synthesis, properties and applications in biomedicine and nanotechnology. *Chemical Society Reviews*, 40(3), 1761–1776. <https://doi.org/10.1039/c0cs00091d>
- Carné Sánchez, A., & Collinson, S. R. (2011). The selective recycling of mixed plastic waste of polylactic acid and polyethylene terephthalate by control of process conditions. *European Polymer Journal*, 47(10), 1970–1976. <https://doi.org/10.1016/j.eurpolymj.2011.07.013>
- Carney Almroth, B., & Eggert, H. (2019). Marine plastic pollution: Sources, impacts, and policy issues. *Review of Environmental Economics and Policy*, 13(2), 317–326. <https://doi.org/10.1093/reep/rez012>
- Carrasco, F., Pérez-Maqueda, L. A., Sánchez-Jiménez, P. E., Perejón, A., Santana, O. O., & MasPOCH, M. Ll. (2013). Enhanced general analytical equation for the kinetics of the thermal degradation of poly(lactic acid) driven by random scission. *Polymer Testing*, 32(5), 937–945. <https://doi.org/https://doi.org/10.1016/j.polymertesting.2013.04.013>
- Castro-Aguirre, E., Iñiguez-Franco, F., Samsudin, H., Fang, X., & Auras, R. (2016). Poly(lactic acid)—Mass production, processing, industrial applications, and end of life. In *Advanced Drug Delivery Reviews*, 107, 333–366. <https://doi.org/10.1016/j.addr.2016.03.010>

- Chae, Y., & An, Y. J. (2018). Current research trends on plastic pollution and ecological impacts on the soil ecosystem: A review. In *Environmental Pollution*, 240, 387–395. <https://doi.org/10.1016/j.envpol.2018.05.008>
- Chaianansutcharit, S., Katsutath, R., Chaisuwan, A., Bhaskar, T., Nigo, A., Muto, A., & Sakata, Y. (2007). Catalytic degradation of polyolefins over hexagonal mesoporous silica: Effect of aluminum addition. *Journal of Analytical and Applied Pyrolysis*, 80(2), 360–368. <https://doi.org/10.1016/j.jaap.2007.04.009>
- Chakraborty, G., Valapa, R. B., Pugazhenth, G., & Katiyar, V. (2018). Investigating the properties of poly (lactic acid)/exfoliated graphene based nanocomposites fabricated by versatile coating approach. *International Journal of Biological Macromolecules*, 113, 1080–1091. <https://doi.org/https://doi.org/10.1016/j.ijbiomac.2018.03.037>
- Chanprateep, S. (2010). Current trends in biodegradable polyhydroxyalkanoates. *Journal of Bioscience and Bioengineering*, 110(6), 621–632. <https://doi.org/10.1016/j.jbiosc.2010.07.014>
- Chaudhry, A. N., & Billingham, N. C. (2001). Characterisation and oxidative degradation of a room-temperature vulcanised poly(dimethylsiloxane) rubber. *Polymer Degradation and Stability*, 73(3), 505–510. [https://doi.org/https://doi.org/10.1016/S0141-3910\(01\)00139-2](https://doi.org/https://doi.org/10.1016/S0141-3910(01)00139-2)
- Chauliac, D., Pullammanappallil, P. C., Ingram, L. O., & Shanmugam, K. T. (2020). A Combined Thermochemical and Microbial Process for Recycling Polylactic Acid Polymer to Optically Pure L-Lactic Acid for Reuse. *Journal of Polymers and the Environment*, 28(5), 1503–1512. <https://doi.org/10.1007/s10924-020-01710-1>
- Chou, Y. H., Cundy, C. S., Garforth, A. A., & Zholobenko, V. L. (2006). Mesoporous ZSM-5 catalysts: Preparation, characterisation and catalytic properties. Part I: Comparison of different synthesis routes. *Microporous and Mesoporous Materials*, 89(1–3), 78–87. <https://doi.org/10.1016/j.micromeso.2005.10.014>
- Chen, J., Duan, Z., Song, Z., Zhu, L., Zhou, Y., Xiang, Y., & Xia, D. (2017). Relationship between surface property and catalytic application of amorphous NiP/H β catalyst for

- n-hexane isomerization. *Applied Surface Science*, 425, 448–460.
<https://doi.org/10.1016/j.apsusc.2017.07.019>
- Chen H, Chen F, Chen H, Liu H, Chen L, Yu L. (2023). Thermal degradation and combustion properties of most popular synthetic biodegradable polymers. *Waste Manag Res*, 41(2):431-441. doi: 10.1177/0734242X221129054. Epub 2022 Oct 15. PMID: 36250214; PMCID: PMC9925886.
- Chrysafi, I., Ainali, N. M., & Bikiaris, D. N. (2021). Thermal Degradation Mechanism and Decomposition Kinetic Studies of Poly (Lactic Acid) and Its Copolymers with Poly(Hexylene Succinate). *Polymers*, 13(9).
<https://doi.org/10.3390/polym13091365>
- Chyxx.com. (2021). Recycling rate of plastic products in China from 2017 to 2020 [Graph]. In Statista. Retrieved February 28, 2023, from <https://www.statista.com/statistics/1257741/plastic-product-recycling-rate-in-china/>
- Clark, J. H., Farmer, T. J., Hunt, A. J., & Sherwood, J. (2015). Opportunities for bio-based solvents created as petrochemical and fuel products transition towards renewable resources. In *International Journal of Molecular Sciences*, 16(8), 17101-17159.
<https://doi.org/10.3390/ijms160817101>
- Clarke, C. J., Tu, W. C., Levers, O., Bröhl, A., & Hallett, J. P. (2018). Green and Sustainable Solvents in Chemical Processes. *Chemical Reviews*, 118(2), 747–800.
<https://doi.org/10.1021/acs.chemrev.7b00571>
- City to Sea. (2022). How Does Plastic Contribute To Climate Available At: Change. Retrieved 17 Nov. 2020, from <https://www.citytosea.org.uk/how-does-plastic-contribute-to-climate-breakdown/>
- Coats, A. W., and J. P. Redfern. (1964). Kinetic Parameters from Thermogravimetric Data. *Nature*, 201, 68-69.

- Čolnik, M., Kotnik, P., Knez, Ž., & Škerget, M. (2022). Chemical Recycling of Polyolefins Waste Materials Using Supercritical Water. *Polymers*, 14(20). <https://doi.org/10.3390/polym14204415>
- Cooper, G.M. (2000). *The Cell: A Molecular Approach*. 2nd Edition, Sunderland (MA): Sinauer Associates, The Development and Causes of Cancer. <https://www.ncbi.nlm.nih.gov/books/NBK9963/>
- Cooper, A.I. (2001). Recent Developments in Materials Synthesis and Processing Using Supercritical CO₂. *Advanced Materials*, 13(14). [https://doi.org/10.1002/1521-4095\(200107\)13:14<1111::AID-ADMA1111>3.0.CO;2-L](https://doi.org/10.1002/1521-4095(200107)13:14<1111::AID-ADMA1111>3.0.CO;2-L)
- Copinat, A., Legin-Copinat, E., & Erre, D. (2009). Compostability of Co-extruded starch/poly(lactic acid) polymeric material degradation in an activated inert solid medium. *Materials*, 2(3), 749–764. <https://doi.org/10.3390/ma2030749>
- Cornelissen, T., Jans, M., Stals, M., Kuppens, T., Thewys, T., Janssens, G. K., Pastijn, H., Yperman, J., Reggers, G., Schreurs, S., & Carleer, R. (2009). Flash co-pyrolysis of biomass: The influence of biopolymers. *Journal of Analytical and Applied Pyrolysis*, 85(1), 87–97. <https://doi.org/https://doi.org/10.1016/j.jaap.2008.12.003>
- Cristina, A. M., Sara, F., Fausto, G., Vincenzo, P., Rocchina, S., & Claudio, V. (2018). Degradation of Post-consumer PLA: Hydrolysis of Polymeric Matrix and Oligomers Stabilization in Aqueous Phase. *Journal of Polymers and the Environment*, 26(12), 4396–4404. <https://doi.org/10.1007/s10924-018-1312-6>
- Das, P., & Tiwari, P. (2017). Thermal degradation kinetics of plastics and model selection. *Thermochimica Acta*, 654, 191–202. <https://doi.org/https://doi.org/10.1016/j.tca.2017.06.001>
- Davis, P. J., C. J. Brinker, D. M. Smith, and R. A. Assink. 1992. Pore Structure Evolution in Silica Gel during Aging/Drying II. Effect of Pore Fluids. *Journal of Non-Crystalline Solids*, 142, 197–207.

- De França, J. O. C., da Silva Valadares, D., Paiva, M. F., Dias, S. C. L., & Dias, J. A. (2022). Polymers Based on PLA from Synthesis Using D,L-Lactic Acid (or Racemic Lactide) and Some Biomedical Applications: A Short Review. *Polymers*, 14(12), 2317. <https://doi.org/10.3390/polym14122317>
- Değirmencioglu, P. (2018). “Methanol Steam Reforming Over Silica Aerogel Supported Catalyst For Hydrogen Production ” <https://open.metu.edu.tr/handle/11511/27341>
- Deshpande, R., Smith, D. M. and Brinker, C. J. (1992). Preparation of High Porosity Xerogels by Chemical Surface Modification. US Patent No. 5565142A.
- Dinçer, B. Y. (2019). Synthesis and Characterization of Metal Loaded New Generation Meso Porous Silica Pillared Catalyst
- Drohsler, P., Yasir, M., Cruz Fabian, D. R., Cisar, J., Yadollahi, Z., & Sedlarik, V. (2022). Comparative degradation study of a biodegradable composite based on polylactide with halloysite nanotubes and a polyacrylic acid copolymer. *Materials Today Communications*, 33, 104400. <https://doi.org/https://doi.org/10.1016/j.mtcomm.2022.104400>
- Drumright, R. E., Gruber, P. R., & Henton, D. E. (2000). Polylactic acid technology. *Advanced Materials*, 12(23), 1841–1846. [https://doi.org/10.1002/1521-4095\(200012\)12:23<1841::AID-ADMA1841>3.0.CO;2-E](https://doi.org/10.1002/1521-4095(200012)12:23<1841::AID-ADMA1841>3.0.CO;2-E)
- Dorcheh, A. S., Abbasi M. H. (2008). Silica aerogel; synthesis, properties and characterization. *Journal of Materials Processing Technology*, 199 (1-3), 10-26. <https://doi.org/10.1016/j.jmatprotec.2007.10.060>
- Duan, Y., Jana, S. C., Lama, B., & Espe, M. P. (2016). Hydrophobic silica aerogels by silylation. *Journal of Non-Crystalline Solids*, 437, 26–33. <https://doi.org/https://doi.org/10.1016/j.jnoncrysol.2016.01.016>
- Dubois, M. A., Dozol, J. F., Massiani, C., & Ambrosio, M. (1996). Reactivities of Polystyrenic Polymers with Supercritical Water under Nitrogen or Air. Identification

and Formation of Degradation Compounds. *Eng. Chem. Res.*, 35 (8), 2743–2747.
<https://doi.org/10.1021/ie950591f>

Dunn, B. C., Cole, P., Covington, D., Webster, M. C., Pugmire, R. J., Ernst, R. D., Eyring, E. M., Shah, N., & Huffman, G. P. (2005). Silica aerogel supported catalysts for Fischer-Tropsch synthesis. *Applied Catalysis A: General*, 278(2), 233–238.
<https://doi.org/10.1016/j.apcata.2004.10.002>

Emadian, S. M., Onay, T. T., & Demirel, B. (2017). Biodegradation of bioplastics in natural environments. *Waste Management*, 59, 526-536.
<https://doi.org/10.1016/j.wasman.2016.10.006>

Ennaert T., Aelst J.V., Dijkmans J., Clercq R. D., Schutyser W., Dusselier M., Verboekend D., Sels B. F. (2016). Potential and challenges of zeolite chemistry in the catalytic conversion of biomass. *Chem. Soc. Rev.*, 45, 584.

European Bioplastics. (2021). Production capacity of bioplastics worldwide from 2020 to 2026, by type (in 1,000 metric tons) [Graph]. In Statista. Retrieved March 01, 2022, from <https://www.statista.com/statistics/678684/global-production-capacity-of-bioplastics-by-type/>

European Bioplastics. (2021). Estimated land use for bioplastics production worldwide from 2021 to 2026 (in million hectares) [Graph]. In Statista. Retrieved October 05, 2022, from <https://www.statista.com/statistics/678929/agricultural-land-use-for-bioplastics-production/>

European Bioplastics. (2021). Production capacity of bioplastics worldwide in 2021 by market segment (in 1,000 metric tons) [Graph]. In Statista. Retrieved March 01, 2022, from <https://www.statista.com/statistics/678908/production-capacity-of-bioplastics-worldwide-by-market-segment/>

European Bioplastics. (2021). Forecasted production capacity of bioplastics worldwide in 2026, by market segment (in 1,000 metric tons) [Graph]. In Statista. Retrieved March 01, 2022, from <https://www.statista.com/statistics/727640/projected-global-bioplatic-production-capacity-by-market-segment/>

- European Bioplastics, Nova Institute. (2022). Global Production Capacities of Bioplastics 2022 (by material type). Retrieved November 6, 2022, from [https://www.european-bioplastics.org/market/#iLightbox\[gallery_image_1\]/0](https://www.european-bioplastics.org/market/#iLightbox[gallery_image_1]/0)
- European Commission. (2018). Changing the way we use plastics. Retrieved January 20, 2023, from <https://ec.europa.eu/environment/pdf/circular-economy/pan-european-factsheet.pdf>
- European Commission. (2020). Communication from the commission to the European parliament, the council, the European economic and social committee and the committee of the regions: A new circular economy action plan-for a cleaner and more competitive Europe”. Retrieved January 20, 2023, from <https://eur-lex.europa.eu/legalcontent/EN/TXT/?qid=1583933814386&uri=COM:2020:98:FIN>
- European Commission. (2021). A European Green Deal: Striving to be the first climate-neutral continent. Retrieved January 20, 2023, from https://ec.europa.eu/info/strategy/priorities-2019-2024/european-green-deal_en
- European Commission. (2022). Biobased, biodegradable and Compostable Plastics. Environment. Retrieved January 20, 2023, from https://environment.ec.europa.eu/topics/plastics/bio-based-biodegradable-and-compostable-plastics_en
- European Environmental Agency. (2021). Impacts of covid-19 on single-use plastic in Europe’s environment. Retrieved January 20, 2023, from <https://www.eea.europa.eu/publications/impacts-of-covid-19-on>
- European Parliament. (2021). Plastic in the ocean: the facts, effects and new EU rules | News | European Parliament. Retrieved January 20, 2023, from <https://www.europarl.europa.eu/news/en/headlines/society/20181005STO15110/plastic-in-the-ocean-the-facts-effects-and-new-eu-rules>
- Eurostat. (2022). Packaging waste statistics. Retrieved January 5, 2023, from <https://ec.europa.eu/eurostat/statistics->

[explained/index.php?title=Packaging_waste_statistics#Waste_generation_by_packaging_material](#)

- Fan, L., & Fujimoto, K. (1999). Fischer-Tropsch synthesis in supercritical fluid: characteristics and application. In *Applied Catalysis A: General*, 186(1-2), 343-354. [https://doi.org/10.1016/S0926-860X\(99\)00153-2](https://doi.org/10.1016/S0926-860X(99)00153-2)
- Fan, Y., Nishida, H., Hoshihara, S., Shirai, Y., Tokiwa, Y., & Endo, T. (2003a). Pyrolysis kinetics of poly(l-lactide) with carboxyl and calcium salt end structures. *Polymer Degradation and Stability*, 79(3), 547–562. [https://doi.org/https://doi.org/10.1016/S0141-3910\(02\)00374-9](https://doi.org/https://doi.org/10.1016/S0141-3910(02)00374-9)
- Fan, Y., Nishida H., Shirai Y., Endo T. (2003b). Racemization on thermal degradation of poly(l-lactide) with calcium salt end structure. *Polymer Degradation and Stability*, 80 (3), 503-511.
- Fan, Y., Nishida, H., Shirai, Y., Tokiwa, Y., & Endo, T. (2004a). Thermal degradation behaviour of poly(lactic acid) stereocomplex. *Polymer Degradation and Stability*, 86(2), 197–208. <https://doi.org/https://doi.org/10.1016/j.polymdegradstab.2004.03.001>
- Fan, Y., Nishida H., Shirai Y., Endo T. (2004b). Thermal Stability of Poly (L-Lactide): Influence of End Protection by Acetyl Group. *Polymer Degradation and Stability*, 84 (1), 143-149.
- Fan, Y., Nishida H., Mori T., Shirai Y., Endo T. (2004c). Thermal degradation of poly(l-lactide): effect of alkali earth metal oxides for selective 1,1-lactide formation. *Polymer*, 45 (4), 1197-1205.
- Fávaro, S. L., Freitas, A. R., Ganzerli, T. A., Pereira, A. G. B., Cardozo, A. L., Baron, O., Muniz, E. C., Giroto, E. M., & Radovanovic, E. (2013). PET and aluminum recycling from multilayer food packaging using supercritical ethanol. *Journal of Supercritical Fluids*, 75, 138–143. <https://doi.org/10.1016/j.supflu.2012.12.015>

- Fernández, J., Etxeberria, A., & Sarasua, J. R. (2013). Effects of repeat unit sequence distribution and residual catalyst on thermal degradation of poly(l-lactide/ε-caprolactone) statistical copolymers. *Polymer Degradation and Stability*, 98(7), 1293–1299. <https://doi.org/10.1016/j.polymdegradstab.2013.04.003>
- Feng, L., Bian, X., Chen, Z., Xiang, S., Liu, Y., Sun, B., Li, G., & Chen, X. (2017). Determination of D-lactide content in lactide stereoisomeric mixture using gas chromatography-polarimetry. *Talanta*, 164, 268–274. <https://doi.org/10.1016/j.talanta.2016.11.038>
- Folino, A., Karageorgiou, A., Calabrò, P. S., & Komilis, D. (2020). Biodegradation of wasted bioplastics in natural and industrial environments: A review. *Sustainability*, 12(15). <https://doi.org/10.3390/su12156030>
- Fortune Business Insights. (2021). Market value of bioplastics worldwide from 2018 to 2021, with a forecast for 2028 (in million U.S. dollars) [Graph]. In Statista. Retrieved March 01, 2022, from <https://www.statista.com/statistics/981762/market-value-bioplastics-worldwide/>
- Fromonteil, C., Bardelle, P., & Cansell, F. (2000). Hydrolysis and oxidation of an epoxy resin in sub- and supercritical water. *Industrial and Engineering Chemistry Research*, 39(4), 922–925. <https://doi.org/10.1021/ie990093x>
- Fuchs, M., Walbeck, M., Jagla, E., Hoffmann, A., & Herres-Pawlis, S. (2022). Guanidine Carboxy Zinc Complexes for the Chemical Recycling of Renewable Polyesters. *Chem Plus Chem*, 87(5), e202200029. <https://doi.org/10.1002/cplu.202200029>
- Gaca, P., Drzewiecka M., Kaleta W., Kozubek H., Nowińska K. (2008). Catalytic Degradation of Polyethylene over Mesoporous Molecular Sieve MCM-41 Modified with Heteropoly Compounds. *Polish J. of Environ. Stud.*, 17(1), 25-31.
- Garforth A, A., Fiddy, S., Lin, Y.-H., Ghanbari-Siakhali, A., Sharratt, R. N., & Dwyer, J. (1997). Catalytic degradation of high density polyethylene: An evaluation of

mesoporous and microporous catalysts using thermal analysis. *Thermochimica Acta*, 294 (1). [https://doi.org/10.1016/S0040-6031\(96\)03145-0](https://doi.org/10.1016/S0040-6031(96)03145-0)

Gartiser, S., Wallrabenstein, M., & Stiene, G. (1998). Assessment of Several Test Methods for the Determination of the Anaerobic Biodegradability of Polymers. *Journal of Environmental Polymer Degradation*, 6(3).

Geyer, R., Jambeck, J. R., & Law, K. L. (2017). Production, use, and fate of all plastics ever made. *Science Advances*, 3(7). DOI: 10.1126/sciadv.1700782

Ghorpade, V. M., Gennadios, A., & Hanna, M. A. (2001). Laboratory composting of extruded poly(lactic acid) sheets. *Bioresource Technology*, 76(1), 57-61. [https://doi.org/10.1016/S0960-8524\(00\)00077-8](https://doi.org/10.1016/S0960-8524(00)00077-8)

Global Citizen. (2020). “10 Plastic Pollution Facts That Show Why We Need To Do More We serious” Retrieved Nov. 20, 2020, from <https://www.globalcitizen.org/de/content/plastic-pollution-facts>

Gigante, V., Cinelli, P., Sandroni, M., D’ambrosio, R., Lazzeri, A., & Seggiani, M. (2021). On the Use of Paper Sludge as Filler in Biocomposites for Injection Moulding. *Materials*, 14(10). <https://doi.org/10.3390/ma14102688>

Göktürk, S. (2021). Hydrogen production via steam reforming of glycerol. <https://open.metu.edu.tr/handle/11511/89722>

Gornall, T. (2011). *Catalytic Degradation of Waste Polymers*. <https://core.ac.uk/download/pdf/1442485.pdf>

Goto, M., Koyamoto, H., Kodama, A., Hirose, T., Nagaoka, S., & Mccoy, B. J. (2002). Degradation Kinetics of Polyethylene Terephthalate in Supercritical Methanol. *J. Phys.: Condens. Matter*, 14(44), 11427. DOI 10.1088/0953-8984/14/44/494

Goto, M. (2009). Chemical recycling of plastics using sub- and supercritical fluids. *Journal of Supercritical Fluids*, 47(3), 500-507. <https://doi.org/10.1016/j.supflu.2008.10.011>

- Goto, M. (2016). Subcritical and supercritical fluid technology for recycling waste plastics. *Journal of the Japan Petroleum Institute*, 59(6), 254-258. <https://doi.org/10.1627/jpi.59.254>
- Grand View Research. (2021). Market size value of plastics worldwide from 2021 to 2030. Retrieved September 10, 2021, from <https://www.statista.com/statistics/1060583/global-market-value-of-plastic/>.
- Grand View Research. (2019). Polylactic Acid Market Size, Share And Trends Analysis Report By End Use (Packaging, Agriculture, Transport, Electronics, Textile, Others), By Region, And Segment Forecasts, 2022 – 2030. <https://www.grandviewresearch.com/industry-analysis/polylactic-acid-pla-market>
- Gregorowicz, J., & Bernatowicz, P. (2009). Phase behaviour of l-lactic acid based polymers of low molecular weight in supercritical carbon dioxide at high pressures. *Journal of Supercritical Fluids*, 51(2), 270–277. <https://doi.org/10.1016/j.supflu.2009.08.002>
- Grewell, D., Srinivasan, G., & Cochran, E. (2014). Depolymerization of post-consumer polylactic acid products. *Journal of Renewable Materials*, 2(3), 157–165. <https://doi.org/10.7569/JRM.2014.634112>
- Grigore, M. E. (2017). Methods of recycling, properties and applications of recycled thermoplastic polymers. *Recycling*, 2(4). <https://doi.org/10.3390/recycling2040024>
- Groot, W. J., & Borén, T. (2010). Life cycle assessment of the manufacture of lactide and PLA biopolymers from sugarcane in Thailand. *International Journal of Life Cycle Assessment*, 15(9), 970–984. <https://doi.org/10.1007/s11367-010-0225-y>
- Güner, Ö. (2007). Acidity Characterization and Adsorption Characteristics of Cobalt and Lead Doped SBA-15 Mesoporous Materials.
- Habib, A. R. (2019). “Production of valuable chemicals from plastic wastes containing polyethylene and polypropylene”. <https://open.metu.edu.tr/handle/11511/44494>

- Hador, R. Shuster, M., Venditto, V., Kol. M. (2022). Stereogradient Poly(Lactic Acid) from meso-Lactide/L-Lactide Mixtures. *Angewandte Chemie*, 61(40), e202207652. <https://doi.org/10.1002/anie.202207652>
- Hanon, M. M., Dobos, J., & Zsidai, L. (2021). The influence of 3D printing process parameters on the mechanical performance of PLA polymer and its correlation with hardness. *Procedia Manufacturing*, 54, 244–249. <https://doi.org/10.1016/j.promfg.2021.07.038>
- Heidbreder, L. M., Bablok, I., Drews, S., & Menzel, C. (2019). Tackling the plastic problem: A review on perceptions, behaviors, and interventions. *Science of the Total Environment* (Vol. 668, pp. 1077–1093). Elsevier B.V. <https://doi.org/10.1016/j.scitotenv.2019.02.437>
- Henton D., G. P., L. J. , R. J. (2005). Polylactic Acid Technology. *Natural Fibers, Biopolymers, and Biocomposites*. 527–577. CRC Press.
- Hernandez-Charpak, Y. D., Trabold, T. A., Lewis, C. L., & Diaz, C. A. (2022). Biochar-filled plastics: Effect of feedstock on thermal and mechanical properties. *Biomass Conversion and Biorefinery*, 12(10), 4349–4360. <https://doi.org/10.1007/s13399-022-02340-4>
- Hirao, K., Nakatsuchi, Y., & Ohara, H. (2010). Alcoholysis of Poly(l-lactic acid) under microwave irradiation. *Polymer Degradation and Stability*, 95(6), 925–928. <https://doi.org/10.1016/j.polymdegradstab.2010.03.027>
- Homa, P., Wenelska, K., & Mijowska, E. (2020). Enhanced thermal properties of poly(lactic acid)/MoS₂/carbon nanotubes composites. *Scientific Reports*, 10(1), 740. <https://doi.org/10.1038/s41598-020-57708-1>
- Hopmann, C., Schippers, S., & Höfs, C. (2015). Influence of recycling of poly(lactic acid) on packaging relevant properties. *Journal of Applied Polymer Science*, 132(9). <https://doi.org/10.1002/app.41532>

- Hosler, D., Burkett, S. L., & Tarkanian, M. J. (1999). Prehistoric Polymers: Rubber Processing in Ancient Mesoamerica. *Science*, 284(5422), 1988–1991. <https://doi.org/10.1126/science.284.5422.1988>
- Huang, K., Tang, L. H., Zhu, Z. bin, & Ying, W. Y. (2006). Continuous distribution kinetics for degradation of polystyrene in sub- and supercritical toluene. *Journal of Analytical and Applied Pyrolysis*, 76(1–2), 186–190. <https://doi.org/10.1016/j.jaap.2005.11.005>
- Huang, Z., Ye, Q. Q., & Teng, L. J. (2015). A comparison study on thermal decomposition behavior of poly(l-lactide) with different kinetic models. *Journal of Thermal Analysis and Calorimetry*, 119(3), 2015–2027. <https://doi.org/10.1007/s10973-014-4311-4>
- Huang, D., Guo, C., Zhang, M., & Shi, L. (2017). Characteristics of nanoporous silica aerogel under high temperature from 950°C to 1200°C. *Materials & Design*, 129, 82–90. <https://doi.org/https://doi.org/10.1016/j.matdes.2017.05.024>
- Hyon, S.-H., Jamshidi, K., & Ikada, Y. (1997). Synthesis of polylactides with different molecular weights. *Biomaterials*, 18(22), 1503-1508. [https://doi.org/10.1016/S0142-9612\(97\)00076-8](https://doi.org/10.1016/S0142-9612(97)00076-8)
- Imran, M., Kim, B. K., Han, M., Cho, B. G., & Kim, D. H. (2010). Sub-and supercritical glycolysis of polyethylene terephthalate (PET) into the monomer bis(2-hydroxyethyl) terephthalate (BHET). *Polymer Degradation and Stability*, 95(9), 1686–1693. <https://doi.org/10.1016/j.polymdegradstab.2010.05.026>
- Iñiguez-Franco, F., Auras, R., Dolan, K., Selke, S., Holmes, D., Rubino, M., & Soto-Valdez, H. (2018). Chemical recycling of poly(lactic acid) by water-ethanol solutions. *Polymer Degradation and Stability*, 149, 28–38. <https://doi.org/https://doi.org/10.1016/j.polymdegradstab.2018.01.016>
- Iwaya, T., Sasaki, M., & Goto, M. (2006). Kinetic analysis for hydrothermal depolymerization of nylon 6. *Polymer Degradation and Stability*, 91(9), 1989–1995. <https://doi.org/10.1016/j.polymdegradstab.2006.02.009>

- IDTechEx. (2020). Revenue of polymer recycling worldwide in 2020 and 2030 (in billion U.S. dollars) [Graph]. In Statista. Retrieved February 28, 2023, from <https://www.statista.com/statistics/1135178/global-polymer-recycling-revenue/>
- Itavaara, M., Karjomaa, S., & Selin, J.-F. (2002). Biodegradation of polylactide in aerobic and anaerobic thermophilic conditions. *Chemosphere*, 46(6), 879-885. DOI: 10.1016/s0045-6535(01)00163-1
- Jarerat, A., Tokiwa, Y., & Tanaka, H. (2006). Production of poly(L-lactide)-degrading enzyme by *Amycolatopsis orientalis* for biological recycling of poly(L-lactide). *Applied Microbiology and Biotechnology*, 72(4), 726–731. <https://doi.org/10.1007/s00253-006-0343-4>
- Jašo, V. (2019). PLA in mechanical and chemical recycling. *Circular and Biobased Performance Materials Symposium Title: PLA in mechanical and chemical recycling*. 19 June 2019, Wageningen, The Netherlands.
- JCPRA. (2022). Average costs for chemical recycling of plastic packaging per ton in Japan from fiscal year 2013 to 2022 (in 1,000 Japanese yen) [Graph]. In Statista. Retrieved September 05, 2022, from <https://www.statista.com/statistics/1263954/japan-plastic-packaging-chemical-recycling-costs-per-ton/>
- Jedliriski, Z., Wafach, W., Kurcok, P., & Adamus, G. (1991). Polymerization of lactones, 12 a) Polymerization of L-dilactide and L, D-dilactide in the presence of potassium methoxide. *Mikromol. Chem*, 192, 205–206. <https://doi.org/10.1002/macp.1991.021920914>
- Jem, K. J., & Tan, B. (2020). The development and challenges of poly (lactic acid) and poly (glycolic acid). *Advanced Industrial and Engineering Polymer Research*, 3(2),60-70. <https://doi.org/10.1016/j.aiepr.2020.01.002>
- Johnston, K. P., & Haynes, C. (1987). Extreme solvent effects on reaction rate constants at supercritical fluid conditions. *AIChE Journal*, 33(12), 2017–2026. <https://doi.org/10.1002/aic.690331212>

- Kale, G., Auras, R., & Singh, S. P. (2007). Comparison of the degradability of poly(lactide) packages in composting and ambient exposure conditions. *Packaging Technology and Science*, 20(1), 49–70. <https://doi.org/10.1002/pts.742>
- Kamimura, A., Oishi, Y., Kaiso, K., Sugimoto, T., & Kashiwagi, K. (2008). Supercritical secondary alcohols as useful media to convert polyamide into monomeric lactams. *ChemSusChem*, 1(1–2), 82–84. <https://doi.org/10.1002/cssc.200700024>
- Karamanlioglu, M., Preziosi, R., & Robson, G. D. (2017). Abiotic and biotic environmental degradation of the bioplastic polymer poly(lactic acid): A review. In *Polymer Degradation and Stability* (Vol. 137, pp. 122–130). Elsevier Ltd. <https://doi.org/10.1016/j.polymdegradstab.2017.01.009>
- Karamanlioglu, M., & Robson, G. D. (2013). The influence of biotic and abiotic factors on the rate of degradation of poly(lactic) acid (PLA) coupons buried in compost and soil. *Polymer Degradation and Stability*, 98(10), 2063–2071. <https://doi.org/10.1016/j.polymdegradstab.2013.07.004>
- Karamanlioglu, M., Preziosi R., Robson G. D. 2017. “Abiotic and Biotic Environmental Degradation of the Bioplastic Polymer Poly(lactic Acid): A Review”, *Polymer Degradation and Stability*, 137, 122-130. <https://doi.org/10.1016/j.polymdegradstab.2017.01.009>
- Karidi, K., Pladis, P., & Kiparissides, C. (2013). A theoretical and experimental kinetic investigation of the ROP of L,L-lactide in the presence of polyalcohols. *Macromolecular Symposia*, 333(1), 206–215. <https://doi.org/10.1002/masy.201300040>
- Kendall, J. L., Canelas, D. A., Young, J. L., & DeSimone, J. M. (1999). Polymerizations in Supercritical Carbon Dioxide. *Chemical Reviews*, 99(2–3), 543–563. <https://doi.org/10.1021/cr9700336>
- Khalil, I., Celis-Cornejo, C. M., Thomas, K., Bazin, P., Travert, A., Pérez-Martínez, D. J., Baldovino-Medrano, V. G., Paul, J. F., & Maugé, F. (2020). In Situ IRATR Study of the Interaction of Nitrogen Heteroaromatic Compounds with HY Zeolites:

- Experimental and Theoretical Approaches. *ChemCatChem*, 12(4), 1095–1108.
<https://doi.org/10.1002/cctc.201901560>
- Knez, Markočič, E., Leitgeb, M., Primožič, M., Knez Hrnčič, M., & Škerget, M. (2014). Industrial applications of supercritical fluids: A review. *Energy*, 77, 235–243.
<https://doi.org/10.1016/j.energy.2014.07.044>
- Kolstad, J. J., Vink, E. T. H., de Wilde, B., & Debeer, L. (2012). Assessment of anaerobic degradation of Ingeo™ polylactides under accelerated landfill conditions. *Polymer Degradation and Stability*, 97(7), 1131–1141.
<https://doi.org/https://doi.org/10.1016/j.polymdegradstab.2012.04.003>
- Komesu, A., Martins Martinez, P. F., Lunelli, B. H., Oliveira, J., Wolf Maciel, M. R., & Maciel Filho, R. (2017). Study of Lactic Acid Thermal Behavior Using Thermoanalytical Techniques. *Journal of Chemistry*, 2017, 4149592.
<https://doi.org/10.1155/2017/4149592>
- Kondo R., Toshima, K., Matsumura K. (2002). Lipase-Catalyzed Selective Transformation of Polycaprolactone into Cyclic Dicaprolactone and Its Repolymerization in Supercritical Carbon Dioxide. *Macromol. Biosci*, 2, 267–271.
- Kong, F., Nie, B., Han, C., Zhao, D., Hou, Y., & Xu, Y. (2022). Flame Retardancy and Thermal Property of Environment-Friendly Poly(lactic acid) Composites Based on Banana Peel Powder. *Materials*, 15(17). <https://doi.org/10.3390/ma15175977>
- Kooli, F., Sasaki, T., Mizukami, F., Watanabe, M., Martin, C., & Rives, V. (2001). Characterization and acidic properties of silica pillared titanates. *Journal of Materials Chemistry*, 11(3), 841–845. <https://doi.org/10.1039/b007315f>
- Kopinke, F.-D., Remmler, M., Mackenzie, K., Möder, M., & Wachsen, O. (1996). Thermal decomposition of biodegradable polyesters—II. Poly(lactic acid). *Polymer Degradation and Stability*, 53(3), 329–342.
[https://doi.org/https://doi.org/10.1016/0141-3910\(96\)00102-4](https://doi.org/https://doi.org/10.1016/0141-3910(96)00102-4)

- Kowalski, A., Libiszowski, J., Duda, A., & Penczek, S. (2000). Polymerization of 1, 1-dilactide initiated by tin(ii) butoxide. *Macromolecules*, 33(6), 1964–1971. <https://doi.org/10.1021/ma991751s>
- Kurcok, P., Matuszowicz, A., Jedliński, Z., Kricheldorf, H. R., Dubois, P., & Jérôme, R. (1995). Substituent effect in anionic polymerization of β -lactones initiated by alkali metal alkoxides. *Macromolecular Rapid Communications*, 16(7), 513–519. <https://doi.org/10.1002/marc.1995.030160709>
- Kuznetsova, T. F., & Eremenko, S. I. (2014). Synthesis of aerogel-type mesoporous silica. *Colloid Journal*, 76(3), 327–333. <https://doi.org/10.1134/S1061933X14030089>
- Lamberti, F. M., Ingram, A., & Wood, J. (2021). Synergistic dual catalytic system and kinetics for the alcoholysis of poly(Lactic acid). *Processes*, 9(6). <https://doi.org/10.3390/pr9060921>
- Lamberti, F. M., Román-Ramírez, L. A., Dove, A. P., & Wood, J. (2022). Methanolysis of Poly(lactic Acid) Using Catalyst Mixtures and the Kinetics of Methyl Lactate Production. *Polymers*, 14(9). <https://doi.org/10.3390/polym14091763>
- Lee, O.-J., Lee, K.-H., Jin Yim, T., Young Kim, S., & Yoo, K.-P. (2002). Determination of mesopore size of aerogels from thermal conductivity measurements. *Journal of Non-Crystalline Solids*, 298(2-3), 287-292. [https://doi.org/10.1016/S0022-3093\(01\)01041-9](https://doi.org/10.1016/S0022-3093(01)01041-9)
- Lee, S.-H., Hyun Kim, S., Han, Y.-K., & Kim, Y. H. (2001). Synthesis and degradation of end-group-functionalized polylactide. *Journal of Polymer Science Part A: Polymer Chemistry*, 39(7), 973–985. [https://doi.org/https://doi.org/10.1002/1099-0518\(20010401\)39:7<973::AID-POLA1073>3.0.CO;2-8](https://doi.org/https://doi.org/10.1002/1099-0518(20010401)39:7<973::AID-POLA1073>3.0.CO;2-8)
- Lei, S., Xuehua, W., Keyu, C., & Shiming, H. (2007). Effect of Increasing Course of Temperature and Pressure on Polypropylene Degradation in Supercritical Water. *Chin. J. Chem. Eng*, 15(5).

- Leitner, W. (2002). Supercritical Carbon Dioxide as a Green Reaction Medium for Catalysis. *Accounts of Chemical Research*, 35(9), 746–756. <https://doi.org/10.1021/ar010070q>
- Lettner, M., Schöggli, J. P., & Stern, T. (2017). Factors influencing the market diffusion of bio-based plastics: Results of four comparative scenario analyses. *Journal of Cleaner Production*, 157, 289–298. <https://doi.org/10.1016/j.jclepro.2017.04.077>
- Leventis, N., Elder, I. A., Rolison, D. R., Anderson, M. L., & Merzbacher, C. I. (1999). Durable modification of silica aerogel monoliths with fluorescent 2,7-diazapyrenium moieties. sensing oxygen near the speed of open-air diffusion. *Chemistry of Materials*, 11(10), 2837–2845. <https://doi.org/10.1021/cm9901966>
- Li, J., Cao, J., Huo, L., & He, X. (2012). One-step synthesis of hydrophobic silica aerogel via in situ surface modification. *Materials Letters*, 87, 146–149. <https://doi.org/https://doi.org/10.1016/j.matlet.2012.07.078>
- Li, J., & Stoliarov, S. I. (2013). Measurement of kinetics and thermodynamics of the thermal degradation for non-charring polymers. *Combustion and Flame*, 160(7), 1287–1297. <https://doi.org/https://doi.org/10.1016/j.combustflame.2013.02.012>
- Li, X.-Y., Zhou, Q., Yang, K.-K., & Wang, Y.-Z. (2014). Degradation of polylactide using basic ionic liquid imidazolium acetates. *Chemical Papers*, 68(10), 1375–1380. <https://doi.org/10.2478/s11696-014-0560-8>
- Li, X. K., Lu, H., Guo, W. Z., Cao, G. P., Liu, H. L., & Shi, Y. H. (2015). Reaction kinetics and mechanism of catalyzed hydrolysis of waste PET using solid acid catalyst in supercritical CO₂. *AIChE Journal*, 61(1), 200–214. <https://doi.org/10.1002/aic.14632>
- Li, D., Shi, Y., Yang, L., Xiao, L., Kehoe, D. K., Gun'ko, Y. K., Boland, J. J., & Wang, J. J. (2020). Microplastic release from the degradation of polypropylene feeding bottles during infant formula preparation. *Nature Food*, 1(11), 746–754. <https://doi.org/10.1038/s43016-020-00171-y>

- Li, K., & Zhen, W. (2020). Performance, structure-property relationship and biodegradability of poly(lactic acid)/amide ammonium acetate organic vermiculite intercalation nanocomposites. *Polymer-Plastics Technology and Materials*, 59(7), 702–721. <https://doi.org/10.1080/25740881.2019.1686763>
- Li, C., Liu, Q., Gong, W., Zhou, Z., Yao, Z., & Meng, X. (2022). Study on the atomic scale of thermal and thermo-oxidative degradation of polylactic acid via reactive molecular dynamics simulation. *Thermochimica Acta*, 709, 179144. <https://doi.org/https://doi.org/10.1016/j.tca.2021.179144>
- Lin, H., Han, L., & Dong, L. (2014). Thermal degradation behavior and gas phase flame-retardant mechanism of polylactide/PCPP blends. *Journal of Applied Polymer Science*, 131(13). <https://doi.org/https://doi.org/10.1002/app.40480>
- Liu, E. K., He, W. Q., & Yan, C. R. (2014). “White revolution” to “white pollution” - Agricultural plastic film mulch in China. *Environmental Research Letters*, 9(9). Institute of Physics Publishing. <https://doi.org/10.1088/1748-9326/9/9/091001>
- Liu, F., Guo, J., Zhao, P., Gu, Y., Gao, J., & Liu, M. (2019). Facile synthesis of DBU-based protic ionic liquid for efficient alcoholysis of waste poly(lactic acid) to lactate esters. *Polymer Degradation and Stability*, 167, 124–129. <https://doi.org/10.1016/j.polymdegradstab.2019.06.028>
- Lizundia, E., Ruiz-Rubio, L., Vilas, J. L., & León, L. M. (2016). Towards the development of eco-friendly disposable polymers: ZnO-initiated thermal and hydrolytic degradation in poly(l-lactide)/ZnO nanocomposites. *RSC Adv.*, 6(19), 15660–15669. <https://doi.org/10.1039/C5RA24604K>
- Longieras, A., Tanchette, J. B., Erre, D., Braud, C., & Copinet, A. (2007). Compostability of Poly(lactide): Degradation in an Inert Solid Medium. *Journal of Polymers and the Environment*, 15(3), 200–206. <https://doi.org/10.1007/s10924-007-0061-8>
- Lowell, S., J.E. Shields, M.A. Thomas, and M. Thommes. (2006). *Characterization of Porous Solids and Powders: Surface Area, Pore Size and Density*, Netherlands: Springer.

- Lucintel. (2022). Polylactic Acid Market: Trends, Opportunities and Competitive Analysis. Retrieved March 10, 2022, from <https://www.lucintel.com/polylactic-acid-market.aspx>
- Lunt, J. (1998). Large-scale production, properties and commercial applications of polylactic acid polymers. *Polymer Degradation and Stability*, 59(1-3), 145-152. [https://doi.org/10.1016/S0141-3910\(97\)00148-1](https://doi.org/10.1016/S0141-3910(97)00148-1)
- Lv, S., Zhang, Y., & Tan, H. (2019). Thermal and thermo-oxidative degradation kinetics and characteristics of poly (lactic acid) and its composites. *Waste Management*, 87, 335–344. <https://doi.org/https://doi.org/10.1016/j.wasman.2019.02.027>
- Maharana, T., Mohanty, B., & Negi, Y. S. (2009). Melt-solid polycondensation of lactic acid and its biodegradability. *Progress in Polymer Science*, 34(1), 99–124. <https://doi.org/10.1016/j.progpolymsci.2008.10.001>
- Mark, L. O., Cendejas, M. C., & Hermans, I. (2020). The Use of Heterogeneous Catalysis in the Chemical Valorization of Plastic Waste. *ChemSusChem*, 13(22), 5808-5836. <https://doi.org/10.1002/cssc.202001905>
- Masanobu, A., Katashi, E., Kazuhiko, S., Akihiro, Y. (1995). The Basic Properties of Poly(lactic Acid) Produced by the Direct Condensation Polymerization of Lactic Acid. *Journal of Enviromental Polymer Degradation* 3(4).
- Massardier-Nageotte, V., Pestre, C., Cruard-Pradet, T., & Bayard, R. (2006). Aerobic and anaerobic biodegradability of polymer films and physico-chemical characterization. *Polymer Degradation and Stability*, 91(3), 620–627. <https://doi.org/10.1016/j.polymdegradstab.2005.02.029>
- Masutani, K., & Kimura, Y. (2014). *Chapter 1. PLA Synthesis. From the Monomer to the Polymer*, 1-36. <https://doi.org/10.1039/9781782624806-00001>
- McCarthy, N. (2018). Plastic Can Take 500 Years to Bio-Degrade In The Ocean [Digital image]. Retrieved February 27, 2022, from

<https://www.statista.com/chart/15905/the-estimated-number-of-years-for-selected-items-to-bio-degrade/>

McLauchlin, A. R., & Ghita, O. R. (2016). Studies on the thermal and mechanical behavior of PLA-PET blends. *Journal of Applied Polymer Science*, 133(43). <https://doi.org/10.1002/app.44147>

McNeill, I. C., & Leiper, H. A. (1985). Degradation studies of some polyesters and polycarbonates-1. Polylactide: General features of the degradation under programmed heating conditions. *Polymer Degradation and Stability*, 11(3), 267–285. [https://doi.org/https://doi.org/10.1016/0141-3910\(85\)90050-3](https://doi.org/https://doi.org/10.1016/0141-3910(85)90050-3)

ME (South Korea). (2022). Recycling rate of plastic waste in South Korea from 2008 to 2020 [Graph]. In Statista. Retrieved February 28, 2023, from <https://www.statista.com/statistics/1074985/south-korea-plastic-waste-recycling-rate/>

Meimoun, J., Favrelle-Huret, A., Winter, J. de, & Zinck, P. (2022). Poly(L-lactide) Epimerization and Chain Scission in the Presence of Organic Bases. *Macromol*, 2(2), 236–246. <https://doi.org/10.3390/macromol2020016>

MRFR. (2021). Distribution of the production capacity of biodegradable plastics worldwide in 2019, by material [Graph]. In Statista. Retrieved March 01, 2022, from <https://www.statista.com/statistics/1283701/global-bioplastic-production-capacity-shares-by-material/>

Miskolczi, N. (2013). Co-pyrolysis of petroleum based waste HDPE, poly-lactic-acid biopolymer and organic waste. *Journal of Industrial and Engineering Chemistry*, 19(5), 1549–1559. <https://doi.org/https://doi.org/10.1016/j.jiec.2013.01.022>

Mlyniec, A., Ekiert, M., Morawska-Chochol, A., & Uhl, T. (2016). Influence of density and environmental factors on decomposition kinetics of amorphous polylactide – Reactive molecular dynamics studies. *Journal of Molecular Graphics and Modelling*, 67, 54–61. <https://doi.org/https://doi.org/10.1016/j.jmglm.2016.04.010>

- Mohd-Adnan, A.-F., Nishida, H., & Shirai, Y. (2008). Evaluation of kinetics parameters for poly(l-lactic acid) hydrolysis under high-pressure steam. *Polymer Degradation and Stability*, 93(6), 1053–1058. <https://doi.org/https://doi.org/10.1016/j.polymdegradstab.2008.03.022>
- Moliner, C., Badia, J. D., Bosio, B., Arato, E., Teruel-Juanes, R., Kittikorn, T., Strömberg, E., Ek, M., Karlsson, S., & Ribes-Greus, A. (2018). Thermal kinetics for the energy valorisation of polylactide/sisal biocomposites. *Thermochimica Acta*, 670, 169–177. <https://doi.org/10.1016/j.tca.2018.10.029>
- Molnár, Á. (2011). Efficient, selective, and recyclable palladium catalysts in carbon-carbon coupling reactions. *Chemical Reviews*, 111(3), 2251–2320. <https://doi.org/10.1021/cr100355b>
- Montalbán, M. G., & VÍllora, G. (2022). Supercritical Fluids: Properties and Applications. *Phase Equilibria With Supercritical Carbon Dioxide*, (1). IntechOpen. <https://doi.org/10.5772/intechopen.105485>
- Moon, S. il, Lee, C. W., Miyamoto, M., & Kimura, Y. (2000). Melt polycondensation of L-lactic acid with Sn(II) catalysts activated by various proton acids: A direct manufacturing route to high molecular weight poly(L-lactic acid). *Journal of Polymer Science, Part A: Polymer Chemistry*, 38(9), 1673–1679. [https://doi.org/10.1002/\(SICI\)1099-0518\(20000501\)38:9<1673::AID-POLA33>3.0.CO;2-T](https://doi.org/10.1002/(SICI)1099-0518(20000501)38:9<1673::AID-POLA33>3.0.CO;2-T)
- Moore W.J. (1972). *Physical Chemistry*, Prentice-Hall, Englewood Cliffs, New Jersey.
- More Than Green (2021). Plastic Soup | The great Pacific garbage patch. Retrieved September 30, 2021, from <https://www.morethangreen.es/en/plastic-soup-the-great-pacific-garbage-patch/>
- Mulyashov, S. A., Sirovski, F. S., & Beksaev, S. G. (2011). Depolymerisation of oligolactic acid: Simulation and pilot plant trial. *Chemical Engineering Journal*, 176–177, 225–230. <https://doi.org/https://doi.org/10.1016/j.cej.2011.03.086>

- Nalawade, S. P., Picchioni, F., & Janssen, L. P. B. M. (2006). Supercritical carbon dioxide as a green solvent for processing polymer melts: Processing aspects and applications. *Progress in Polymer Science*, 31(1), 19–43. <https://doi.org/https://doi.org/10.1016/j.progpolymsci.2005.08.002>
- Nanda, S., Patra, B. R., Patel, R., Bakos, J., & Dalai, A. K. (2022). Innovations in applications and prospects of bioplastics and biopolymers: a review. In *Environmental Chemistry Letters*, 20(1), 379-395. <https://doi.org/10.1007/s10311-021-01334-4>
- Nayak, J. P., and J. Bera. 2009. Preparation of Silica Aerogel by Ambient Pressure Drying Process Using Rice Husk Ash as Raw. *Material Transactions of the Indian Ceramic Society*, 68(2): 91–94. <https://doi.org/10.1080/0371750X.2009.11082163>
- NatureWorks LLC. (2023). Composting. Retrieved December 10, 2022, from <https://www.Natureworksllc.Com/What-Is-Ingeo/Where-It-Goes/Composting>.
- Ni, C., Luo, R., Xu, K., & Chen, G.-Q. (2009). Thermal and crystallinity property studies of poly (L-lactic acid) blended with oligomers of 3-hydroxybutyrate or dendrimers of hydroxyalkanoic acids. *Journal of Applied Polymer Science*, 111(4), 1720–1727. <https://doi.org/https://doi.org/10.1002/app.29182>
- Nicholson, S. R., Rorrer, J. E., Singh, A., Konev, M. O., Rorrer, N. A., Carpenter, A. C., Jacobsen, A. J., Román-Leshkov, Y., & Beckham, G. T. (2022). The Critical Role of Process Analysis in Chemical Recycling and Upcycling of Waste Plastics. *Annual Review of Chemical and Biomolecular Engineering*, 13(1), 301–324. <https://doi.org/10.1146/annurev-chembioeng-100521-085846>
- Nim, B., Opaprakasit, M., Petchsuk, A., & Opaprakasit, P. (2020). Microwave-assisted chemical recycling of polylactide (PLA) by alcoholysis with various diols. *Polymer Degradation and Stability*, 181, 109363. <https://doi.org/https://doi.org/10.1016/j.polymdegradstab.2020.109363>

- Obalı, Z., Sezgi, N. A., & Doğu, T. (2009). Performance of acidic MCM-Like aluminosilicate catalysts in pyrolysis of polypropylene. *Chemical Engineering Communications*, 196(1–2), 116–130. <https://doi.org/10.1080/00986440802301537>
- Obalı, Z., Sezgi, N. A., & Doğu, T. (2011). The synthesis and characterization of aluminum loaded SBA-type materials as catalyst for polypropylene degradation reaction. *Chemical Engineering Journal*, 176–177, 202–210. <https://doi.org/10.1016/j.cej.2011.04.063>
- Obalı Z., Sezgi N.A., Doğu T. (2012). Catalytic Degradation of Polypropylene over Alumina Loaded Mesoporous Catalysts. *Chemical Engineering Journal*, 207-208, 421-425.
- OECD. (2021). Plastic pollution is growing relentlessly as waste management and recycling fall short. Retrieved November 6, 2022, from <https://www.oecd.org/environment/plastic-pollution-is-growing-relentlessly-as-waste-management-and-recycling-fall-short.htm>
- OECD. (2022). Plastic use and waste projection scenarios worldwide in 2060, by type (in million metric tons) [Graph]. In Statista. Retrieved February 28, 2023, from <https://www.statista.com/statistics/1316016/global-plastic-waste-outlook-by-scenario/>
- Okajima, I., & Sako, T. (2014). Energy Conversion of Biomass and Recycling of Waste Plastics Using Supercritical Fluid, Subcritical Fluid and High-Pressure Superheated Steam. *Supercritical Fluid Technology for Energy and Environmental Applications* (pp. 249–267). Elsevier B.V. <https://doi.org/10.1016/B978-0-444-62696-7.00013-7>
- Onwudili, J. A., Yildirim, E., & Williams, P. T. (2013). Catalytic hydrothermal degradation of carbon reinforced plastic wastes for carbon fibre and chemical feedstock recovery. *Waste and Biomass Valorization*, 4(1), 87–93. <https://doi.org/10.1007/s12649-013-9204-4>
- Onwudili, J. A., & Williams, P. T. (2016). Catalytic supercritical water gasification of plastics with supported RuO₂: A potential solution to hydrocarbons-water pollution

- problem. *Process Safety and Environmental*, 102, 140-149. <https://doi.org/10.1016/j.psep.2016.02.009>
- Ozdemir, E., & Hacaloglu, J. (2018a). Thermal degradation of Polylactide/Poly(ethylene glycol) fibers and composite fibers involving organoclay. *Journal of Analytical and Applied Pyrolysis*, 129, 181–188. <https://doi.org/10.1016/j.jaap.2017.11.014>
- Ozdemir, E., & Hacaloglu, J. (2018b). Characterization of polymer/nanoclay composites via direct pyrolysis mass spectrometry. *Journal of Analytical and Applied Pyrolysis*, 134, 395–404. <https://doi.org/10.1016/j.jaap.2018.07.006>
- Papong, S., Malakul, P., Trungkavashirakun, R., Wenunun, P., Chom-In, T., Nithitanakul, M., & Sarobol, E. (2014). Comparative assessment of the environmental profile of PLA and PET drinking water bottles from a life cycle perspective. *Journal of Cleaner Production*, 65, 539–550. <https://doi.org/10.1016/j.jclepro.2013.09.030>
- Palmay, P., Mora, M., Barzallo, D., & Bruno, J. C. (2021). Determination of Thermodynamic Parameters of Polylactic Acid by Thermogravimetry under Pyrolysis Conditions. *Applied Sciences*, 11(21). <https://doi.org/10.3390/app112110192>
- Park, Y., Hool, J. N., Curtis, C. W., & Roberts, C. B. (2001). Depolymerization of styrene-butadiene copolymer in near-critical and supercritical water. *Industrial and Engineering Chemistry Research*, 40(3), 756–767. <https://doi.org/10.1021/ie0005021>
- Pérez Davila, S., González Rodríguez, L., Chiussi, S., Serra, J., & González, P. (2021). How to sterilize polylactic acid based medical devices?. *Polymers*, 13(13), 2115. <https://doi.org/10.3390/polym13132115>
- Petrus, R., Bykowski, D., & Sobota, P. (2016). Solvothermal Alcoholysis Routes for Recycling Polylactide Waste as Lactic Acid Esters. *ACS Catalysis*, 6(8), 5222–5235. <https://doi.org/10.1021/acscatal.6b01009>
- Petrus, R., & Sobota, P. (2019). Magnesium and zinc alkoxides and aryloxides supported by commercially available ligands as promoters of chemical transformations of lactic

acid derivatives to industrially important fine chemicals. *Coordination Chemistry Reviews*, 396, 72-88. <https://doi.org/10.1016/j.ccr.2019.06.002>

Piemonte, V., & Gironi, F. (2013a). Kinetics of Hydrolytic Degradation of PLA. *Journal of Polymers and the Environment*, 21(2), 313–318. <https://doi.org/10.1007/s10924-012-0547-x>

Piemonte, V., & Gironi, F. (2013b). Lactic Acid Production by Hydrolysis of Poly(Lactic Acid) in Aqueous Solutions: An Experimental and Kinetic Study. *Journal of Polymers and the Environment*, 21(1), 275–279. <https://doi.org/10.1007/s10924-012-0468-8>

Plastics Europe. (2020). Plastics-the Facts 2020 An analysis of European plastics production, demand and waste data. Retrieved November 10, 2022, from https://plasticseurope.org/wp-content/uploads/2021/09/Plastics_the_facts-WEB-2020_versionJun21_final.pdf

Plastics Europe. (2021). Plastics - the Facts 2021. Retrieved September 3, 2022, from <https://Plasticseurope.Org/Knowledge-Hub/Plastics-the-Facts-2021/>.

Plastics Europe (PEMRG). (2022). Distribution of global plastic materials production in 2021, by region [Graph]. In Statista. Retrieved January 1, 2023, from <https://www.statista.com/statistics/281126/global-plastics-production-share-of-various-countries-and-regions/>

Plichta, A., Lisowska, P., Kundys, A., Zychewicz, A., Dębowski, M., & Florjańczyk, Z. (2014). Chemical recycling of poly(lactic acid) via controlled degradation with protic (macro)molecules. *Polymer Degradation and Stability*, 108, 288–296. <https://doi.org/10.1016/j.polymdegradstab.2014.03.006>

Ponce, G., Rodríguez-Llamazares, S., Rivera, P. C., Castaño, J., Oporto-Velásquez, G., Sabando, C., Ide, W., Nesic, A., & Cabrera-Barjas, G. (2022). Biocomposites of polylactic acid/ poly(butylene adipate-co-terephthalate) blends loaded with quinoa husk agro-waste: thermal and mechanical properties. *Journal of Polymer Research*, 29(8), 356. <https://doi.org/10.1007/s10965-022-03196-y>

- Prabu, S., & Chiang, K. Y. (2022). Highly active Ni-Mg-Al Ni–Mg–Al catalyst effect on carbon nanotube production from waste biodegradable plastic catalytic pyrolysis. *Environmental Technology and Innovation*, 28, 102845. <https://doi.org/10.1016/j.eti.2022.102845>
- PR Newswire. (2016). Market value of recycled plastic and plastic waste-to-oil worldwide in 2014 and 2024 (in million U.S. dollars) [Graph]. In Statista. Retrieved December 24, 2021, from <https://www.statista.com/statistics/1010111/global-recycled-plastic-and-plastic-waste-to-oil-market-value/>
- Ragusa, A., Svelato, A., Santacroce, C., Catalano, P., Notarstefano, V., Carnevali, O., Papa, F., Rongioletti, M. C. A., Baiocco, F., Draghi, S., D'Amore, E., Rinaldo, D., Matta, M., & Giorgini, E. (2021). Plasticenta: First evidence of microplastics in human placenta. In *Environment International*, 146, 106274. <https://doi.org/10.1016/j.envint.2020.106274>
- Rahimi, A. R., & Garcíá, J. M. (2017). Chemical recycling of waste plastics for new materials production. *Nature Reviews Chemistry* 1, 0046. <https://doi.org/10.1038/s41570-017-0046>
- Rajan, K. P., Thomas, S. P., Gopanna, A., Al-Ghamdi, A., & Chavali, M. (2018). Rheology, mechanical properties and thermal degradation kinetics of polypropylene (PP) and polylactic acid (PLA) blends. *Materials Research Express*, 5(8), 85304. <https://doi.org/10.1088/2053-1591/aad1d3>
- Rao, A. P., Pajonk, G. M., & Rao, A. v. (2005). Effect of preparation conditions on the physical and hydrophobic properties of two step processed ambient pressure dried silica aerogels. *Journal of Materials Science*, 40, 3481–3489. <https://doi.org/10.1007/s10853-005-2853-3>
- Ramsey, E. D., Sun, Q., Zhang, Z., Zhang, C., & Gou, W. (2009). Mini-review: green sustainable processes using supercritical fluid carbon dioxide. *Journal of Environmental Sciences*, 21(6), 720–726.

- Rezvani Ghomi, E., Khosravi, F., Saedi Ardahaei, A., Dai, Y., Neisiany, R. E., Foroughi, F., Wu, M., Das, O., & Ramakrishna, S. (2021). The life cycle assessment for polylactic acid (PLA) to make it a low-carbon material. *Polymers*, 13(11), 1854. <https://doi.org/10.3390/polym13111854>
- Rezwan, K., Chen, Q. Z., Blaker, J. J., & Boccaccini, A. R. (2006). Biodegradable and bioactive porous polymer/inorganic composite scaffolds for bone tissue engineering. *Biomaterials*, 27(18), 3413-3431. <https://doi.org/10.1016/j.biomaterials.2006.01.039>
- Román-Ramírez, L. A., McKeown, P., Jones, M. D., & Wood, J. (2020). Kinetics of Methyl Lactate Formation from the Transesterification of Polylactic Acid Catalyzed by Zn(II) Complexes. *ACS Omega*, 5(10), 5556–5564. <https://doi.org/10.1021/acsomega.0c00291>
- Rosen, S.L. (1982). *Fundamental Principles of Polymeric Materials*, Wiley, New York.
- Rosenboom, J. G., Langer, R., & Traverso, G. (2022). Bioplastics for a circular economy. In *Nature Reviews Materials*, 7(2), 117-137. <https://doi.org/10.1038/s41578-021-00407-8>
- Roura, P., Farjas, J., Camps, J., Ricart, S., Arbiol, J., Puig, T., & Obradors, X. (2011). Decomposition processes and structural transformations of cerium propionate into nanocrystalline ceria at different oxygen partial pressures. *Journal of Nanoparticle Research*, 13(9), 4085–4096. <https://doi.org/10.1007/s11051-011-0352-9>
- Saadi, Z., Rasmont, A., Cesar, G., Bewa, H., & Benguigui, L. (2012). Fungal Degradation of Poly(l-lactide) in Soil and in Compost. *Journal of Polymers and the Environment*, 20(2), 273–282. <https://doi.org/10.1007/s10924-011-0399-9>
- Saeang, K., Phusunti, N., Phetwarotai, W., Assabumrungrat, S., & Cheirsilp, B. (2021). Catalytic pyrolysis of petroleum-based and biodegradable plastic waste to obtain high-value chemicals. *Waste Management*, 127, 101–111. <https://doi.org/https://doi.org/10.1016/j.wasman.2021.04.024>

- Salak, F., Uemura, S., & Sugimoto, K. (2015). Thermal pretreatment of kudzu biomass (*pueraria lobata*) as filler in cost-effective pla biocomposite fabrication process. *Polymer Engineering & Science*, 55(2), 340–348. <https://doi.org/https://doi.org/10.1002/pen.23909>
- Samir, A., Ashour, F. H., Hakim, A. A. A., & Bassyouni, M. (2022). Recent advances in biodegradable polymers for sustainable applications. *Npj Materials Degradation*, 6, 68 . <https://doi.org/10.1038/s41529-022-00277-7>
- Sangwan, P., & Wu, D. Y. (2008). New insights into polylactide biodegradation from molecular ecological techniques. *Macromolecular Bioscience*, 8(4), 304–315. <https://doi.org/10.1002/mabi.200700317>
- Santulli, F., Lamberti, M., Annunziata, A., Lastra, R. C., & Mazzeo, M. (2022). The Contribution of Commercial Metal Amides to the Chemical Recycling of Waste Polyesters. *Catalysts*, 12(10). <https://doi.org/10.3390/catal12101193>
- Savage, P. E., Gopalan, S., Mizan, T. I., Martino, C. J., & Brock, E. E. (1995). Reactions at Supercritical Conditions: Applications and Fundamentals. *AIChE Journal*, 41(7), 1723-1778. <https://doi.org/10.1002/aic.690410712>
- Schlexer, Philomena. (2017). Computational Modeling in Heterogeneous Catalysis. *Reference Module in Chemistry, Molecular Sciences and Chemical Engineering*. Elsevier. <https://doi.org/10.1016/b978-0-12-409547-2.14273-8>
- Schmidt, M., & Schwertfeger, F. (1998). Applications for silica aerogel products. *Journal of Non-Crystalline Solids*, 225, 364-368. [https://doi.org/10.1016/S0022-3093\(98\)00054-4](https://doi.org/10.1016/S0022-3093(98)00054-4)
- Schwark, F. (2009). Influence factors for scenario analysis for new environmental technologies - the case for biopolymer technology. *Journal of Cleaner Production*, 17(7), 644–652. <https://doi.org/10.1016/j.jclepro.2008.11.017>

- Schwertfeger, F., Frank, D., & Schmidt, M. (1998). Hydrophobic waterglass based aerogels without solvent exchange or supercritical drying. *Journal of Non-Crystalline Solids*, 225, 24-29. [https://doi.org/10.1016/S0022-3093\(98\)00102-1](https://doi.org/10.1016/S0022-3093(98)00102-1)
- Sciencing. (2020). The Eight Most Abundant Elements in the Earth's Crust. Retrieved March 10, 2022, from <https://sciencing.com/eight-abundant-elements-earths-crust-8120554.html>
- Serra, T., Mateos-Timoneda, M. A., Planell, J. A., & Navarro, M. (2013). 3D printed PLA-based scaffolds: A versatile tool in regenerative medicine. *Organogenesis*, 9(4), 239-244. <https://doi.org/10.4161/org.26048>
- Serra, T., Ortiz-Hernandez, M., Engel, E., Planell, J. A., & Navarro, M. (2014). Relevance of PEG in PLA-based blends for tissue engineering 3D-printed scaffolds. *Materials Science and Engineering C*, 38(1), 55–62. <https://doi.org/10.1016/j.msec.2014.01.003>
- Shoemaker D.P. Garland, C.W., Steinfeld, I.J. (1974). Experiments in Physical Chemistry, McGraw-Hill, New York.
- Shogren, R. L., Doane, W. M., Garlotta, D., Lawton, J. W., & Willett, J. L. (2003). Biodegradation of starch/polylactic acid/poly(hydroxyester-ether) composite bars in soil. *Polymer Degradation and Stability*.79(3), 405-411. [https://doi.org/10.1016/S0141-3910\(02\)00356-7](https://doi.org/10.1016/S0141-3910(02)00356-7)
- Shogren, R., Wood, D., Orts, W., & Glenn, G. (2019). Plant-based materials and transitioning to a circular economy. In *Sustainable Production and Consumption*, 19, 194-215. <https://doi.org/10.1016/j.spc.2019.04.007>
- Siddiqui, M. N., Kolokotsiou, L., Vouvoudi, E., Redhwi, H. H., Al-Arfaj, A. A., & Achilias, D. S. (2020). Depolymerization of PLA by Phase Transfer Catalysed Alkaline Hydrolysis in a Microwave Reactor. *Journal of Polymers and the Environment*, 28(6), 1664–1672. <https://doi.org/10.1007/s10924-020-01716-9>

- Siddiqui, M. N., Redhwi, H. H., Al-Arfaj, A. A., & Achilias, D. S. (2021). Chemical Recycling of PET in the Presence of the Bio-Based Polymers, PLA, PHB and PEF: A Review. *Sustainability*, 13(19). <https://doi.org/10.3390/su131910528>
- Silva, D., Kaduri, M., Poley, M., Adir, O., Krinsky, N., Shainsky-Roitman, J., & Schroeder, A. (2018). Biocompatibility, biodegradation and excretion of polylactic acid (PLA) in medical implants and theranostic systems. *Chemical Engineering Journal*, 340, 9–14. <https://doi.org/10.1016/j.cej.2018.01.010>
- Sin, L.T, Rahmat, A. R., Rahman W.A. (2012). “Polylactic Acid Biopolymer Technology and Applications”, USA, Elsevier Inc.
- Sivri, S., Dilek, C., & Sezgi, N. A. (2019). Synthesis and characterization of aluminum containing silica aerogel catalysts for degradation of PLA. *International Journal of Chemical Reactor Engineering*, 17(5). <https://doi.org/10.1515/ijcre-2018-0163>
- Sohn, Y. J., Kim, H. T., Baritugo, K. A., Jo, S. Y., Song, H. M., Park, S. Y., Park, S. K., Pyo, J., Cha, H. G., Kim, H., Na, J. G., Park, C., Choi, J. il, Joo, J. C., & Park, S. J. (2020). Recent Advances in Sustainable Plastic Upcycling and Biopolymers. *Biotechnology Journal*, 15(6). <https://doi.org/10.1002/biot.201900489>
- Song, X., Zhang, X., Wang, H., Liu, F., Yu, S., & Liu, S. (2013). Methanolysis of poly(lactic acid) (PLA) catalyzed by ionic liquids. *Polymer Degradation and Stability*, 98(12), 2760–2764. <https://doi.org/https://doi.org/10.1016/j.polymdegradstab.2013.10.012>
- Song, X., Wang, H., Yang, X., Liu, F., Yu, S., & Liu, S. (2014). Hydrolysis of poly(lactic acid) into calcium lactate using ionic liquid [Bmim][OAc] for chemical recycling. *Polymer Degradation and Stability*, 110, 65–70. <https://doi.org/https://doi.org/10.1016/j.polymdegradstab.2014.08.020>
- Spierling, S., Röttger, C., Venkatachalam, V., Mudersbach, M., Herrmann, C., & Endres, H.-J. (2018). Bio-based Plastics - A Building Block for the Circular Economy. *Procedia CIRP*, 69, 573–578. <https://doi.org/https://doi.org/10.1016/j.procir.2017.11.017>

- Stassin, F., & Jérôme, R. (2005). Polymerization of (L,L)-lactide and copolymerization with ϵ -caprolactone initiated by dibutyltin dimethoxide in supercritical carbon dioxide. *Journal of Polymer Science, Part A: Polymer Chemistry*, 43(13), 2777–2789. <https://doi.org/10.1002/pola.20735>
- Statista. (2019). Market value forecast of polylactic acid in the United States from 2019 to 2025, by application (in million U.S. dollars) [Graph]. In Statista. Retrieved March 01, 2022, from <https://www.statista.com/statistics/964727/polylactic-acid-market-value-us-by-application/?locale=en>
- Statista. (2019). Flow of plastic materials worldwide between 1950 and 2017* (in million metric tons) <https://www.statista.com/study/65164/plastic-waste-worldwide/>
- Statista. (2021) *Global plastic waste*. Statista. Retrieved January 20, 2023, from <https://www.statista.com/study/65164/plastic-waste-worldwide/>
- Stefaniak, K., & Masek, A. (2021). *jMaterials*, 14(18), 52-54. <https://doi.org/10.3390/ma14185254>
- Steinmetz, Z., Wollmann, C., Schaefer, M., Buchmann, C., David, J., Tröger, J., Muñoz, K., Frör, O., & Schaumann, G. E. (2016). Plastic mulching in agriculture. Trading short-term agronomic benefits for long-term soil degradation? *Science of the Total Environment*, 550, 690-705. <https://doi.org/10.1016/j.scitotenv.2016.01.153>
- Stoppato, M., Carletti, E., Sidarovich, V., Quattrone, A., Unger, R. E., Kirkpatrick, C. J., Migliaresi, C., & Motta, A. (2013). Influence of scaffold pore size on collagen I development: A new in vitro evaluation perspective. *Journal of Bioactive and Compatible Polymers*, 28(1), 16–32. <https://doi.org/10.1177/0883911512470885>
- Su, X., Zhao, Y., Zhang, R., & Bi, J. (2004). Investigation on degradation of polyethylene to oils in supercritical water. *Fuel Processing Technology*, 85(8–10), 1249–1258. <https://doi.org/10.1016/j.fuproc.2003.11.044>
- Sun, Y., Zheng, Z., Wang, Y., Yang, B., Wang, J., & Mu, W. (2022). PLA composites reinforced with rice residues or glass fiber—a review of mechanical properties,

- thermal properties, and biodegradation properties. *Journal of Polymer Research*, 29(10), 422. <https://doi.org/10.1007/s10965-022-03274-1>
- Tai, H. S., & Chen, C. Y. (2016). Kinetic Study of Copyrolysis of Waste Polyethylene Terephthalate, Polylactic Acid, and Rice Straw. *Environmental Engineering Science*, 33(9), 671–680. <https://doi.org/10.1089/ees.2015.0522>
- Tanjung, F. A., Arifin, Y., & Kuswardani, R. A. (2021). Influence of newly organosolv lignin-based interface modifier on mechanical and thermal properties, and enzymatic degradation of polylactic acid/chitosan biocomposites. *Polymers*, 13(19), 3355. <https://doi.org/10.3390/polym13193355>
- Taubner, V. and Shishoo, R. (2001), Influence of processing parameters on the degradation of poly(L-lactide) during extrusion. *J. Appl. Polym. Sci.*, 79: 2128-2135. [https://doi.org/10.1002/1097-4628\(20010321\)79:12<2128::AID-APP1020>3.0.CO;2-#](https://doi.org/10.1002/1097-4628(20010321)79:12<2128::AID-APP1020>3.0.CO;2-#)
- The Brooklyn Rail. (2005). *A Brief History of Plastic*. Retrieved November 18, 2021, from. <https://Brooklynrail.Org/2005/05/Express/a-Brief-History-of-Plastic>.
- The Guardian. (2021). Distribution of mismanaged plastic waste attributable to the COVID-19 pandemic as of August 2021, by source [Graph]. In Statista. Retrieved February 27, 2023, from <https://www.statista.com/statistics/1275568/mismanaged-plastic-waste-caused-by-covid-19-by-type/>
- Thomas, P. A., & Marvey, B. B. (2016). Room temperature ionic liquids as green solvent alternatives in the metathesis of oleochemical feedstocks. *Molecules*, 21(2), 184. <https://doi.org/10.3390/molecules21020184>
- Thompson, R. C., Swan, S. H., Moore, C. J., & vom Saal, F. S. (2009). Our plastic age. *Philosophical Transactions of the Royal Society B: Biological Sciences*, 364(1526), 1973-1976. <https://doi.org/10.1098/rstb.2009.0054>

- Tisserat, B., & Finkenstadt, V. L. (2011). Degradation of Poly(l-Lactic Acid) and Bio-Composites by Alkaline Medium Under Various Temperatures. *Journal of Polymers and the Environment*, 19(3), 766–775. <https://doi.org/10.1007/s10924-011-0319-z>
- Tokiwa, Y., & Jarerat, A. (2004). Biodegradation of poly(L-lactide). In *Biotechnology Letters*, 26, 771-777. DOI:10.1023/B:BILE.0000025927.31028.e3
- Torres, A., Li, S. M., Roussos, S., & Vert, M. (1996). Poly(lactic acid) degradation in soil or under controlled conditions. *Journal of Applied Polymer Science*, 62(13), 2295–2302. [https://doi.org/10.1002/\(SICI\)1097-4628\(19961226\)62:13<2295::AID-APP14>3.0.CO;2-2](https://doi.org/10.1002/(SICI)1097-4628(19961226)62:13<2295::AID-APP14>3.0.CO;2-2)
- Toussaint, B., Raffael, B., Angers-Loustau, A., Gilliland, D., Kestens, V., Petrillo, M., Rio-Echevarria, I. M., & van den Eede, G. (2019). Review of micro- and nanoplastic contamination in the food chain. In *Food Additives and Contaminants - Part A Chemistry, Analysis, Control, Exposure and Risk Assessment*, 36(5), 639-673. <https://doi.org/10.1080/19440049.2019.1583381>
- Transparency Market Research. (2021). Market value of plastic recycling worldwide in 2019 and 2027 (in billion U.S. dollars) [Graph]. In Statista. Retrieved February 28, 2022, from <https://www.statista.com/statistics/987522/global-market-size-plastic-recycling/>
- Tripathi, N., Monika, & Katiyar, V. (2017). Poly(lactic acid)/modified gum arabic based bionanocomposite films: Thermal degradation kinetics. *Polymer Engineering & Science*, 57(11), 1193–1206. <https://doi.org/https://doi.org/10.1002/pen.24497>
- Tsukegi, T., Motoyama, T., Shirai, Y., Nishida, H., & Endo, T. (2007). Racemization behavior of l,l-lactide during heating. *Polymer Degradation and Stability*, 92(4), 552–559. <https://doi.org/https://doi.org/10.1016/j.polymdegradstab.2007.01.009>
- Tsuji, H., Fukui, I., Daimon, H., & Fujie, K. (2003). Poly(l-lactide) XI. Lactide formation by thermal depolymerisation of poly(l-lactide) in a closed system. *Polymer Degradation and Stability*, 81(3), 501–509. [https://doi.org/https://doi.org/10.1016/S0141-3910\(03\)00150-2](https://doi.org/https://doi.org/10.1016/S0141-3910(03)00150-2)

- Tsuji, H., & Kondoh, F. (2017). Synthesis of meso-lactide by thermal configurational inversion and depolymerization of poly(l-lactide) and thermal configurational inversion of lactides. *Polymer Degradation and Stability*, 141, 77–83. <https://doi.org/https://doi.org/10.1016/j.polymdegradstab.2017.05.016>
- Tsuji, H., Saeki, T., Tsukegi, T., Daimon, H., & Fujie, K. (2008). Comparative study on hydrolytic degradation and monomer recovery of poly(l-lactic acid) in the solid and in the melt. *Polymer Degradation and Stability*, 93(10), 1956–1963. <https://doi.org/10.1016/j.polymdegradstab.2008.06.009>
- Turkstat. 2015, 2019, 2020. Polilaktik Asit Dış Ticaret İstatistik Raporu.. Available at: <http://rapory.tuik.gov.tr/07-11-2019-15:28:50-16764501492135650475721075775.html?>; <http://rapory.tuik.gov.tr/07-11-2019-15:31:48-15513959277534119421852769870.html?>, [Accessed 15 Sep. 2019].
- Tutek, K., Masek, A., Kosmalska, A., & Cichosz, S. (2021). Application of fluids in supercritical conditions in the polymer industry. *Polymers*,13(5), 1-17. <https://doi.org/10.3390/polym13050729>
- Uddin, M. A., Sakata Y., Muto A., Shiraga Y., Koizumi K., Kanada Y., Murata K. (1998). Catalytic degradation of polyethylene and polypropylene into liquid hydrocarbons with mesoporous silica. *Microporous Mesoporous Mater.* 21 (4-6), 557-564. [https://doi.org/10.1016/S1387-1811\(98\)00036-5](https://doi.org/10.1016/S1387-1811(98)00036-5)
- Undri, A., Rosi, L., Frediani, M., & Frediani, P. (2014). Conversion of poly(lactic acid) to lactide via microwave assisted pyrolysis. *Journal of Analytical and Applied Pyrolysis*, 110, 55–65. <https://doi.org/https://doi.org/10.1016/j.jaap.2014.08.003>
- UN. (2015). Transforming Our World: The 2030 Agenda For Sustainable Development. Retrieved November 15, 2020, from <https://sustainabledevelopment.un.org/content/documents/21252030%20Agenda%20for%20Sustainable%20Development%20web.pdf>
- Usachev, S. v, Lomakin, S. M., Koverzanova, E. v, Shilkina, N. G., Levina, I. I., Prut, E. v, Rogovina, S. Z., & Berlin, A. A. (2022). Thermal degradation of various types of

polylactides research. The effect of reduced graphite oxide on the composition of the PLA4042D pyrolysis products. *Thermochimica Acta*, 712, 179227. <https://doi.org/https://doi.org/10.1016/j.tca.2022.179227>

Vallés, E., Sarmoria, C., Villar, M., Lazzari, M., & Chiantore, O. (2000). Model polydimethylsiloxanes subjected to thermal weathering: effect on molecular weight distributions. *Polymer Degradation and Stability*, 69(1), 67–71. [https://doi.org/https://doi.org/10.1016/S0141-3910\(00\)00041-0](https://doi.org/https://doi.org/10.1016/S0141-3910(00)00041-0)

Velders, G. J. M., Andersen, S. O., Daniel, J. S., Fahey, D. W., & Mcfarland, M. (2007). The importance of the Montreal Protocol in protecting climate. *Environmental Sciences*, 04(12), 4814-4819. <https://doi.org/10.1073/pnas.0610328104>

Vink, E. T. H., Rábago, K. R., Glassner, D. A., Springs, B., O'Connor, R. P., Kolstad, J., & Gruber, P. R. (2004). The sustainability of nature works™ polylactide polymers and ingeo™ polylactide fibers: An update of the future. *Macromolecular Bioscience*, 25;4(6), 551–564. <https://doi.org/10.1002/mabi.200400023>

Viretto, A., Sonnier, R., Taguet, A., Otazaghine, B., Ferry, L., Lopez-Cuesta, J. M., & Lagrève, C. (2016). Thermal degradation of polyesters filled with magnesium dihydroxide and magnesium oxide. *Fire and Materials*, 40(3), 445–463. <https://doi.org/10.1002/fam.2299>

Vroman, I., & Tighzert, L. (2009). Biodegradable polymers. *Materials*, 2(2), 307-344. <https://doi.org/10.3390/ma2020307>

Watanabe ', S., Komura ', K., Nagaya ', S., Morita, H., Nakamoto, T., Hirai ', S., & Aida, F. (2003). Development of Cross-Linked Polymer Material Recycling Technology by Supercritical Water, Proceedings of the 7th International Conference on Properties and Applications of Dielectric Materials, Nagoya, Japan, 2, 595-598. doi: 10.1109/ICPADM.2003.1218487.

Wei, J., Cruz, A., Xu, C., Haque, F., Park, C., & Graber, L. (2020). A Review on Dielectric Properties of Supercritical Fluids. *2020 IEEE Electrical Insulation Conference (EIC)*, 107–113. <https://doi.org/10.1109/EIC47619.2020.9158733>

- Wei, L., Yan, N., & Chen, Q. (2011). Converting Poly(ethylene terephthalate) Waste into Carbon Microspheres in a Supercritical CO₂ System. *Environmental Science & Technology*, 45(2), 534–539. <https://doi.org/10.1021/es102431e>
- Winkler, C.A., Hinshelwood, C.N. (1934). Thermal Decomposition of Acetaldehyde. *Proceedings of the Royal Society of London. Series A, Mathematical and Physical Sciences*, 149 (867), 340-354.
- Wu, D., & Hakkarainen, M. (2015). Recycling PLA to multifunctional oligomeric compatibilizers for PLA/starch composites. *European Polymer Journal*, 64, 126–137. <https://doi.org/10.1016/j.eurpolymj.2015.01.004>
- Wu, X., M. Fan, J. F. Mclaughlin, X. Shen, and G. Tan. (2018). A Novel Low-Cost Method of Silica Aerogel Fabrication Using Fly Ash and Trona Ore with Ambient Pressure Drying Technique. *Powder Technology* 323, 310–22. <https://doi.org/10.1016/j.powtec.2017.10.022>
- WWF. (2022). Impacts of Plastic Pollution in the Oceans on Marine Species, Biodiversity and Ecosystems. Retrieved March 1, 2022, from https://www.Wwf.de/Fileadmin/Fm-Wwf/Publikationen-PDF/Plastik/WWF-Impacts_of_plastic_pollution_in_the_ocean_on_marine_species_biodiversity_and_ecosystems.Pdf.
- Xie, S., Sun, Z., Liu, T., Zhang, J., Li, T., Ouyang, X., Qiu, X., Luo, S., Fan, W., & Lin, H. (2021). Beyond biodegradation: Chemical upcycling of poly(lactic acid) plastic waste to methyl lactate catalyzed by quaternary ammonium fluoride. *Journal of Catalysis*, 402, 61–71. <https://doi.org/https://doi.org/10.1016/j.jcat.2021.08.032>
- Xiu, F. R., & Zhang, F. S. (2010). Materials recovery from waste printed circuit boards by supercritical methanol. *Journal of Hazardous Materials*, 178(1–3), 628–634. <https://doi.org/10.1016/j.jhazmat.2010.01.131>
- Xu, J., Bartholomew, C. H., Sudweeks, J., & Eggett, D. L. (2003). Design, synthesis, and catalytic properties of silica-supported, Pt-promoted iron Fischer-Tropsch catalysts.

Topics in Catalysis, 26, 55-71.
<https://doi.org/10.1023/B:TOCA.0000012987.76556.63>

Yagihashi, M., & Funazukuri, T. (2010). Recovery of l-Lactic Acid from Poly(l-lactic acid) under Hydrothermal Conditions of Dilute Aqueous Sodium Hydroxide Solution. *Industrial & Engineering Chemistry Research*, 49(3), 1247–1251. <https://doi.org/10.1021/ie9008925>

Yanagihara, N., & Ohgane, K. (2013). Studies on the oxidative degradation of nylons by nitrogen dioxide in supercritical carbon dioxide. *Polymer Degradation and Stability*, 98(12), 2735–2741. <https://doi.org/10.1016/j.polymdegradstab.2013.10.010>

Yang, J., Huang, J., Chyu, M. K., Wang, Q. M., Xiong, D., & Zhu, Z. (2010). Degradation of poly(butylene terephthalate) in different supercritical alcohol solvents. *Journal of Applied Polymer Science*, 116(4), 2269–2274. <https://doi.org/10.1002/app.31649>

Ye, Q. qiao, Huang, Z., Hao, Y. hua, Wang, J. wen, Yang, X. yu, & Fan, X. yue. (2016). Kinetic study of thermal degradation of poly(l-lactide) filled with β -zeolite. *Journal of Thermal Analysis and Calorimetry*, 124(3), 1471–1484. <https://doi.org/10.1007/s10973-016-5314-0>

Yi, W. J., Li, L. J., Hao, Z., Jiang, M., Lu, C., Shen, Y., & Chao, Z. S. (2017). Synthesis of l -Lactide via Degradation of Various Telechelic Oligomeric Poly(l -lactic acid) Intermediates. *Industrial and Engineering Chemistry Research*, 56(16), 4867–4877. <https://doi.org/10.1021/acs.iecr.6b04082>

York. P., Kompella. U.D., Shekunov. B.Y. (2014). *Supercritical Fluid Technology for Drug Product Development*, CRC Press, Boca Raton. <https://doi.org/10.1201/9780203021378>

Zenkiewicz, M., & Richert, J. (2009). Synthesis, properties and applications of polylactide. *Przetwórstwo Tworzyw*, 15, 192-199.

- Zhang, C.-C., & Zhang, F.-S. (2020). Enhanced dehalogenation and coupled recovery of complex electronic display housing plastics by sub/supercritical CO₂. *Journal of Hazardous Materials*, 382, 121140. <https://doi.org/10.1016/j.jhazmat.2019.121140>
- Zhang, S., Liang, Y., Qian, X., Hui, D., & Sheng, K. (2020). *Pyrolysis kinetics and mechanical properties of poly(lactic acid)/bamboo particle biocomposites: Effect of particle size distribution*. 9(1), 524–533. <https://doi.org/doi:10.1515/ntrev-2020-0037>
- Zhang, X., Heinonen, S., & Levänen, E. (2014). Applications of supercritical carbon dioxide in materials processing and synthesis. *RSC Adv.*, 4(105), 61137–61152. <https://doi.org/10.1039/C4RA10662H>
- Zhao, X., Gao, S., & Liu, G. (2016). A THEIC-based polyphosphate melamine intumescent flame retardant and its flame retardancy properties for polylactide. *Journal of Analytical and Applied Pyrolysis*, 122, 24–34. <https://doi.org/https://doi.org/10.1016/j.jaap.2016.10.029>
- 3D Hubs. (2018). Worldwide most used 3D printing materials, as of July 2018* [Graph]. In Statista. Retrieved January 20, 2022, from <https://www.statista.com/statistics/800454/worldwide-most-used-3d-printing-materials/>

APPENDICES

A. Determination of Activation Energy for Thermal Degradation Reaction of PLA

The kinetic parameters of the PLA degradation reaction with or without catalyst were evaluated based on a standard power law model and following the procedure reported in the study of Coats and Redfern (1964). The rate of disappearance of PLA is expressed as follows:

$$\frac{d\alpha}{dt} = A e^{\frac{-E_a}{RT}} (1-\alpha)^n \quad (\text{A.1})$$

where α is the fraction of PLA decomposed at time t and n is the overall reaction order. A and E_a are the pre-exponential factor and activation energy of the reaction, respectively. α values are calculated using equation A.2.

$$\alpha = \frac{W_0 - W_t}{W_0 - W_\infty} \quad (\text{A.2})$$

where W_0 , W_t , and W_∞ are the sample weights at initial, time t and infinite time, respectively. Using a linear heating rate ($q=dT/dt$), equation A.3 is obtained by taking integral of equation A.1.

$$\frac{1-(1-\alpha)^{(1-n)}}{(1-n)T^2} = \frac{AR}{qE_a} \left(1 - \frac{2RT}{E_a}\right) e^{(-E_a/RT)} \quad \text{for } n \neq 1 \quad (\text{A.3})$$

The term “ $2RT/E_a$ ” in equation A.3 is negligible compared to A.1. By taking the natural logarithm of both sides, equation A.3 is simplified to equation A.4.

$$\ln \frac{1-(1-\alpha)^{(1-n)}}{(1-n)T^2} = \ln \frac{AR}{qE_A} - \frac{E_A}{RT} \text{ for } n \neq 1 \quad (\text{A.4})$$

A similar analysis for a first order reaction yields equation 5.

$$\ln \frac{-\ln(1-\alpha)}{T^2} = \ln \frac{AR}{qE_A} - \frac{E_A}{RT} \text{ for } n = 1 \quad (\text{A.5})$$

A linear relation is attained between the left side of the equations and $1/T$ term in equations A.4 and A.5. Activation energy is estimated from the slope of these linear relations and the overall order of the PLA degradation reaction is found. A typical result showing the agreement of the data with the first order reaction model is presented in Figure A.1 for the degradation of PLA.

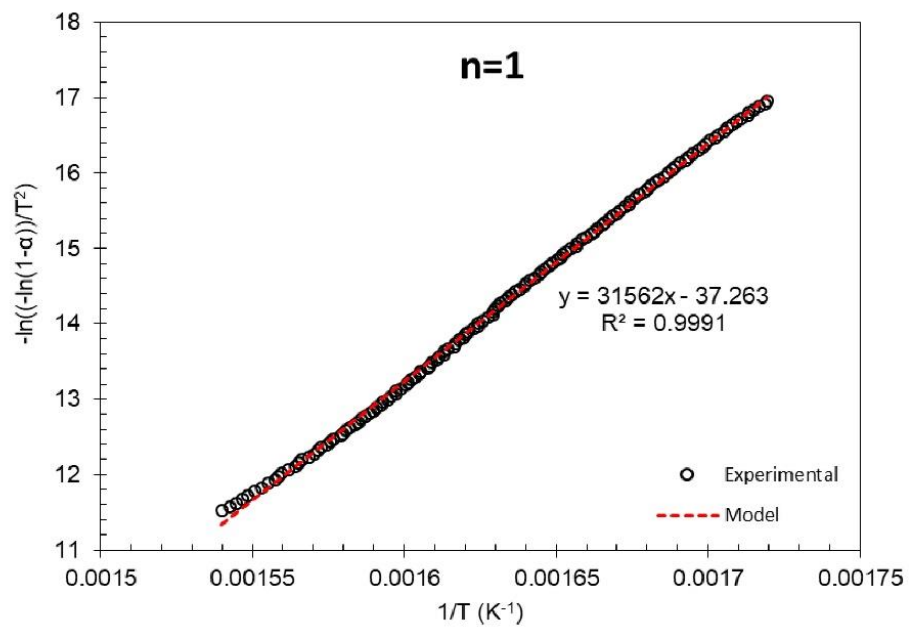


Figure A.1. Determination of Activation Energy of Thermal Degradation Reaction of PLA.

B. Calculation of Solid, Condensable and Non-condensable Product Yields and Weight Fraction of Compounds in Condensable Product for the Pyrolysis System

The yields of the solid, condensable and non-condensable products were calculated based on the equation B.1. The solid products were basically determined by measuring the weight of the sample in the reactor. Similarly, condensable products were also calculated by measuring the amount in the condenser vessels. The amount of non-condensable products were then calculated by applying equation B.1.

$$m_{\text{non-condensable}} = m_{\text{initial PLA}} - m_{\text{solid}} - m_{\text{condensable}} \quad (\text{B.1})$$

m_{solid} , $m_{\text{condensable}}$, and $m_{\text{non-condensable}}$ represent the weight of the solid, condensable and non-condensable products, respectively.

Then the yield of reaction product or compound was obtained as in equation B.2.

$$Yield_i (\text{wt. \%}) = \frac{m_i}{m_{\text{initial PLA}}} * 100 \quad (\text{B.2})$$

m_i represents the weight of the product while $m_{\text{initial PLA}}$ shows the initial weight of the PLA polymer. Weight fraction of the condensable product is defined as in equation B.3.

$$W_i (\text{wt. \%}) = \frac{m_i}{m_{\text{condensable}}} * 100 \quad (\text{B.3})$$

C. Calculations of Relative Response Factor and Number of Moles of the Components in the Condensable and Solid Products

RRF technique was used for the calculation of the amounts of condensable products in pyrolysis experiment and solid products in supercritical reaction experiment. The condensable products and solid were dissolved in acetone and the relative response factor values of the components were determined based on acetone. Response factor (RF) and relative response factor (RRF) of the components were calculated using Equations C.1 and C.2, respectively.

The area of each component was read from the gas chromatogram.

$$RF_i = \frac{A_i}{n_i} \quad (C.1)$$

$$RRF_i = \frac{RF_i}{RF_{C_3H_6O}} \quad (C.2)$$

In equation C.1, the units of area $A_{C_3H_6O}$ and $n_{C_3H_6O}$ are $mV^2 \cdot sec$ and mol, respectively. To determine, RRF values of components, the calibration samples in the range of 5-20 mg/ml in acetone which were D, L lactide, meso lactide, lactic acid and propionic acid were used. The RRF_i values of the components are tabulated in Table C.1.

Table C.1. RRF values and the retention times of the compounds.

Compound	Molecular Weight (g/mol)	Retention Times (min)	RRF
D L,L	144.1	15.3	1.41
Meso L	144.1	14.2	1.41
LA	90.08	8.3	0.36
PA	74.08	7.3	1

The number of moles of compounds in condensable and solid products are calculated using the following equations C.3-C.4.

$$n_{C_3H_6O} = \frac{V_{C_3H_6O}}{M_{C_3H_6O}} * \rho_{C_3H_6O} \quad (C.3)$$

In equation C.3, the units of $V_{C_3H_6O}$, $M_{C_3H_6O}$ and $\rho_{C_3H_6O}$ are in ml, mol/g and g/ml, respectively. Densities of compounds are tabulated in Table C.2.

Table C.2. Densities of the compounds.

Compound	Density (g/cm ³)
D L,L	1.186
Meso L	1.186
LA	1.209
PA	0.988

$$n_i = \frac{A_i}{A_{C_3H_6O}} * \frac{1}{RRF_i} * n_{C_3H_6O} \quad (C.4)$$

The mass and weight fraction of compounds were found from equations C.5-C.7.

$$m_i = n_i * MW_i \quad (C.5)$$

$$m_{condensable} = \sum_{i=1}^j m_i \quad (C.6)$$

$$w_i = \frac{m_i}{m_{condensable}} * 100\% \quad (C.7)$$

D. Calculation of Mole Fraction of Components in Non-condensable Product

Beta factors were used to calculate number of moles of components in non-condensable products. The calibration factors of the gas were obtained with calibration gas containing of hydrogen (%1), methane (%1), ethane (%1), carbon monoxide (%1), carbon dioxide (%1) in argon, by mole. Acetaldehyde was also fed to the system with these gases. The beta factor of carbon dioxide was taken as 1. The beta factors of the other components were calculated using equation D.1. In Table D.1, the retention times and calibration factors of the gas products are given.

$$\beta_i = \frac{A_{CO_2} * \beta_{CO_2}}{A_i} * \frac{n_i}{n_{CO_2}} \quad (D.1)$$

Table D.1. Beta factors and the retention times of the gas compounds.

Compound	Retention Times (min)	β
Hydrogen (H ₂)	2.7	0.14
Carbon monoxide (CO)	5	1.42
Methane (CH ₄)	9.8	0.35
Carbon dioxide (CO ₂)	13.1	1.00
Ethylene (C ₂ H ₄)	17.5	0.39
Acetaldehyde (CH ₃ CHO)	26.4	3.06

Number of moles of gases in the non-condensable was calculated using equation D.2.

$$n_i = A_i * \beta_i \quad (D.2)$$

Total number of moles of gas is equal to equation D.3.

$$n_{non-condensable} = n_{CO} + n_{CO_2} + n_{C_2H_4O} + n_{H_2} \quad (D.3)$$

Mole fraction of the gas components is defined as in equation D.4.

$$y_i (\text{mol } \%) = \frac{n_i}{n_{\text{non-condensable}}} * 100 \quad (\text{D.4})$$

n_i represents the number of moles of the gas product while $n_{\text{non-condensable}}$ shows the total number of moles of the non-condensable products.

E. DSC Analysis of PLA-2003D

DSC spectrum of PLA-2003D is given in Figure E.1.

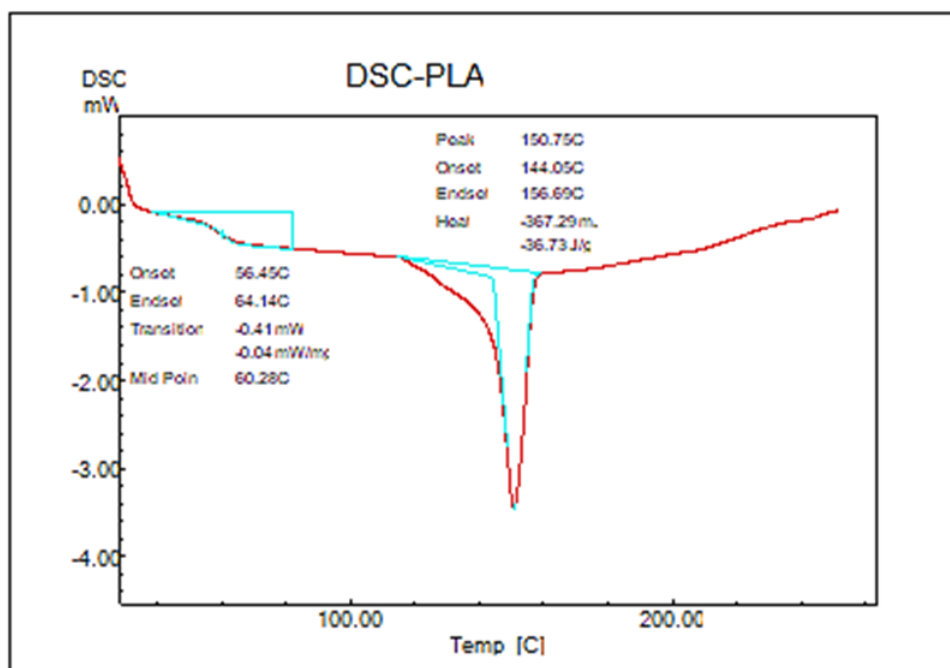


Figure E.1. DSC spectrum of PLA-2003D.

F. Determination of the Viscosity Average Molecular Weight of the Solid in the Reactor

The viscosity average molecular weights of the PLA and degraded PLA were determined using Hagen-Poiseuille equation (Rosen, 1982, Brandrup, 1966, Moore, 1972, Shoemaker, 1974).

$$\eta = \frac{\pi \times r^4 \times \Delta P \times t}{8 \times V \times l} \quad (\text{F.1})$$

ΔP is the hydrostatic pressure head generated, where t denotes the time elapsed as the fluid in the upper meniscus flows between the upper and lower collimating marks. To simplify, the hydrostatic pressure head can be represented by $g.h$ rather than ΔP , where ρ is the fluid's density. The equation becomes:

$$\eta = \frac{\pi \times r^4 \cdot \rho \cdot g \cdot h \cdot t}{8 \cdot V \cdot l} \quad (\text{F.2})$$

Due to the fact that the terms on the right-hand side of the equation (F.2) are constant with the exception of density and time, the equation can be rewritten as

$$\eta = A \cdot \rho \cdot t \quad (\text{F.3})$$

where A is a constant defined by a fluid's viscosity and density. In equation (F.3), the variables are fluid density and the time necessary for the fluid to flow through an Ubbelohde viscometer; hence, the relative viscosity of fluids A and B is defined as

$$\eta_{rel} = \frac{\eta_A}{\eta_B} = \frac{\rho_A \cdot t_A}{\rho_B \cdot t_B} \quad (\text{F.4})$$

In dilute polymeric solutions, the densities of the polymer solutions are close to one another; hence, in equation (F.4), the ratio of density of fluids can be considered as unity and the relative viscosity is just the ratio of time. Using intrinsic viscosity and the Mark-Kuhn-Houwink-Sakurada equation, it is feasible to estimate the viscosity average molecular weight of polymers. (Atkins & Paula, 2006)

$$[\eta] = \lim_{c \rightarrow 0} \left(\frac{\eta - \eta_0}{c \times \eta_0} \right) = \lim_{c \rightarrow 0} \left(\frac{\ln(\eta_{rel})}{c} \right) \quad (F.5)$$

When $[\eta]$ denotes intrinsic viscosity, η denotes viscosity of the solution, η_0 denotes viscosity of the solvent, viscosity of the solution the expressions in the first parenthesis denote reduced viscosity, the expression in the second parenthesis denotes inherent viscosity, c denotes polymeric solution concentration.

$$\eta_{sp} = \frac{\eta - \eta_0}{\eta_0} \quad (F.6)$$

$$\eta_{red} = \frac{\eta - \eta_0}{c \times \eta_0} = \frac{\eta_{sp}}{c} \quad (F.7)$$

Since intrinsic viscosity is the limit of both reduced viscosity and inherent viscosity as concentration approaches zero. As in the case of the Mark-Kuhn-Houwink-Sakarada equation, the viscosity average molecular weight of polymers can be related to their intrinsic viscosity.

$$M_v = \left(\frac{[\eta]}{K} \right)^{1/\alpha} \quad (F.8)$$

M_v is the viscosity average molecular weight of the polymer, where K and α are the solvent and polymer type-dependent constants. (Atkins & Paula, 2006). Using an Ubbelohde viscometer, the inherent viscosity of PLA in chloroform was formed at 25 °C. K and α corresponds to $22.1 \cdot 10^{-5}$ dL/g and 0.77, respectively (Köhn et al., 2003). A sample calculation was given for PLA 2003D. The flow times and concentration of PLA solutions are given in Table F.1. The intrinsic viscosity and reduced viscosity plots for PLA (Natureworks, 2003D) are given in Figure F.1.

Table F.1. The flow times and concentration of PLA-chloroform solution

Concentration (g/dl)	Time (s)	Time Solvent (s)
0.25	107.4	64.5
0.5	154.6	64.5
0.75	207.8	64.5
1	267.2	64.5

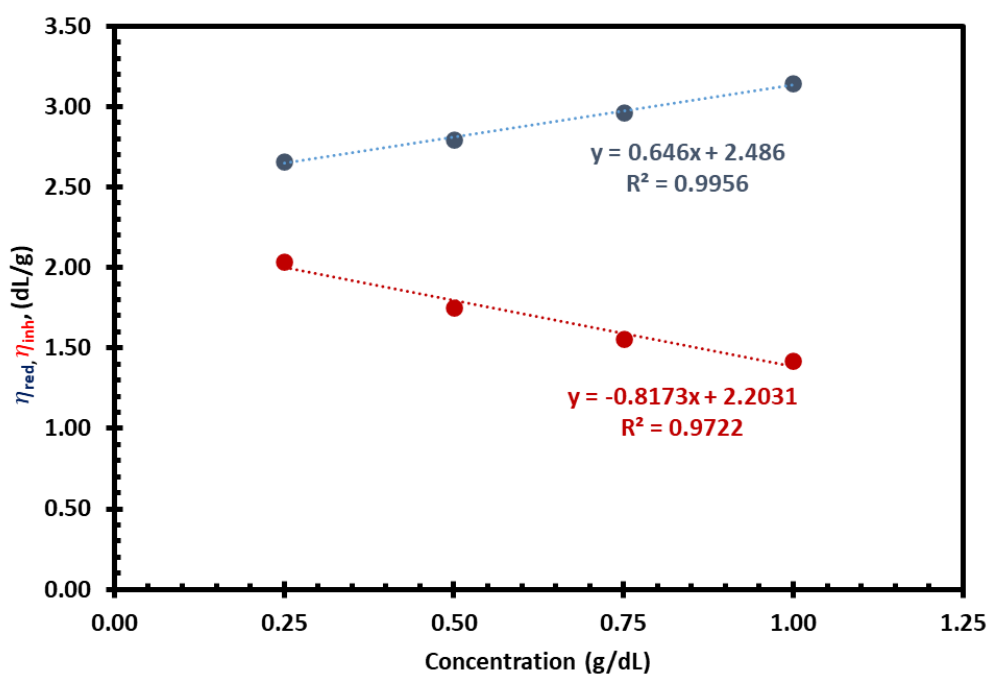


Figure F.1. Change of the intrinsic and reduced viscosities of PLA as a function of PLA-chloroform solution.

The flow times and concentration of degraded PLA solution at 200 °C are given in Table F.2. The intrinsic viscosity and reduced viscosity plots for degraded PLA at 200 °C are given in Figure F.2.

Table F.2. The flow times and concentration of degraded PLA at 200 °C.

Concentration (g/dl)	Time (s)	Time Solvent (s)
0.25	91.5	64.5
0.5	123	64.5
0.75	158.5	64.5
1	195	64.5

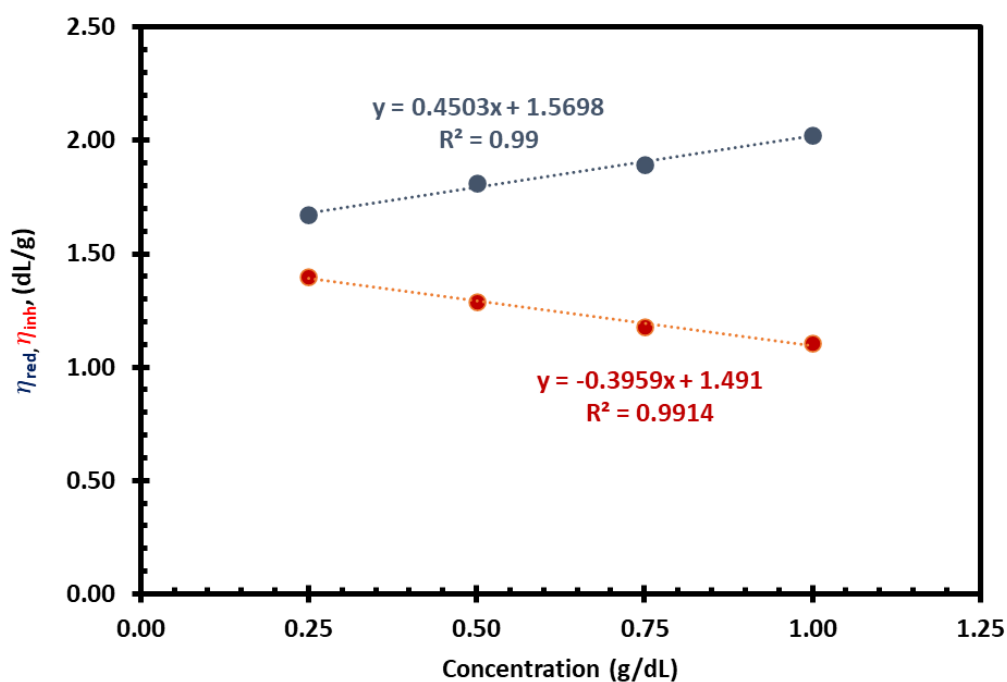


Figure F.2. Change of the intrinsic and reduced viscosities of degraded PLA at 200 °C as a function of degraded PLA-chloroform solution.

The flow times and concentration of degraded PLA solution at 200 °C are given in Table F.3. The intrinsic viscosity and reduced viscosity plots for degraded PLA at 200 °C are given in Figure F.3.

Table F.3. The flow times and concentration of degraded PLA at 250 °C.

Concentration (g/dl)	Time (s)	Time Solvent (s)
0.25	68	64.5
0.5	72	64.5
0.75	77.8	64.5
1	82	64.5

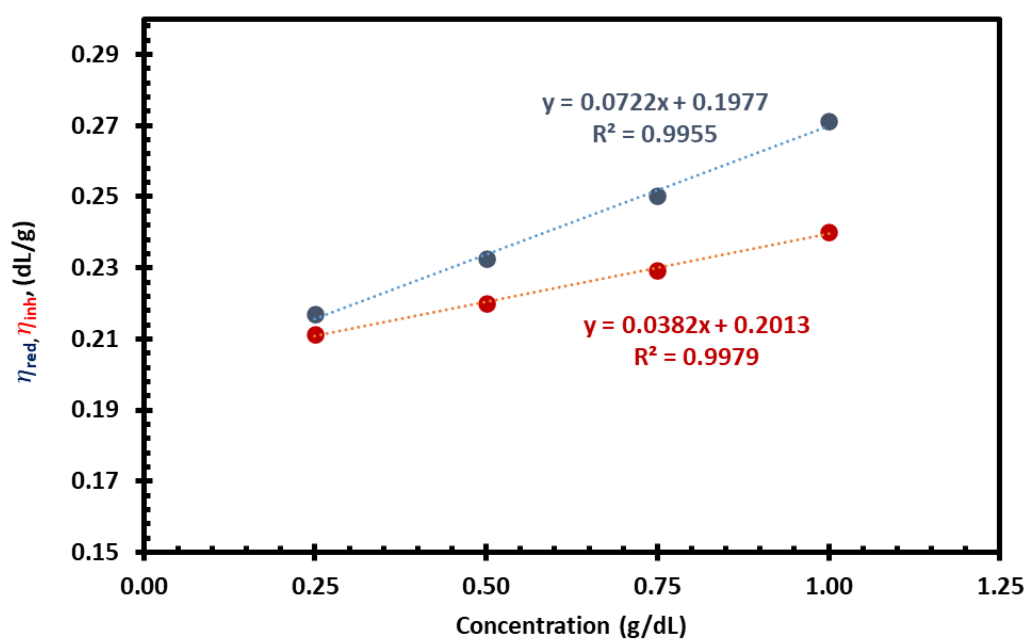


Figure F.3. Change of the intrinsic and reduced viscosities of degraded PLA at 200 °C as a function of degraded PLA-chloroform solution.

G. Calculation of the Solid and Gas Yields in Supercritical Reaction System

The solid product in the reactor was basically determined by measuring the weight of the solid in the reactor. The amount of gas product was calculated by applying equation G.1.

$$m_{\text{gas}} = m_{\text{initial PLA}} - m_{\text{solid}} \quad (\text{G.1})$$

m_{solid} and m_{gas} represent the weight of the solid in the reactor and gas product, respectively. Then the yields of solid and gas were obtained using equation G.2.

$$\text{Yield}_i(\text{wt. \%}) = \frac{m_i}{m_{\text{initial PLA}}} * 100 \quad (\text{G.2})$$

m_i represents the weight of the reaction product while $m_{\text{initial PLA}}$ shows the initial weight of the PLA polymer. Weight fractions of the compounds in the solid were found from equation G.3.

$$w_i(\text{wt. \%}) = \frac{m_i}{m_{\text{solid}}} * 100 \quad (\text{G.3})$$

m_i represents the mass of the compound while m_{solid} shows the weight of the PLA polymer.

H. XRD Data

XRD data of hematite, cubic iron and carbon are given in Figures H.1-H.4.

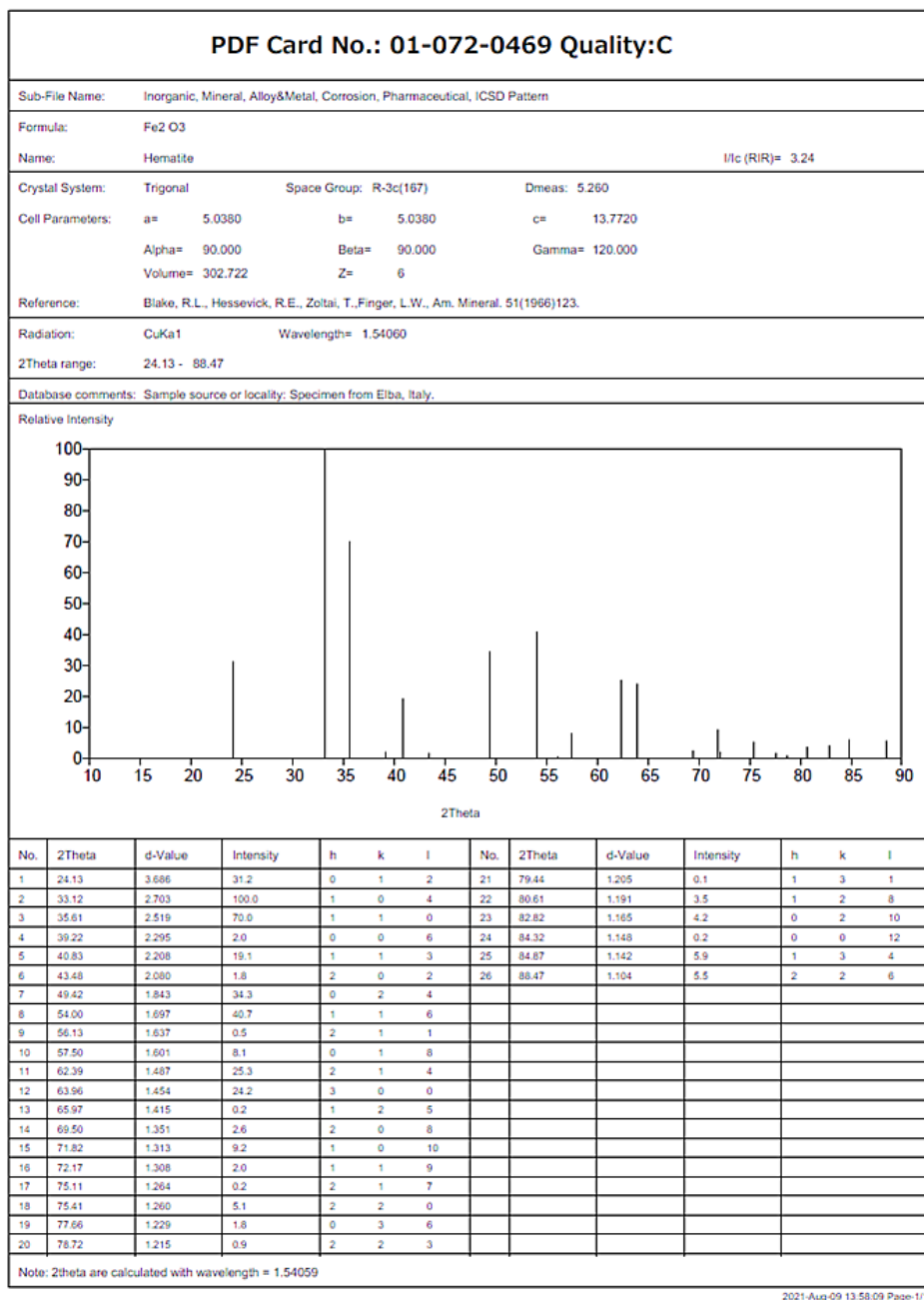
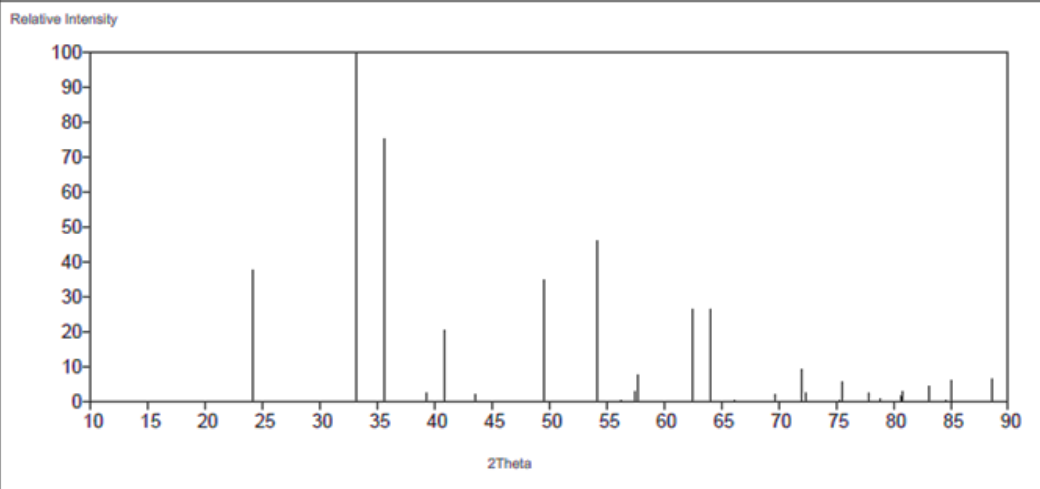


Figure H.1. XRD Data of Hematite

PDF Card No.: 01-089-0599 Quality:C

Sub-File Name:	Inorganic, Mineral, Alloy&Metal, Corrosion, Pharmaceutical, ICSD Pattern		
Formula:	Fe ₂ O ₃		
Name:	Hematite, syn		I/c (RIR)= 3.09
Crystal System:	Trigonal	Space Group: R-3c(167)	Dmeas:
Cell Parameters:	a= 5.0320	b= 5.0320	c= 13.7330
	Alpha= 90.000	Beta= 90.000	Gamma= 120.000
	Volume= 301.146	Z= 6	
Reference:	Sadykov, V.A., Isupova, L.A., Tsybulya, S.V., Cherepanova, S.V., Litvak, G.S., Burgina, E.B....		
Radiation:	CuKα1	Wavelength= 1.54060	
2Theta range:	24.17 - 88.65		

Database comments:



No.	2Theta	d-Value	Intensity	h	k	l	No.	2Theta	d-Value	Intensity	h	k	l
1	24.17	3.679	37.5	0	1	2	21	78.84	1.213	1.0	2	2	3
2	33.19	2.697	100.0	1	0	4	22	79.55	1.204	0.1	1	3	1
3	35.66	2.516	75.1	1	1	0	23	80.65	1.190	1.8	3	1	2
4	39.33	2.289	2.5	0	0	6	24	80.80	1.188	2.8	1	2	8
5	40.90	2.205	20.3	1	1	3	25	83.06	1.162	4.5	0	2	10
6	43.54	2.077	2.2	2	0	2	26	84.61	1.144	0.3	0	0	12
7	49.51	1.840	34.7	0	2	4	27	85.01	1.140	6.2	1	3	4
8	54.13	1.693	46.0	1	1	6	28	88.65	1.102	6.5	2	2	6
9	56.20	1.635	0.6	2	1	1							
10	57.49	1.602	2.7	1	2	2							
11	57.87	1.597	7.5	0	1	8							
12	62.49	1.485	26.4	2	1	4							
13	64.05	1.453	26.6	3	0	0							
14	66.09	1.413	0.3	1	2	5							
15	69.88	1.348	1.9	2	0	8							
16	72.04	1.310	9.4	1	0	10							
17	72.37	1.305	2.3	1	1	9							
18	75.27	1.261	0.3	2	1	7							
19	75.51	1.258	5.5	2	2	0							
20	77.81	1.228	2.3	0	3	6							

Note: 2theta are calculated with wavelength = 1.54059

Figure H.2. XRD Data of Hematite, syn.

Catalog No: 06-0696			
Cubic iron			
Radiation: CuKα1(λ:1.5406Å)			
d(Å)	2θ (°)	Intensity(I/I₀)	h k l
2.026	44.67	100	1 1 0
1.433	65.20	20	2 0 0
1.170	82.33	30	2 1 1
1.013	98.94	10	2 2 0
0.906	116.38	12	3 1 0
0.827	137.13	6	2 2 2

Figure H.3. XRD Data of Cubic Iron

Formula: C			
PDF Card No: 00-041-1487			
Radiation: CuKα1			
Wavelength: 1.54060 Å			
2θ (°)	d spacing (Å)	Intensity (%)	h k l
26.38	3.376	100	0 0 2
42.22	2.139	2.0	1 0 0
44.39	2.039	6.0	1 0 1
50.45	1.807	1.0	1 0 2
54.54	1.681	4.0	0 0 4
59.69	1.548	1.0	1 0 3
77.24	1.234	3.0	1 1 0
83.18	1.160	3.0	1 1 2
86.82	1.121	1.0	0 0 6
93.59	1.057	1.0	2 0 1

Figure H.4. XRD Data of Carbon

CURRICULUM VITAE

Surname, Name: Sivri, Seda

EDUCATION

Degree	Institution	Year of Graduation
MS	METU Chemical Engineering	2016
BS	Gazi University Chemical Engineering	2012

WORK EXPERIENCE

Research Assistant, Middle East Technical University, Department of Chemical Engineering, 2014 -2023

Sales Engineer, Likrom Analytical Solutions Marketing Corporation, 2012-2013

FOREIGN LANGUAGES

Advanced English, Elementary Spanish

PUBLICATIONS

1. Sivri S., Dilek Hacıhabiboğlu Ç., Sezgi N. A. 2019. "Synthesis and Characterization of Aluminum Containing Silica Aerogel Catalysts for Degradation of PLA", International Journal of Chemical Reactor Engineering, 17, 20180163.

REFEREED CONGRESS/SYMPOSIUM PUBLICATIONS IN PROCEEDINGS

1. Sivri S., Dilek Hacıhabiboğlu Ç., Sezgi N. A. Feedstock Recycling of PLA in the Presence of Mesoporous Catalysts. NCC 8, Ankara, Turkey, 9 -12 September 2021.
2. Sivri S., Dilek Hacıhabiboğlu Ç., Sezgi N. A. The Contribution of Metal Loaded Mesoporous Catalysts to Recycling of Polylactic Acid. EuropaCat 2019:14th EuropeanCongress on Catalysis, Aachen, Germany, 18 -23 August 2019.
3. Sivri S., Dilek Hacıhabiboğlu Ç., Sezgi N. A. Metal Yüklü Silika Aerojel Destekli Katalizörlerin Polilaktik Asidin (PLA) Bozunması Üzerine Etkisinin İncelenmesi. UKMK13, Van, Turkey, 3 -6 September 2018.
4. Sivri S., Dilek Hacıhabiboğlu Ç., Sezgi N. A. Recycling of Polylactic Acid by Pyrolysis over Aluminum Loaded Silica Aerogel. EMCC9, Ankara, Turkey , 31 August-2 September 2018.
5. Sivri S., Yılmaz Ü., Bat. E. Kontrollü Protein Salımına Yönelik Nanokompozit Hidrojel Geliştirilmesi. 6.Ulusal Polimer Bilim ve Teknoloji Kongresi,Turkey, 4 -7 September 2016.

PATENTS

1. Sezgi N. A., Dilek Hacıhabiboğlu Ç., Sivri S. 2020. "High Yield, Eco-Friendly Recycling Method of Polylactic Acid using Supercritical or Dense Gas Carbon Dioxide", PCT, CHAPTER C Chemistry; Metallurgy, The Invention Registration Number: PCT/TR2020/050252.
2. Sezgi N. A., Dilek Hacıhabiboğlu Ç., Sivri S. 2020. "Polilaktik Asitin Süperkritik Karbondioksit ile Yüksek Verimde Temiz Geri Dönüşüm Metodu", Turkish Patent, CHAPTER C Chemistry; Metallurgy, The Invention Registration Number: TR 2019 09479 B, Initial Registration.

DISSERTATION

MS, “Development of Nanocomposite Hydrogels for Controlled Release of Proteins, Middle East Technical University”, Graduate School of Natural and Applied Sciences, Department of Chemical Engineering, 2016.

INTERNATIONAL RESEARCHER IDS

ORCID:0000-0003-3601-0537

Yoksis Researcher ID:217494